Analysis of historic rammed earth construction

Jaquin, Paul A.

Analysis of Historic Rammed Earth Construction

Paul A. Jaquin

A thesis submitted in partial fulfilment
of the requirements for the degree of
Doctor of Philosophy

School of Engineering
Durham University
02 January 2008

Analysis of Historic Rammed Earth Construction

Paul A. Jaquin

Volume I

Abstract

Rammed earth is an ancient construction technique which has recently become popular for sustainable building. Soil is compacted in removable formwork to make a homogeneous wall. A lack of experimental evidence and a poor fundamental understanding means that current design guidelines are highly conservative and inappropriate for the analysis of historic rammed earth buildings. This thesis shows that rammed earth can be viewed in a geotechnical engineering framework and that doing so helps to explain many aspects of the material behaviour. Rammed earth walls were built and tested in the laboratory then modelled using techniques available to practising engineers. Unsaturated soil mechanics was considered useful in explaining much of the behaviour of rammed earth. This was investigated through a series of uniaxial compression tests and the results are explained using unsaturated soil mechanics. Visits to Spain and India were made to investigate rammed earth in the field. Historic construction techniques, modes of failure and repair strategies were studied. The unsaturated nature of rammed earth is used to explain modes of failure and to suggest the most appropriate repair strategies.

Declaration

I confirm that no part of the material offered has previously been submitted by myself for a degree in this or any other University. Where material has been generated through joint work, the work of others has been indicated.

Paul A. Jaquin

Durham, January 02, 2008

Acknowledgements

There are many people who have made this thesis possible. Thanks must go primarily to Dr Chris Gerrard who first wondered how best to deal with a failing rammed earth structure and to Dr Charles Augarde who realised that this would be an interesting field of study. The study of rammed earth was the subject of my final year MEng project, and thanks must go to Dr Augarde for seeing the potential of a PhD in both me and in the subject area. At the time we did not know quite where the research would lead.

As a newcomer to the field of rammed earth, I contacted many people for information. Special thanks to Cob builders Linda Watson and Barry Honeysett in Cornwall, and to rammed earth builders David Easton in California and Meror Krackenhoff in Vancouver. In the field of historic building conservation, thanks to Richard Hughes of Arup, John Hurd of the World Monuments Fund and Randolph Langenbach who provided information about specific sites.

In January 2006 I travelled to southern Spain with Mr Phillip Jones who assisted me in both navigating and communicating in rural Spain. In October 2006 I travelled in northern Spain and was greatly assisted by Mr Nick Watson who provided a great deal of assistance and information during this visit. In November 2006 I visited north India, and many thanks to Miss Eleanor Trueman and Rimo Expeditions for organising a superb few days in Ladakh. Thanks to the Institution of Structural Engineers, whose Rowen Travel Award allowed the October and November travel.

A large amount of work was done in the laboratories, and thanks to Tony Garrett of Rivergreen Construction who allowed us to use material from the site, and to Professor Peter Walker of Bath University who provided us with information about the material. Thanks must also go to Dr David Toll who, on looking at a rammed earth wall in the laboratory, commented that it might be suction providing the additional strength in the rammed earth. Thanks to the technicians in the laboratory Mr Bernard McEleavey and Mr Stephen Richardson who assisted me with both rammed earth construction and suction measurement.

To fellow PhD students in the laboratory Sergio Lourenco, Joao Mendes and Cathy Dowding I owe a debt of thanks, for debate, argument and discussion about unsaturated soil and soil chemistry, which greatly help in my understanding of rammed earth.

During my PhD I have been lucky to work with a number of MEng and MSc students who have helped me to study the material of rammed earth. Thanks to Cindy Hendy (nee McChlery), Tom Horncastle, Tom Howard and Lucie Legrand,

Finally, thanks to my office mates Gareth Bird, Robert Simpson and Dimosthensis Koungelis, to my housemates and my family, and for support throughout the PhD and a mammoth proofreading effort, to my girlfriend Eleanor Trueman.

Publications

Parts of this thesis have been presented at external conferences or submitted for publication in journals.

Journal publications

Accepted

Jaquin, P. A. **Study of historic rammed earth structures in Spain and India**. *The Structural Engineer*

Jaquin, P.A. Augarde, C.E. Gerrard, C.M. **Historic rammed earth distribution**. *International Journal of Architectural Heritage*

Under review

Jaquin, P. A., Augarde, C. E., Gallipoli, D. and Toll, D.G. **The strength of rammed earth materials**. *Geotechnique*

Conference proceedings

Papers

Jaquin, P. A., Augarde C.E and Legrande, L. **Unsaturated characteristics of rammed earth** *First European Conference on Unsaturated Soils,* Durham, July 2008

Jaquin, P.A., Augarde, C. E. and Gerrard, C.M. **Historic Rammed Earth Structures in Spain** *International Symposium on Earthen Structures,* Bangalore, August 2007

Jaquin, P.A., **Analysis of Historic Rammed Earth Construction** *9th Young Geotechnical Engineers Symposium*, Belfast, September 2006

Jaquin, P. A., Augarde, C. E. and Gerrard, C.M. **Analysis of Historic Rammed Earth Construction**. *Structural Analysis of Historic Constructions*, New Delhi, November 2006

Jaquin, P. A., Augarde, C. E. and Gerrard, C.M. **Analysis of Tapial structures for modern use and conservation.** *Structural Analysis of Historic Constructions,* Padova, November 2004

Posters

Jaquin, P. **Analysis of Historic Rammed Earth Structures** *Presentations by Britain's Top Younger Scientists and Engineers, Houses of Parliament,* London, October 2006

Jaquin, P. **Historic Rammed Earth Construction** *Institution of Structural Engineers Young Researchers Conference,* London, September 2006

Contents

List of Figures

List of Tables

Nomenclature

D	Diameter
D_n	Percentage smaller than n
E	Young's modulus
E^{ref}	Reference modulus
E_{50}	Shear hardening modulus (HS model)
E_i	Initial modulus (HS model)
E_{oed}	Volumetric hardening modulus (HS model)
F	Yield function
G	Shear modulus
G_s	Specific gravity
K	Bulk modulus
K_0	Ratio of horizontal to vertical stresses
M	Critical State Friction angle, Yield locus multiplier (HS model)
M_a	Total stress ratio (Toll (1990), Critical State model)
M_w	Suctions ratio (Toll (1990), Critical State model)
M_s	Mass of solids
M_w	Mass of water
R	Radius
R_v	Gas constant
R_f	Failure ratio (HS model)
S_r	Degree of Saturation
S_u	Undrained strength
T	Temperature
T_s	Surface tension

V_v	Volume of voids
V_w	Volume of water
AE	Actual Evaporation
AEV	Air Entry Value
PE	Potential Evaporation
RH	Relative humidity
c	Apparent cohesion
d	Diameter
e	Void ratio
$f(u)$	Turbulent exchange function
g	Acceleration due to gravity
h	Relative humidity, height
h_c	Height of capillary rise
i	Hydraulic gradient
k	Coefficient of permeability
k_s	Coefficient of saturated permeability
m	Level of stress dependency (HS)
n	Grading coefficient, soil porosity
p	Pressure, volumetric stress, proportion of grains of a given diameter
p_0	Pressure of saturated water vapour, Preconsolidation stress (CSSM, BBM)
p_0^*	Initial preconsolidation stress (BBM)
p^c	Net mean reference stress at the saturated virgin state (BBM)
p_v	Pressure of water vapour
q	Deviator stress
q_a	Asymptotic value of deviator stress (HS model)
q_{ult}	Ultimate value of deviator stress (HS model)
r	Radius
r_{AEV}	Air entry pore radius
s	Suction
t	Time

u	Pressure
u_a	Water pressure
u_w	Air pressure
v	Velocity, specific volume
w	Volumetric water content

χ	Bishop's effective stress parameter
$\boldsymbol{\varepsilon}$	Strain
ε_1	Maximum principal strain
ε_2	Intermediate principal strain
ε_3	Minimum principal strain
ε^e	Elastic strain
ε^p	Plastic strain
ϕ	Friction angle
ϕ^b	Nonlinear variation of shear strength with respect to suction
γ	Free surface energy, shear strain
γ^p	Plastic shear strain
ν	Poisson's ratio
π	Osmotic suction, pi
θ	Wetting angle
ρ	Density, bulk density
ρ_0	Density of saturated water vapour
ρ_d	Dry density
ρ_v	Density of water vapour
ρ_w	Density of liquid water
σ	Stress
σ'	Effective stress
σ_1	Maximum principal stress
σ_2	Intermediate principal stress

σ_3	Minimum principal stress
τ	Shear stress
υ	Poisson's ratio
ψ	Dilatancy angle
ψ_m	Mobilised dilatancy angle

Chapter 1

Introduction and Literature Review

1.1 Introduction

This thesis studies historic rammed earth. Two parallel threads are drawn together, one based on the construction, testing and analysis of rammed earth which was constructed for the research, the other on observations of historic rammed earth at a large number of sites in Spain and India. Rammed earth is an ancient construction technique which has recently gained popularity as a sustainable construction material. The behaviour of rammed earth is acknowledged to be little understood, which makes the conservation of historic sites and design of new construction difficult. This thesis looks at historic construction techniques, failures of rammed earth buildings and repair methods which have been implemented, and seeks to show that rammed earth can be better understood as a highly unsaturated soil.

1.2 Rammed earth

Rammed earth is an ancient construction technique, based on compacting soil between formwork boards to create a homogenous mass wall. Rammed earth been seen as a quick, easy construction technique for the building of fortifications; a cheap way for a man to build his own home; and a sustainable construction technique which uses only what is available at the site. Rammed earth buildings are found around the Mediterranean, and along the same latitude in Iran, Pakistan, India and China. Rammed earth was taken by the Europeans to South America, and many colonial buildings in parts of Brazil and Columbia are constructed in rammed earth. The rediscovery of rammed earth as a sustainable building material prompted its use in Australia and the southern United States from the early 1970s onward. Today rammed earth is receiving increased interest as sustainable construction practices become more mainstream. Examples of the historic use of rammed earth are given in Appendix A.

To build a traditional rammed earth wall, a formwork box is constructed using two parallel timber sides, supported on two or more horizontal timbers (Figure 1.1). Vertical timbers are then placed through holes in the ends of the horizontal timbers thereby restraining the formwork. These vertical timbers are connected at the top using rope, forming an open box. Soil is taken from the ground and if necessary sieved to remove larger particles. Additives such as straw or lime may be mixed into the soil, which is then dropped into the formwork in layers, usually around 150mm high. The layer is then compacted using a heavy rammer. Upon compaction of one layer, another layer of earth is placed in the formwork and the process repeated until the formwork is full. The formwork is then removed and placed on the next set of horizontal timbers where the process is repeated. Once the formwork has been moved on, the horizontal timbers are removed from the wall leaving characteristic holes usually called *putlog* (*mechinales* in Spanish) holes by architectural historians. Upon completion of one horizontal level the formwork is moved vertically, the mass of standing wall being known as a *lift*. A rammed earth wall can thus be constructed using very little manpower and crucially without recourse to temporary works such as external scaffolding.

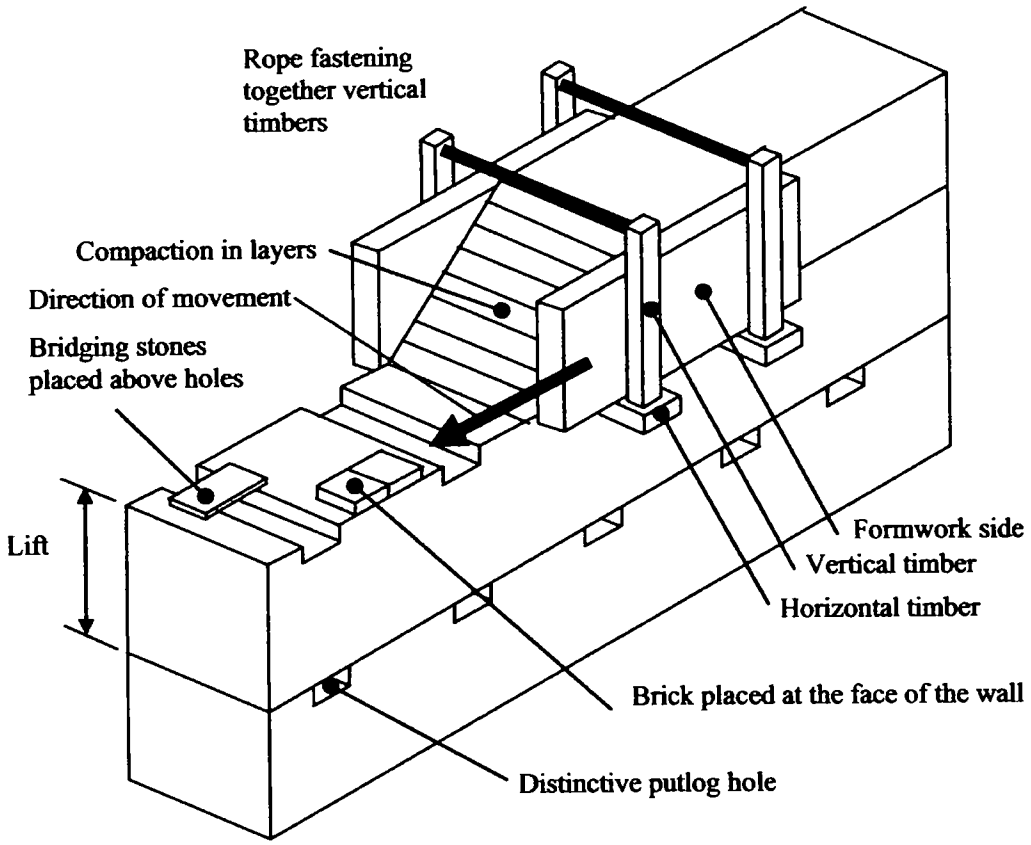

Figure 1.1 Aspects of rammed earth construction

1.3 Objectives and methods

The aim of this thesis is to better understand the structural behaviour of historic rammed earth structures in order to improve analysis and repair techniques. It is generally acknowledged that the current understanding of rammed earth construction is incomplete. This thesis shows that it is possible to analyse historic rammed earth using geotechnical engineering methods available to practising engineers, and that it is important to consider rammed earth as a highly unsaturated soil. Viewing rammed earth as a highly unsaturated soil leads to an improved understanding of the structural performance and failure of historic rammed earth buildings. Repair techniques are discussed and an appreciation of the unsaturated nature of rammed earth will properly infom analysis and repair techniques for historic rammed earth buildings.

To achieve this, two strands of research were undertaken. One strand was the physical and numerical modelling of rammed earth and the other strand was fieldwork visits to a number of historic rammed earth sites. Work on both strands proceeded in parallel, often with the observations from fieldwork informing activity in the laboratory and results in the laboratory being used to understand what was observed in the field. In addition to the laboratory and fieldwork described below, numerical modelling using finite element software was carried out and a small amount of theory developed to help explain behaviour observed both in the laboratory and the field.

1.3.1 Physical and numerical modelling

The laboratory investigations were in two parts, described in Chapters 2 and 3. Chapter 2 uses existing geotechnical engineering techniques to investigate rammed earth. The construction and testing of a small number of walls in the laboratory is described. Finite element numerical models of these walls were constructed and two different approaches used to simulate the behaviour of rammed earth. The numerical models were tuned so that their behaviour matched that observed in the physical testing. The issues with such modelling are discussed and it is proposed that the unsaturated nature of rammed earth be taken into account.

Chapter 3 looks at the unsaturated nature of rammed earth. The concepts of unsaturated soil mechanics are outlined and it is explained how these may be linked to rammed

earth construction. A link between negative pore water pressure (suction), water content and sample strength is proposed and unconfined uniaxial compression tests measuring suction to confirm this hypothesis are described. The test results are explained in a double structure framework of unsaturated soil mechanics and it is shown that treating rammed earth as a highly unsaturated soil allows prediction of its absorption and evaporation characteristics.

1.3.2 Fieldwork

Three different field visits were carried out during the course of this research. A large number of sites in southern Spain were visited during January 2006 and are described in Appendix C. This visit served to increase understanding of historic rammed earth construction and Spain was chosen for its high density of historic rammed earth buildings and excellent transport links, allowing access to a large number of sites in a short time span. A smaller number of sites were visited and observed in much greater detail in northern Spain which are discussed in Appendix B. Full surveys of a sample of sites were undertaken, and scale plans were drawn of a number of structural details and failures which had been identified in southern Spain. A small number of sites were visited in Ladakh in north India prior to a conference in the region and are described in Appendix D. These sites were constructed in the 16^{th} century by Buddhist and Muslim rulers. While only three sites were visited there proved to be a remarkable similarity between Indian and Spanish sites in spite of their geographical separation. Based on these field visits, research was carried out into different types of historic rammed earth construction, the failures which affect historic rammed earth strutures and mitigation and repair strategies which have been attempted.

Different types of historic rammed earth construction are discussed in Chapter 4. A review of existing classifications of historic rammed earth construction typologies is undertaken and expanded upon based on field work carried out in Spain and India. Different aspects of the mix, lift bond, formwork and design are used to produce a framework within which a large number of historic rammed earth techniques can be incorporated. This framework makes it much simpler to describe failures in historic rammed earth.

incorporated. This framework makes it much simpler to describe failures in historic rammed earth.

Chapter 5 describes failures in historic rammed earth. Failures observed in other types of historic earth building are discussed and compared to those found during fieldwork. Failures specific to rammed earth are identified and many of these are explained in a new light based on the unsaturated nature explained in Chapter 3. By distinguishing between different discrete failure mechanisms it is easier to understand and assess a structure prior to repair.

Repair of historic rammed earth buildings is discussed in Chapter 6. The recommendations of earth building experts are considered, and compared to observations of buildings in Spain and India. A range of repair techniques which have been suggested suitable for historic earth buildings are judged, and those though acceptable for rammed earth repair highlighted. Recommendations are made regarding repair with specific reference to the previously ignored unsaturated nature of rammed earth.

Appendix A presents a chronological study of the spatial distribution of historic rammed earth. While many texts give a small number of examples of very famous rammed earth sites, it is shown that rammed earth exists in many parts of the world. Because the international distribution of rammed earth is offered, it is possible to describe the spread of rammed earth around the world over time. Field visits to northern and southern Spain and India are described in Appendices B, C and D. The sites visited are uniquely identified and a brief history and survey of each site is provided.Each site is given a unique two letter identifier based on the site name, and each structure within that site numbered. Thus two sites in the Spanish city of Jaen are named Ja1 and Ja2 respectively.

Modern rammed earth construction is not investigated, except to compare historic and modern building and analysis techniques. Cement stabilised rammed earth is not studied, neither is the thermal performance considered. Unsaturated soil mechanics is used as a framework in which rammed earth may be better understood, and the testing described must be considered as simple tests performed on rammed earth rather than

specific unsaturated soil testing. Numerical modelling using finite elements is described as a tool to better understand rammed earth behaviour but the finite element method is not described.

1.4 Literature review

This section presents a review of literature relating to rammed earth construction. It is argued that while some research has been carried out, and guidelines exist for the construction of new rammed earth buildings, there is a lack of understanding of many of the concepts which underpin earth building, and this means that many basic questions about the nature of rammed earth remain unanswered. While these questions have been posed, and it has been argued that rammed earth be treated in a geotechnical engineering framework, it is shown that work to date has not achieved this.

Rammed earth can be considered within the field of earthen architecture. Research into earthen architecture conservation began around 1973, with the First International Conference on the Conservation of Earthen Architecture (ICOMOS 1972). This corresponds with the rediscovery of earthen architecture as a sustainable building material and the inception of the modern rammed earth industry in the USA, Australia and Europe (see Appendix A).

The majority of published work on rammed earth construction concentrates on either modern construction or architectural case studies of specific historic sites. There is little literature on the fundamental bonding and cohesion mechanisms within earthen architecture or global problems associated with rammed earth structures. Much of the published engineering literature on rammed earth construction discusses thermal and erosional performance of the material.

A survey of the publications from seven international conferences (1972 – 1993) showed that only 8% of papers related to rammed earth (Matero and Cancino 2000). An international study of rammed earth (Oliver 1986) noted that testing and experimental source material was hard to find. While European aid institutions were developing traditional rammed earth techniques in developing countries, north American and Australian contractors were experimenting with cement stabilised rammed earth and developing proprietary formwork systems. Therefore although rammed earth was being used as both a traditional and modern building technique, there was little investigation into the behaviour and fundamental properties of the material.

This review therefore extends slightly outside literature relating to historic rammed earth structures to touch on modern rammed earth construction and other historic earthen architecture such as cob and layered earth construction. The intention is to understand historic rammed both in the context of modern rammed earth and of other historic earthen architecture. Research into historic rammed earth is first outlined, followed by a discussion of some aspects of modern rammed earth building which are relevant to the understanding of historic buildings and to the testing of rammed earth. Finally research needs in earthen architecture are discussed, it is shown that may issues have been identified which require further investigation. Because this thesis introduces many themes and ideas which have not previously been discussed in the field of earthen architecture, literature pertaining to these themes (such as soil mechanics) is presented in the relevant chapter as required.

1.5 Historic rammed earth

A relatively large number of case studies about historic rammed earth constructions have been published, most of which are included in Appendix A. The majority of these deal with the architectural restoration of specific sites, or are reviews of buildings constructed as a legacy of a particular rammed earth practitioner. However, there is very little published academic work regarding the engineering behaviour of historic rammed earth construction. A team at Granada University have performed a series of tests on historic samples and a group at Seville University have looked at typological descriptions of historic rammed earth in their local area.

Arango Gonzalez (1999) cored samples from the city walls of Granada. Six 150mm diameter cores were taken, but the method of drilling is not revealed. Cyclic unconfined compression tests were carried out on five of the samples and a Brazilian test was performed on the remaining sample. Elastic behaviour was observed up between 1 and 2.5MPa, and following this there was a decrease in stiffness to a final compressive failure stress of between 6.5 and 10MPa. The single Brazilian test yielded a tensile resistance of 0.7MPa. The elastic modulus was found to vary between 51.4 and 56.6 GPa.

Typological descriptions allow historians to accurately date historic structures, and allow engineers to be informed of the method of construction of a wall without destructive intervention. García and Rodríguez (2003) highlight the lack of typological descriptions of historic rammed earth techniques, and offer a typological framework based on their studies of the city of Seville. The lack of such descriptions hindered investigation during the fieldwork, and so the framework was expanded upon as explained in Chapter 4.

1.6 Modern rammed earth construction

Modern rammed earth construction is flourishing in many parts of the world. Since the 1970s, Western Australia has led the way in cement stabilised rammed earth building, with the technique now definitely part of mainstream construction. In north America, cement stabilised rammed earth has also gained a substantial footing in the domestic property market. In Europe the trend has been towards one of high sustainability, with many practitioners in Austria, Germany and the UK advocating the use of unstabilised rammed earth.

A recent UK Department of Trade and Industry (DTI) funded project *Developing rammed earth walling for UK housing construction* performed a state-of-the-art review into modern rammed earth construction. The resulting document (Walker and Maniatidis 2003) forms the basis of a book (Walker, Keable et al. 2005) which was published following completion of the project.

A wide range of different norms and standards exist around the world and this section highlights a number of areas which are relevant to this thesis. Standards or guidelines exist in a number of countries and these are briefly outlined below. Different approaches to the characterisation of the material are described, together with methods for testing rammed earth samples. Erosion testing is discussed, as are in-situ methods for the determination of strength of rammed earth and other testing and investigations which have been carried out on rammed earth.

1.6.1 Design

It is hoped that design guidelines for modern rammed earth buildings will help inform engineers investigating historic rammed earth buildings. There are two series of guidelines which may help in understanding historic rammed earth, those regarding material specification and those looking at structural design. The modern rammed earth building community is split into two sectors, practitioners looking at cement stabilised rammed earth, and more 'ecological' builders, who promote *unstabilised* rammed earth. Unfortunately a lack of materials testing and case studies means that guidelines for modern construction are simplistic with structural design guidelines being based on those for unreinforced masonry, and materials specifications being compliance rather

than method based. Because of this lack of understanding, large material safety factors must be used in structural design, Walker, Keable et al. (2005) recommend that material safety factors of between 3 and 6 should be used, depending on the experience of the contractor and knowledge of the material properties. These factors are obviously unacceptable for efficient building design, and for the analysis of historic structures, owing more to geotechnical than to structural design. As the use of rammed earth becomes more widespread there is an increasing need for rational structural design guidelines. A review of design guidelines in different countries is given in Walker and Maniatidis (2003) and a brief overview is given here.

1.6.1.1 North America

In the USA three buildings codes are available; in the Southern States the Southern Building Code is used, which concentrates on hurricanes; in the North East and Midwest, the Standard Building Code concentrates on snow and wind loading; and in the West states the Uniform Building Code (UBC) concentrates on earthquake loading. Earth buildings are not covered by any of these codes, but the UBC has been adapted for use with earth buildings, mainly by taking masonry design values. The resulting guidelines are published in King (1997).

The UBC is a permissive stress design guide, and these are defined as a function of a material's ultimate compressive strength (King 1997). This approach may not be entirely valid for rammed earth, and the small amount of testing data available means that many of the figures are educated guesses. Using this approach each permissive stress value is dependant on compressive strength testing of similar rammed earth. King recommends unconfined compression testing of 6 inch (150mm) test cylinders. Material partial safety factors are decided by the designer, and King (1997) recommends that although a factor of 2 is recommended for uninspected masonry, factors of between 4 and 8 should be employed for the ultimate compressive strength. Easton (2005) notes that the guidelines recommended in King (1997) are highly conservative. In some cases rammed earth may be considered as a weak concrete (due to the addition of cement as a stabiliser) and then design follows more exact UBC rules for unreinforced concrete.

1.6.1.2 Australia and New Zealand

Research work detailed in Appendix A resulted in the publication of *Bulletin No.5* (Middleton 1952) which sets out 'requirements and capabilities' of rammed earth. This document provided a basis for the design in rammed earth in Australia from its publication until very recently. Walker (2002) produced a Standards Australia Handbook which while not carrying the weight of a full standard (which is prepared by a technical committee), aims to provide state-of-the-art guidance. In 2001 the Earth Building Association of Australia published a draft document (EBAA 2001) outlining alternative design guidelines, but this document remains in draft form.

Earth building standards in New Zealand were begun in 1991 sponsored by the Earth Building Association of New Zealand. In 1994 Standards New Zealand took responsibility for the project, which was to be a joint project with the Australian Standards board. However this joint approach failed and in 1997 drafts were published in New Zealand but not Australia. These are the only current rammed earth standards which were prepared by a technical committee and are legally binding. Three standards were produced, covering *Engineered Design of Buildings* (NZS 4297:1998), *Materials and Workmanship* (NZS 4298:1998) and *Buildings not Requiring Specific Design* (NZS 4299:1998). Buildings less than 3.3m tall do not require specific design, although the rammed earth must pass the specifications laid out in NZS 4298:1998. Buildings between 3.3m and 6.5m must in addition be designed to NZS 4297:1998. Walls are usually considered to be constructed in cement stabilised rammed earth between 230mm and 400mm thick, and in New Zealand the critical loading condition is usually seismic.

1.6.1.3 Europe

West Germany published documents in 1947 and 1956 about rammed earth construction, and it is assumed that the large number of rammed earth constructions in East Germany (Guntzel 1990) were constructed to these guidelines following the Second World War. The standards were withdrawn in 1971, but Volhard and Röhlen (1999) published a 'state of the art (earth building) technical rule'. This document specifies types of material suitable for earthen construction together with selection tests, detail of rammed earth formwork and structure design. Material properties such as density, permeability and insulation are given. This document does not carry the same

weight as a national DIN standard, but a document of this level is currently being prepared.

A guidance document was published in Spain (MOPT 1992) detailing the design and construction of earthen structures, with specific emphasis on rammed earth. Advice on formwork and ramming is given. Design principles for compression, tension and buckling are outlined with detailing of footings and corners discussed. Quality control measures for the production of rammed earth are also provided.

1.6.1.4 Africa

The design guidelines for Zimbabwe (SAZS 2001) are virtually identical to those in Keable (1996) which is based in part on work carried out by Lilley and Robinson (1995). In addition the Zimbabwe design guidelines include a spray erosion test, detailed in Middleton (1952). Information on formwork and design are given, with an emphasis on compression design, structural stability and reinforcement over openings. Formwork design and material specification are also covered, together with footing and roof detailing.

1.6.2 Material Characteristics

Characterisation of materials suitable for rammed earth construction is noted as being difficult (Houben and Avrami 2000), as much of the material used could fit into narrow definitions within a broader geotechnical framework. However attempts have been made to describe suitable properties for a rammed earth material, and these are outlined below.

1.6.2.1 Particle size distribution

Walker and Maniatidis (2003) show particle size distributions recommended for unstabilised rammed earth given by a wide range of authors (reproduced in Figure 1.2). It can be seen that the percentage of clay varies from a minimum of 10% to a maximum of 80%, with the same figures for the proportion of silt. Acceptable ranges of sand range from 5% to 40%. For stabilised rammed earth the recommended proportions of cement vary from 25% to 40% by volume (Walker and Maniatidis 2003).

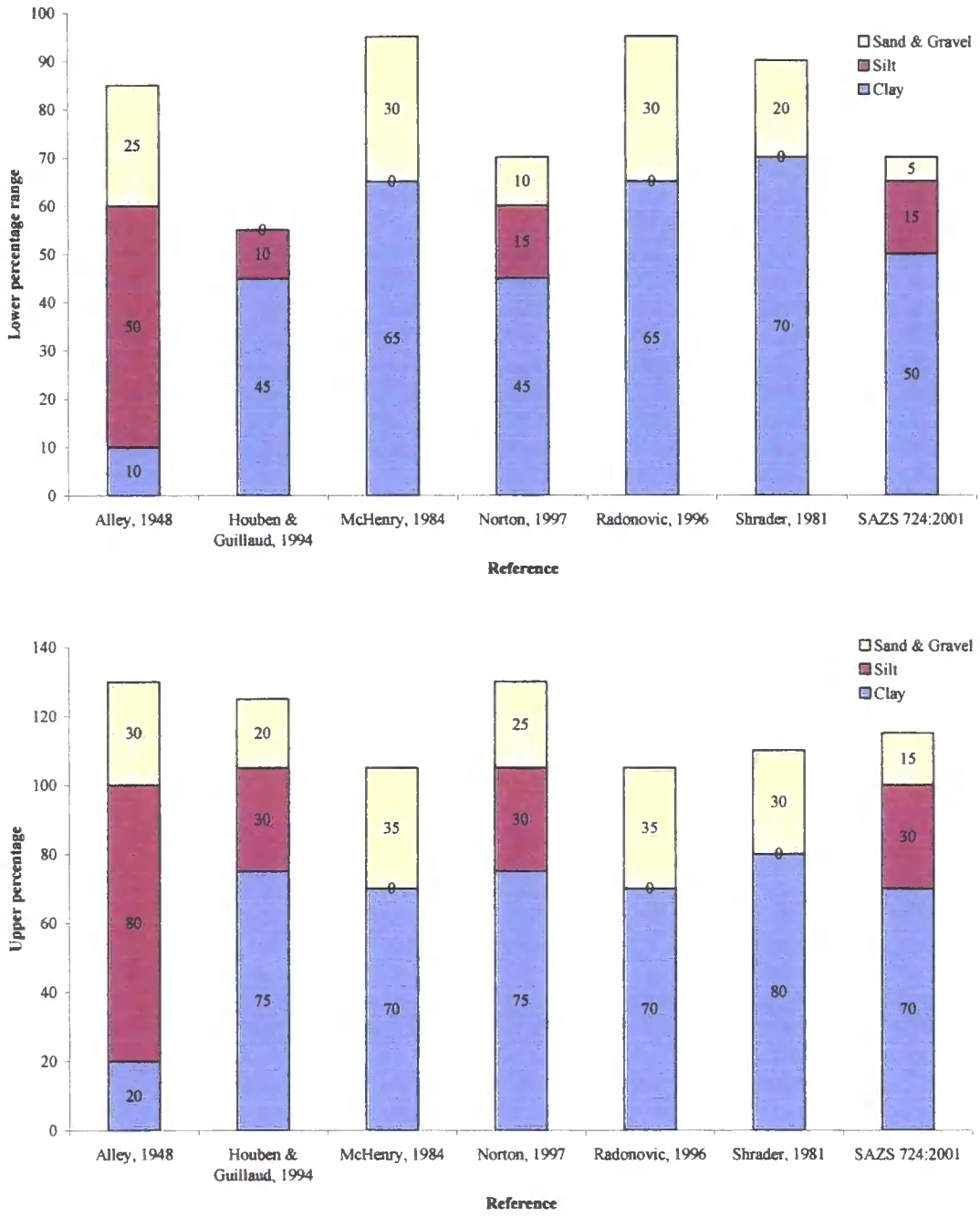

Figure 1.2 Suggested upper and lower particle size distributions suitable for rammed earth. After Walker, Keable et al. (2005)

1.6.3 Dry density

The density of rammed earth is dependent on particle size distribution, moisture content during compaction and compactive effort applied. The concepts of dry density and optimum moisture content are outlined in Section 2.2.2. Testing methods outlined in Section 1.6.4 recommend that rammed earth is compacted close to the optimum moisture content, although Keable (1996) and Lilley and Robinson (1995) note that

soil compacted at the optimum tends to adhere to the formwork sides, and thus a slightly lower moisture content is used in practice. The compactive effort applied by modern pneumatic and electric rammers is considered to be significantly higher than that achieved by manual compaction, but it can be seen that the densities achieved in historic samples are similar to those achieved in modern rammed earth construction. Densities of modern rammed earth range from 1700kg/m^3 to 2200kg/m^3 (Walker and Maniatidis 2003), and the only quoted density of a historic sample is 1770kg/m^3 – 1990kg/m^3 (Arango Gonzalez 1999).

1.6.4 Compressive strength

Walker and Maniatidis (2003) note that the range of compressive strength of unstabilised soils tends to be very large, and as such experimental testing should always be undertaken prior to design. It is widely observed that the compressive strength of a rammed earth sample increases when cement is added. It is assumed that the testing of rammed earth samples takes place at a fixed moisture content, which is in equilibrium with the humidity of the air. However the moisture content of a sample will change depending on the surrounding humidity and Greer (1996) observed that the strength of cob samples varied by around 80% depending on their moisture content. It is assumed that a similar relationship will hold for rammed earth.

Minimum permissible compressive strength values for unstabilised rammed earth vary from 0.25MPa (Middleton 1952) to 0.6MPa (EBAA 2001), while values for stabilised rammed earth range between 1MPa and 15MPa (Walker and Maniatidis 2003), although this obviously depends on the amount of stabilisation added. The strength of the only historic samples tested varied between 6.5MPa and 10MPa (Arango Gonzalez 1999). Burroughs (2001) notes that compliance-based testing is used at all modern rammed earth construction sites in Australia.

Cylinder, cube and wallet tests are outlined below. A number of institutions have now undertaken tests on rammed earth, and tests where published results are available are presented. Samples are usually tested in a similar manner to concrete (cubes and cylinders) or masonry (wallets). Measurement of load and displacement allows the elastic modulus to be determined.

Based on a large amount of experimental test data, the relationship between the compressive strength of concrete cubes and cylinders is known to be close to 0.7 (BCA 2004) but this relationship has not been established for rammed earth. Roach (1994) undertook cylinder and wallet tests, and found that the compressive strength of walls was similar to that predicted by 150mm diameter cylinders.

Font and Hidalgo (1991) performed three compression tests on unstabilised rammed earth cylinders made from material used to construct a test dwelling in the Els Port region of Spain. A relationship between density and compressive strength was established with increasing density giving a higher compressive strength. The maximum density achieved was 2138 kg/m^3, which gave a compressive strength of 2.94MPa.

Testing undertaken by Lilley and Robinson (1995) used 150mm cubes compacted in layers 100mm deep. The soil used is described in Section 1.6.5.1. A metal rammer weighing 7.5kg was dropped 18 times on each layer (height not known), and the cubes tested after 24 hours, 7 days and 28 days. The optimum moisture content was determined and drying cubes tested at six different moisture contents. It was found that the cube strength increased to a maximum after 7 days, being between 1.8 and 2.3MPa. It was thought that the lower strength after 28 days was a result of shrinkage cracking.

Burroughs (2001) tested 149 unique soil samples, with the aim of identifying suitable soils in New South Wales for use in rammed earth construction. Standard geotechnical tests were undertaken and unconfined compressive strength testing performed on all of the samples. The majority of the tests were undertaken on stabilised material, and different types of stabilisers were added to the mixture. The samples were first screened through a 19mm sieve, then the required amount of stabiliser was added. The samples were always compacted at their predetermined optimum moisture content. Compaction took place in a 105mm diameter, 115mm high mould lightly coated with castor oil. Each 3kg sample was compacted in five equal layers, subjected to 25 uniformly distributed blows by a 4.9kg rammer falling freely 450mm above the compacting surface. 300g of excess mixture was used to determine the moisture content by oven drying. Each specimen was allowed to cure in

a humidity cabinet at 22°C for 28 days, after which it was immersed in water for 4 hours, and allowed to drain for 15 minutes. The 28 day cured samples were then compression tested to failure at a loading rate of 0.10MPa/second.

A procedure given in Walker, Keable et al. (2005) is based on work by David Clark, due to be published as a PhD thesis at some point in the future. 100mm diameter, 200mm tall cylinders are used to determine the compressive strength. The maximum aggregate size should not exceed one sixth of the diameter of the cylinder. Compaction is carried out at either the optimum or the 'as used' moisture content and the cylinders are then stored at 15°-20° in a relative humidity of 40-60% for 28 days. Cylinders should be capped with dental cement or similar to ensure a parallel top and bottom faces. The cylinders should be loaded at a constant strain rate of 1.0mm/min.

Hall and Djerbib (2004b) detail a method for compaction of rammed earth cube samples based on the Proctor compaction method. The Proctor method is usually used to determine the Optimum Moisture Content (OMC) of a sample. The total energy input is fixed for a Proctor test, while Hall and Djerbib (2004b) allow the energy to be varied, the amount of compaction controlled the particle size distribution and the optimum moisture content. Compaction was then carried out to NZS 4298:1998, which states that a 6.5kg hand rammer must 'ring' when dropped from 300mm onto the soil. It is assumed that when the rammer rings, compaction of that layer is complete and the next layer begun.

1.6.5 Wallet testing

Wallet (small wall) testing has been carried out at a number of centres, and the results have usually been incorporated into the code of practice for the country where the testing has taken place. Where published work is available, it is presented below, although a number of other tests are known to have been conducted, the results of which are not now available, for example Kornouchow (1933).

1.6.5.1 Newcastle University

Lilley and Robinson carried out compression tests on wallets with openings, and attempted to strengthen the openings with steel reinforcement as used in concrete construction. The walls were manufactured by Andy Simmonds, now an architect

working in rammed earth consultancy, and the work was incorporated into Keable (1996) for use in Zimbabwe rammed earth guidelines (Section 1.6.1.4).

Four different soils were imported from Ghana with clay contents varying from 4% to 21%. Initially the walls were compacted at their optimum moisture content, but this led to the soils adhering to the shuttering, so a lower moisture content was used, defined using a technique where the soils were dried until they did not stick to the hands when pressed into a small ball. This was considered the new optimum moisture content for compaction. 14 walls were constructed within concrete formwork, with mould release oil applied to the formwork to aid removal. Blanks were used to form openings and filleted corners were used at the intersection of two walls. Initially each 100mm layer was hand rammed for around four minutes before the next layer was placed, but both manual and pneumatic ramming methods were used. Only small differences were observed in the dry densities achieved using each technique.

Arched, pointed and rectangular openings were constructed in the rammed earth, and reinforcing steel bars were added to some of the wallets. In some walls point loads were applied directly above the openings and in others loads were applied to simulate floor and roof joists acting through a timber ring beam. Global failure of the unreinforced walls occurred through 45 degree cracks from the corners of the walls, which caused a triangular section above the wall to fail. Reinforced walls allowed this section to remain intact and thus did not lead to the collapse of the wall. It was therefore deemed to be a safety feature to have reinforcement above the openings, however there was no gain in strength using reinforcement. While failure loads are provided, they are of little use because of the unique failures of the walls, which makes failure stresses within the rammed earth difficult to establish.

1.6.5.2 New Zealand Standards

Walker and Morris (1997) performed tests on wall panels, the results of which were incorporated into NZS 4297:1998. Two panels were tested, made from a soil of 5% clay, 40% silt and 55% sand. Wall panel A was 1.8m square and 250mm thick and reinforced with three (two 16mm and one 20mm) reinforcing rods running vertically, with a timber bond beam fixed to the top of the wall. Wall panel B was 2.4m high, 1.8m wide and 300mm thick, two 20mm reinforcing rods ran vertically through the

wall connected to a concrete bond beam at the top. Wall A proved stronger than the concrete foundation plinth it stood on, and the foundation failed at a vertical load of 130kN. Wall B failed in brittle diagonal tension following yielding of the reinforcing steel. The equivalent shear strength was found to be 0.14MPa.

1.6.6 Erosion tests

Although structural performance of rammed earth is important, because much rammed earth is low rise compression only buildings, it is often erosional performance which determines whether a rammed earth mix can be used in construction.

1.6.6.1 Ralph Patty, South Dakota Experiment Station

Professor Ralph Patty conducted early pioneering field trials of wall tests (Patty 1936), the results of which are reproduced in Burroughs (2001). Patty aimed to examine the resistance to weathering of rammed earth walls constructed from different soil types, and undertook work varying the proportions of sand in each wall mixture. 29 walls were constructed in an East-West run, leaving the north and south faces exposed. The walls were 0.910m long, 0.760m high and 0.300m thick and were built on a concrete plinth, and topped with a metal cap.

After five years Patty examined the resistance of the walls to weathering, giving each wall a performance rating based on visual inspection. Patty found that three of the best walls contained over 75% sand, two with fine sand and one with a coarser sand. Patty inferred that the size of the sand grains has little effect on the resistance to weathering. He concluded that the clay content of the walls was the most important factor in determining the degree of deterioration and stated that soils containing more than 40% clay should not be used for rammed earth wall construction, with the best range being between 30 and 39% (Burroughs 2001).

1.6.6.2 George Middleton, Commonwealth Experimental Building Station, New South Wales

Middleton set out to define a reliable method for accurately identifying favourable soils for rammed earth construction, and to determine the structural characteristics of suitable soils. He aimed to determine the optimum sand:clay ratio and the optimum

moisture content for both strength and weathering resistance (Middleton 1947). 23 walls were constructed, based on the work of Patty. These walls were also in an East-West arrangement, leaving the north and south faces exposed. The walls were 1.2m long, 0.9m high and 0.3m thick. Middleton found that soils containing more than 40% sand had a higher weathering resistance (Burroughs 2001). The tests were published (Middleton 1952), and his results remained for a long time the standard for rammed earth construction in Australia and other parts of the world.

1.6.6.3 Other erosion tests

Hall (2006) made use of a climatic chamber to simulate erosion on a stabilised rammed earth wall. A number of organisations also have conducted erosional tests on a number of rammed earth walls, but none of the results are published. These organisations include

- *Fundacion Navapalos*, Spain
- Arc Architects, Earth Structures, Renders & Plasters Project (Morton and Little 2007).

1.6.7 *In situ* testing

Indirect density tests such as nuclear density tests, as used in the geotechnical industry, have been suggested by Keable (1996) and Walker, Keable et al. (2005) but there is no evidence of this being undertaken in practice.

Strength testing using rebound hammers has been investigated (McChlery 2004; SREB 2006). This attempts to match compressive strength to rebound values, and this work seemed to meet with some success, though Walker, Keable et al. (2005) suggest that the results can prove variable and unreliable.

Assessment of as built rammed earth is usually limited to a visual inspection of the surface. Walker, Keable et al. (2005) suggest a minimum performance specification states 'no cracks wider than 3mm and longer than 75mm' but the depth of the cracks is not specified.

1.6.8 Other types of tests

Walker and Maniatidis (2003) performed tests on rammed earth columns. The columns were 300mm square in cross section and between 1.8m and 3m high. Compressive loading at increasing eccentricities was carried out. Hall and Djerbib (2004a) investigated absorption of moisture into rammed earth samples, looking at the effect of particle size distribution on the rate of capillary suction from free and pressure driven water. Taylor and Luther (2004) investigated the thermal performance of rammed earth walls and Treloar, Owen et al. (2001) conducted a life cycle analysis on a rammed earth structure. McChlery (2004) and an undergraduate student at Bath University have performed pullout test of reinforcement bar embedded in rammed earth.

Coring of rammed earth walls has been successfully achieved by Arango Gonzalez (1999), who performed compression tests on the cored samples (Section 1.6.4), though they do not specify the coring method used. Lilley and Robinson (1995) attempted to core their test falls following failure to obtain the density of the samples, but this proved difficult as the rotary corers used were unsuitable for the dense, coarse grained rammed earth.

1.7 Research needs in earthen architecture

This section deals with research into both the conservation and engineering of historic earthen architecture, with an emphasis on historic rammed earth buildings. Hughes (2001) notes there is a perceived lack of research in the whole field of earthen architecture. In 2000, following the 8th International Conference on the Conservation of Earthen Architecture, *Project Terra* was set up, with the aim of 'outlining research needs in the field of earthen architecture conservation' (Houben and Avrami 2000). Much of the work outlined in this thesis follows directly from the needs outlined by this group.

The further aims of this group were to instigate cooperation and corroboration between partner organisations in the field of earthen architecture conservation. Crocker and Rojas (2000) note that prior to the instigation of *Project Terra* the discipline appeared to the lacking structure, and it was hoped that these collaborations would take forward the field of earthen architecture conservation. However, Morton and Little (2001) note that 'research relating to earthen architecture conservation...remains somewhat disparate, lacking the focus and support that a better linked and developed community of investigators could provide'. Crocker and Rojas (2000) also observe that the field of earthen architecture conservation is small, with too few practitioners for the amount of work

A number of publications relating to the conservation of earthen architecture have been produced by the *Project Terra* partners, for example Oliver (2000) and Tolles, Kimbro et al. (2000) but all of these focus on reports for specific case studies, and do not address fundamental engineering aspects of earthen architecture defined as currently lacking by Houben and Avrami (2000). Hughes (2001), Langenbach (2004) and Velde (2003c) and have all expressed the need to consider earthen architecture within a soil mechanics framework, but as yet no literature has been published in this field. This thesis aims to answer some of the research needs outlined by Houben and Avrami (2000) and a review of those needs is given below.

1.7.1 Binding mechanisms

Houben and Avrami (2000) identify an understanding of the binding mechanisms in earthen architecture as 'fundamental to advancing knowledge in the diagnosis and conservation of earthen architecture'. While it is considered that the macro-mechanisms of structural decay are well known, the micro mechanisms which trigger the failure of the physio-chemical matrix are not considered to be the subject of speculation. A research priority is defined as the requirement to

- Understand the relative parts of electromagnetic forces, ion exchange potential, friction, capillary forces and microbiological effects.

Guillaud and Avrami (2003) draw heavily on Velde (2003a, 2003b,2003c) in pointing out that much research is required into the understanding of the actions of clay minerals within earthen architecture conservation. While this is valid, it is assumed that the high proportion of clay present within adobe bricks means that research in adobe should concentrate on clay mineralogy. Rammed earth however, is seen to have a much broader particle size distribution, and thus investigation of other binding mechanisms, as outlined by Houben and Avrami (2000) is warranted.

1.7.1.1 Soil mechanics

Hughes (2001) has noted that consideration of soil mechanics within the field of earthen architecture conservation is desired, but is currently treated in a superficial way and there is a 'lack of application of fundamental principles and material parameters of soil mechanics by architects and structural engineers'. Hughes (2001) considers that there is a large amount of technology transfer which can take place from the road construction and soil mechanics industries to the conservation of earthen buildings.

Langenbach (2004), in investigating causes of failure in the 2003 Bam earthquake in Iran, noted that traditional seismic masonry theory did not explain the failures observed at Bam. While seismic masonry analysis usually considers discrete blocks subject to accelerations, Langenbach (2004) observed a total loss of cohesion of soil structures, which must be explained in soil mechanics terms rather than by treating earthen structures as weak masonry. This is considered to be doubly important in the

case of rammed earth, as the earthen walls at Bam were generally constructed in adobe brick, and as such could be considered as masonry. Rammed earth however is much more akin to a homogenous soil body albeit with material inhomogeneities introduced by the variability of the soil, and non-isotropy by the presence of compaction layers. However, taking into account the compaction layers, and by using average properties, it is possible to consider rammed earth as a soil

1.7.1.2 Water

Houben and Avrami (2000) acknowledge that water plays a critical role in both the decay and cohesion of earthen architecture, but that the influence is qualitatively observed and there is a complete lack in quantitative data. The behaviour of water within a structure (absorption, adsorption and migration) is described as unknown and as such the processes of decay are not understood. The following research priority is suggested:

- Understanding the relationship between strength of earthen materials and small variations in water content (0.5%- 1.5%)

Houben and Avrami (2000) note that most geotechnical and rock mechanics literature focuses on fully or partially saturated materials, whereas most earthen architecture constructions are operating at 2-7% moisture content. Houben and Avrami (2000) highlight suction as playing an important, not yet understood role in the non-structural decay of earthen architecture, and observe that earthen buildings are known to be able to recover some cohesion, up to a limiting water content. However the value of this limiting water content and the reasons for it, are not understood.

Houben and Avrami (2000) also observe the practicality of testing in-situ water contents of historic buildings, given that existing methods have proved inadequate at the low moisture contents observed. In addition the non-uniformity of water content through a wall is noted.

1.7.2 Structural mechanisms

Hughes (2001) outlines the lack of standard engineering principles applied to soil structures, and a lack of appreciation of the unique structural behaviour of earthen

architecture. Very few case histories on the analysis and repair of earthen structures are published where engineering is a key concern. No mention is made of the structural modelling of historic earthen structures, and Houben and Avrami (2000) concentrate instead on identifying the relationships between microscale interactions and structural behaviour, suggesting that relationships exist through all levels of earthen architecture, and that microscale actions impact on the structural behaviour of a building. Particular note is made of the relationship between water content and the strength and stiffness of a structure. It is assumed that strength is sensitive to moisture content, but the relationship is not known. The phenomenon of creep in historic earthen structures is examined, and the extent of 'safe' creep is questioned.

Houben and Avrami (2000) and Hughes (2001) highlight the abundance of cracks in earthen buildings, and observe that cracks in earthen buildings can be considered as normal and part of the functioning system of the structure. In unreinforced non-earthen buildings cracks are almost always considered to be detrimental to structural behaviour, but this is not always the case in earthen buildings. Houben and Avrami (2000) recognise the need to educate structural engineers in the mechanics of earthen buildings, to allow them to discern threatening and non-threatening cracking, and seismic and structural cracks.

Hughes (2001) investigates structural repair of earthen buildings and notes that there is a tendency to use modern repair solutions to earth buildings. These repair techniques often employ artificial stiffening of the structure, such as recreating of structural continuity across cracks and other defects, which changes the structural system of the building. Hughes (2001) calls for the following research areas to be investigated:

Modelling

- Wall failure modelling, to model typical failure modes, backed up by structural analysis.
- Evaluation of the effects of conservation on how a structure performs, accounting for actions in a decayed structure, which will change over time.

- Analysis of structural connections of soil (wall) to soil (ground) and timber to soil.
- Prediction of future building performance, assessment of building stiffness and definition and measurement of critical tensile strains, leading to development of a generalised comparative performance model, such as exists for stone and brick structures.
- Investigation of fracture mechanics of soil walls, relating the stress-strain conditions to the creation and propagation of crack systems.

Decay

- Assessment of the historic tradition of the building type and setting.
- The influence of fabric condition on loading and load paths, looking at both surface condition and overall wall structure.
- Relative humidity and dew effects on the wall fabric.

Conservation

- Assessment of the compatibility of new structural support systems with earthen structures.
- Assessment and documentation of the processes and techniques which have been applied in active conservation projects.

1.8 Concluding remarks

The scarcity of published work in the engineering of historic rammed earth structures has been identified, and the need for an improved understanding of engineering processes within historic rammed earth structures highlighted. The current level of understanding of modern rammed earth construction has been outlined, and it is argued that this cannot be reasonably used to model historic rammed earth structures.

The range of micromechanical and structural issues outlined by Houben and Avrami (2000) are a good guide to future research into earthen architecture conservation. While *Project Terra* continues to operate, there are a range of issues highlighted which have yet to be resolved, mainly due to their falling within the remit of engineers, rather than architects and conservators who are the main participants in *Project Terra*. A gap in understanding is presented, it is shown that practitioners of architectural conservation of historic rammed earth structures are not fully aware of the advantages which an understanding of soil mechanics can bring to the conservation of rammed earth structures. It is shown that there is already an acknowledgement of a lack of understanding of the fundamental processes within rammed earth, without which good conservation practices cannot be undertaken. Issues of structural engineering and soil mechanics, raised by Houben and Avrami (2000) and Hughes (2001) are yet to be tackled, but an understanding of these, as outlined above, would be of great value to the earthen architecture conservation community.

Walker and Maniatidis (2003) point out that the standard soil characterisation tests (particle size distribution, liquid and plastic limit) are not reliable in establishing the suitability of a certain soil for rammed earth construction. As such soil for modern rammed earth construction is selected on performance criteria defined at the beginning of each project. This situation obviously cannot occur in historic structures, and as such a more fundamental understanding of the binding mechanisms of rammed earth is required, as outlined in Section 1.7.1.

It is clear from the assessment by Walker and Maniatidis (2003) that while the development of design guidelines for rammed earth is progressing, there is not the depth of understanding or consistency which is found in concrete or masonry design guides. The lack of established test methods means comparisions between different rammed earth samples are close to meaningless, with each institution using, for example different size and shape of samples and different loading rates. Therefore modelling techniques and a fundamental understanding of rammed earth as a building material must be developed. It thought that the best way to achieve this is to model rammed earth as a soil, which can both lead to an improved understanding of the fundamental processes, and guide modelling strategies.

The lack of typological descriptions of historic rammed earth constructions has been emphasised. As highlighted by Hughes (2001) the typological differences observed in historic rammed earth constructions have a large bearing on the erosional and structural performance. The lack of engineering analysis of historic rammed earth sites has been identified and as such the body of fieldwork undertaken aims to provide engineering explanations of damage and failure observed in historic rammed earth structures. A large number of different repair techniques have been suggested and identified as being used at historic sites. These are evaluated and best practice repair techniques suggested.

Investigators of historic structures do not usually have the luxury of destructive testing to determine performance characteristics for the material they are investigating, and must rely on modelling and a fundamental understanding to judge the safety of a structure. This thesis aims to provide both modelling strategies and a deeper fundamental understanding of historic rammed earth structures, such that they can be better understood and thus better managed.

Chapter 2

Classical testing and modelling

2.1 Introduction

The design guidelines outlined in Section 1.6 are unsatisfactory for use with historic rammed earth. This is because they are based heavily on masonry or concrete guidelines and have been adapted for use in modern rammed earth. The lack of definitive testing and these adapted guidelines mean that large factors of safety must be used. When investigating a historic building possibility close to collapse, such safety factors cannot be used. Therefore improved modelling strategies must be developed.

This chapter uses simple physical modelling to inform numerical modelling. Physical modelling involved the construction of five walls in the laboratory. These walls were differently shaped and loaded in different ways because construction of the next wall was informed by the behaviour of the previous wall. The tests were intentionally simple and only limited instrumentation was used. These walls improved our understanding of the construction technique and provided insights into the types of failure which occur when loading rammed earth. The layered nature of rammed earth is highlighted.

Simple numerical models, available to practising engineers were used to represent rammed earth behaviour. Finite elements models of some of the physical walls were developed. The layered nature, highlighted in physical modelling was investigated first. A layered rammed earth model was developed based on the Mohr-Coulomb yield criteria, with the layers being assigned different properties to the body of the rammed earth. A second approach looked at the compaction of rammed earth using an elasto-plastic hardening approach also making use of the Mohr-Coulomb yield criteria. In both cases a parametric study of Mohr-Coulomb parameters was carried out.

The first part of this chapter discusses soil from a geotechnical engineering perspective. A range of constitutive models are then described. The construction and testing of walls in the laboratory is then explained, and this leads to the development of the numerical modelling based on the constitutive models.

2.2 Soil

Soil can be considered as any uncemented or weakly bonded accumulation of mineral particles formed by the weathering of rocks; the type of soil depends on the rock from which the soil originates and the processes it has undergone since it was weathered, (Craig 2002). A soil may be defined by the distribution of different sized particles it contains, and names given to ranges of particle sizes are shown in Table 2.1. Particles smaller than 0.002mm are clay sized and some of these particles are *clay*, while others are merely small inert particles. Clay is considered unique amongst soil particles as it is electrostatically charged and additional forces are observed between clay particles, which are further discussed in Section 3.6.1.

Name	**Maximum dimension (mm)**
Clay	0.002
Silt	0.06
Sand	2
Gravel	60
Cobbles	200
Boulders	> 200

Table 2.1 Particle sizes, from BS1377-2:1990

2.2.1 Phase relationships

Soil consists of interlocked solid particles with voids between. These voids are be filled with fluid, generally air or water, but other fluids may be present. Where all of the voids in the soil are filled with water, the soil is described as saturated, and where air is present in some of the voids, the soil is described as unsaturated. In unsaturated soils, additional forces are present across the voids by virtue of the meniscus. In this chapter saturation is assumed, as is the case in most engineering soil mechanics, and hence the presence of these additional forces is ignored. The studies undertaken here thus match the approach taken conventionally. In Chapter 3 the issue is revisited and rammed earth considered as unsaturated.

Some definitions required for the description of soils are as follows (Craig 2002)

- The *water content* w of a soil is the ratio of the mass of water M_w to the mass of solids M_s in the soil.

$$w = \frac{M_w}{M_s} \tag{2.1}$$

- The *degree of saturation* S_r is the ratio of the volume of the water V_w to the total volume of the void spaces V_v. This ranges between 0 for a completely dry soil to 1 for a saturated soil.

$$S_r = \frac{V_w}{V_v} \tag{2.2}$$

- The *void ratio* e is the ratio of the volume of void spaces to the volume of solids V_v.

$$e = \frac{V_v}{V_s} \tag{2.3}$$

- The *specific volume* v is the total volume of soil which contains unit volume of solids.

$$v = 1 + e \tag{2.4}$$

- The *bulk density* of a soil is the ratio of the total mass to the total volume

$$\rho = \frac{M}{V} \tag{2.5}$$

- The *specific gravity* G_s of the soil particles is given by

$$G_s = \frac{M_s}{V_s \rho_w} = \frac{\rho_s}{\rho_w} \tag{2.6}$$

where ρ_s is the particle density and ρ_w is the density of water.

- The *degree of saturation* S_r can be expressed as

$$S_r = \frac{wG_s}{e} \tag{2.7}$$

- The *dry density* ρ_d of a soil is the mass of solids per unit volume of the soil, and is a measure of the compaction

$$\rho_d = \frac{\rho}{1 + w} \tag{2.8}$$

2.2.2 Soil compaction and optimum water content

Compaction is the process where the volume of a soil is reduced by removal of air from the pore spaces, leading to an increase in the density of the soil. The degree of compaction of a soil is measured by the dry density (Equation (2.8)) and depends on the initial water content of the soil and the amount of energy supplied, known as the compactive effort. For a given soil and compactive effort there is a particular water content at which maximum compaction will occur, if the soil is too dry the particles are not able to be rearranged and if the soil is too wet, the voids are mostly filled with water so then the compactive effort will simply attempt to compress the water, which can be considered to be incompressible, and thus maximum density cannot be achieved. The maximum possible dry density is known as the *zero air voids* density and can be calculated from Equation (2.9).

$$\rho_d = \frac{G_s}{1 + wG_s}\rho_w \tag{2.9}$$

There are a number of tests to determine the optimum water content for compaction of a sample. Figure 2.1 shows the zero air voids line for a given soil from which it can be appreciated that the optimum water content decreases with increasing compactive effort. The three main tests used in geotechnical engineering are the Standard and Heavy Proctor tests and the vibrating hammer test (all described in BS1377-2:1990). In each test a number of different samples are compacted at different water contents and the water content for the greatest dry density determined as the optimum water content. The Standard Proctor test uses a 2.5kg hammer dropped from 300mm onto soil in a 1 litre mould, compacted in three layers with each receiving 27 blows. The Heavy Proctor test is similar, but uses a larger 2.3 litre mould with a 4.5kg hammer falling 450mm to compact five layers, each receiving 27 blows. A vibrating hammer test compacts the soil in a 2.3 litre mould, three layers each receiving 60s of dynamic compaction. The Proctor tests are known as semi-confined, where material is allowed to flow around the hammer foot, whereas the foot in the vibrating hammer test fills the entire mould (Figure 2.2). Each test provides a different amount of compactive effort, and is used for different soils. Soils with larger particles are compacted in larger moulds, thus the optimum water content for a gravel would be determined using a vibrating hammer test, while a Standard Proctor test would be used for a clayey material. Walker, Keable et al.

(2005) recommend use of the Standard Proctor test when determining the optimum water content for rammed earth compaction, but it should be appreciated that the method used for construction should be used to determine the optimum water content for compaction

An alternative method of determining the optimum water content for compaction of rammed earth requiring no laboratory apparatus is the drop test method. This method is outlined in Houben and Guillaud ; Keable (1996) and Walker, Keable et al. (2005) and defines the optimum water content for compaction as reached when a ball of the soil can just be formed in the palm of a hand, which on dropping breaks into two or three equal sized parts. While perhaps a good estimate, this empirical method is subject to user competence, and results will obviously differ between individuals, making use of this method difficult to justify in scientific investigation.

The maximum possible density of the soil is obviously equal to the density of the actual soil particles, and would represent a state with no voids between particles, and thus also no air or water present. This situation, while impossible to achieve in practice, can be modelled using a particle size distribution curve following the formula known as the *Fuller* formula (Fuller and Thompson 1907)

$$p = 100\left(\frac{d}{D}\right)^n \tag{2.10}$$

where p is the proportion of particles of a given diameter; d is the diameter of particles, D is the largest grain diameter and n is a grading coefficient. $n = 0.50$ for spherical grains, but is assumed to be between 0.20 and 0.25 for earth construction (Houben and Guillaud 1994). Figure 2.13 shows the particle size distribution of the soils used compared to Equation (2.10).

Knowledge of the properties such as those described above is useful in understanding the behaviour of soil. However such properties much be combined with laboratory testing and constitutive models to allow understanding and prediction of soil performance.

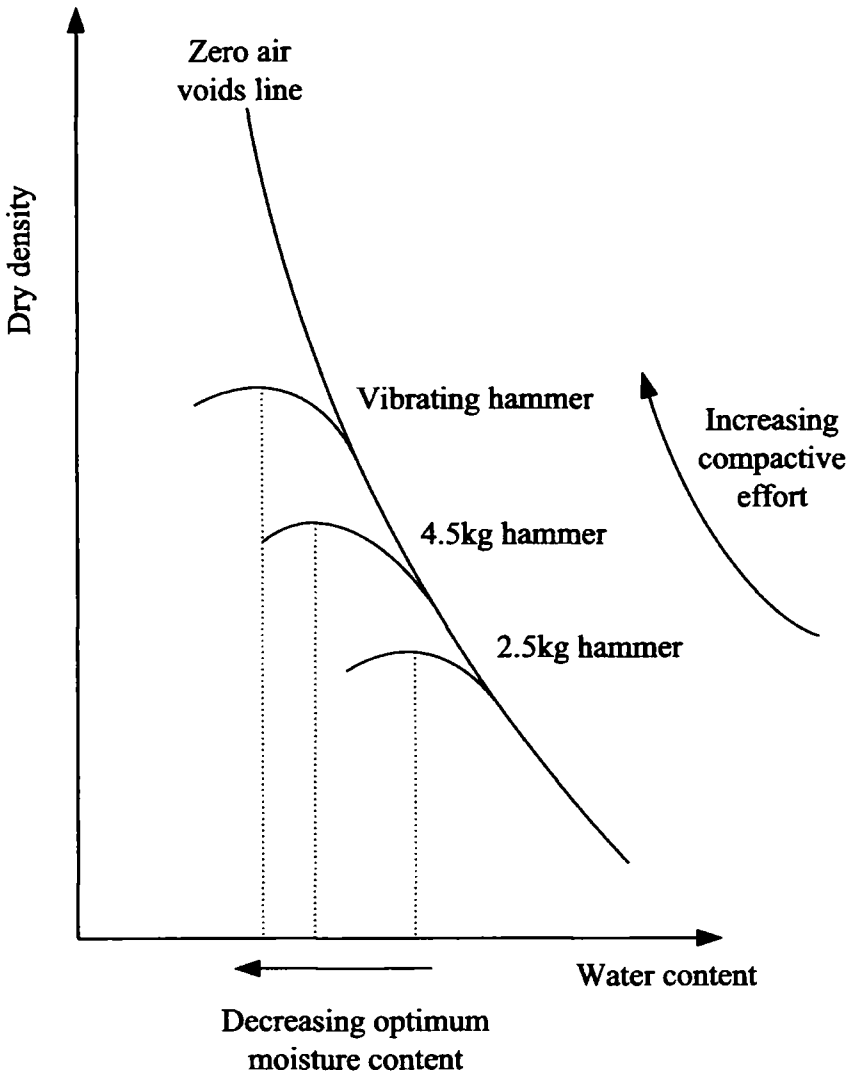

Figure 2.1 Optimum water content graph

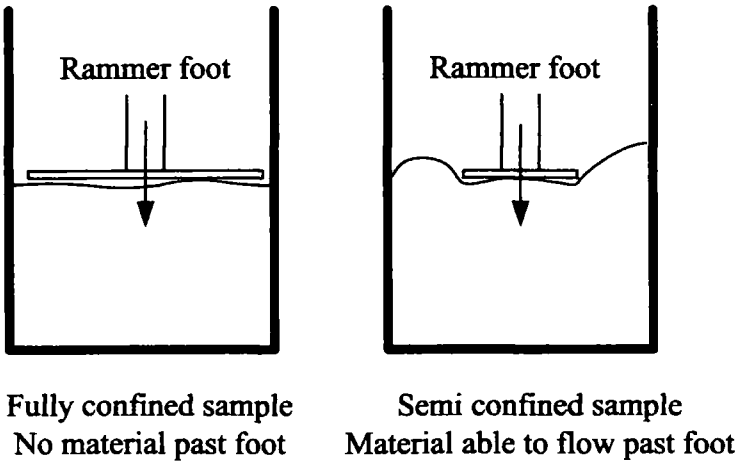

Figure 2.2 Confined and semi confined samples

2.3 Elasto-plastic constitutive models

A material is considered *elastic* if it deforms (extends or contracts) because of an applied stress (force per unit area), but returns to its original size and shape when the stress is removed. *Strain* (change in length / length) is a measure of the deformation. If the stress exceeds a certain value, then *plastic* material behaviour will occur, and the deformation is irreversible. The transition between elastic and plastic behaviour is called *yield.* A *ductile* material allows large plastic deformations without fracture, whereas a *brittle* material cannot sustain such deformations and fracture occurs at yield. In the region before yield the rate of change of stress with strain is known as the *elastic modulus.* A *linear* material, obeys *Hooke's law* , with stress being directly proportional to strain until yield. At the yield stress (or *elastic limit*) a material ceases to obey Hookes law and begins to behave plastically. The maximum stress a material can sustain is known as the *peak* stress, and the stress prior to failure is known as the *ultimate* stress.

In two dimensions, if two opposite faces of a linearly elastic square are considered, compressive stresses normal to these faces will result in an elongation of the square in the direction of the stresses, and a contraction in the directions perpendicular to the stresses. These stresses and the resulting strains on the cube are called the *normal stress* (σ) and *normal strain* (ε). The constant of proportionality between orthogonal strains is called *Poisson's ratio* (ν). The normal stress is directly proportional to the normal strain, and the constant of proportionality is known as *Young's Modulus* (E). If a stress is applied to the top and bottom edges of the square parallel to the edges, then the square will deform to become a parallelogram. The stress is called *shear stress* (τ) and the deviation of the parallelogram from square is given by the shear strain (γ). The shear stress is proportional to the shear strain and the constant of proportionality is known as the *shear modulus* (G).

For a given two dimensional system, it is always possible to find two orthogonal planes, where the shear stress is zero, which correspond to planes of maximum and minimum normal stress. These planes are the *principal planes*, on which the *principal stresses* act.

The maximum principal stress is denoted σ_1 and the minimum principal stress σ_2. The principal stresses and principal planes may be found through construction of a *Mohr's circle.*

In a three dimensional problem, an element may be subject to triaixal normal stresses σ_x, σ_y and σ_z and corresponding normal strains ε_x, ε_y, ε_z, as well as shear stresses τ_{xy}, τ_{xz} and τ_{yz} and shear strains γ_{xy}, γ_{xz} and γ_{yz}. Here there are three orthogonal principal stresses, the smallest being denoted σ_3. A stress state in which all three principal stresses are equal, is described as *volumetric.* In this stress state an isotropic body will only change in volume. This situation is also known as *hydrostatic*, because the same pressure exists all around a body, such as one under water. Volumetric stress p is the average of the three principal stresses

$$p = \frac{\sigma_1 + \sigma_2 + \sigma_3}{3} \tag{2.11}$$

If the principal stresses acting on a body are not equal, then the body will change shape, and the difference between the principal stresses (the deviation from a volumetric stress state) is known as the *deviatoric* stress q

$$q = \sqrt{\frac{(\sigma_1 - \sigma_2)^2 + (\sigma_2 - \sigma_3)^2 + (\sigma_1 - \sigma_3)^2}{2}} \tag{2.12}$$

In a triaxial stress state, such as that used to model the uniaxial compression $\sigma_2 = \sigma_3$ so Equations (2.11) and (2.12) become

$$p = \frac{(\sigma_1 + 2\sigma_3)}{3} \tag{2.13}$$

$$q = (\sigma_1 - \sigma_3) \tag{2.14}$$

A constitutive model is made up of a series of constitutive relations. These are relations between two physical quantities which do not follow directly from a physical law. Hooke's law, which relates normal stress and normal strain is an example of a constitutive relationship. Constitutive relations may be combined with other equations which are based on physical laws to solve real problems. Many constitutive models for a wide range of situations were discovered in the 19th century and are now widely used

(for example Ohm's law and Darcy's law). As explained in Section 2.1 it is hoped that treating rammed earth as a soil will lead to a better understanding of its behaviour. A first step in this process is the use of constitutive models for soil to model rammed earth. This section describes a number of constitutive models, some of which will be used to model rammed earth walls.

2.3.1 Defining constitutive models

There are four simple elastoplastic constitutive models, which can be used to model some aspects of simple soil behaviour and form the basis of classical soil mechanics theory. Elastoplastic and some constitutive models are outlined below. Further detailed expositions are available in many texts (e.g. Potts and Zdravkovic 2001; Craig 2002). There are four essential components to an elastoplastic constitutive model: an elasticity relation, a yield function, a plastic potential function and a hardening/softening rule. With these specified the full elastoplastic behaviour of material may be modelled. Each component is described below.

One of the major assumptions in conventional elastoplasticity is coincidence of axes. To explain this, during elastic behaviour the principal directions of *incremental* stress and *incremental* strain coincide whereas during plastic behaviour the strain increments are a function of the current stress state and therefore the principal directions of *accumulated* stress and *incremental* plastic strain coincide. A yield function separates purely elastic behaviour from elasto-plastic behaviour, and cannot be exceeded. The function is a scalar multiplier of stress (usually expressed in invariants) and state parameters (parameters which describe the current stress state) $\{k\}$.

$$F(\{\sigma\},\{k\}) = 0 \tag{2.15}$$

The function is plotted as a surface in stress space, its size changing as a function of the state parameters, which can be related to hardening and softening. For perfect plasticity $\{k\}$ is constant and represents the magnitude of the stresses at yield. For hardening and softening behaviour $\{k\}$ varies with plastic strain to represent how the magnitude of the stress state at yield changes. The type of material behaviour is determined by the yield function, elastic behaviour occurs for $F < 0$ and elastoplastic behaviour occurs for $F = 0$. $F > 0$ represents an impossible situation (Potts and Zdravkovic 2001).

The plastic potential defines the direction of plastic straining. A *flow rule* specifies the direction of plastic strains for every stress state. This takes the form

$$d\varepsilon_i^p = \Lambda \frac{\partial P(\{\sigma\},\{m\})}{\partial \sigma_i} \tag{2.16}$$

where $d\varepsilon_i^p$ represents the six components of incremental plastic strain $(d\varepsilon_x, d\varepsilon_y, d\varepsilon_z, d\gamma_{xy}, d\gamma_{xz}, d\gamma_{yz})$, Λ is a scalar multiplier dependent on hardening/softening rules and P is the *plastic potential function* of the form

$$P(\{\sigma\},\{m\}) = 0 \tag{2.17}$$

The plastic potential function is thus a function of the total stress components. The relative magnitudes of the incremental strain components are represented by a vector normal to these stress components (i.e. $\sigma_x, \sigma_y, \sigma_z, \tau_{xy}, \tau_{xz}, \tau_{yz}$) in six dimensional stress space at the current stress state. A simplification is introduced if it is assumed that the plastic potential function is the same is the yield function. In this case the flow rule is said to be *associated* and the incremental plastic strain vectors are normal to the yield surface.

2.3.1.1 Hardening and softening rules

Hardening and softening rules prescribe how the state parameters vary with plastic straining. A hardening/softening rule which relates changes in size of the yield surface to accumulated plastic strain is known as a *strain* hardening/softening rule, and one which relates the change in size to increase in plastic work is known as a *work* hardening/softening rule.

2.3.2 Tresca and von Mises

The simplest yield criteria are attributed to Tresca and von Mises. The Tresca model assumes that yielding of a sample occurs at a maximum shear stress, and the magnitude of this shear stress can be determined by the plotting of Mohr's circles. Sample strength is derived purely from cohesion between particles. Triaxial tests on undrained (where a build up of pore pressure is allowed, see Section 3.8.1) saturated clay are found to plot as shown in Figure 2.3. This shows that if two similar samples are tested at two different confining pressures, the shear strength of the samples will be the same, and thus the Mohr's circles will have the same radius. However, given that the samples were

tested at different confining (horizontal) pressures, the Mohr's circles plot at different points on the stress axis. A failure criterion is adopted which relates the undrained strength s_u to the diameter of the Mohr's circles at failure.

$$\sigma_1 - \sigma_3 = 2S_u \tag{2.18}$$

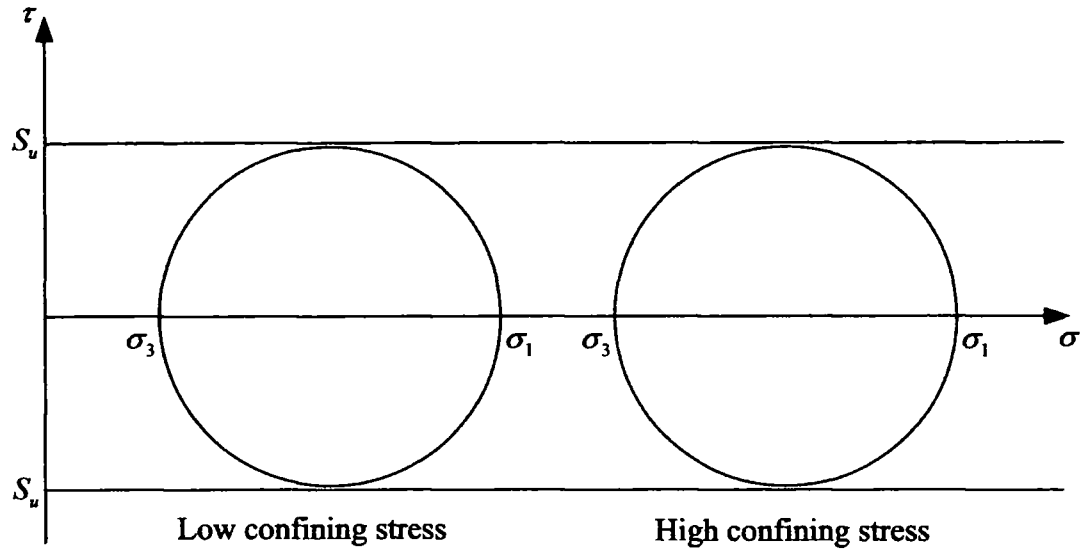

Figure 2.3 Tresca failure criterion

The Tresca failure criterion plots as a regular hexagonal cylinder centred on the space diagonal in principal stress space, with the corners of the hexagon representing the various combinations of the major and minor principal stresses ($\sigma_a \geq \sigma_b \geq \sigma_c, \sigma_b \geq \sigma_a \geq \sigma_c$, ... etc). These corners imply singularities in the yield function, which cause problems during numerical implementation. In order to overcome this a yield function approximating the hexagon, with a circle on the deviatoric plane was proposed, to produce the von Mises failure criterion (Figure 2.4) (Potts and Zdravkovic 2001).

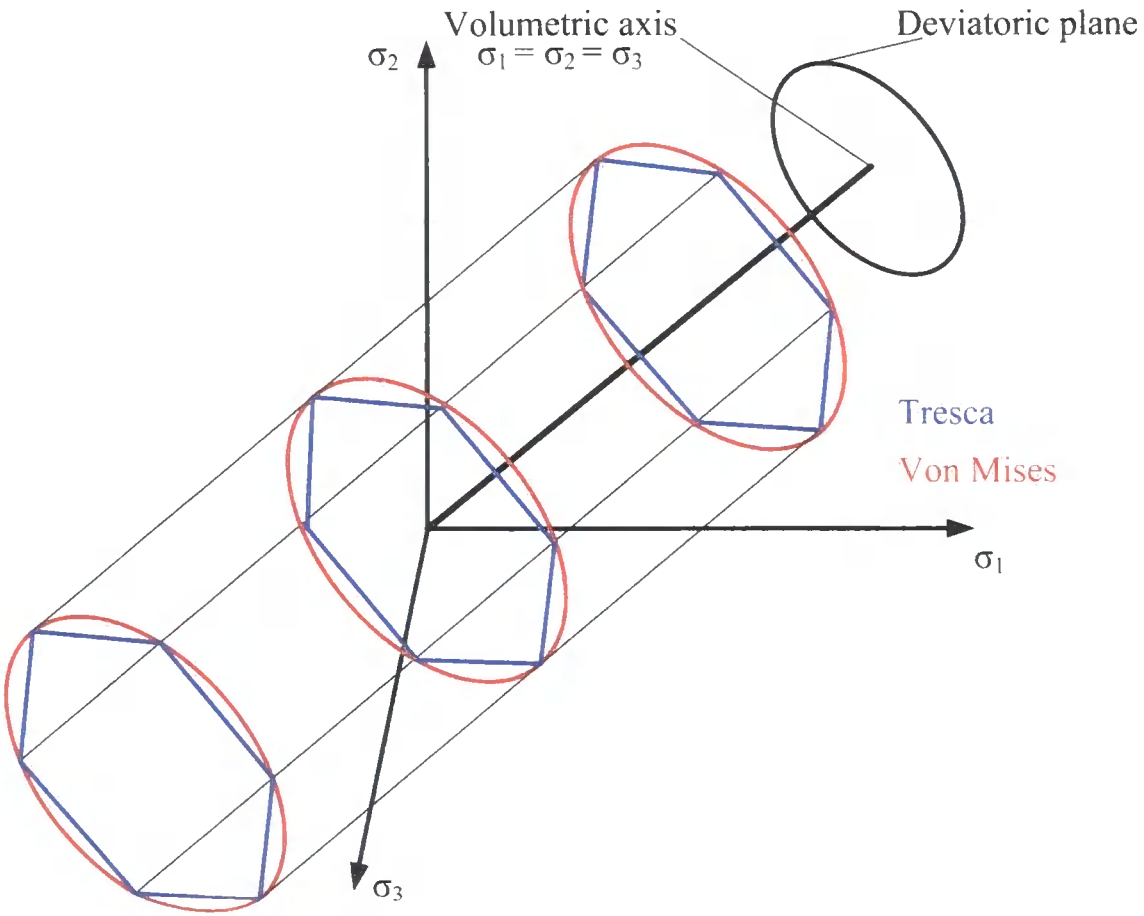

Figure 2.4 Tresca and von Mises yield criteria

2.3.3 Mohr-Coulomb and Drucker-Prager

If an interlocking frictional material (such as a sand) is considered, then samples tested at different confining pressures are found to have increased shear strength depending on the confining pressure. Mohr's circle plots of tests of these materials are as shown in Figure 2.5. If several tests are carried out at different confining pressures, then a best fit straight line may be drawn linking the shear strengths of the samples tested at different confining pressures. This line is known as the Mohr-Coulomb yield line and has two parameters: the angle of the line with respect to the normal stress axis is known as the angle of friction ϕ', and the shear strength at no normal load is known as the apparent cohesion, denoted c. If the angle of friction is zero, then the Mohr-Coulomb model becomes the von Mises model. The equation of the failure line can be expressed in terms of the normal and shear stresses as

$$\tau_f = \sigma'_n \tan\phi' + c' \tag{2.19}$$

or in terms of principal stresses

$$\sigma_1 - \sigma_3 = (\sigma_1 + \sigma_3)\sin\phi' + 2c\cos\phi' \quad (2.20)$$

The Mohr-Coulomb criteria plots as an irregular hexagonal cone in principal stress space (the Tresca criterion plots as a regular hexagon), and in order to remove the singularities presented by the corners, the Drucker-Prager criterion was developed, in which the hexagon on the deviatoric plane is replaced by an equivalent circle.

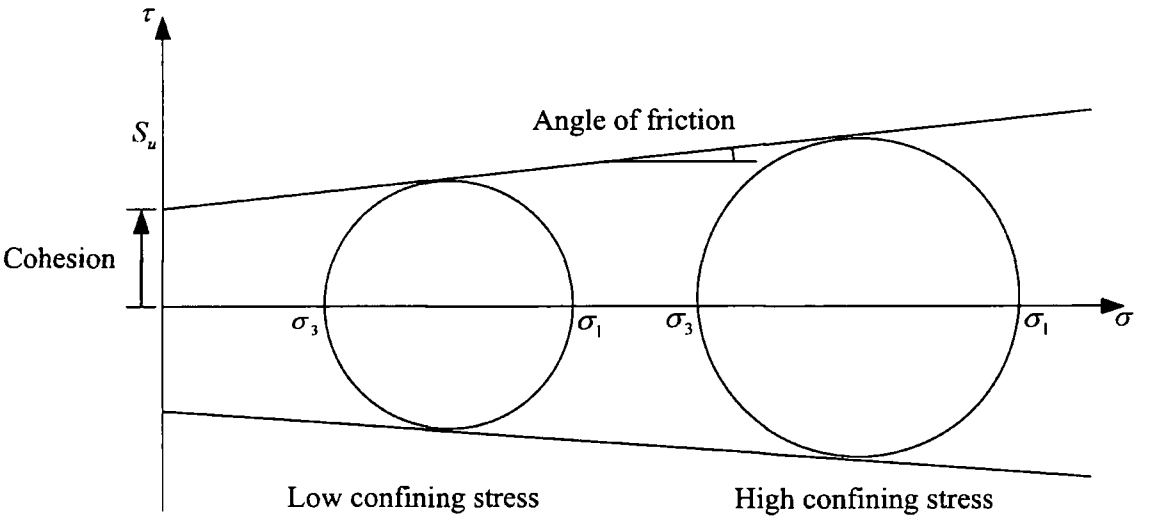

Figure 2.5 Mohr-Coulomb failure criterion

2.3.3.1 Planes of weakness

Jaeger and Cook (1979) outline the *plane of weakness* theory where the strength of a sample of intact rock with a single discontinuity can be established. The stress applied to the sample is resolved into normal and shear components on the plane of weakness and the Mohr-Coulomb failure criterion applied. Figure 2.6 shows three Mohr's circles, representing the lowest, intermediate and highest strength of the system. Circle A represents the case when failure occurs within the discontinuity, and Circle B is a case when failure can occur along the discontinuity for a range of angles. Circle C represents the case where failure occurs in the intact rock if it has not already done so along the discontinuity.

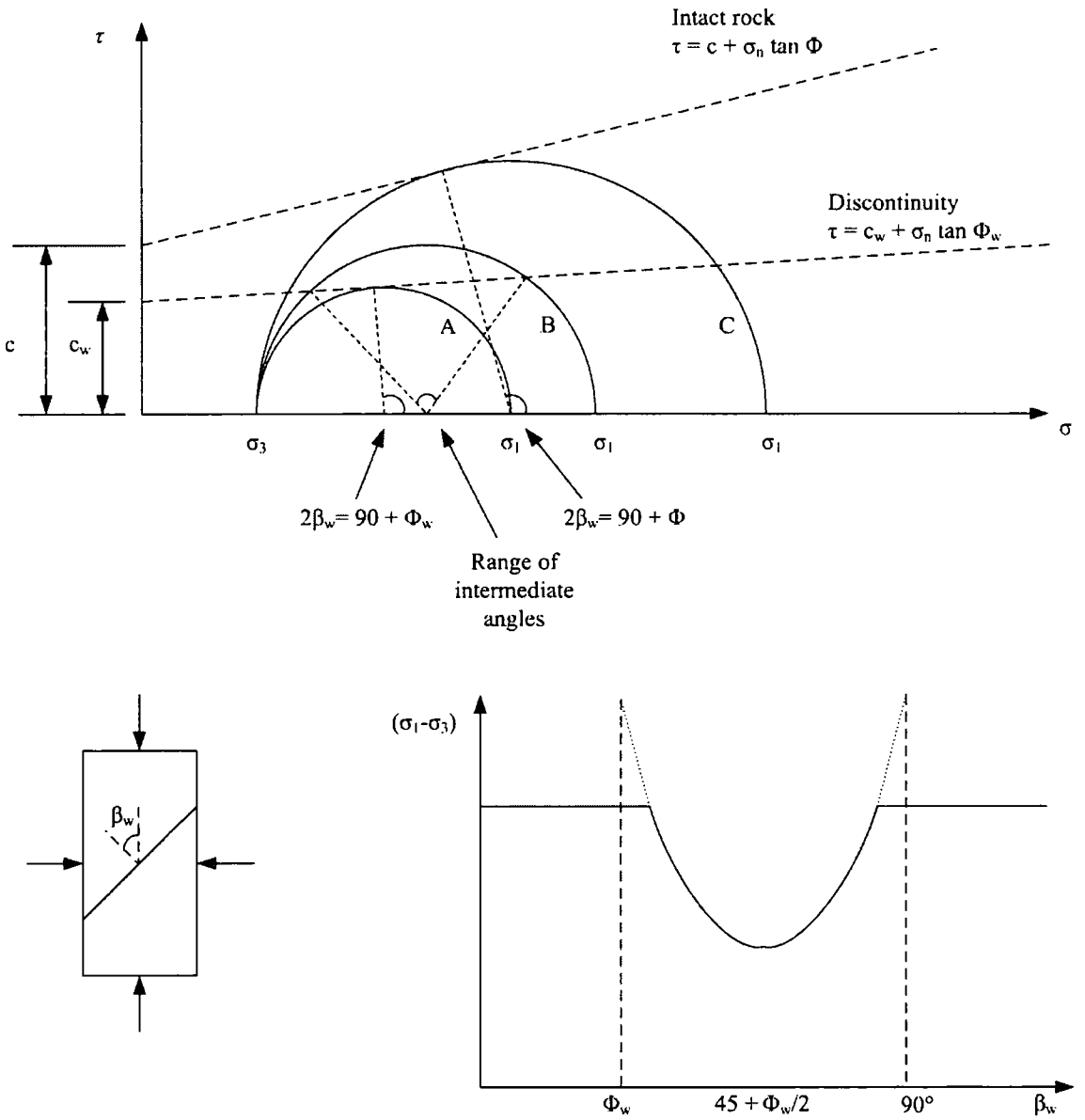

Figure 2.6 Single plane of weakness theory, after Hudson and Harrison (1997)

2.3.4 Hardening/softening plasticity models

The assumption of linear elasticity and perfect plasticity upon reaching a yield criterion does not hold for the vast majority of materials. Instead most materials exhibit a softening or hardening behaviour, and often a combination of the two.

An elastic-perfectly plastic material will, upon reaching the yield surface, continue to strain indefinitely with the stresses never exceeding the yield surface. A hardening material, upon reaching the yield surface requires an increased applied stress to produce further strain. This is seen as an increase in the size of the yield surface. A softening material requires a smaller applied stress to produce further strain. Thus hardening

materials increase in strength with plastic deformation and softening materials reduce in strength with plastic deformation, which is seen as a reduction in size of the yield surface (Figure 2.7).

Both hardening and softening behaviour can be observed in soils. Soil behaviour in an oedometer test is very similar to that of a hardening material, the virgin consolidation line resembling a primary loading curve, and elastic unloading and reloading following swelling lines. Shear box testing leads to soil response similar to that of uniaxial testing of a softening material (Potts and Zdravkovic 2001).

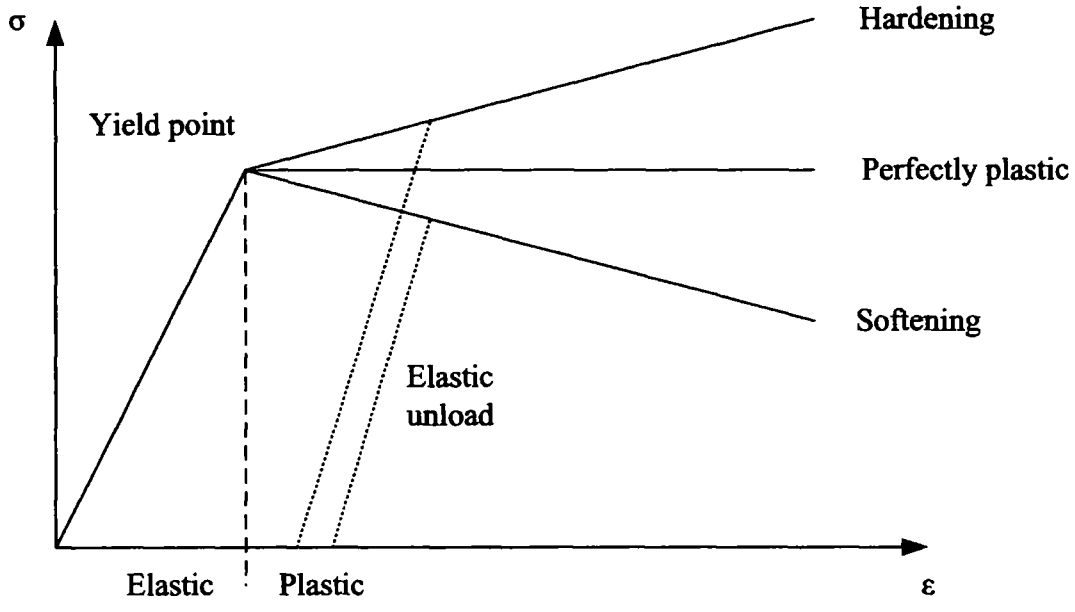

Figure 2.7 Hardening, perfectly plastic and softening material behaviour

2.3.5 Schanz, Vermeer et al. (1999) Hardening Soil (HS) model

Various attempts have been made over the years to develop models for soils that incorporate nonlinear elasticity. Konder and Zelasko (1963) observed a hyperbolic relationship between the deviatoric stress and the maximum principal strain during the triaxial testing of a wide range of soils. When subject to primary deviatoric loading the soil in their tests showed decreasing stiffness and the development irreversible plastic strains. The relationship was used as the basis for the *hyperbolic model* (Duncan and Chang 1970) expressed in Equation (2.21).

$$(\sigma_1 - \sigma_3) = \frac{\varepsilon}{a + b\varepsilon} \tag{2.21}$$

where a and b are material constants.

Equation (2.21) can be rewritten as

$$\frac{\varepsilon}{(\sigma_1-\sigma_3)} = a + b\varepsilon \tag{2.22}$$

which allows the plotting of laboratory stress-strain data on axes as shown in Figure 2.8B to easily determine the parameters a and b.

Differentiation of Equation (2.21) leads to the variation of the tangent Young's modulus E_i with the stress level $(\sigma_1-\sigma_3)$.

$$E_i = \frac{\partial(\sigma_1-\sigma_3)}{\partial\varepsilon} = \frac{a}{(a+b\varepsilon)^2} \tag{2.23}$$

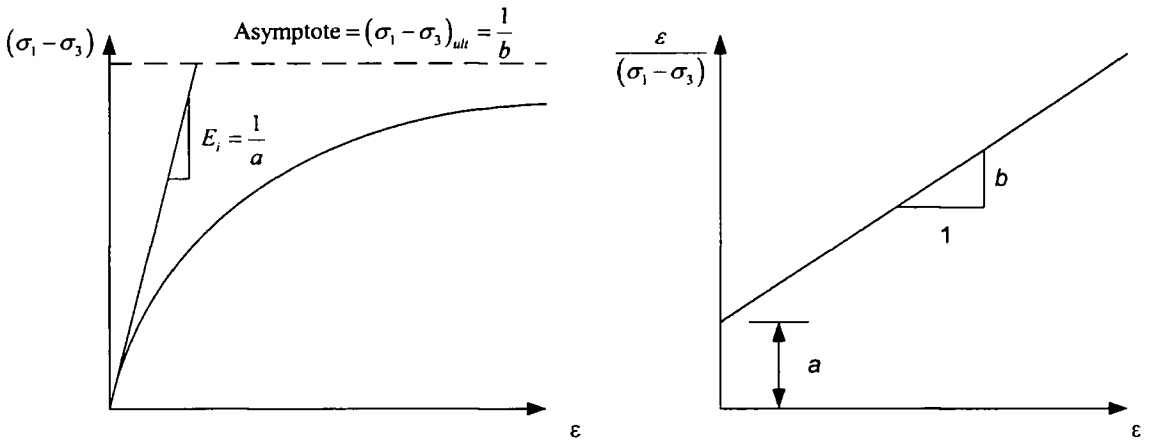

Figure 2.8 Hyperbolic elastic model. After Duncan and Chang (1970). A - Deviator stress-strain axes, B - transformed axes.

While widely used in the past, the Duncan and Chang (1970) model is now regarded as somewhat unsophisticated because it does not distinguish between loading and unloading, may not be thermodynamically consistent and cannot be used to calculate collapse loads when in the fully plastic range (Schanz, Vermeer et al. 1999). However, the nonlinear elastic relationship between principal strain and primary deviatoric stress implemented in this model is used as the basis of the more advanced Hardening Soil (HS) model of Schanz, Vermeer et al. (2000) who added volumetric and shear plastic potential functions. The model is available in the Plaxis geotechnical engineering finite element package (Brinkgreve and Vermeer 1998), which is widely used in the geotechnical engineering industry.

Section 2.4 describes rammed earth walls which were built and tested in the laboratory. The HS model implemented in the Plaxis package was one of the analysis methods used to investigate these walls (which is described in Section 2.5.3), and thus the formulation is now described in detail.

The HS model is a nonlinear elasto–plastic model and assumes a linear relationship between increments of stress and strain, with nonlinear elastic behaviour achieved by varying the Young's modulus at each increment. Total strains are calculated using a stress dependent stiffness, and the plastic strains calculated using a two surface yield criterion: one for shear behaviour and one for volumetric behaviour.

Hardening behaviour is controlled by stress dependent stiffness. Two types of hardening are defined – shear hardening is used to model shear irreversible strain, defined by the parameter E_{50} (used in preference to E_i as explained below) and volumetric compression hardening , defined by the parameter E_{oed} (after *oedometer* stiffness).

2.3.5.1 Shear hardening behaviour in primary loading

The hyperbolic relationship between deviatoric stress and normal strain observed by Konder and Zelasko (1963) and given in Equation (2.22) may be expressed as

$$\varepsilon_1 = \frac{a}{\frac{1}{q} - b} . \tag{2.24}$$

Defining

$$a = \frac{1}{E_i} \quad b = \frac{1}{q_{ult}} \tag{2.25}$$

allows Equation (2.24) to be expressed as

$$\varepsilon_1 = \frac{1}{E_i} \frac{q}{1 - \frac{q}{q_{ult}}} \tag{2.26}$$

where q_{ult} is the asymptotic value of shear strength and E_i is the initial stiffness.

As the behaviour of the soil is modelled as hyperbolic, failure cannot be considered by the reaching of the asymptotic q_a value (see Figure 2.9), and so failure is assumed upon

reaching a lower value defined as q_{ult} where the ratio between q_a and q_{ult} is known as the failure ratio $\left(R_f\right)$ and is taken as 0.9. The ultimate (ie peak) deviatoric stress q_{ult} is derived from the Mohr-Coulomb failure criterion and is defined as

$$q_{ult} = (c\cot\phi' - \sigma_3)\frac{2\sin\phi'}{1-\sin\phi'} \tag{2.27}$$

When $q = q_{ult}$ the Mohr-Coulomb failure criterion is satisfied and perfectly plastic yielding occurs.

The initial stiffness is not used in the HS model, as it is found to be difficult to obtain through experiment, therefore the parameter E_{50} is introduced, which is usually determined from a triaxial stress-strain curve for a mobilisation of 50% of the maximum shear strength. The relationship between E_i and E_{50} is given by Equation (2.28)

$$E_i = \frac{2E_{50}}{2-R_f} \tag{2.28}$$

The actual modulus used is a multiplier of a reference stress $\left(E_{ref}^{50}\right)$ and depends on the confining stress σ_3 and a level of dependency, given by a power (m).

$$E_{50} = E_{50}^{ref}\left(\frac{c\cos\phi' - \sigma_3\sin\phi'}{c\cos\phi' - \sigma^{ref}\sin\phi'}\right)^m \tag{2.29}$$

To simulate logarithmic behaviour (as observed for soft clays) m should be set to 1.0, however for sands, values of 0.5 should be used (Schanz, Vermeer et al. 1999).

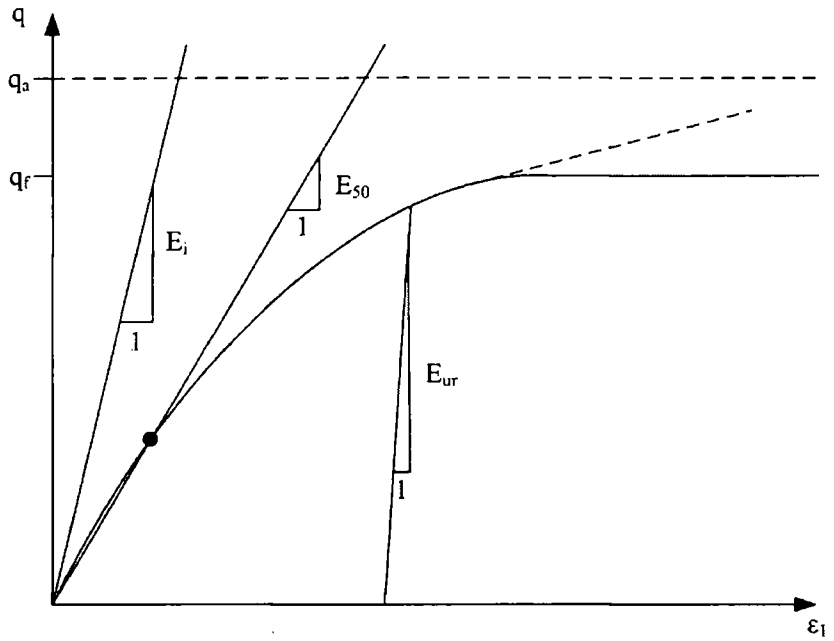

Figure 2.9 Hyperbolic assumptions. After Schanz, Vermeer *et al.* (1999). Compare to Figure 2.8

2.3.5.2 Volumetric hardening/softening behaviour on primary loading

Volumetric hardening is modelled using the oedometer stiffness E_{oed}, which is taken as a tangent stiffness on primary loading, and is defined as

$$E_{oed} = E_{oed}^{ref}\left(\frac{\sigma_1 + c\cot\phi}{\sigma^{ref} + c\cot\phi}\right)^m \tag{2.30}$$

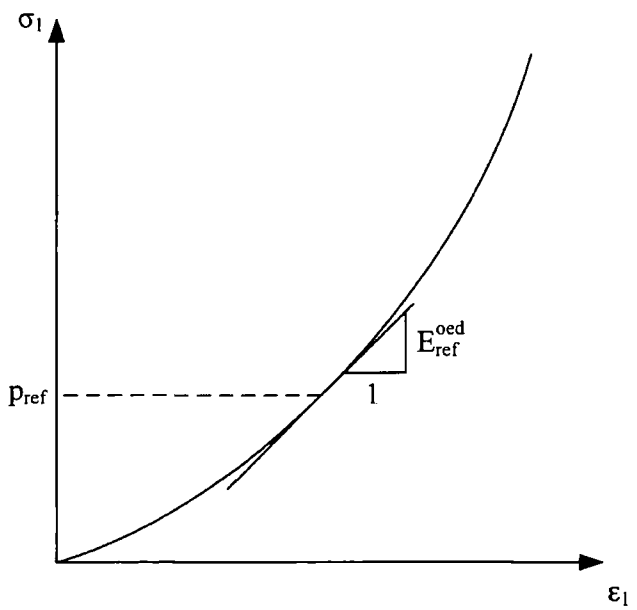

Figure 2.10 Volumetric stress-strain relationships used in the Hardening Soil model. After Schanz, Vermeer et al. (2000)

2.3.5.3 Elastic unload/reload stiffness

The unload/reload stiffness is assumed to be nonlinear elastic, but dependent on the minor principal stress, based on a reference Young's modulus for unloading and reloading, and is given by

$$E_{ur} = E_{ur}^{ref}\left(\frac{\sigma_3 + c\cot\phi}{\sigma_{ref} + c\cot\phi}\right)^m \tag{2.31}$$

which may be seen in Figure 2.9.

2.3.6 Yield surfaces

Two main yield surfaces are defined, a shear yield surface, which expands due to shear plastic straining, and is limited by the Mohr-Coulomb failure criterion, and a volumetric yield cap, which expands on volumetric hardening.

2.3.6.1 Shear yield function

A shear strain yield function is defined as

$$f = \bar{f} - \gamma^p \tag{2.32}$$

$\bar{f}$ matches the hyperbolic law defined by Konder and Zelasko (1963) and given in Equations (2.21) with an additional component of elastic behaviour.

$$\bar{f} = \frac{2}{E_i}\frac{q}{1-\frac{q}{q_a}} - \frac{2q}{E_{ur}} \tag{2.33}$$

The plastic shear strain γ^p is taken as the strain hardening parameter. It is assumed that plastic volumetric strains are small in comparison to shear strains, and thus

$$\gamma^p = -\left(2\varepsilon_1^p - \varepsilon_v^p\right) \approx -2\varepsilon_1^p \tag{2.34}$$

For the yield condition $f = 0$, it can be seen that Equation (2.32) gives

$$-\varepsilon_1^p \approx \frac{1}{2}\bar{f} = \frac{1}{E_i}\frac{q}{1-\frac{q}{q_a}} - \frac{q}{E_{ur}} \tag{2.35}$$

which is the same as Equation (2.26) with an additional component of elastic strain. The elastic strains are present in both primary loading and unload/reload cycles, and are calculated using

$$-\varepsilon_1^e = \frac{q}{E_{ur}} \qquad \varepsilon_2^e = \varepsilon_3^e = -\varepsilon_1^e \upsilon_{ur} \tag{2.36}$$

The yield condition $(f=0)$ can be visualised as a yield locus in the (p,q) plane. Figure 2.11 shows successive yield loci for $m=0.5$

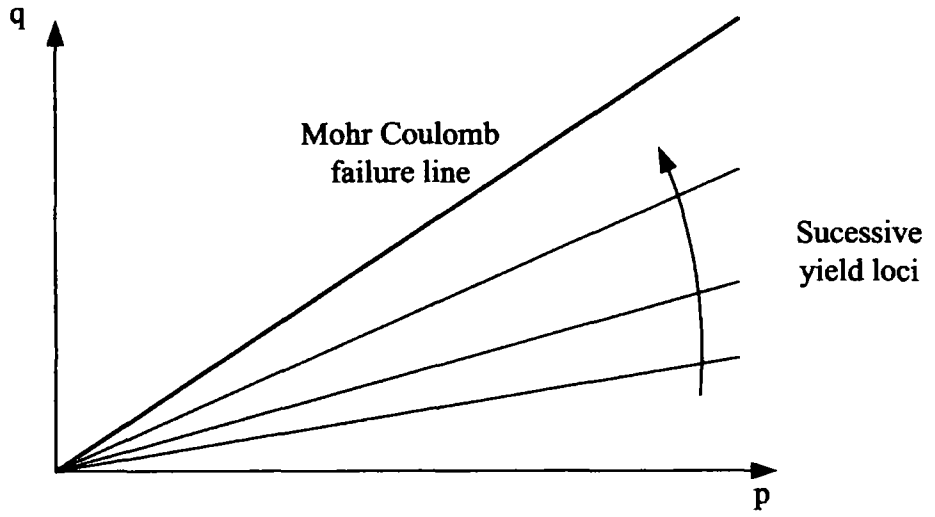

Figure 2.11 Successive yield loci. After Brinkgreve and Vermeer (2007)

Shear hardening yield surfaces (Figure 2.11) do not account for plastic volume strain in volumetric compression. A cap yield surface is thus introduced to close the elastic region for compressive (compaction hardening) stress paths (Figure 2.12). The size of the yield cap is determined by the effective preconsolidation stress (p_c)

The yield cap surface is defined as

$$f_c = \frac{\tilde{q}^2}{M^2} + (p+a)^2 - (p_c+a)^2 \tag{2.37}$$

where M is a model parameter and $\tilde{q}$ is a special measure of deviatoric stress and

$$a = c\cot\phi \tag{2.38}$$

The yield function thus plots as an ellipse in $(p,q)$of length p_c+a and height $M(p_c+a)$. A relationship of the form

$$E_{oed} = f(M)E_{oed}^{ref} \tag{2.39}$$

is used by Plaxis to determine the magnitude of the yield surface, however this nor the exact nature of $\tilde{q}$ is not explained in either Schanz, Vermeer et al. (1999) or Brinkgreve and Vermeer (2007).

The plastic volumetric strain rate at the cap is determined using a linear relationship between the rates of deviatoric and volumetric plastic flow, the coefficient being the mobilised dilatancy angle (ψ_m).

$$\dot{\varepsilon}_v^p = \sin\psi_m \dot{\gamma}^p \tag{2.40}$$

The mobilised dilatancy angle used is adapted from the stress dilatancy theory of Rowe (1962). The essential property of the stress dilatancy theory is that a granular material contracts for small stress ratios and dilates for high stress ratios.

Plaxis calculates the mobilised dilatancy angle and mobilised friction angles as functions of the principal stresses, apparent cohesion and ultimate friction and dilation angles which are specified by the user.

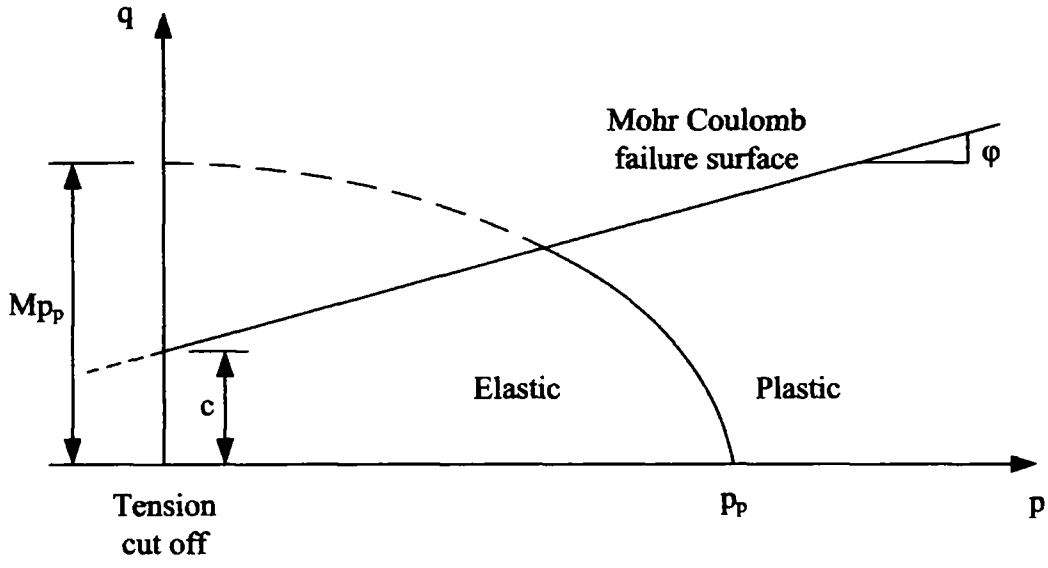

Figure 2.12 Yield surfaces in p-q space

Level of stress dependency	m
Primary deviatoric secant stiffness (usually derived from triaxial testing at 50% of ultimate shear strength)	E_{50}^{ref}
Primary volumetric tangent stiffness (usually derived from oedometer testing)	E_{oed}^{ref}
Elastic unload/reload stiffness	E_{ur}^{ref}, ν_{ur}
Ultimate failure parameters	c, ϕ, ψ

Table 2.2 Hardening Soil parameters. After Schanz, Vermeer et al. (1999)

The Mohr-Coulomb and Hardening Soil models were used to model a number of rammed earth walls whose construction and testing are now outlined.

2.4 Wall construction and testing

In order to better understand rammed earth as a construction material, a number of walls were constructed in the laboratory. This section describes the construction, drying and loading of five walls. Two mixes of soil were used, one blended from material available in the laboratory, and one taken from a local rammed earth construction. Section 2.4.1 describes the classification of these soils and the determination of the moisture content for compaction. Custom formwork was made to facilitate the construction of different height walls, and a method was developed to create voids beneath the walls. The construction, drying and testing of the walls is outlined in Section 2.4.4. Five different walls were constructed with each wall being a refinement based on the previous experience. The mixing and compaction improved over time and incremental changes were made in procedures as testing progressed. Because the aim the wall construction was to gain a better understanding of the material, the tests are discrete and non repeatable, because changes were made to the configuration of the walls and the mixing and compaction procedure over time. The simple monitoring in place during the testing means that it is difficult to obtain conclusive evidence from these walls, but they served to inform us of the construction material and allowed for simple numerical modelling to be carried out (detailed in Section 2.5), based on the soil models described in Section 2.3.

2.4.1 Soil

Two soils were used for the construction of the walls. The first soil was blended using materials available in the laboratory and the second used was sourced from a local rammed earth construction project (Rivergreen Developments, Aykley Heads, Durham). One walls was constructed using the blended soil, and the rest used the Aykley Heads soil.

The Aykley Heads soil consisted of purchased aggregate, alluvial sand dug from the site, and purchased powdered clay/silt. Testing performed at Bath University, and detailed in Walker (2007), recommended mixing the materials by the following mass fractions - 25% aggregate, 60% alluvial sand, 15% powered clay/silt. On site the materials were mixed in a horizontal axis mixer then left to dry in windrows at the site,

covered in plastic sheeting to reduce water loss. Two tonnes of material were sourced from the site for use in the laboratory.

Wet sieving of both samples and a sedimentation analysis of the Aykley Heads sample were carried out in accordance with BS1377-2:1990, and the resulting particle size distributions are shown in Figure 2.13. The relative percentages of sand, silt and clay, and percentage of particle diameter smaller (D_{60} etc), of the Aykley Heads sample is shown in Table 2.3. Plotting of the Liquid and Plastic Limits puts the soil above the horizontal part of the A line on a plasticity chart, making it a silt of low plasticity (ML). A particle density analysis of the Aykley Heads samples was carried out in accordance with BS1377-2:1990 Two sample sets were tested, one set of the whole sample and one set of material passing a 425μm sieve. The average particle density of the whole sample was found to be 2560kg/m^3, and that passing 425μm, 2649kg/m^3.

Table 2.3 summarises the classification of the Aykley Heads mix, which was used for the majority of the walls constructed, and compares with the values suggested by Walker, Keable et al. (2005). This suggests that the soil contains a little too much clay, and is excessively silty, containing too little sand. However the liquid limit and plasticity index are acceptable. The particle size distribution recommend by the Fuller formula (Equation (2.10)) for a largest grain diameter of 14mm, and a grading coefficient n of 0.25 is shown in Figure 2.13 for comparison. This shows that the Aykley Heads sample contains too much sand, too little silt, and roughly the correct amount of clay. As outlined in Chapter 1, an optimum particle size distribution for rammed earth is difficult to define and harder to justify. The Aykley Heads sample was used for the majority of the testing as it was felt sufficient to represent a correctly engineered rammed earth mix.

A vibrating hammer and a standard Proctor test were carried out in accordance with BS1377-2 1990. These tests determined the optimum water content required to achieve maximum density for the given compactive effort and are shown in Figure 2.14. This appears to be 8% when using a vibrating hammer and 10.5% for a standard Proctor test. The water content of a *drop test* sample was found to be 12%, and this water content was used for construction of the walls as recommended by Walker, Keable et al. (2005).

The zero, 5% and 10% air voids lines are also shown for the two different values of G_s obtained. The vibrating hammer test touches the zero air voids line for a G_s of 2.65 (particle density of the material passing 425μm) indicating that the maximum density has been achieved for the given water content. Figure 2.14 also highlights the current confusion within the rammed earth community. While the *drop test* would recommend a water content for optimum compaction of 12%, the soil is to be compacted using a vibrating hammer, and thus a water content of 8% should be used. The standard Proctor test, as recommended by Walker, Keable et al. (2005) recommends compacting at an intermediate water content of 11.5%. Despite the lower water content suggested by the vibrating hammer tests it was decided to compact soil for the walls at a water content of 12%, as this was considered to be representative based on experience of rammed earth in the field.

Constituent (%)	**Aykley Heads material (measured)**	**Recommendations (Walker, Keable et al. 2005)**
Sand	21.5	45-80
Silt	52.3	10-30
Clay	26.2	5-20
Percentage smaller (%)	**μm**	
D10	2.1	N/A
D30	85.9	N/A
D60	345.0	N/A
Liquid Limit	22.7	< 45
Plastic Limit	16.0	N/A
Plasticity Index	6.7	2-30

Table 2.3 Classification of Aykley Heads material

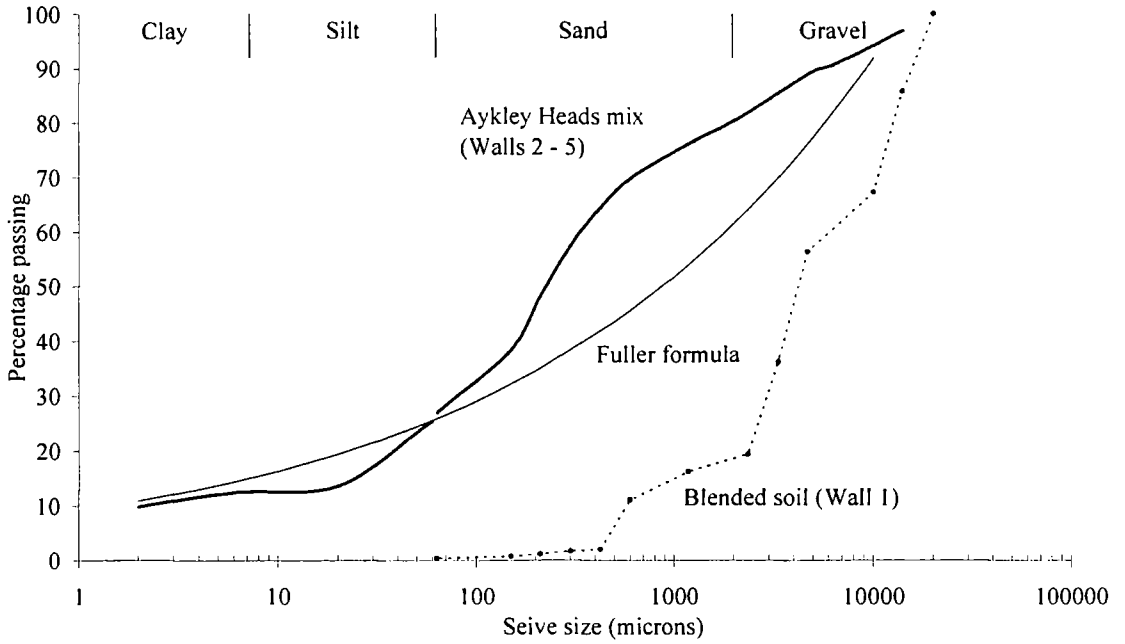

Figure 2.13 Particle size distribution of soils used

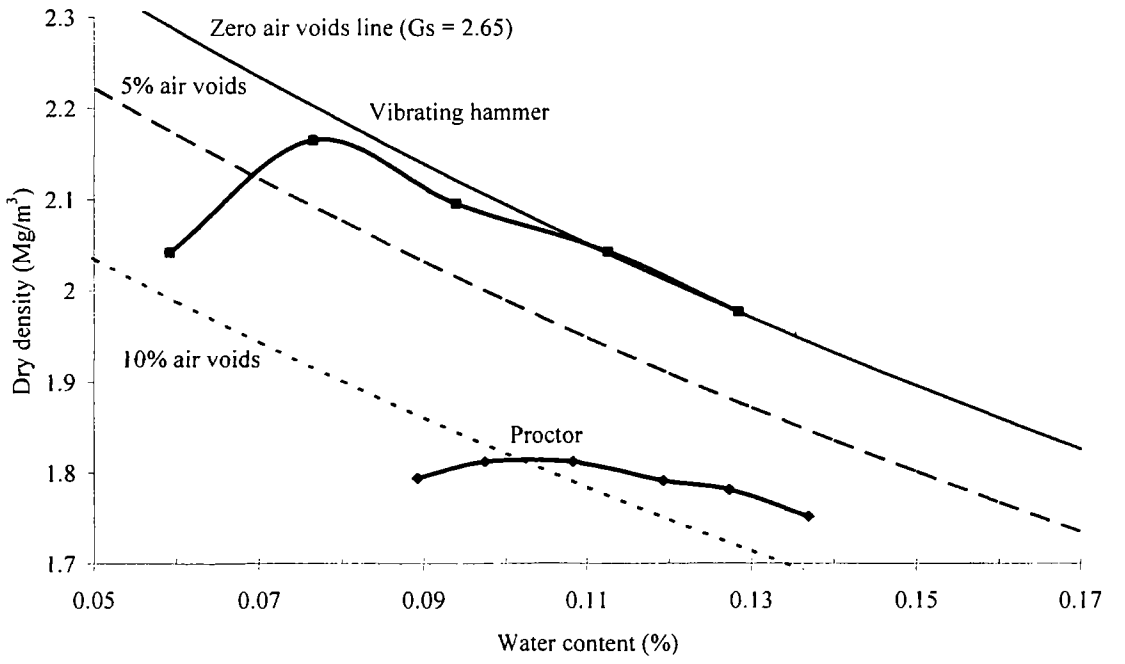

Figure 2.14 Optimum water content curve for vibrating hammer and Proctor test

2.4.2 Mixing procedure

The material was mixed in a vertical axis cement mixer, with a capacity of around 300kg mass of soil. A horizontal axis mixer was tried, but it was found that this caused the soil to form into spheres, due to the constant rolling action they were experiencing, so larger angular particles became coated in clay and silt sized particles, the whole

mixture becoming an assembly of different sized balls, largely increasing the minimum particle size. On compaction of this material large voids were present within the walls and a much lower density was achieved. Thus a vertical axis machine was used, which was of larger capacity and which mixed the soil more evenly. Water was sprayed from a hose as a fine mist into the mixer. The mixer was then turned on and allowed to rotate for 60 seconds. A sample was taken to check the water content using the *drop test* as described above, and the process repeated until the desired water content was reached. When this water content was reached the soil was then mixed for a further five minutes, to allow the water within the soil to distribute evenly.

2.4.3 Formwork description

Custom formwork was made such that walls could be constructed and load tested. The formwork consisted of two side sections, 1000mm x 1000mm, and two end pieces, 1000mm high and 300mm wide. This enabled the construction of a wall 1000mm long by 300mm wide, of any height (up to 1000mm). The formwork sides were fastened together by 15mm diameter threaded steel bolts 350mm long. The formwork was made using 12mm thick plywood reinforced with 25mm square timbers as shown in Figure 2.15. Holes were drilled though the reinforcement to allow the threading of the joining bolts. Thus constructed, the formwork became an open box into which the mixture was placed.

Initially walls were constructed directly onto the floor of the laboratory, but a refinement was later added to allow the formation of voids below the wall, to load the walls as beams or cantilevers. To do this timber blocks, cut to size, were placed in the bottom of the formwork. The blocks were 300mm long, allowing them to be placed across the width of the formwork, and 50mm square, meaning 20 blocks were placed along the base. These blocks were covered in a sheet of polythene prior to the addition of the mixture, to ensure that the wall was not constrained at the base and was allowed to move freely. This also provided a continuous surface on which to place the mixture. Where a void was required, sand was placed instead of blocks, and levelled to provide a flat surface. The wall was then rammed as normal, but on removal of the formwork the sand flowed out, leaving the wall unsupported at that section (Figure 2.16).

2.4.4 Compaction, drying and testing

The walls were compacted immediately following the mixing of the soil, to ensure that they were constructed at the correct water content. Compaction was carried out using a Milwaukee Tools Kango 900K electric rammer (Milwaukee 2006) with a rectangular foot 100mm square. Material was added to the formwork in layers of around 150mm, using a method described by Keable (1996). Soil is taken from the mixer with a spade and placed against the inside edges of the formwork. In this way a valley formed within the formwork. When subsequent material is added to this slope in the same manner, the larger particles roll down the slope, to the centre of the wall. In this way the face of the wall contains only smaller sized particles, which gives the face a smoother finish on removal of the formwork. The layers were methodically compacted using the rammer, until the rammer made no further impression on the surface, or until material was forced to rise above the compacting foot on application of the load. When one layer was completed, the next layer was added and compacted, increasing the height of the wall. When the full height of the wall was reached, the top layer was skimmed using material from the mixer, to provide a flat loading surface. The walls were observed as they dried and a colour change was noted as drying occurred (Figure 2.17, Figure 2.18 and Figure 2.19).

Loading was carried out using a hydraulic ram fixed to an large steel frame to ensure no movement of the ram, with a digital load cell placed between the ram and the loaded section. Each of the walls was loaded over its full width, the load being spread using a timber 60mm x 300mm. As the tests were intentionally simple, and due to difficulties in placing instrumentation, displacements were not recorded. The intention of the experiments was to determine the failure modes and approximate stresses on collapse. Following failure soil samples were taken from the failure planes at the centre of the wall. At least three samples were taken and used to determine the water content at failure.

Figure 2.15 Compaction of the wall within formwork

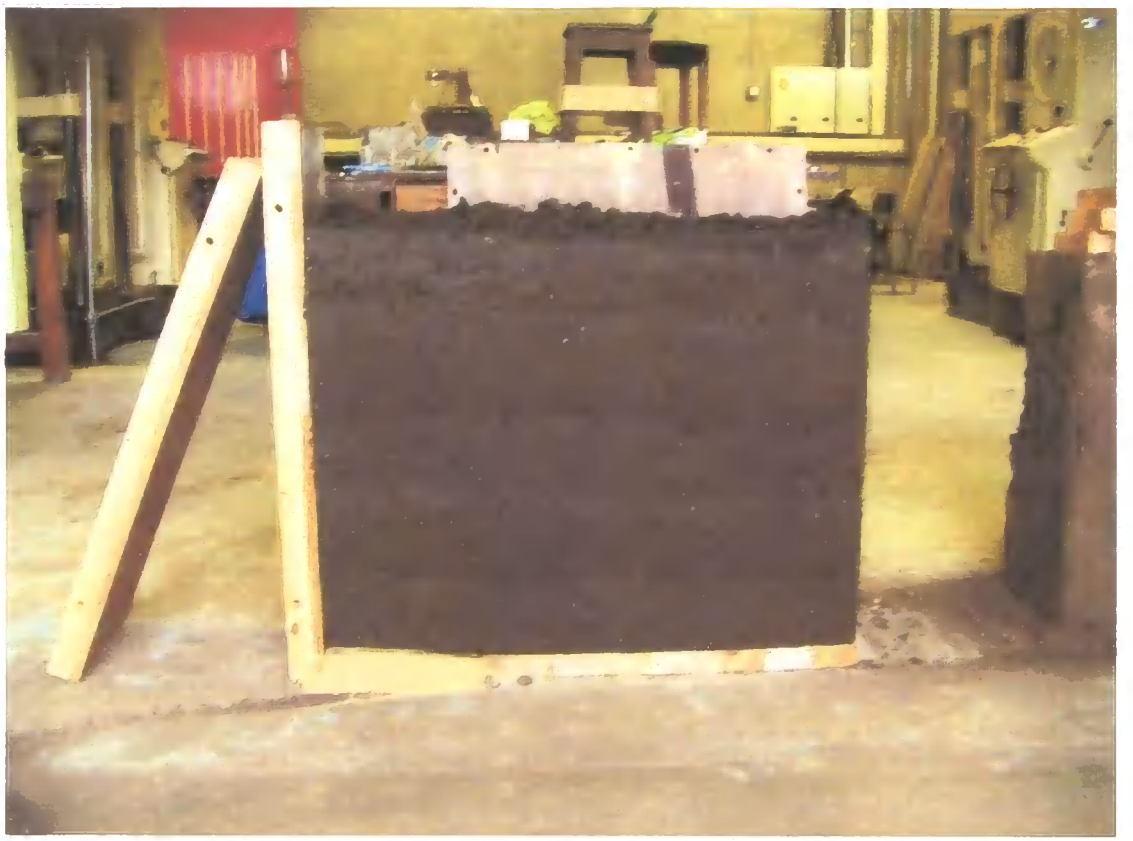

Figure 2.16 Sand and timbers beneath wall 4

Figure 2.17 Wall 2 drying, 24/05/05, day 1

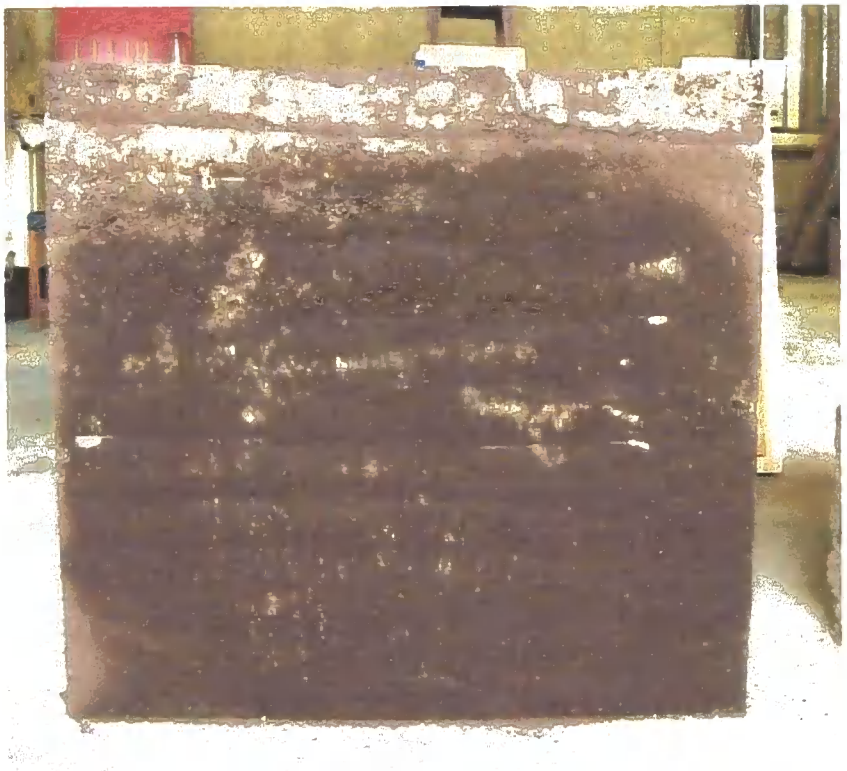

Figure 2.18 Wall 2 drying, 27/05/05, day 4

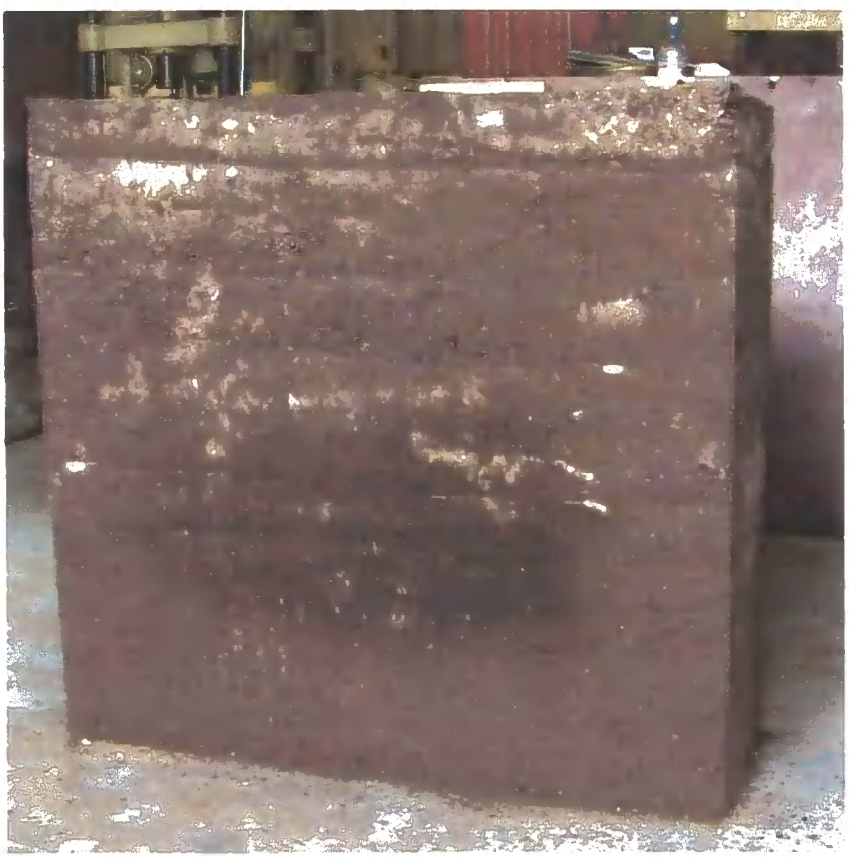

Figure 2.19 Wall 2 drying, 31/05/05, day 8

2.4.5 Observations

Four walls were constructed and each was load tested after 14 days. A description of the mechanism of failure of each wall follows, which may also be seen in Figure 2.20 to Figure 2.32. The water content of the wall was determined by taking at least three samples from the failure plane following testing. A summary of the observations is given in Table 2.4.

2.4.5.1 Wall 1

Wall 1 was the first attempt by the author to make a rammed earth wall. The soil used was not the Aykley Heads mix described in detail above but soil from the laboratory was blended, and the moisture content for compaction was determined using the drop test recommended by Walker, Keable et al. (2005). The wall was left to dry for 14 days prior to testing then loaded across its full width at its centre. Failure occurred first though out-of-plane disintegration, then through the formation of two solid hexahedral blocks, which moved in the out-of-plane direction (Figure 2.20 and Figure 2.21). Later construction and observation led to the conclusion that Wall 1 was constructed rather dry, and as such was very brittle. The mean contact pressure at failure was 0.64MPa. Shortly after the construction of Wall 1, the material from Aykley Heads was sourced, and was used in all subsequent experimentation.

Figure 2.20 Wall 1 diagonal shear and out-of-plane failure

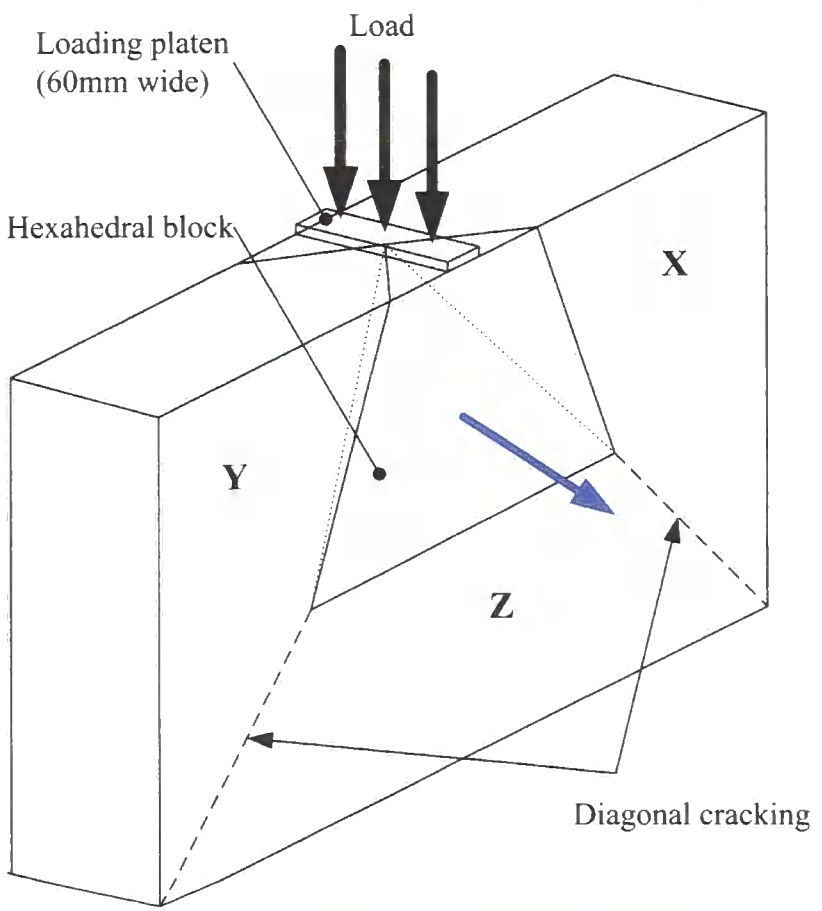

Figure 2.21 Wall 1, Wall 2.2 side B and wall 3 failure diagram

2.4.5.2 Wall 2, initial test (Wall 2.1)

Wall 2 was constructed using the Aykley Heads mix, and a much better finish was achieved than with Wall 1. This was due to the improved technique in the mixing and the compacting of the rammed earth that the author developed during this period. The wall was left to dry for 14 days, during which a change in colour was observed (Figure 2.17, Figure 2.18 and Figure 2.19). This colour change occurred over 8 days, so it was assumed that by 14 days drying to the core of the wall would have been completed.

Upon initial loading there was a delamination of the top layer of rammed earth (Figure 2.22 and Figure 2.23), which was not expected. The reason for the failure is thought to be lack of shear strength of the bond between the compaction layers. The mean contact pressure was 0.61MPa. This phenomenon was also observed later in Wall 4 (Figure 2.29 and Figure 2.30).

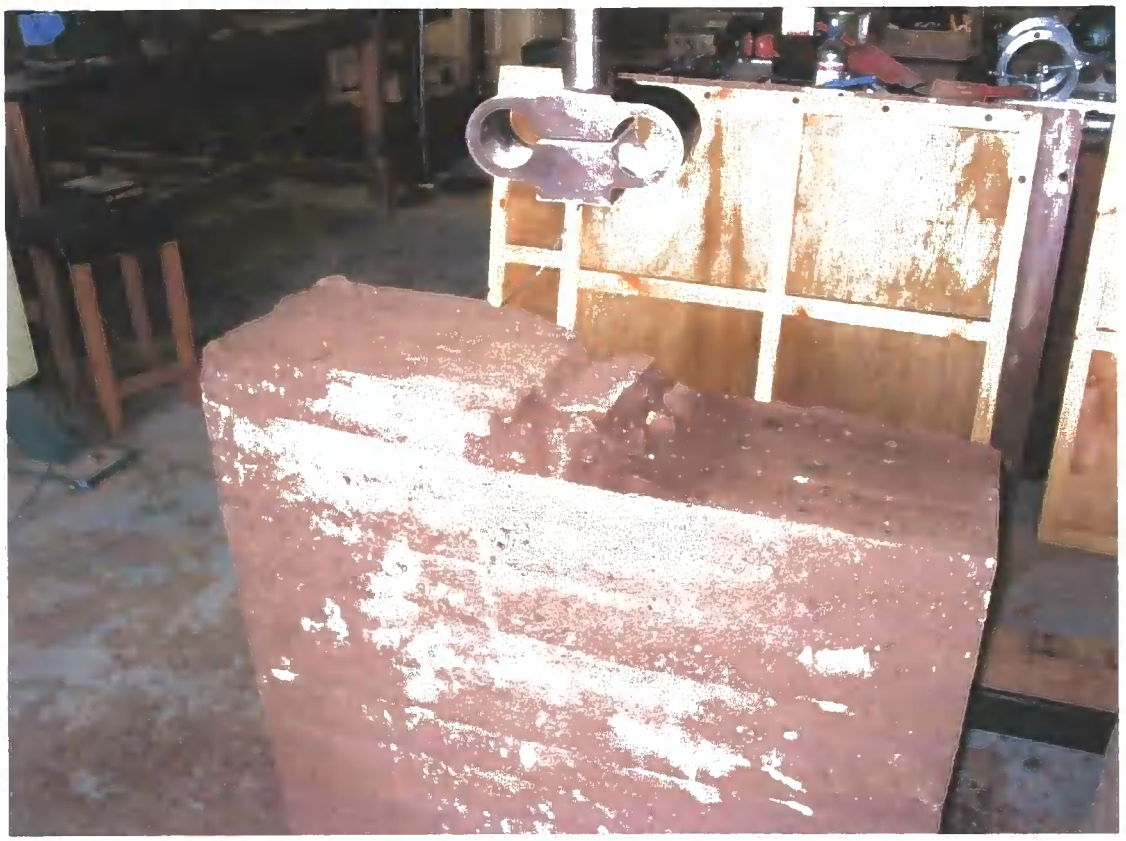

Figure 2.22 Wall 2.1 failure through delamination

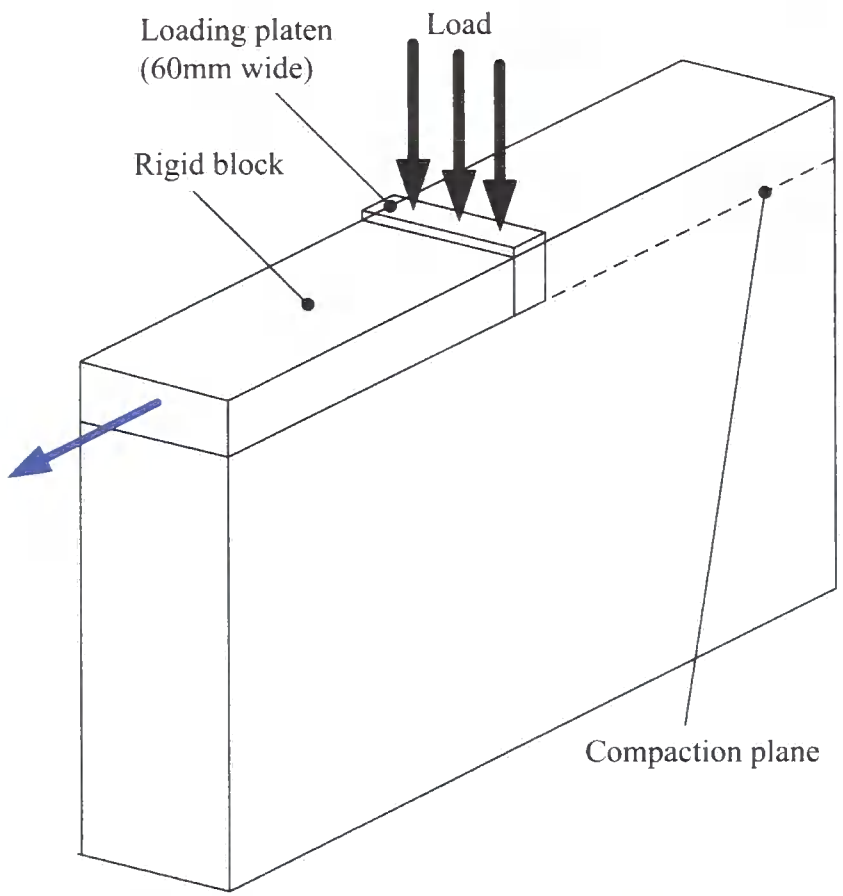

Figure 2.23 Wall 2.1 failure diagram

2.4.5.3 Wall 2, second testing (Wall 2.2)

The wall was then cleaned such that a clean top surface was produced, and load tested again. Failure was by the same modes observed for Wall 1, out-of-plane block failure and diagonal cracking. Side A (Figure 2.24) showed a smaller amount of out-of-plane failure than side B (Figure 2.25), which is thought to be due to slightly eccentric loading applied through the loading ram. In-plane failure occurred through compression of the lower central triangular section (Z, Figure 2.26), which induced shear forces between blocks Y and Z causing shear cracking. Block Z also dilated on compression (a-b, Figure 2.26) causing block X and Y to be forced outwards, and causing a crushing of material at the toe. The mean contact pressure required to cause failure was 0.71MPa, and the water content following testing was 2.7%.

Figure 2.24 Wall 2.2 side A, diagonal shear failure

Figure 2.25 Wall 2.2 side B, diagonal shear failure

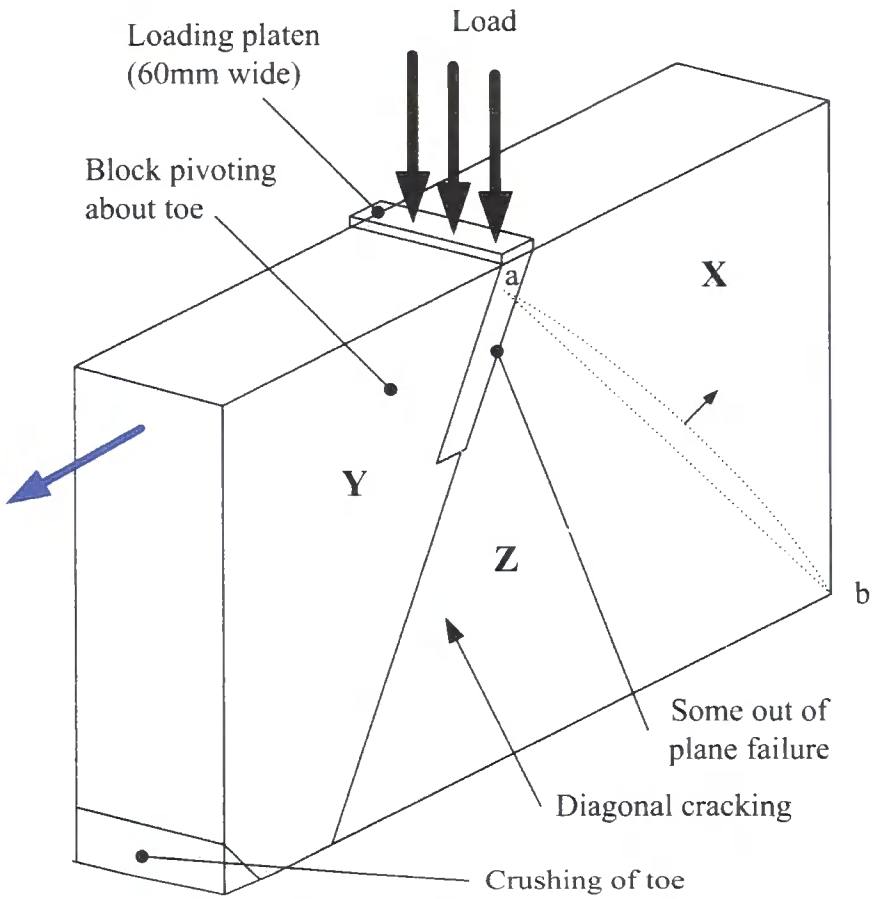

Figure 2.26 Wall 2.2 side A failure diagram

2.4.5.4 Wall 2, third testing (Wall 2.3)

The wall was later finally destroyed using the loading ram. The final water content was observed to be 1% higher than the previous testing, suggesting that the wall had absorbed water between testing. This testing was carried in exactly the same way as the previous tests, with a line load applied across the width of the wall. As loading occurred very close to the edge of the wall, there was no constraint in the in-plane direction, causing the end section of the wall to move outwards, creating a tension crack vertically through the wall. The mean contact pressure at failure of the wall was 0.69MPa, which is remarkably close to the 0.71MPa strength of the previous test.

Figure 2.27 Wall 2.3 failure through vertical shear cracking

2.4.5.5 Wall 3

Wall 3 was constructed at a lower initial water content than Wall 2 (5.2%) and a worse surface finish was obtained on removal of the formwork. This wall was loaded in an identical way to wall 2, but failure occurred in the out-of-plane direction and no in-plane cracking was observed. This may be due to the weaker and more brittle nature of the material meaning that section Z (see Figure 2.21) was not able to deform enough prior to yield because of its lower strength to initiate a shear crack between sections X and Y and section Z, thus failure of the wall was through brittle out-of-plane breakdown, rather than shear cracking.

Figure 2.28 Wall 3 out-of-plane failure

2.4.5.6 Wall 4

Wall 4 was constructed in an attempt to model settlement of one end of a wall. The intention was to load the wall sufficiently to develop a tension crack at the top face. The wall was constructed by placing timber blocks within the formwork as described in Section 2.4.4, and by placing sand in the region where a void under the wall was to be made (Figure 2.16). This enabled compaction while still producing a homogeneous wall. A plastic sheet was placed above the base timbers, to provide a continous surface against which to compact, and to allow free movement of the base of the wall upon loading. Following compaction three of the formwork sides were removed, leaving one end to support the sand in the void (Figure 2.16). After three days the end section and the sand were removed, leaving one end of the wall unsupported. The behaviour of this unsupported section was unknown, and thus experimentation developed, in an attempt to cause the wall to fail.

The wall was left to dry for 14 days, during which time the unsupported section was observed not to move. It was suspected that the wall might 'flow' slightly, being unsupported and not yet dry. The wall was then loaded using steel weights (used for application of a normal load in a shear box test) across the whole of the top surface of

the wall. 234kg was applied, equating to a uniform stress of 7.65kPa. This load was applied for two days, but again no movement of the wall was observed. Finally the wall was loaded using the loading ram over the unsupported section as shown in Figure 2.30. The failure observed following this loading was quite complex and required video analysis of the loading to understand the cracking observed.

Upon loading to the left hand side of the wall (as seen in Figure 2.29 and Figure 2.30), the wall remains as a block and begins to pivot about the end of the support (A). This causes some crushing at the toe, but otherwise the wall remains intact. Because of the pivot, the right hand end of the wall is lifted from the base, and because of its self-weight a tensile crack is opened up at the compaction plane. This crack initiates at the right hand end of the wall, then spreads towards the centre of the wall. As the crack spreads, section X falls back and crack C is initiated from the base upwards. Crack C meets crack B and section X is thus separate from the still combined sections Y and Z. Crack D is then initiated as section Z falls back, crack D rising through the full height of the wall. Section Y then hits the ground causing crack E to form.

While the sequence of cracking is difficult to establish, the initial cracking is due to a tearing of the compaction plane at mid height of the wall. This further highlights the situation observed in Wall 2.1 (Figure 2.22 and Figure 2.23), where a lack of vertical compressive load across the compaction plane led to failure of this plane. The mean contact pressure at failure was 0.04MPa and the final water content was 2.9%.

Figure 2.29 Wall 4 loaded and unsupported at left

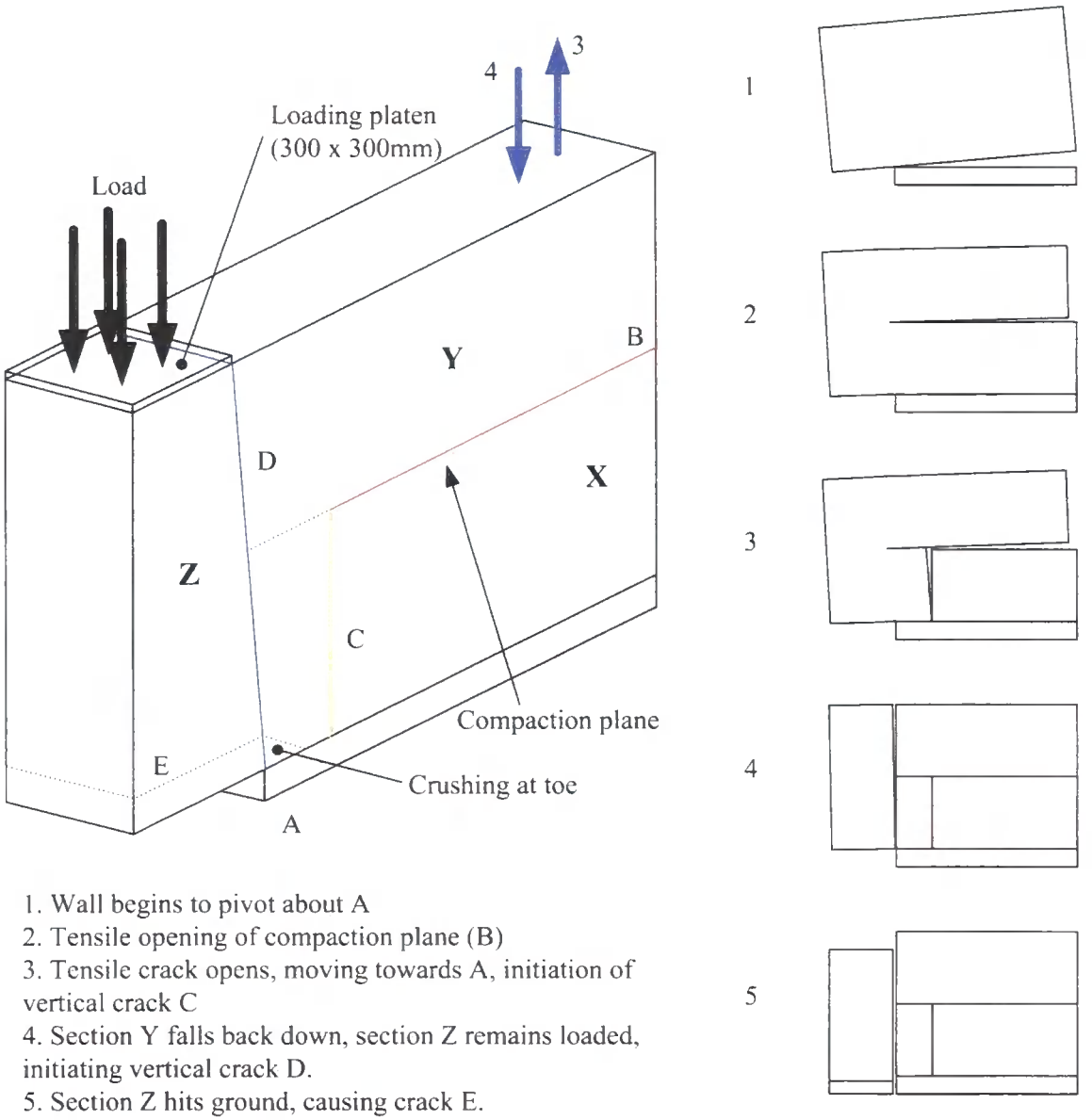

1. Wall begins to pivot about A
2. Tensile opening of compaction plane (B)
3. Tensile crack opens, moving towards A, initiation of vertical crack C
4. Section Y falls back down, section Z remains loaded, initiating vertical crack D.
5. Section Z hits ground, causing crack E.

Figure 2.30 Wall 4 failure diagram

2.4.5.7 Wall 5

Wall 5 was constructed to understand how a rammed earth beam would behave. The wall was constructed using the same methods as the previous walls, but only two layers of earth were used, making the wall 250mm high. Sand was again placed within the formwork to allow the formation of a void beneath the rammed surface. The wall was left to dry for 17 days prior to testing. On loading a tensile crack (A, Figure 2.32) was observed to form at the base of the wall. This crack grew to around 25mm long, however failure occurred through the formation of a diagonal crack (B). The movement downwards of section Z, and the non-moving of sections Y caused shear crack (B) to form between the edge of the support and the loading point. This crack initiated at the

support, growing as section Z moved downward. As crack B formed, crack C also formed, initiating in the body of the beam. This crack then spread to mirror crack B. Cracks D and E then formed as tension cracks as sections W and V were loaded as cantilevers. The cause of failure of the wall is the formation of diagonal shear planes running from the loading point to the supports, which occurred at a mean contact pressure of 0.2MPa.

Figure 2.31 Wall 5 unsupported and loaded over centre

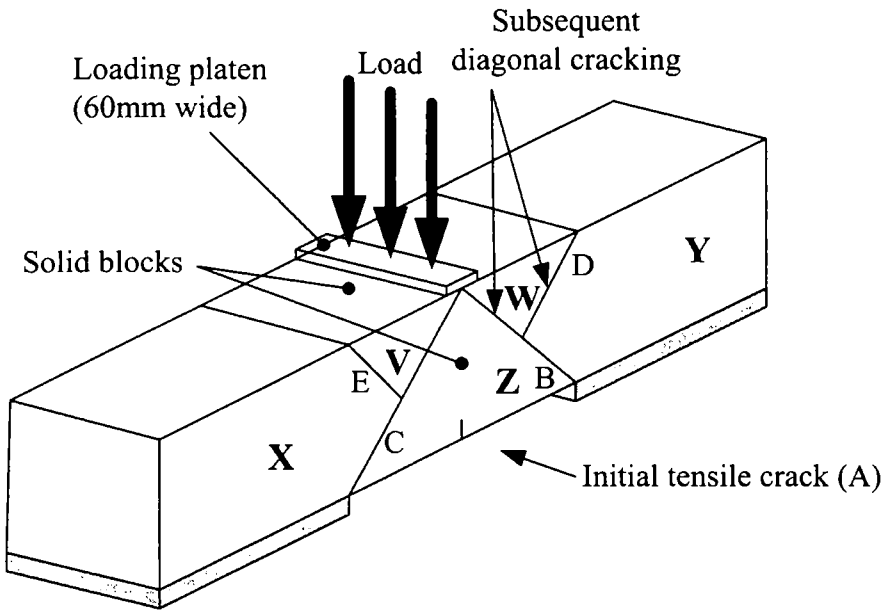

Figure 2.32 Wall 5 failure diagram

Wall ID	1	2.1	2.2	2.3	3	4	5
Construction	19/05/2005	24/05/2005	24/05/2005	24/05/2005	27/06/2005	05/07/2005	19/7/2005
Testing date	07/06/2005	07/06/2005	07/06/2005	22/06/2005	11/07/2005	22/07/2005	01/08/2005
Age (days)	19	14	14	29	14	17	13
Material source	Laboratory	Aykley Heads	Aykley Heads	Aykley Heads	Aykley Heads	Aykley Heads	Aykley Heads
Height	Not measured	990	770	770	Not measured	840	220
Initial water content	Not measured	Not measured	Not measured	Not measured	5.2	12.0	Not measured
Final water content	Not measured	2.7	2.7	3.8	3.0	2.9	Not measured
Loading method	Line load	Line load	Line load	Line load	Line Load	Area load over 0.3 x 0.3 at end	Line Load
Failure type	Diagonal cracking	Delamination	Diagonal Cracking	Diagonal cracking	Vertical cracking	Vertical and horizontal shear	Tension crack
Peak load (kN)	14.3	13.7	16	15.5	3.4	3.8	3.7
Peak stress (MPa)	0.64	0.61	0.71	0.69	0.15	0.04	0.2

Table 2.4 Wall statistics

2.4.6 Discussion

The rammed earth walls were constructed and tested initially to gain further insights into the macroscale nature of rammed earth, concentrating on construction and behaviour under loading. A number of different loading configurations were attempted, and methods developed to produce voids beneath the wall base. The quality of the construction improved as more walls were constructed, but meaningful conclusions may be taken from each of the experiments. Four distinct failure types were observed. Out-of-plane failure was observed in Walls 1, 2.2 and 3. Failure of the compaction plane was observed in Walls 2.1 and 4. In-plane shear cracking was seen in Walls 2.2, 2.3, 4 and 5, and in-plane tensile cracking was observed in Wall 5. A trend may be observed of local out-of-plane failure, directly beneath the loading point, but global in-plane failure of the walls.

The local out-of-plane failure can be considered most akin to exceeding of the unconfined compressive strength of the material, and failure is similar to that of unconfined cube tests (Figure 2.33). This would help to explain the similar compressive strengths of the walls where out-of-plane failure occurred (Wall 1 – 0.64MPa, Wall 2.2 – 0.71MPa). Wall 3 also failed through out-of-plane failure, but at a much reduced stress. This is thought to be due to the reduced strength of the wall which is discussed below.

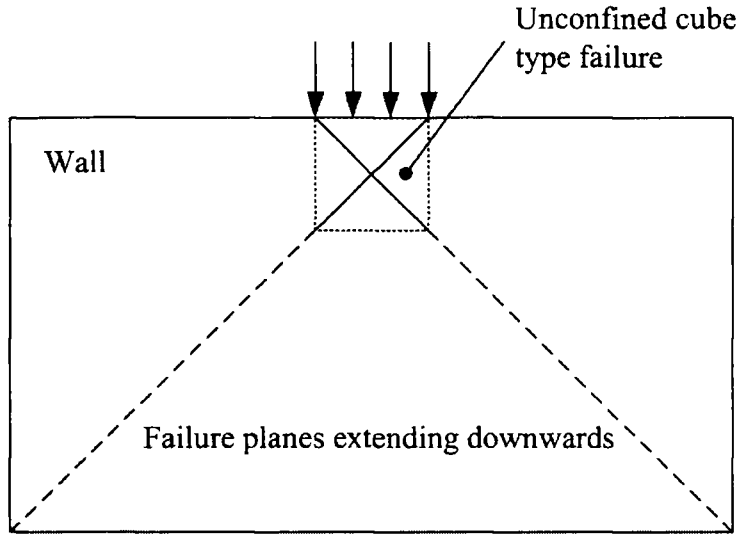

Figure 2.33 Out-of-plane failure, compare to Figure 2.21

In-plane cracking occurs when a mechanism forms through the creation of a failure plane, in much the same manner as the development of a slip circle when considering slope stability. The material properties, geometry of the loading and of the wall dictate the distribution of stresses, and failure occurs along planes where the shear strength of the soil is exceeded.

Failure of the compaction plane was observed in Walls 2.1 and 4. This is also known to be a problem in modern rammed earth construction (Hodsdon 2006). The bond between each compacted layer is known to be weaker than the rammed earth layer, and so under certain stress conditions is liable to fail in preference to the rammed earth between layers. This occurred in Wall 2.1 where the vertical load at the top layer was relatively low (comprising only the self weight of one lift of rammed earth), thus it is assumed that the shear strength is also very low. Failure of Wall 4 occurred due to a rotation of the wall about the end of the support, and led to a direct tensile stress across the compaction plane, which exceeded the strength of the compaction plane, leading to failure.

The difference between the failure loads of Wall 2.2 and Wall 3 highlights the differences caused by compaction at different initial water contents. The initial water content of Wall 2 was determined using the *drop test* (around 12%) and that of Wall 3 was measured as 5.2%. Soil fabric is defined as the geometrical arrangement of particles and Toll (1991) highlights the differences in soil fabric caused by compaction at different water contents. Compaction dry of optimum water content

leads to an aggregated fabric, with smaller particles sticking together leading to a coarser soil than justified by the grading, whereas soil compacted wet of optimum is dispersed, and the behaviour is closer to that expected from the particle size distribution. Figure 2.14 shows the optimum water content for the Aykley Heads soil used for both Wall 2 and Wall 3. Given that the wall was compacted using a vibrating hammer, it may be seen that Wall 2 was compacted wet of optimum and Wall 3 dry of optimum, and the differences in soil fabric are apparent when comparing Figure 2.25 and Figure 2.28. The role of water within rammed earth is explored in much greater detail in Chapter 3. In the next section numerical modelling of these tests is described.

2.5 Numerical modelling

Modelling is a particularly useful tool for the engineer, and becomes increasingly important when observing historic structures, where the material properties and applied stresses are usually not well understood (Yeomans 2006). A large number of models have been developed for soil but numerical modelling of rammed earth has been little discussed (only Bui, Hans et al. 2007).

The aim of this work is to demonstrate the ability of conventional approaches (as might routinely be used by engineers in industry) to simulate rammed earth and the shortcomings of such modelling. It was hoped that the modelling described below would be able to reproduce the behaviour of rammed earth as observed in the laboratory and to allow predictions of the behaviour of historic rammed earth to be made. In the case of historic rammed earth, it is usually impossible to take representative samples of a structure for destructive testing and thus representative parameters should be determined by other means. The main features of rammed earth which it was hoped would be captured were compaction in layers leading to the different strengths of each layer and of layer interfaces, and onset of in-plane cracking.

Two different types of analysis were carried out. The analyses both aimed to model the behaviour of the walls described in Section 2.4.5. The Mohr-Coulomb criterion was used for both analyses and a parametric study of the Mohr-Coulomb parameters was carried out in both cases to determine which parameters could be used to best describe the behaviour of the walls as observed during physical testing.

The first analysis (Section 2.5.2) looked at the layered nature of rammed earth. Because the wall testing had highlighted the weakness of the compaction planes, a model was constructed which introduced horizontal planes of weakness into the wall (Section 2.3.3.1), in a similar manner to that described by Jaeger and Cook (1979). An elastic-perfectly plastic Mohr-Coulomb failure criterion was chosen, but layers of reduced strength were introduced to simulate the compaction planes. The second approach (Section 2.5.3) used the Hardening Soil model, described in Section 2.3.5.

This attempted to model the compaction of the rammed earth and removal of formwork in addition to loading of the walls.

As the construction and testing of walls in the laboratory was crude, this modelling was not intended to allow accurate quantitative predictions of the behaviour of rammed earth. Rather, it was attempted in order to show that current modelling strategies employed by practising engineers may be used for modelling rammed earth, and to highlight the drawbacks of such techniques.

2.5.1 Rammed earth modelled as a soil

In modelling rammed earth as soil, it is important to note how standard geotechnical assumptions may not be as valid when applied to structures.

2.5.1.1 Plane strain assumption

The assumption of plane strain is common in many geotechnical analyses, and is used in the following analyses. Plane strain is usually assumed when one dimension is significantly larger than the others, and if the applied boundary conditions are perpendicular to and independent of the largest dimension (usually denoted z). If the z dimension of the problem is large, then it may be assumed that the strain in the z direction is zero although the stress is likely to be non zero. In geotechnical engineering the assumption of plane strain is usually applied to structures such as embankments and dams, where the structure is long in comparison to its width and height, and stresses along the length of the structure are assumed to be small in comparison to those perpendicular.

The walls tested failed in both in- and out-of-plane directions, and thus a full three dimensional analysis would be required in order to fully capture the behaviour. However given that such analysis would be computationally expensive, the assumption of plane strain may be used to capture the in-plane behaviour.

The plane strain assumption (Figure 2.34) would be valid for the compaction of material if the formwork were infinitely stiff and perfectly smooth and if the compaction was carried out over the full horizontal surface of the soil. In this manner all plane sections would remain plane. The plane strain assumption is valid for

compaction of material within the formwork because the formwork acts to limit displacements in the z direction to zero, and the horizontal components of the compaction stresses are non-zero.

Justification of the assumption of plane strain is more problematic in the analysis of the loading of the walls. The z direction is taken as the width of the wall and although the boundary conditions are perpendicular to this direction, but it is not the largest dimension. Failure of some of the walls occurred out-of-plane, which cannot be modelled with the plane strain assumption, but modelling of the in-plane cracking may be attempted using the plane strain assumption.

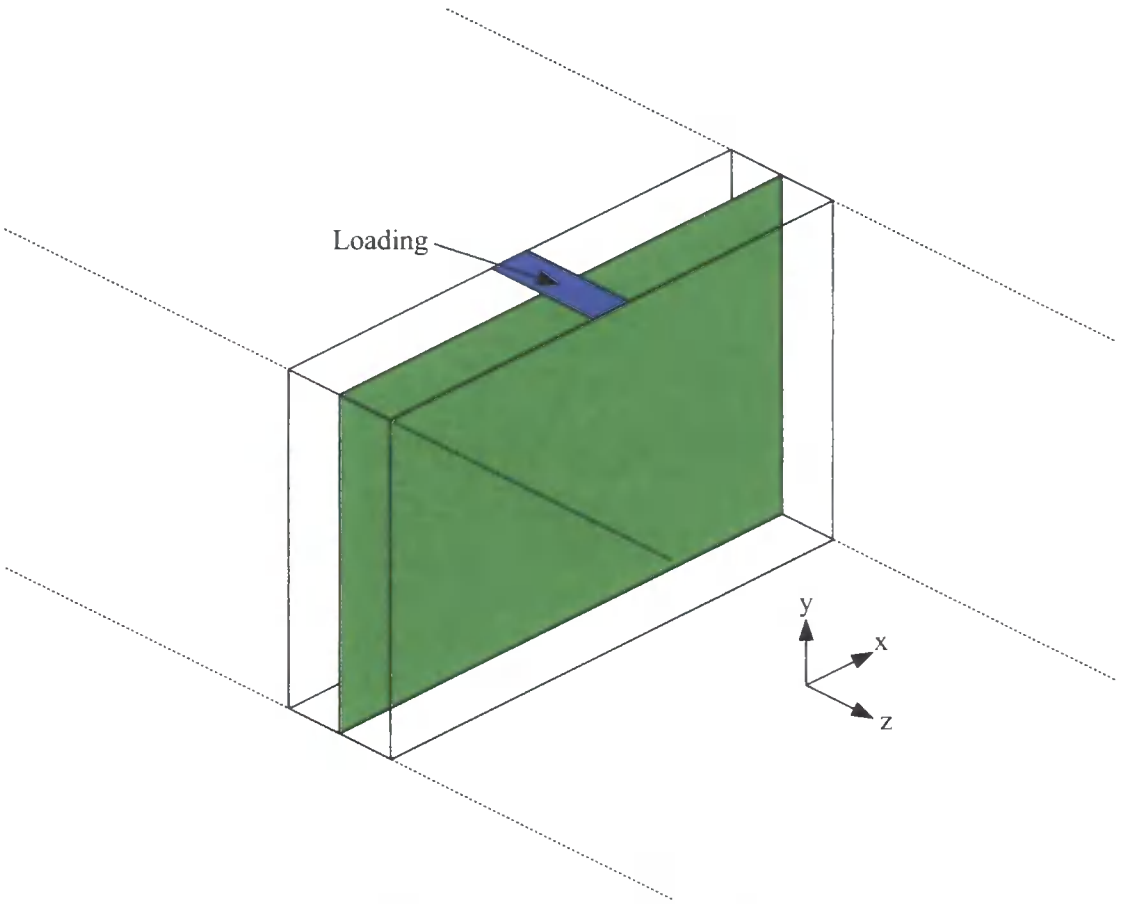

Figure 2.34 Plane strain assumptions

2.5.1.2 Pore water pressure

The concept of effective stress is outlined in Section 3.8.1, but briefly, where a stress is applied to saturated soils, it is carried by both the soil skeleton and the water in the pores. The water is considered to be an incompressible fluid and thus the total stress

normal to any plane in the soil is divided into two parts; the pressure of the pore water u_w, and the stress carried by the soil skeleton, which is known as the effective stress σ'. This is neatly summarised in Terzaghi's equation

$$\sigma = \sigma' + u_w \tag{2.41}$$

If loading of a saturated sample is carried out quickly, without allowing water to leave the sample (known as a *quick, undrained test*) then the pressure of the water in the soil pores increases, which leads to reduced strength samples because some of the total stress is taken as an increase in pore water pressure, leading to a reduced effective normal stress and thus strength (Equation (2.19)) . However, if the loading takes place over a long period of time and water is allowed to drain from the sample (the test is *drained*) then a more accurate representation of soil behaviour in the field is observed. Numerical modelling of soil allows both drained and undrained conditions to be simulated and in both cases described here drained modelling was assumed.

2.5.2 Mohr-Coulomb layered model

In order to capture the in-plane failures observed in the laboratory, a simple model based on the Mohr-Coulomb failure criterion and similar to the *Planes of weakness* model described in Section 2.3.3.1 was developed. The rammed earth is modelled as elasto-plastic with a Mohr-Coulomb failure criterion but the lower strength of the compaction layers, as observed in Walls 2.1 and 4 is modelled by the introduction of layers with reduced strengths.

2.5.2.1 Formulation

A linear elastic-perfectly plastic Mohr-Coulomb constitutive model was used for both the layer and the main wall body sections (Figure 2.35). Finite element modelling using the commercial software Strand7 finite element analysis program. Nine node quadrilateral and seven node triangular elements were used, and assigned Mohr-Coulomb properties which could be tuned in order to match the failure stress and mode observed in the physical modelling. The adopted meshes were chosen on the basis of achieving reasonable accuracy within a reasonable runtime. It is recognised that further refinement of the meshes will influence the results. An elastic modulus of 50GPa and Poisson's ratio of 0.3 were used, based on Gonzalez (1999) and Walker,

Keable et al. (2005) as outlined in Chapter 1. A density of 2000kg/m^3 was chosen based on measurements of density taken during the physical testing.

Although it was possible to model only half of the wall to take advantage of symmetry, a model of the whole walls was constructed, and used to model each of the walls as constructed in the laboratory. Therefore although computing time for each simulation was increased, it was considered that this was outweighed by the time saved by producing a number of different models for the parametric studies. As conventional continuum finite elements were used it was not possible to model cracking failure as actually observed. This can be seen as a critical shortcoming of the modelling. However it is important to reiterate that the study was meant to replicate the type of analysis that might be undertaken by a practising engineer who would be unlikely to have access to complex numerical modelling techniques. As an approximation to this the perfectly plastic behaviour of the model allowed the elements to strain indefinitely, which was considered as a failure of the individual element. This can be seen as the 'failure' of the element, but does not obvisouly mean failure of the whole system. Failure was assumed to be approaching when there was a loss of convergence to a solution, due to the formation of a mechanism, which is manifested as a singular stiffness matrix thus making convergence to a solution impossible (Potts and Zdravkovic 2001). Models of each of the walls tested were constructed and a nonlinear load stepping analysis was carried out, increasing the load until the model showed failure.

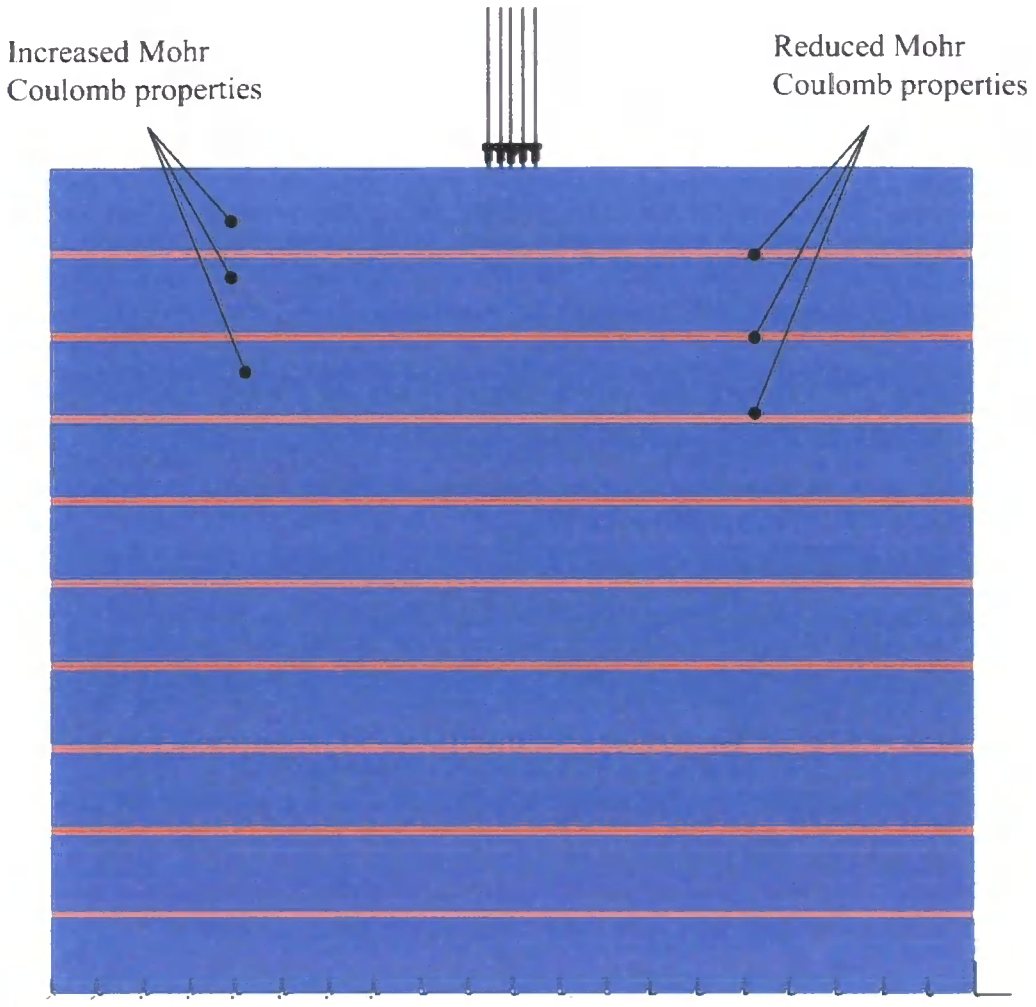

Figure 2.35 Layered Mohr-Coulomb model of rammed earth

2.5.2.2 Results

Not all of the walls tested were used to validate the finite element model. Wall 1 was not used as the soil mix used was different to that used for the other walls, and as such would have different properties to the soil used for the rest of the testing. Wall 3 failed in the out-of-plane direction (Figure 2.28) and thus its failure could not be modelled under the conditions outlined. As a result the model was tuned using only three walls, one of which (Wall 2) was tested twice. Two different failure types were observed in these walls, namely shear failure within the body of the rammed earth, and failure about the compaction plane. These two aspects are modelled.

Models of the walls were first constructed, then the parameters tuned until the failure mode and stress matched that observed during physical testing. First the load steps

were set to match the failure load, for example if the failure load from physical testing was 0.71MPa, this was set as a load factor of 1.0, and load factors of 0.80, 0.85, 0.90 0.95, 1.00, 1.05 and 1.10 were set. The four Mohr-Coulomb parameters values were set to those found in Table 2.7 and an analysis carried out to see if failure occurred. The properties were then reduced or increased until the failure mode observed occurred at the required load.

Figure 2.36 to Figure 2.39 show the walls at a load factor of 1.0 where the Mohr-Coulomb parameter (ϕ and c for the rammed earth parts; and ϕ_{layer} and c_{layer} for the compaction plane layer) were such that failure occurred at the same stress and in the same way as was observed in the laboratory walls. Figure 2.36 and Figure 2.37 show the results in terms of Mohr-Coulomb plate stress, which is the maximum shear stress in the plate, based on the Mohr-Coulomb criterion (Equation (2.19). Figure 2.38 and Figure 2.39 show a different way of looking at the failure of elements. Because continuum finite elements are used, it is not possible to model cracking. Therefore cracking is assumed where yielding of the brittle rammed earth occurs. As perfect plasticity was assumed, yielding leads to greatly increased strain in the element. Therefore the maximum principal strain is shown, and those element exhibiting a large strain can quickly be identified as failed.

Physical testing of Wall 2.1 revealed delamination of the upper-most layer of rammed earth, failing along the compaction plane. It was assumed that this could be modelled as a failure of the compaction layer region, which was given reduced properties compared to the rammed earth. The required parameters for failure of the layer at the same load as the physical testing are shown in Table 2.6. It was observed that at loads close to the failure load (load factor of 0.97) elements in the centre of upper-most layer region had failed, and become perfectly plastic, although the whole system did not fail. Failure of the whole wall occurred when 50% of the layer elements reached failure, and it is assumed that this would physically manifest itself as a shearing of the top layer of rammed earth, as is shown in Figure 2.22 and Figure 2.23.

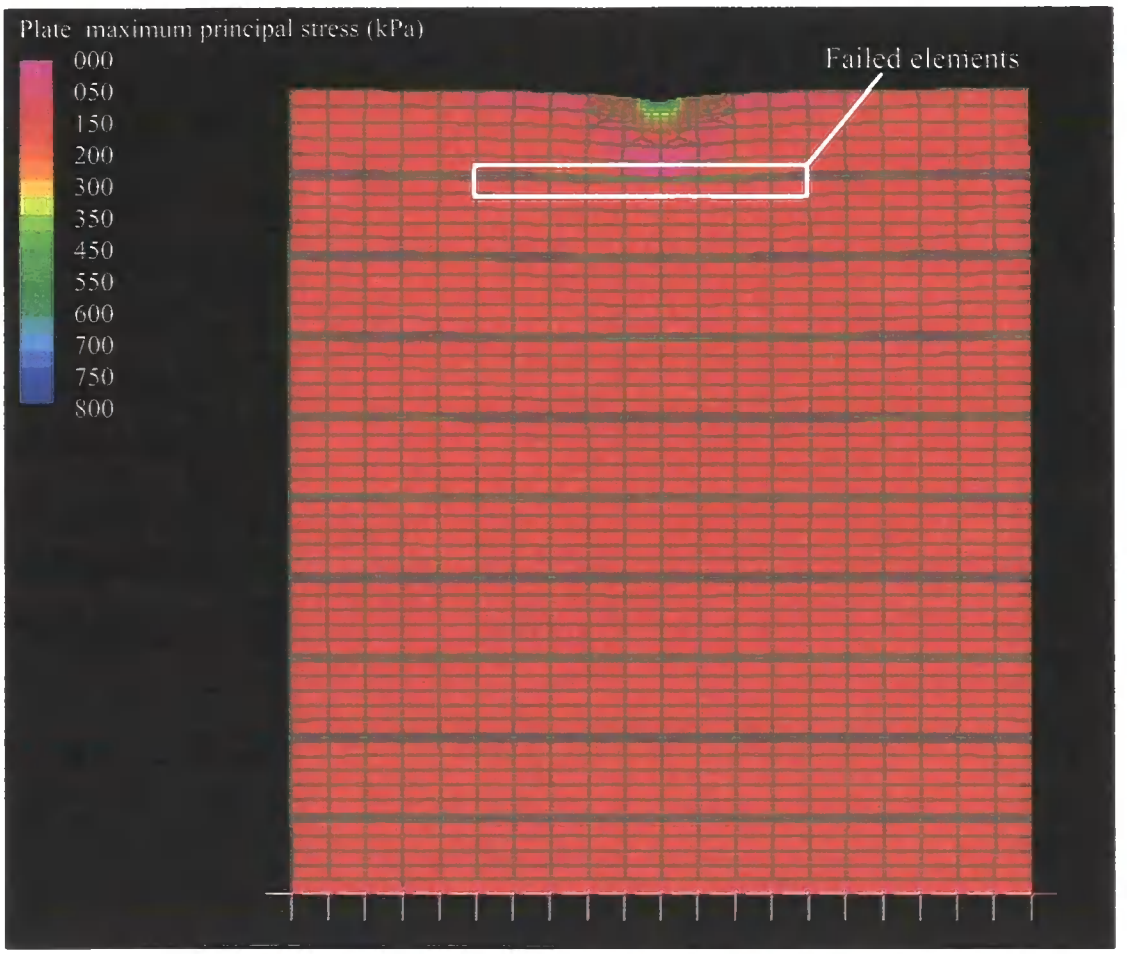

Figure 2.36 Maximum principal stress contour plot close to failure of model. Mean applied pressure = 0.61MPa. Layered model, Wall 2.1

Initially Wall 2.2 was given the same material properties as Wall 2.1, the only difference between the two walls being the height; Wall 2.1 was one lift higher than Wall 2.2. While giving the walls the same material properties, in reality the lower layers of the wall will have received more compaction (assuming that each layer receives some compaction from the layer above it). Therefore the cohesion value of the layer was increased from $c_{layer} = 20kPa$ to $c_{layer} = 35kPa$, and this led to failure in shear in the rammed earth close to the loading point. Where the strength of the layer region was too low, it was observed that this layer failed, and behaved as though 'pulling' the layer below, leading to high tensile stresses at the base of the topmost layer. This is unlikely to occur in practice due to the actual zero thickness of the compaction layer.

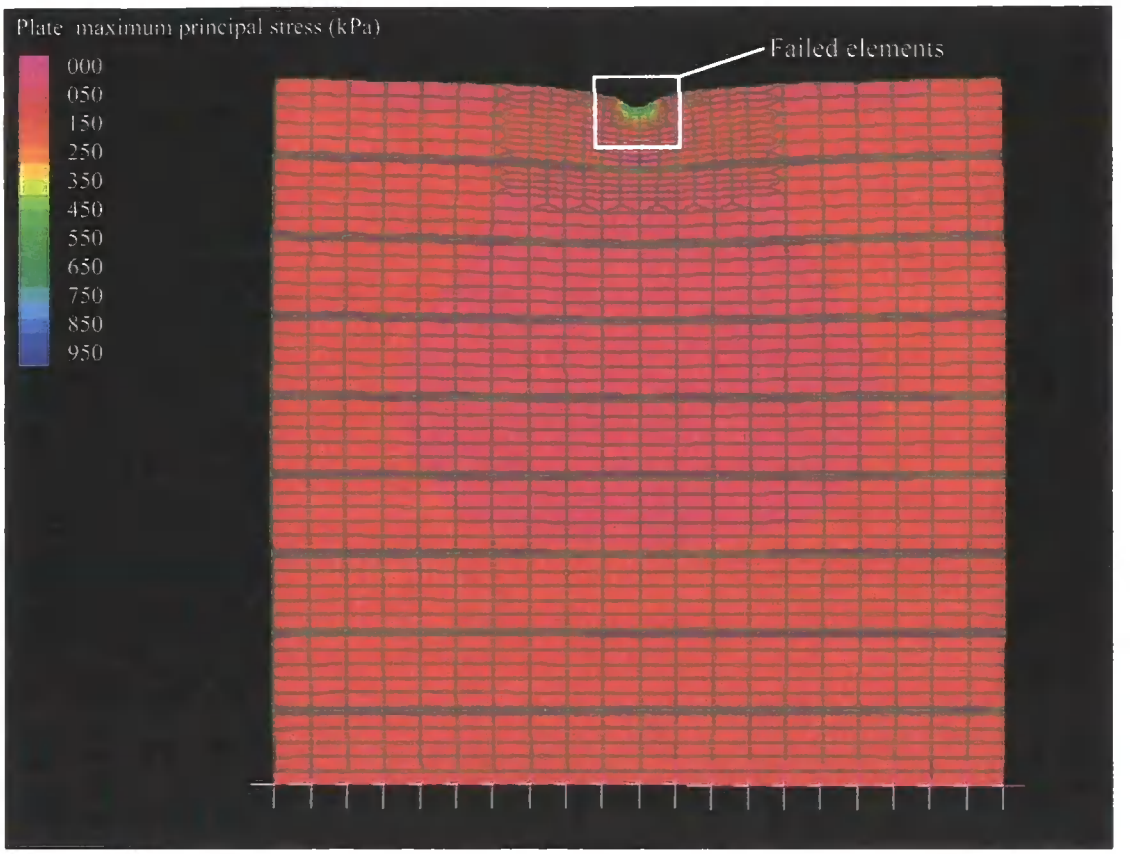

Figure 2.37 Maximum principal stress contour plot close to failure of model. Mean applied pressure = 0.71MPa. Layered model, Wall 2.2

Wall 4 was difficult to construct and test due to the complex failure method. The main issue was that failure in Wall 4 was initiated as section X (Figure 2.30) lifted from the base, which induced caused tension across the compaction plane, initiating a crack. It was not possible to model lifting of the base of the wall in a simple manner. The solution was simplified by reducing the cohesion of the compaction layer from $c_{layer} = 20kPa$ to $c_{layer} = 10kPa$. This gave failure at the correct load, but also induced failure above the pivot point, as can be seen in Figure 2.38. However, given the complex failure pattern it is sufficient to understand that this model shows that failure initiated through direct tension across the compaction plane. As the problem is treated as one of kinematics, pivoting of the wall, and subsequent crack opening and closing, as occurred during physical modelling, cannot be modelled.

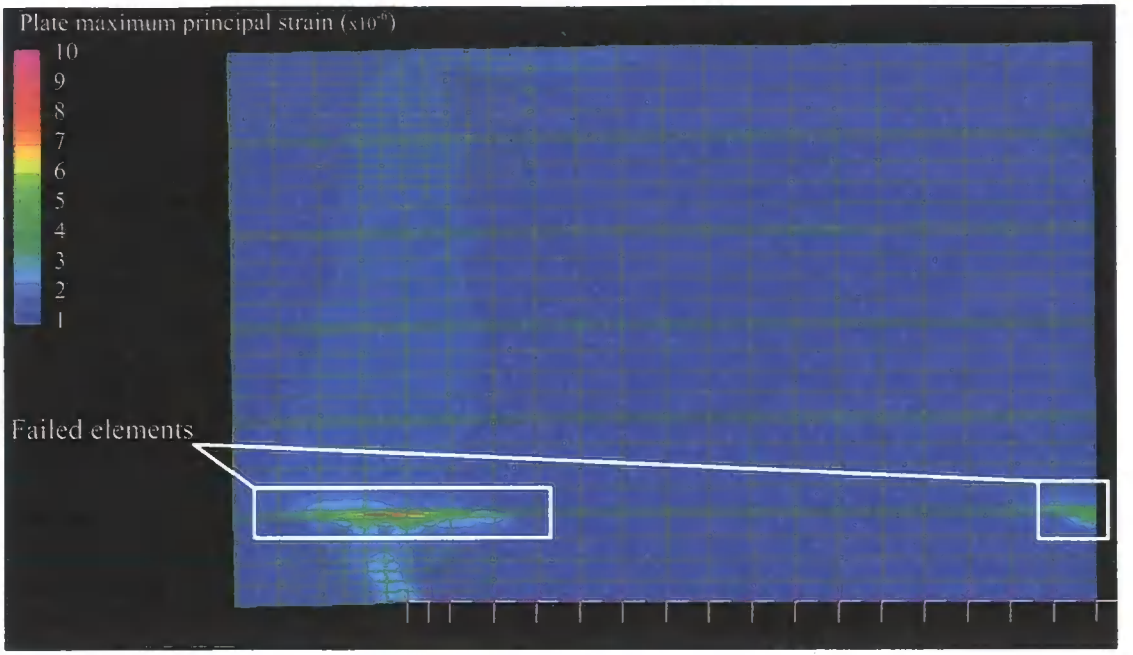

Figure 2.38 Maximum principal stress contour plot close to failure of model. Mean applied pressure = 0.04MPa. Layered model, Wall 4

Wall 5 failed through shear failure of the rammed earth, but this was preceded by a tension crack forming at the base of the beam. It was difficult to model failure in the finite element model of the wall as the system was very tolerant to a large degree of shear failure in the elements prior to failure of the whole system. Figure 2.39 shows failed elements, but it can be seen that the beam is still able to support the loading, due to the action of arching towards each end of the beam. During physical modelling the beam was not able to support this arching action, and the ends of the beam moved outwards as the limiting friction between the ground and the beam was exceeded. It was not possible to model this movement in the finite element model.

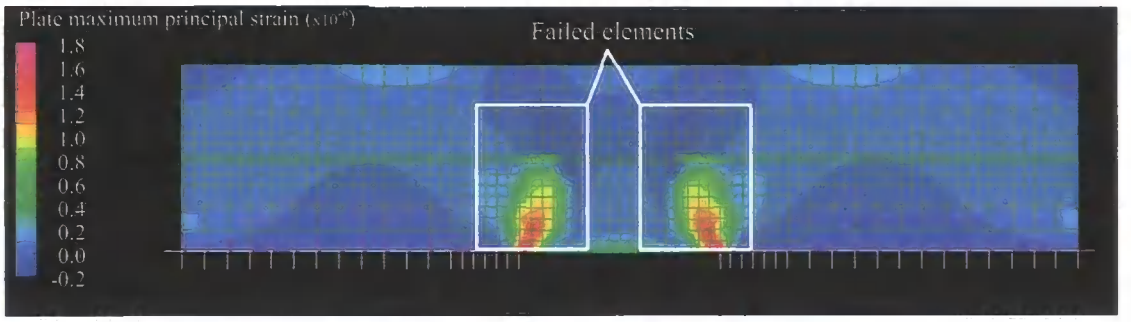

Figure 2.39 Maximum principal stress contour plot close to failure of model. Mean applied pressure = 0.71MPa. Layered model, Wall 5

2.5.3 Modelling with the Hardening Soil model

While modelling using a layered Mohr-Coulomb approach, as described above proved useful, it was thought that modelling the compaction of rammed earth would allow a capturing the real behaviour.

The Hardening Soil model (described in Section 2.3.5) is a formulation available to practising engineers which offers several advantages over the Mohr-Coulomb model used in Section 2.5.2. A hyperbolic (rather than bilinear) stress strain curve could be implemented, and the cap yield surface could be used to model plastic volume strain. Coupled with the dependence of stiffness on stress level, this means that the compaction of rammed earth may be modelled.

The compaction procedure may be modelled as a series of discrete loading steps, with a new layer of soil added prior to a new load being applied to the top most layer. It was proposed that the stiffness of each subsequently compacted layer would differ from the one below because of the stiffness of the layers below. This would mean that the bottom layer would increase in stiffness as more layers above were compacted, and that the top layer would be the least stiff because it had only been compacted once. It was though that the strength of each layer would also vary, for similar reasons. Increased compaction of the lower layers would lead to reduced height of the layer (reduced soil volume) which would probably lead to an increase in strength.

In the HS model, the soil strength is defined by the Mohr-Coulomb parameters (Equation (2.27)) and parametric study of the Mohr-Coulomb parameters was carried out.

A model of Wall 2 (section 2.4.5.2) was constructed and is shown in Figure 2.40. The model consists of a central 'wall' with 'formwork' sections to the left and right, which are removed prior to loading. The wall is made up by compacting ten layers sequentially by applying a displacement to the top of each layer. The wall consists of ten layers each of 100mm height, resulting in a 1m high wall (uncompacted height). Upon completion of compaction the wall is allowed to recover with no load applied, then the 'formwork' ends are removed, allowing the walls to deform laterally. An

increasing displacement is then applied to the centre of the wall, to simulate loading as carried out in the laboratory.

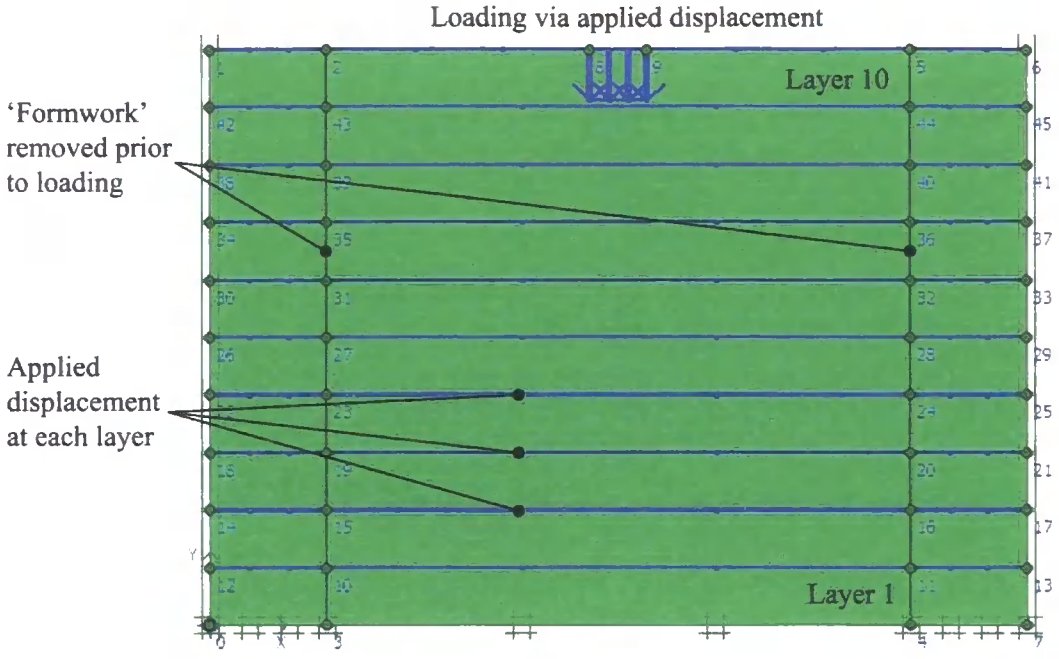

Figure 2.40 Hardening Soil model

2.5.3.1 Selection of material parameters for the HS model

A parametric study was carried out in order to find which strength parameters best fitted the results obtained through laboratory wall testing outlined in Section 2.4. Other parameters were kept constant, and were chosen based on recommended values (for example m and E_{ur}^{ref}) or on the results of uniaxial compression testing detailed in Chapter 3 (for example E_{50}^{ref}). Values of ϕ were varied from 25° to 45° and c from 75kPa to 300kPa. These values represent a wide range of 'classical' soil properties. The grading of the soil (shown in Figure 2.13) indicates it to be a well graded, blended mix, resulting in proportions of both sand and clay, giving rise to both a high friction angle from the sand particles, and a non-zero apparent cohesion from the clay particles. The high values of apparent cohesion used are likely to result from the fact that the soil is actually *unsaturated* (a feature which is investigated further in Chapter 3). Other model parameters (detailed in Table 2.2) were kept constant, and values are given in Table 2.5. Stiffness values were derived from previous testing, detailed by Horncastle (2006).

Some combinations of Mohr-Coulomb strength parameters used here treat the soil as close to a Tresca type material (low angle of friction and high apparent cohesion, analogous to s_u) while other approximate the behaviour of a sharp sand type material, with almost no apparent cohesion and a high angle of friction. The lowest value of cohesion which it was possible to use was 75kPa, values lower than this resulted in collapse of the wall on removal of the formwork, and so analyses were not performed using lower values. A maximum value of 300kPa was used, which would represent an unconfined compressive strength of 0.6MPa for a Tresca type material. As the Mohr-Coulomb material model was used additional strength would be gained through frictional interlock. A cohesion value of 75kPa corresponds to a strong clay, while 300kPa would be expected for a weakly cemented rock. Friction angles of 25°, 35° and 45° were used, which correspond very roughly to a silty clay, a smooth and a sharp sand.

Increasing the Mohr-Coulomb parameters in the HS model has the effect of increasing the potential size of the elastic region upon full hardening, as perfectly plastic yielding occurs at the Mohr-Coulomb failure line. The ultimate (peak) shear strength of the material is determined by Equation (2.27), and obviously increases with both increasing apparent cohesion (c) and friction angle (ϕ')

Equations (2.29), (2.30) and (2.31) show how the stiffness of the material should be affected by changing the Mohr-Coulomb parameters. The secent stiffness (E_{50}) and unload/reload stiffness (E_{ur}) are controlled by the minor principal stress and the tangent stiffness for oedometer loading (E_{oed}) is controlled by the major principal stress. The exponent (m) was maintained at 0.5, recommended by Brinkgreve and Vermeer (2007) to model the behaviour of a sand type material.

Parameter	Meaning	Value	Units
E_{50}^{ref}	Reference primary deviatoric modulus	160	MPa
E_{oed}^{ref}	Reference primary volumetric modulus	150	MPa
E_{ur}^{ref}	Reference unload/reload modulus	460	MPa
m	Stress dependent stiffness	0.5	
c_{ref}	Apparent cohesion	Varied	kPa
ϕ'	Angle of friction	Varied	degrees
ψ	Dilatancy angle	20	degrees
γ	Unit weight	24	kPa

Table 2.5 Hardening Soil model parameters used

2.5.3.2 Compaction

The layered nature of compaction of rammed earth means that the compaction applied to the layer is not homogeneous and that a variation in density occurs from the top to the bottom of a layer. The difference in density manifests itself as weaker horizontal layers within a rammed earth wall, along which failure is more likely to occur.

Compaction of modern rammed earth is generally achieved using a vibrating hammer, with a small foot impacting the soil. Historic rammed earth was usually compacted manually, using a slower vibrating action. The size of the foot ensures that material is able to flow around the foot when close to maximum compaction. Compaction reduces the volume of the sample, increasing the density and reducing the void ratio. An increase in density in soil mechanics is usually linked to an increase in bulk stiffness, seen as volumetric hardening. As rammed earth compaction is performed in layers, it is likely that the lower previously compacted layer is of greater stiffness (having hardened) than the topmost layer which is undergoing compaction. Therefore the topmost layer will reduce in volume and increase in stiffness until of equal stiffness to the layers below.

Modelling of compaction using Plaxis was achieved through the application of an applied 10mm displacement across the full length of the wall, with compaction also applied to the 'formwork' at both ends. This simulates volumetric compression of the sample, and should lead to volumetric hardening as shown in Figure 2.10. This volumetric hardening should 'push out' the yield cap, as shown in Figure 2.12, giving each different layer different cap positions.

2.5.3.3 Behaviour of the HS model

The model accurately captured the volumetric hardening behaviour of the rammed earth on compaction, but was not tuned to quantitatively record the behaviour as described in Sections 2.4.5.2 and 2.4.5.3. A major shortcoming of the fixed applied displacement was the fact that the applied strain varied greatly with increasing height of the wall. Thus a 10mm compaction to the base layer (100mm wall height) provides a 10% strain, while a 10mm compaction to the top layer of the wall (1000mm wall height) provides only a 1% strain. However this is considered to be more realistic, as each compacted layer acts as almost rigid in comparison to the loose soil about to be rammed above.

Figure 2.41 shows vertical displacement of the top of each (odd numbered) layer through compaction of the whole wall. The final position represents a summation of the amount of plastic deformation and elastic deformation due to self weight. This figure shows that the base layers recover the most and the top layers recover the least, with the base layer (1) undergoing only 2mm of permanent deformation, and the top layer undergoing 5mm of permanent deformation.

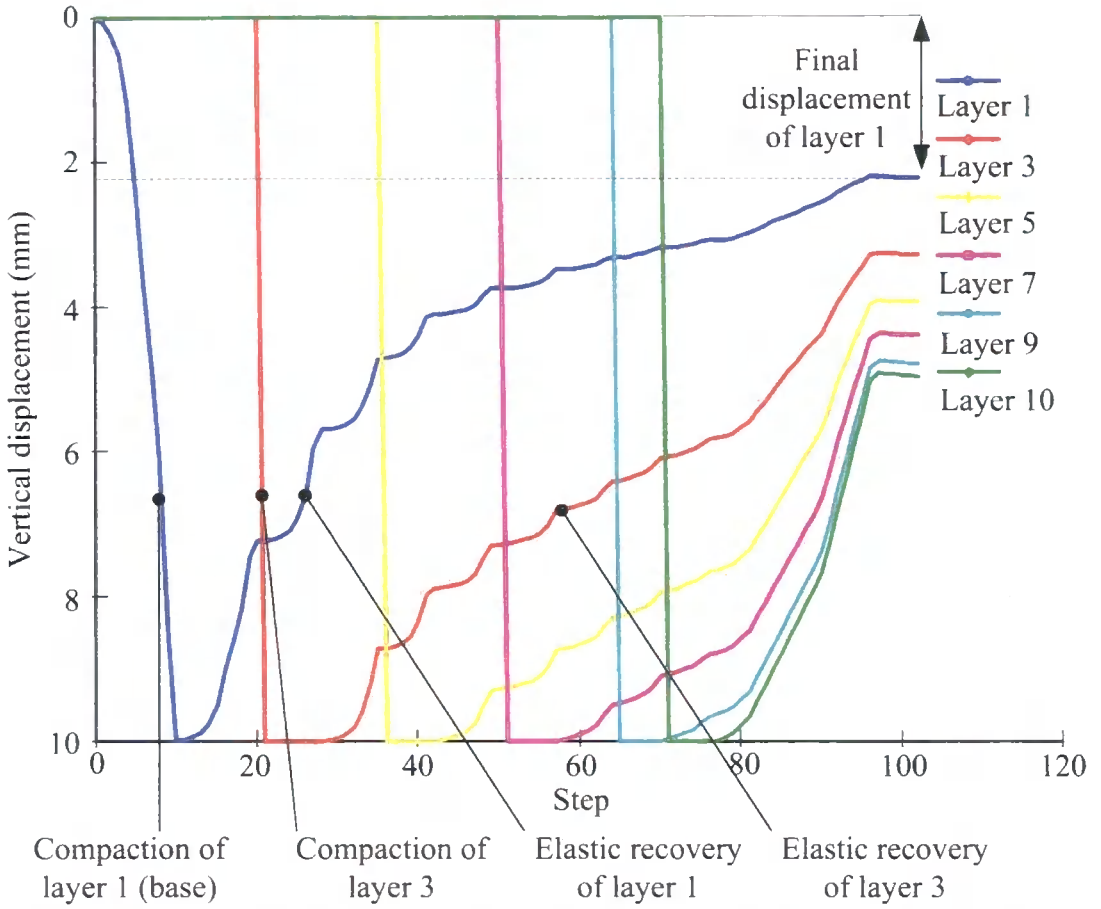

Figure 2.41 Vertical displacement of odd layers and layer 10 during compaction process

$$\phi = 25°, c = 40\text{kN/m}^2$$

Figure 2.42 shows the vertical and horizontal stresses at the top of the layers on compaction of the wall. It may be observed that both the vertical and horizontal stresses in the base layer are significantly larger than those in the subsequently compacted layer. This may be explained by considering the hyperbolic volumetric hardening behaviour described by Equation (2.30), and that as an applied displacement must be reached, a large force must be applied in order to achieve that displacement. This large increase in stiffness may be seen in Figure 2.43, where the large volumetric and corresponding shear stress applied to the base layer may be seen in comparison to that applied to the subsequent layers. This high stress (200MPa) is unrealistic and should be ignored.

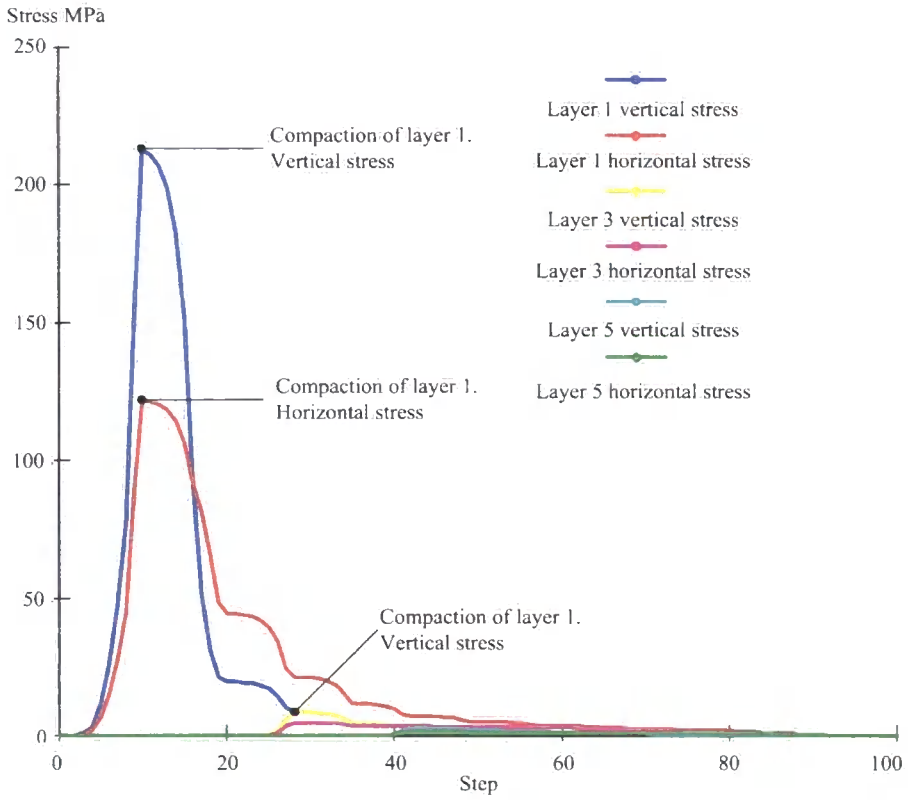

Figure 2.42 Horizontal and vertical stresses on compaction $\phi = 25°, c = 40\text{kN/m}^2$

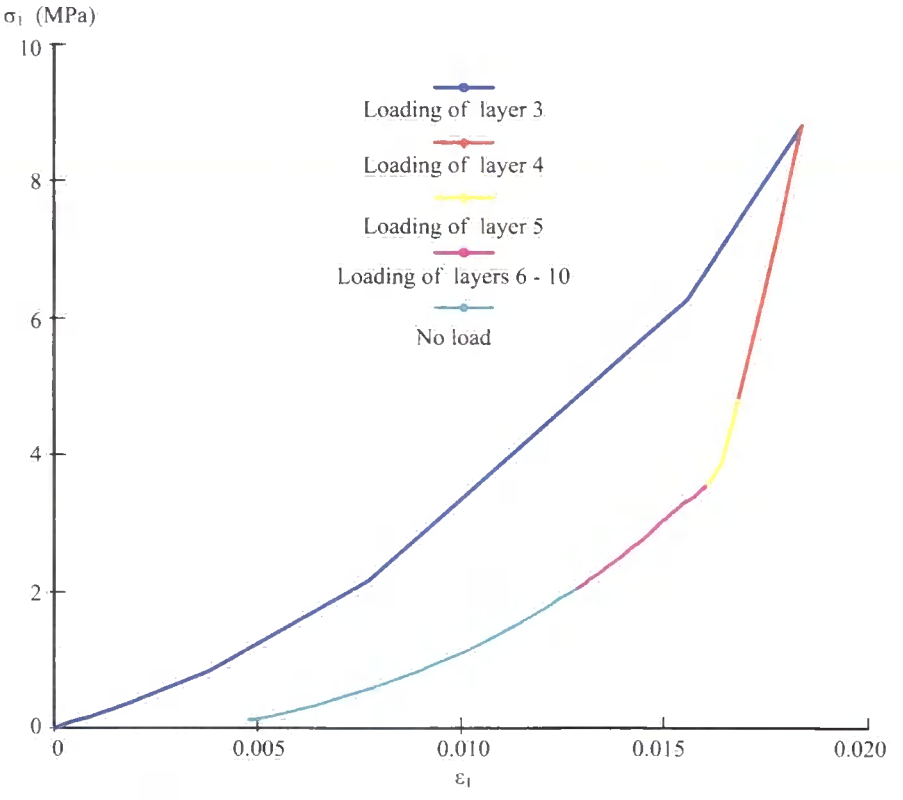

Figure 2.43 Volumetric hardening behaviour on compaction $\phi = 25°, c = 40\text{kN/m}^2$**. Compare to Figure 2.10.**

Figure 2.44 shows shear hardening behaviour on compaction. The third compaction layer is shown as an example, and shows (q, ε_1) behaviour on compaction of the layer and loading of subsequent layers. Shear hardening occurs on the initial loading of each layer through the shear stresses induced by the different horizontal and vertical stresses on loading (e.g Figure 2.45). Upon loading of the subsequent layer, the shear stresses are reduced and the layers are allowed to volumetrically expand elastically, which explains the reduction in ε_1. The change in direction of the deviatoric stress may be explained by the changing magnitudes of the horizontal and vertical stresses. On initial compaction of the layer the vertical stresses exceed the horizontal stresses, but these reduce on compaction of subsequent layers until they are equal, at which point the deviatoric stress is equal to zero (Figure 2.45 and Figure 2.46). On compaction of further layers, the vertical stress further reduces leading to an increase in deviatoric stress, until the initial compaction line is reached, at which point the deviatoric stress also reduces to zero.

Unfortunately, on compaction of the base layer, the Mohr-Coulomb failure surface has been exceeded, and perfectly plastic yielding has occurred, which can be seen in Figure 2.46. The combination of normal and shear stresses will cause failure and plastic yielding through the exceeding of the Mohr-Coulomb criterion, but the fully contained nature of the problem means that no failure mechanisms are able to form, and the problem is then simply one of perfect plasticity.

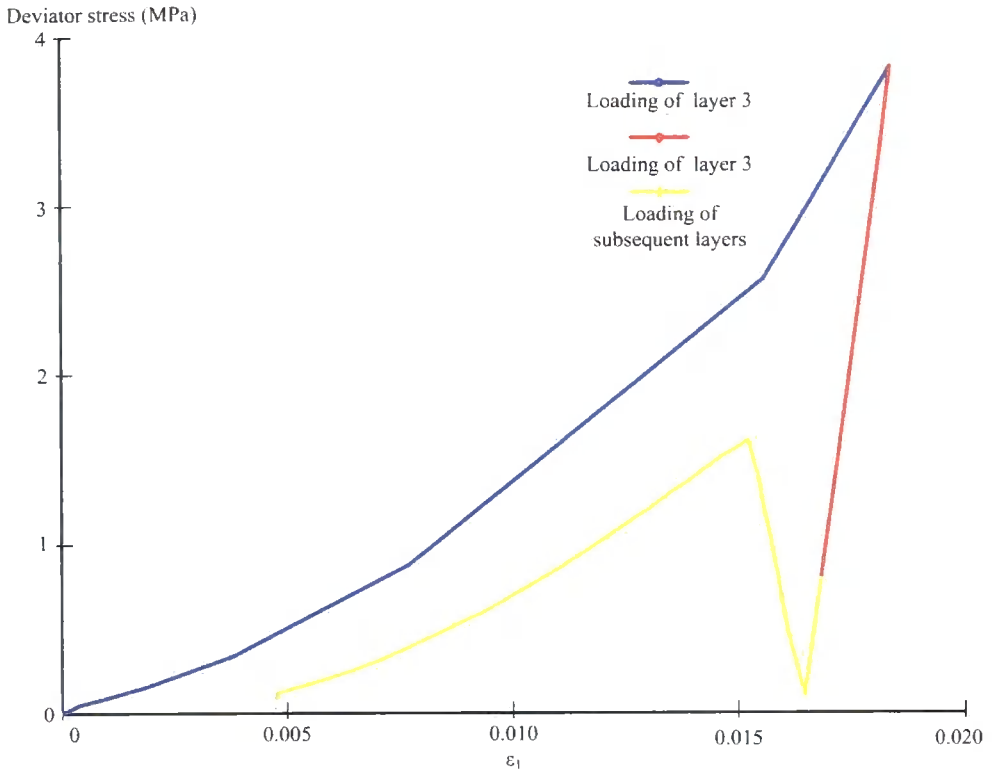

Figure 2.44 Shear hardening behaviour, layer 3 $\phi = 25°, c = 40\text{kN/m}^2$

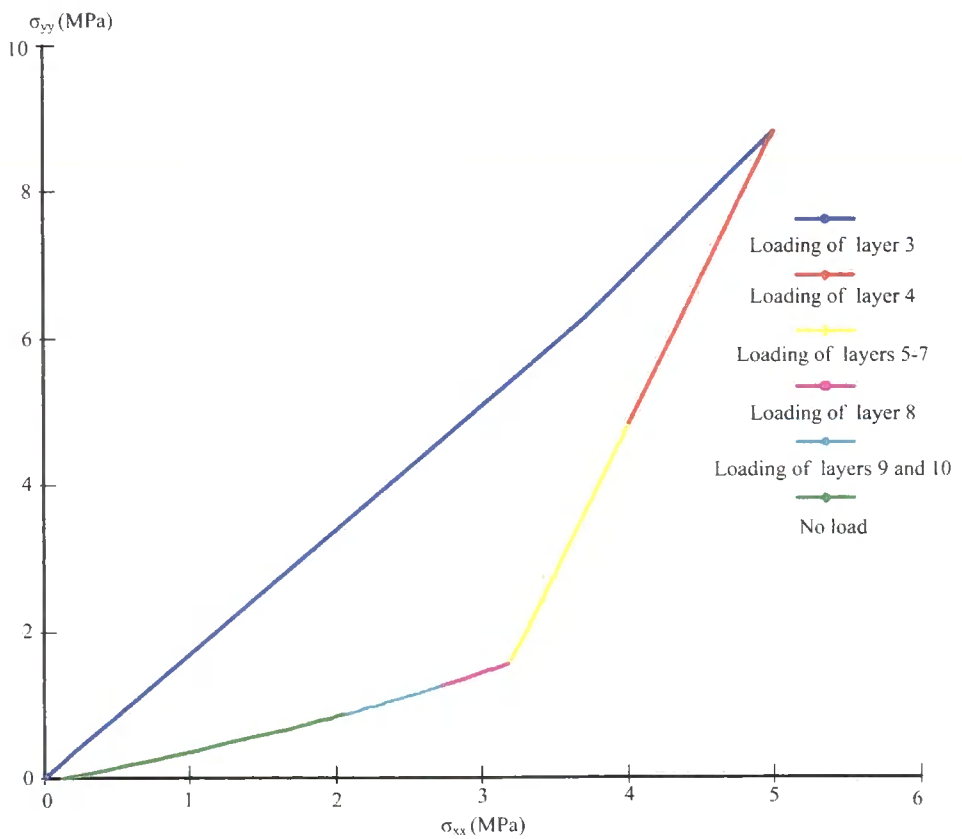

Figure 2.45 Horizontal and vertical stresses on compaction, layer 3 $\phi = 25°, c = 40\text{kN/m}^2$

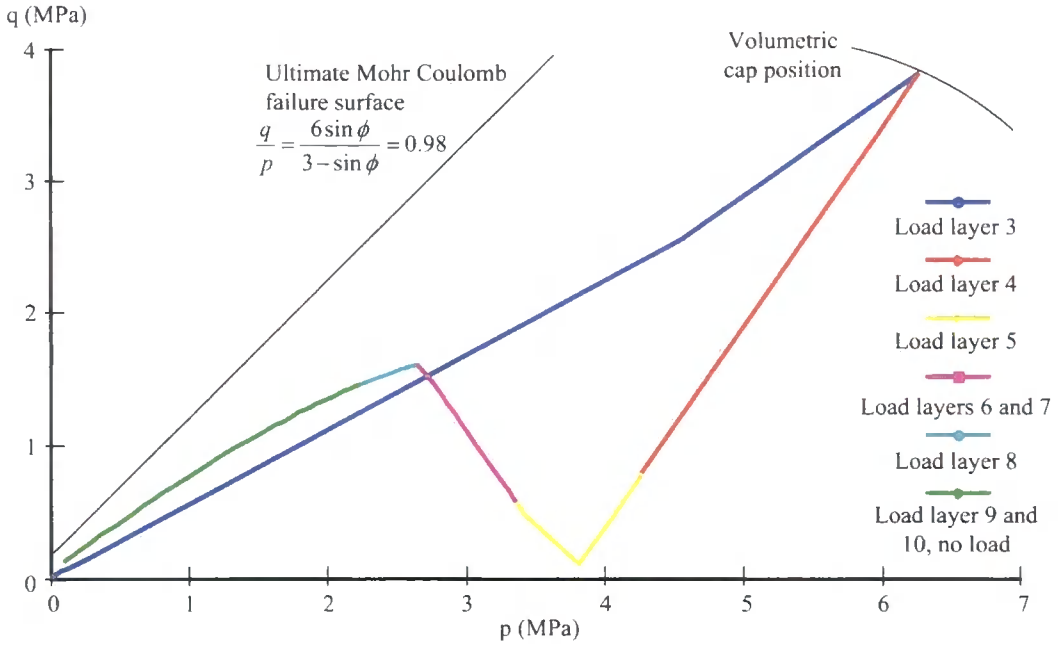

Figure 2.46 p-q behaviour on compaction $\phi = 25°, c = 40\text{kN/m}^2$

2.5.3.4 Removal of the formwork

The removal of the formwork is critical in rammed earth construction. If the rammed earth is too weak on removal of the formwork, the resulting wall may deform excessively. The manner of removal of formwork is discussed in Section 2.4.4 but for this series of analyses, it is assumed that the formwork simply disappears.

The wall has been modelled as fixed at the base. This is a reasonable assumption given that there is friction between the wall at its foundation. However in the finite element model displacements are limited to zero in the horizontal direction, whereas it is possible that a real wall will displace horizontally, working against the wall-foundation interface friction. Vertical stresses are a result only due to self weight, and horizontal stresses increase from a maximum at the centre to zero at the vertical sides of the structure.

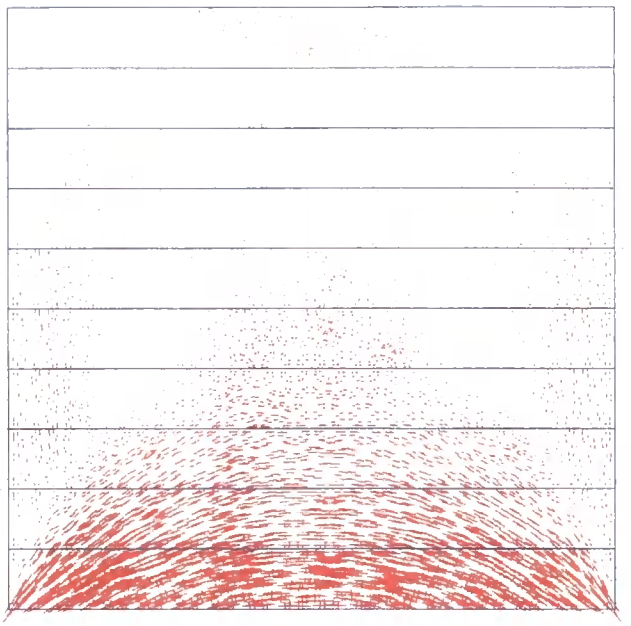

Figure 2.47 Principal stress distribution on removal of the formwork. Extreme total principal stress 430kN/m². $\phi = 25°, c = 40\text{kN/m}^2$

2.5.3.5 Loading

The processes of compaction and removal of the formwork, the loading of the wall is now described. The general failure mechanism observed for all walls is first described, using a sample wall with Mohr-Coulomb parameters of $\phi = 25°, c = 40\text{kN/m}^2$ in addition to those parameters described in Table 2.5. A parametric study of changing friction angle and cohesion was then carried out, and the results of parametric study are then compared with the physical testing which was described in Section 2.4.5 to give an indication of the friction angle and cohesion which may be expected for the walls.

The model was loaded using an applied displacement at the centre, over a length of 60mm to simulate the loading of Walls 1 and 2.2. The applied displacement was increased until failure of the soil body occurred. Figure 2.51 to 2.63 show the development of plastic points for a sample wall model with Mohr-Coulomb parameters $\phi = 25°, c = 40\text{kN/m}^2$. Figure 2.50 is a legend for the different types of plastic points developed during loading. Observation of the development of elements

which are behaving plastically is useful in describing the behaviour of loaded walls, as cracking cannot be directly viewed using continuum finite element modelling. In these analyses perfectly plastic behaviour occurs when the Mohr-Coulomb failure criterion is satisfied in an element. Cracking and failure of a wall may be assumed when a sufficient number of plastic points are present to allow formation of a mechanism, leading to collapse of the soil body.

Figure 2.49 shows the shear stress behaviour of an element in the centre of layer 8, and indicates the peak strength of the element has been reached at a compressive displacement of 1mm. This behaviour would be repeated in the other elements shown in red in Figure 2.51, which represents elements which have reached the Mohr-Coulomb failure criterion according to Equation (2.27). The behaviour of such elements is shown in Figure 2.48. Shear hardening is also experienced by those elements coloured green in Figure 2.51. Failed elements do not extend through the full wall, and as such a mechanism cannot form at an applied displacement of 1mm.

As the load is increased, the shear stress in the wall increases, leading to failure of more elements. When the failed elements reach the edge of the wall, as can be seen in Figure 2.52, then cracking and collapse would occur. Rigid block type movement, such as can be seen in Figure 2.24 may be observed by considering Figure 2.54 where the base triangle remains static while the two triangular elements above move outwards.

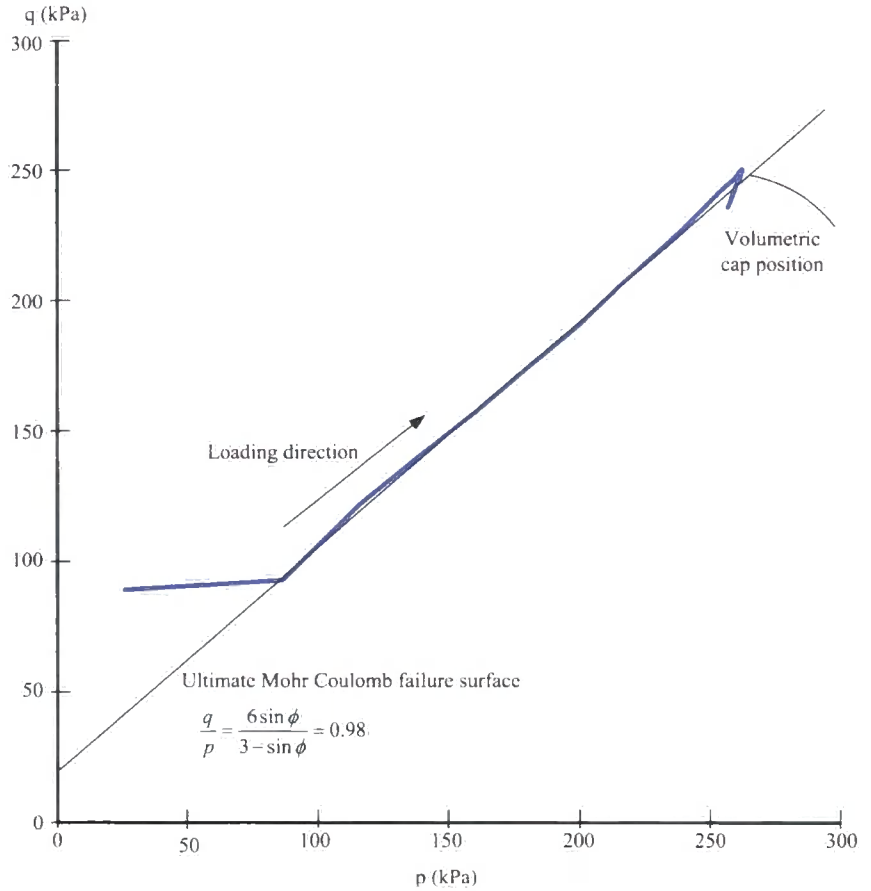

Figure 2.48 $p' - q$ **graph showing perfectly plastic behaviour following reaching of Mohr Coulomb failure surface. Layer 8 centre** $\phi = 25°, c = 40\text{kN/m}^2$.

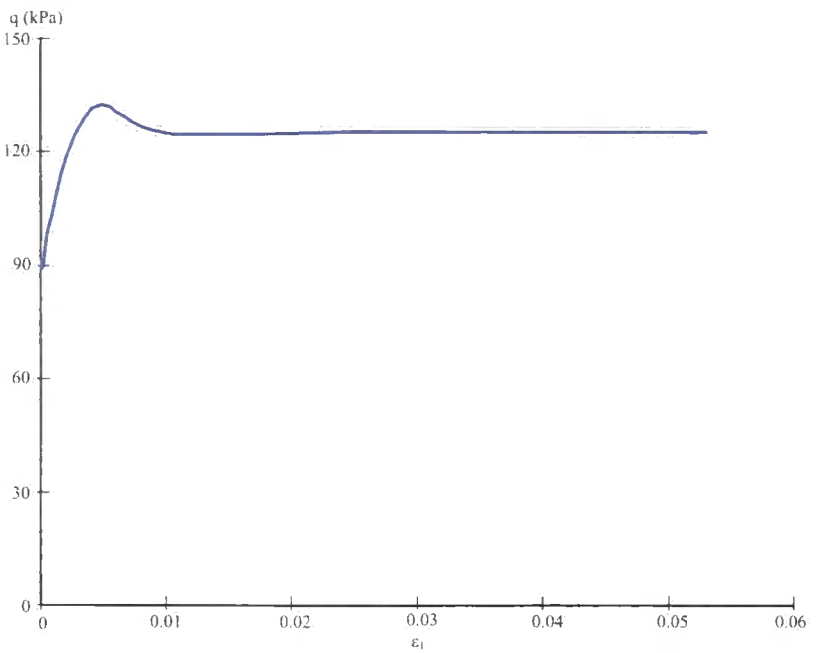

Figure 2.49 Shear behaviour. Layer 8 centre. $\phi = 25°, c = 40\text{kN/m}^2$

Mohr Coulomb failure
Volumetric and shear hardening
Volumetric hardening
Tension cut off
Shear hardening
Not yielded

Figure 2.50 Legend for plastic points in HS model (Figure 2.51 to Figure 2.63)

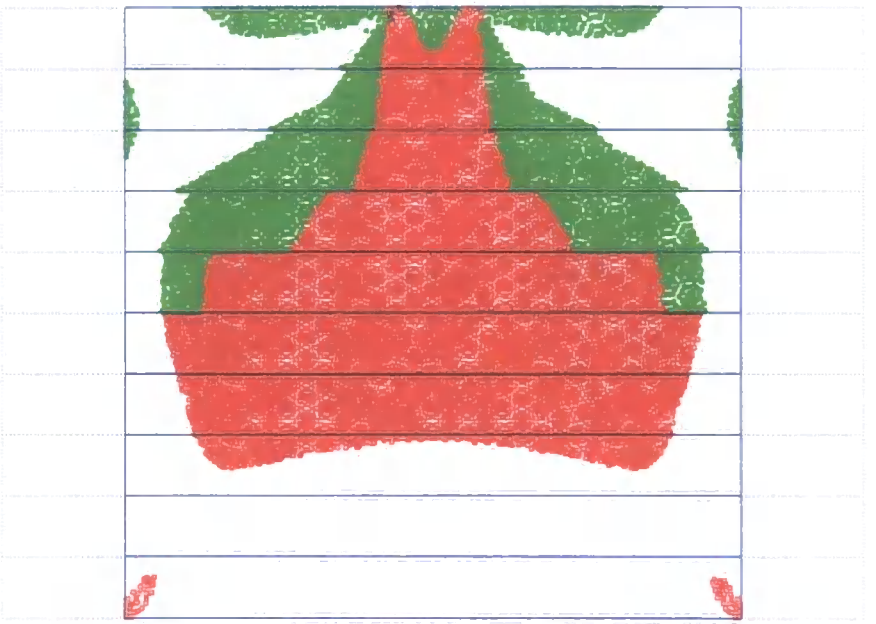

Figure 2.51 Development of plasticity on loading. 1mm applied displacement. Mohr Coulomb parameters of $\phi = 25°, c = 40kPa$

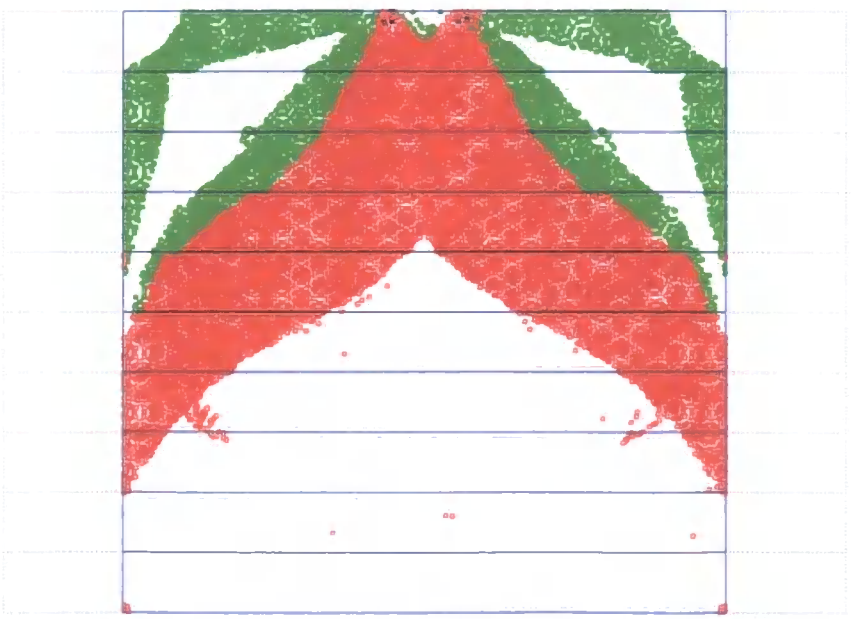

Figure 2.52 Development of plasticity on loading. 5mm applied displacement. Mohr Coulomb parameters of $\phi = 25°, c = 40kPa$

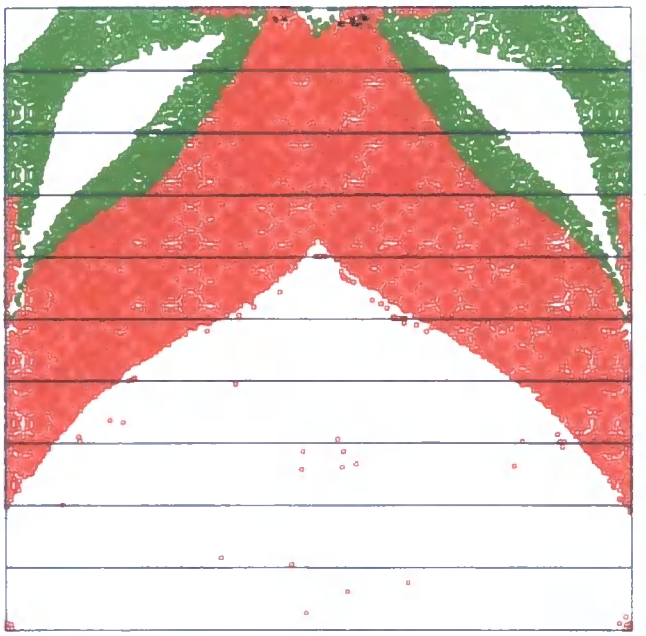

Figure 2.53 Development of plasticity on loading. 14mm applied displacement. Mohr Coulomb parameters of $\phi = 25°, c = 40kPa$

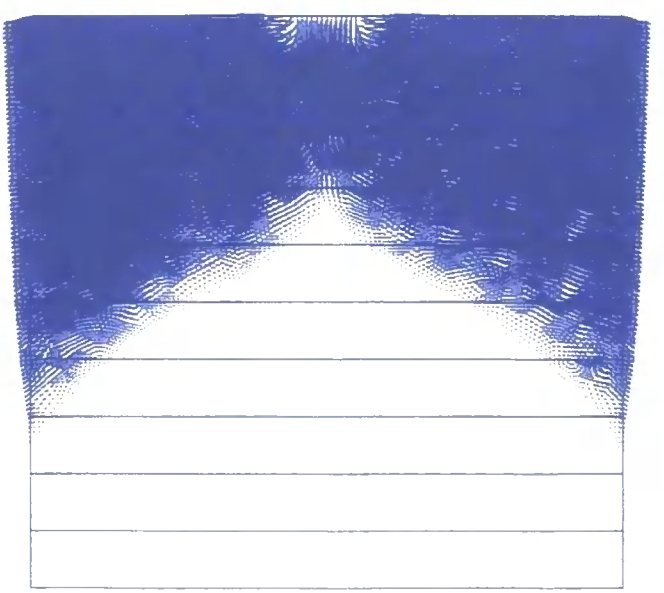

Figure 2.54 Example total displacement vectors on loading. Maximum displacement = 0.84mm. Mohr Coulomb parameters of $\phi = 25°, c = 200kPa$

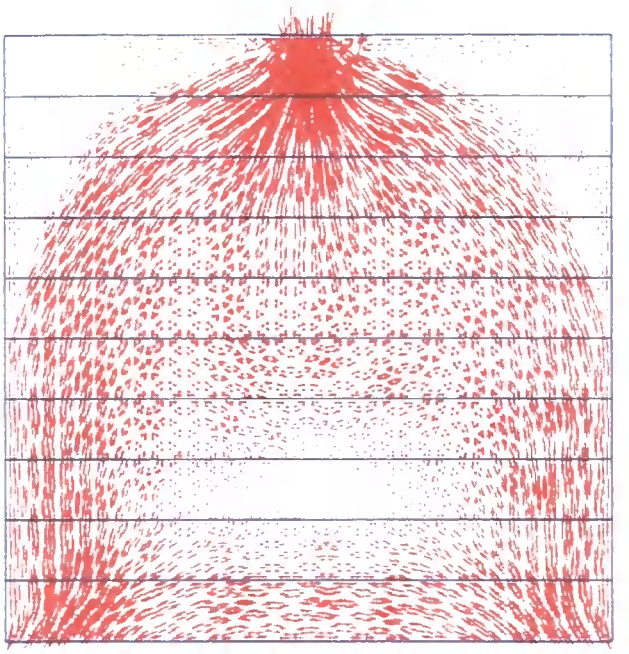

Figure 2.55 Maximum and minimum principal stress vectors at 14mm displacement. Peak applied pressure = 0.86MPa. Mohr Coulomb parameters of $\phi = 25°, c = 200kPa$

Figure 2.56 to Figure 2.60 show the final plastic points at a prescribed displacement of 12mm for varying values of cohesion and a constant friction angle of 35°. It can be observed that the distribution of plastic points is broadly similar for the range of cohesion values, with the Mohr-Coulomb failure surface being reached at many points in the wall. The formation of wide 'shear bands' in an inverted Y shape follows the cracking pattern as observed in laboratory testing (Figure 2.25 and Figure 2.26) and appears to be almost independent of cohesive strength. Formation of these shear bands would lead to rigid block movement of the upper left and right section of the wall. For high values of cohesion ($c = 250$ and $c = 300$ kPa) the shear bands do not reach the edge of the wall, and as such the wall may be considered to still be functioning even at this extreme displacement.

Figure 2.56 Distribution of plastic points on loading of wall. Applied displacement = 12mm. Mohr Coulomb parameters $\phi = 35°, c = 75kPa$

Figure 2.57 Distribution of plastic points on loading of wall. Applied displacement = 12mm. Mohr Coulomb parameters $\phi = 35°, c = 150kPa$

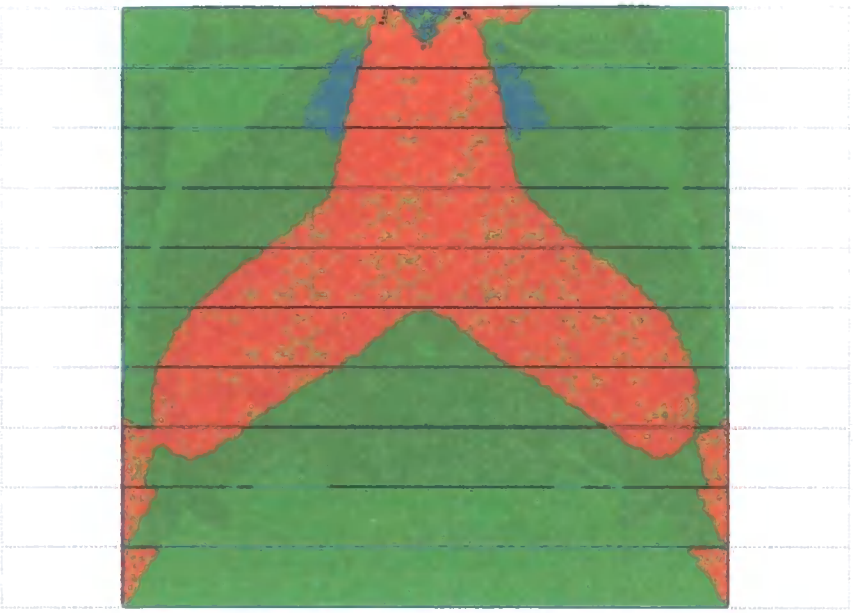

Figure 2.58 Distribution of plastic points on loading of wall. Applied displacement = 12mm. Mohr Coulomb parameters $\phi = 35°, c = 250kPa$

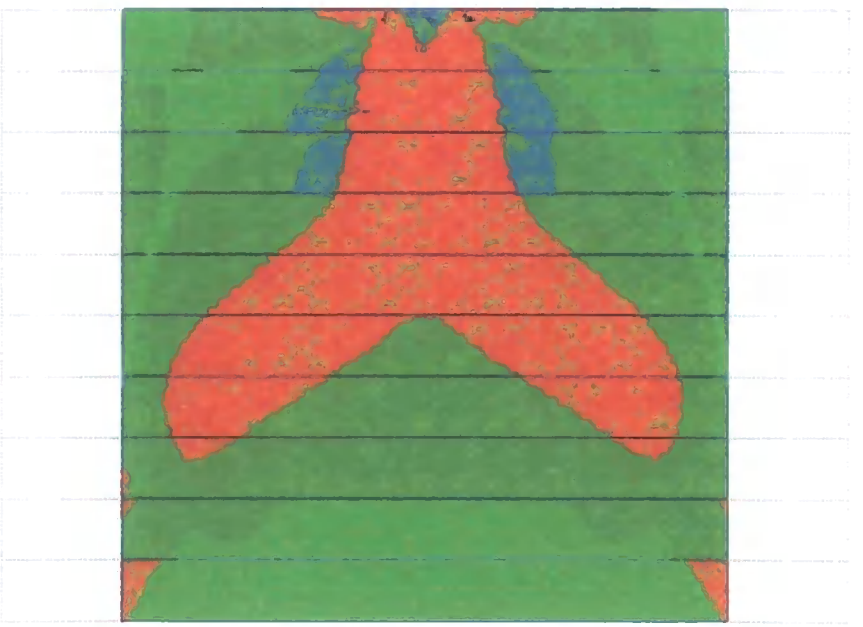

Figure 2.59 Distribution of plastic points on loading of wall. Applied displacement = 12mm. Mohr Coulomb parameters $\phi = 35°, c = 300kPa$

Figure 2.57, Figure 2.60 and Figure 2.61 show the distribution of plastic points at 12mm displacement for constant cohesion value of 150kPa and varying angles of friction (35°, 25° and 45° respectively). Here the different shapes of the shear bands are apparent, with a friction angle of 25° producing higher broad shear bands, at an angle close to 25°, which diverge from each other 600mm from the base of the wall, and intersect the vertical faces around 150mm from the base. This is a sharp contrast to a friction angle of 45°, where the shear bands diverge from each other lower down the wall (500mm from the base) and travel at 45° to intersect the wall at the base. In all three cases, a steepening of the angle of the shear band is seen close to the edge of the wall. The shape of the shear bands directly below the loading point also vary considerably with changing angle of friction, and appear to be approximately double that of the lower section. Thus for a friction angle of 25°, the angle of the shear band directly below the loading point is close to 50°, whereas for a friction angle of 45°, the angle is approximately 90°.

A comparison between the failure of the walls tested in the laboratory (photographs Figure 2.24 and Figure 2.25, diagram Figure 2.26) and the formation of shear bands modelled using finite elements (Figure 2.56 to Figure 2.61) would lead to the conclusion that the angle of friction of the walls studied in the laboratory is closer to 50°, which is the angle at which the cracks appear to travel on failure of the laboratory walls. Side A of Wall 2.2 (Figure 2.24) showed a small out-of-plane failure below the loading point, also running at 50°, indicating that perhaps this angle of friction is constant on this side of the wall. However, side B of wall 2.2 (Figure 2.25) showed a larger region of out-of-plane failure below the loading point, with an increased angle at the face, closer to 85°. This is consistent with the upper and lower angle change as described above, where the angle of the shear band directly below the loading point is approximately double that once the shear bands diverge.

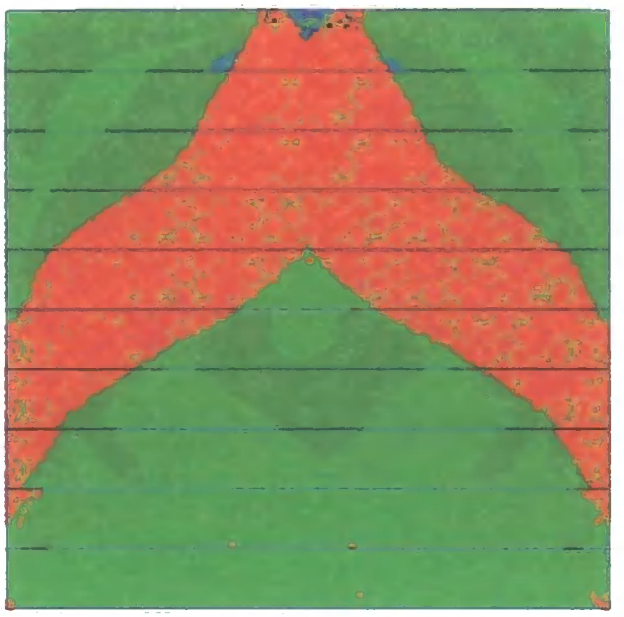

Figure 2.60 Distribution of plastic points on loading of wall. Applied displacement = 12mm. Mohr Coulomb parameters $\phi = 25°, c = 150kPa$

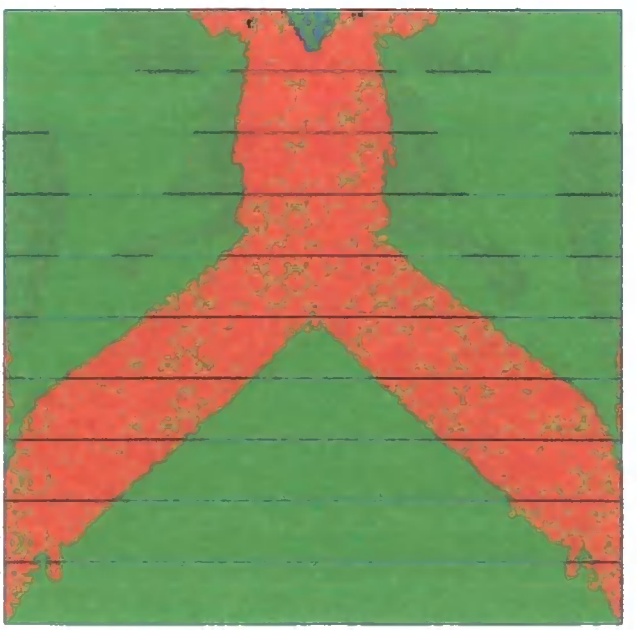

Figure 2.61 Distribution of plastic points on loading of wall. Applied displacement = 12mm. Mohr Coulomb parameters $\phi = 45°, c = 150kPa$

Figure 2.62 and Figure 2.63 shows the maximum principal stress at failure of the wall, and can be considered as the ultimate strength of the wall. This shows that the maximum vertical stress which a wall can sustain prior to failure increases with increasing Mohr-Coulomb properties. Three curves are shown, for friction angles of $\phi = 25$, $\phi = 35$ and $\phi = 45$ for different values of cohesion. Figure 2.62 shows the cohesion range from $c = 0$ to $c = 100$ and Figure 2.63 shows the range from $c = 0$ to $c = 300$. In Figure 2.62 the wall strength are identical in the range $c = 0$ to $c = 50$ for $\phi = 25$ and $\phi = 35$, with $\phi = 45$ strength being slightly increased. At a cohesion of $c = 100$ the $\phi = 35$ line 'overtakes' the $\phi = 45$ line and the $\phi = 35$ walls continue to exhibit higher failure loads in the range $c = 0$ to $c = 300$. This was unexpected and further work should be undertaken to establish the exact cause of this. It is thought that reason for the increased strength may be due to the differing patterns of failure between $\phi = 25$ (Figure 2.60), $\phi = 35$ (Figure 2.57) and $\phi = 45$ (Figure 2.61). At $\phi = 25$ there is a large region of material which has yielded and is acting perfectly plastically (shown in red), whereas at $\phi = 45$ the yielded material described a much tighter inverted Y shape, and the $\phi = 35$ wall falls somewhere between.

The ultimate strength of a similar wall tested in the laboratory (Wall 2.2) was 0.71MPa, which can be seen to correspond to a cohesion value of 35kPa for friction angles of 25° and 35°, and a cohesion value of 27 kPa for a friction angle of 45°. The cracking pattern observed in Wall 2.2 is most similar to the 45° pattern of points at failure (red in Figure 2.61), so it is assumed that a reasonable set of Mohr-Coulomb parameters for the modelling of Wall 2.2 is $\phi = 45$, $c = 27$.

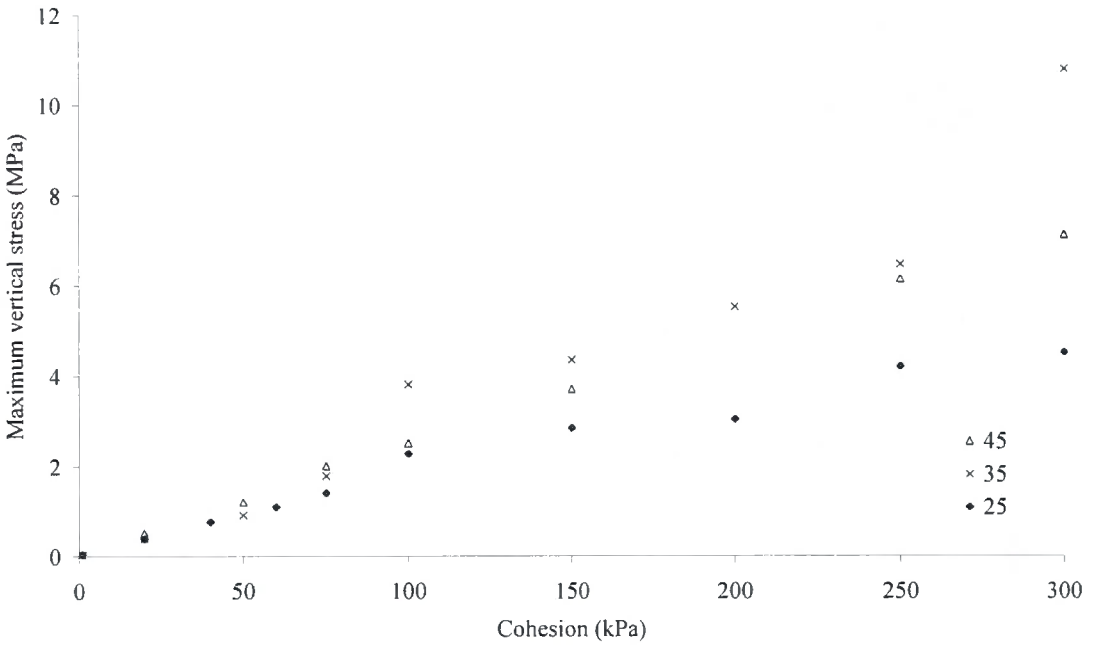

Figure 2.62 Maximum vertical stress at 14mm applied displacement for different cohesion values from zero to 100kPa.

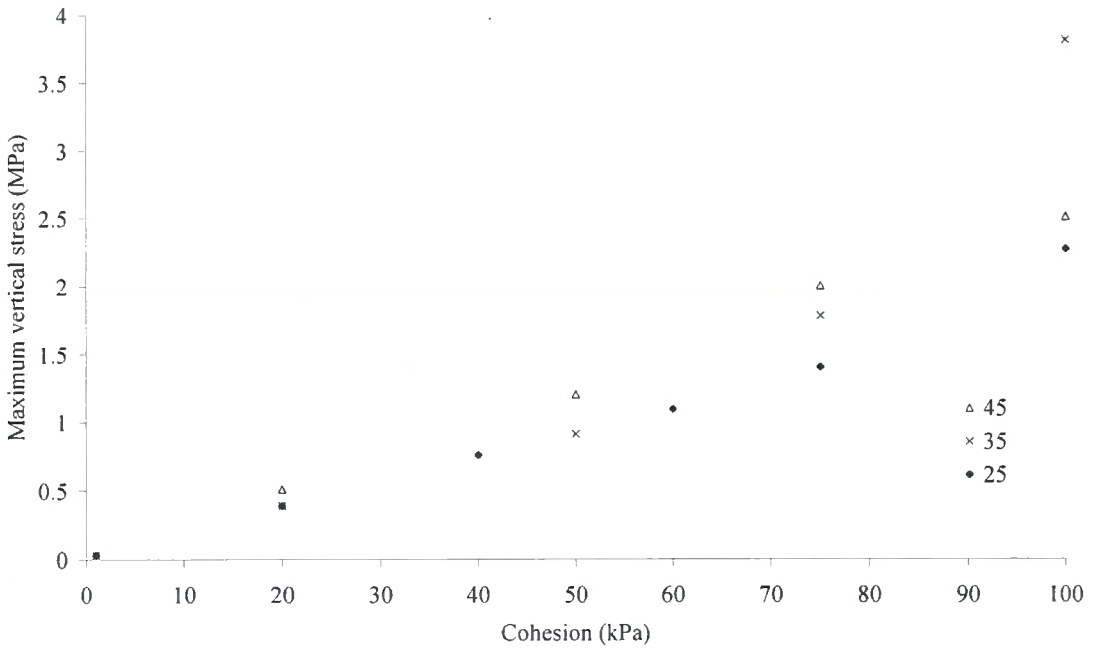

Figure 2.63 Maximum vertical stress at 14mm applied displacement for cohesion values from zero to 350kPa.

2.6 Evaluation of numerical modelling

The two modelling strategies presented aim to capture some of the in-plane behaviour of rammed earth. The small number, and different geometries of the physical testing, meant that the behaviour observed was not repeatable and results were very specific. Because of this the modelling was deliberately simple, aiming to probe the methods which could be used, rather than to provide definitive expressions of the behaviour of rammed earth.

2.6.1 Mohr-Coulomb layered model

Table 2.6 shows the parameters required for failure of each of the walls. It can be seen that the strength of the rammed earth always exceeds that of the layer, and that the properties required for Walls 2.1, 2.2 and 4 are broadly similar. Wall 5 required reduced properties, and it is considered that this is due to a tension crack initially appearing at the base of the wall which did not actually cause failure. The most relevant properties are those in the failed region, and these are shown in bold in Table 2.6. However some of the properties required increasing in order that failure did not occur in that regions, so for example the layer properties of Wall 2.2 and Wall 5 are greater than those required to cause failure in Walls 2.1 and 5 (Equation (2.27)). This highlights the fact that the combination of shear angle and value of cohesion can be devised to match a given shear strength is not unique.

The use of the Mohr-Coulomb failure criterion to model the interface layer has been presented on the grounds that the shear strength of the layer is proportional to the normal load across the layer. This method allows the modelling of the decrease in shear strength across the compaction layer with increasing building height. The ability to model both full lifts and compaction layers means that both modern and historic rammed earth can be analysed, and layers of lime, brick or stone, such as are found in historic structures (see Chapter 4) can also be incorporated into the model. However prediction of failure through delamination requires a careful choice of parameters for the compacted layer, and these parameters may not actually accurately represent the properties of the layer.

2.6.2 Hardening Soil model

The Hardening Soil model is a slightly more advanced formulation than the layered Mohr-Coulomb described above. This allows the use of a hyperbolic stress strain curve, with the stiffness depending on the stress level and a volumetric yield cap. The HS formulation was used to model the compaction, formwork removal and loading of rammed earth. Wall 2.2 was modelled and a parametric study of the Mohr-Coulomb parameters (ϕ and c) required to accurately model the behaviour of the wall was carried out.

Compaction of the rammed earth was modelled by applying a fixed displacement to the topmost surface of the wall. This induced stresses in the wall, which were different for each layer because of each layer's different stiffness due to the hardening behaviour. This is thought to be similar to the physical compaction of rammed earth, where a layer is highly compacted before the next layer is placed. On being compacted a layer reduces in volume and increases in stiffness, until a minimum volume and maximum density is reached (see Figure 2.1). The Hardening Soil model is able to model this type of behaviour, but the application of a fixed displacement meant that the compaction of the base layer was artificially high, leading to greatly inflated stresses (Figure 2.45). However with a more precise choosing of the parameters for compaction, it is thought that the HS layer could be used to accurately model compaction.

The removal of the formwork and loading was then discussed. The general failure mechanism which occurred in the models was outlined, and this is broadly similar to that observed in the physical walls discussed in Section 2.4. A parametric study of the Mohr-Coulomb parameters was carried out to determine if the behaviour of Wall 2.2 could be modelled. It was not possible to model Wall 2.2 extremely accurately because the displacement was not measured, therefore only the failure load and cracking pattern were used to determine which parameters would be most appropriate. It was found that parameters of $\phi = 45°$ and $c = 27kPa$ would approximate the behaviour of the model to the behaviour observed during physical testing.

2.6.3 Conclusions

The physical walls constructed and tested highlighted the layered nature of rammed earth and the importance of water content and mix design on behaviour at both compaction and testing.

The numerical models showed that it is possible to used techniques available to practising engineers to represent rammed earth. The Mohr-Coulomb criteria was used at the interface layer because it was assumed that the strength of the interface layer was proportional to the normal load across it. This may prove useful for the modelling of *males* which are described in Chapter 4. The body of the rammed earth was also assigned a Mohr-Coulomb yield criteria with properties reflecting those of the wall. Further work may make use of a different criteria for the rammed earth part. The Hardening Soil model was used to portray compaction of the rammed earth within formwork. The increased stiffness within increasing volumetric stress represents the behaviour of rammed earth layers being compacted. Although this modelling used an applied displacement at each layer, it is considered that it may be more realistic to instead apply a fixed strain to model compaction of layeres of rammed earth. To accurately model compaction of rammed earth further physical and numerical modelling is required.

The parametric studies of Mohr-Coulomb parameters were used to chose parameters such that the behaviour of the model matched the physical behaviour observed. This also occurs in the modelling of historic buildings where material properties are generally unknown. Table 2.6 shows the parameters required to match the behaviour to that observed, and Table 2.7 shows a range of values for different soils and rammed earth rests for comparison. This shows that the rammed earth in the walls may be seen as having a friction angle (ϕ) equivalent to that of a sand, and a cohesion (c) of a clay, as justified by its particle size distribution, shown in Figure 1.2.

The plane strain assumption was used for both of simulations carried out, and in Section 2.5.1.1 it was argued that this assumption may be considered valid for the compaction of rammed earth within formwork. However, justification of the plane strain assumption is more problematic when considering loading of walls. A plane

stress approach means that the out-of-plane stress is considered zero $(\sigma_z = 0)$ meaning the peak load would be lower than that in plane strain, and that an artificially low cohesion value may have been obtained by analysing in plane strain. A full 3D analysis, taking into account out-of-plane movement, would result in a much more accurate representation of the material properties required to model rammed earth.

Both the physical and numerical modelling have highlighted the fact that many material properties of rammed earth depend on the water content. The strength and stiffness properties of wall being compacted are very different to those of a dry wall. Chapter 3 therefore looks at the role of water within rammed earth, showing that both the strength and stiffness properties may be explained by treating the material as an unsaturated soil.

Wall	**Failure stress (MPa)**	**Failure mode**	ϕ	c **(kPa)**	ϕ_{layer}	c_{layer} **(kPa)**
Layered						
2.1	0.610	Delamination	45	150	**45**	**20**
2.2	0.710	Shear	**45**	**150**	45	35
4	0.042	Delamination	45	150	**45**	**10**
5	0.610	Shear	**45**	**150**	45	20
HS						
2.2	0.710	N/A	**45**	**27**		

Table 2.6 Required parameters for finite element models

Material	ϕ	c **(kPa)**
Stiff Clay Craig 2002)	25-35	100-150
Dense Uniform Sand (Craig 2002)	45	0
Rammed earth Shear box (Howard 2007)	40	36
Rammed earth Triaxial (Horncastle 2006)	30-40	75-230

Table 2.7 Mohr-Coulomb parameters for comparison

Chapter 3

Advanced testing and modelling

3.1 Introduction

Classical soil mechanics is well suited to a wide range of geotechnical engineering problems. The use of simple formulae and experience based safety factors leads to efficient design of geotechnical structures and can be used to predict the behaviour of a wide range of soil types under different loading conditions. However there are situations where classical soil mechanics cannot accurately predict the behaviour of a body of soil (as described by Jennings and Burland 1962). This usually occurs when the soil becomes unsaturated, that is there is a mixture of air and water within the pores of the soil, and the pore water within the soil is not continuous. Menisci form between the soil particles and these add to the strength of the soil when it is in its unsaturated state. This source of strength is lost when the soil becomes fully saturated or completely dry. Geotechnical engineering examples of this phenomenon include rainfall-induced landslides, where a slope initially unsaturated, becomes saturated at the surface due to intense rainfall and loses strength causing a landslide. A simpler example is the sandcastle whose strength cannot be accounted for by saturated soil mechanics and Schiffer (2005) and Nowak, Samadani et al. (2005) argue that the unsaturated nature of these simple structures must be taken into account. It is in this light that rammed earth, and other types of earthen architecture must be considered as unsaturated soils.

This chapter first outlines the concepts of tensile strength of water and of surface tension. The notion of suction is outlined by explaining the phenomenon of capillary rise which is then linked to the relative humidity of the surrounding air. Suction in soil mechanics is then explained and the concept of equilibrium pore radius defined. The idea of a liquid bridge is outlined and the attractive force across the liquid described. The volume of water held within a soil due to suction is then described through the idea of a Soil Water Characteristic Curve.

The differences between the behaviour of saturated and unsaturated soils; and ideas for the conceptualisation of unsaturated soils are described, highlighting the double structure theory and evidence of liquid bridges. Constitutive models which distinguish between the behaviour of saturated and unsaturated soils are then outlined.

The origins of strength in rammed earth are discussed. Rammed earth practitioners disagree on the reasons for strength in the construction material (for example King 1997; Norton 1997 and Houben and Avrami 2000), and attempts are being made in the field of unsaturated soil mechanics to quantify the magnitudes of the different actions. Electrostatic actions such as van der Waals forces and Double Layer attraction are combined as DLVO theory, and it is shown that it is suction rather than DLVO forces which provide additional strength to highlight unsaturated soils such as rammed earth. Cementing is briefly introduced to later explain why there is an optimum cement content for stabilised rammed earth building.

A short series of unconfined compression tests were carried out, where suction was measured to establish a link between sample strength and suction. Tensiometers were introduced as a way of measuring suction. The testing procedure, and the way in which issues in the experimentation were resolved are described.

As a result of the experimentation is it possible to describe the relationship between a number of the measured parameters such as water content and strength. A change in suction on loading; and the increased strength and brittleness of drier samples was observed. The results are then explained within a double structure framework and it is argued that this concept may be of use in explaining the behaviour of earthen structures.

The nature of water in rammed earth is then discussed. It is argued that the concepts outlined previously may also be used to explain the infiltration to and evaporation from rammed earth structures. Finally further work is suggested and implications for modern rammed earth buildings are highlighted. The work in this chapter allows a much fuller understanding of the failure of and repair to rammed earth structures which are discussed in Chapters 5 and 6.

3.2 Key concepts in unsaturated soil mechanics

Saturated soil mechanics treats soil at the microscale, as a two phase material consisting of soil particles and water. Unsaturated soil mechanics is required when an air phase is introduced into the microscale and the additional interactions between water and air become important in determining the properties of the soil. There are a number of concepts which are vital to an understanding of unsaturated soil mechanics.

3.2.1 Tensile strength of water

The discovery that water was able to withstand a tensile stress was made by Daniel and Jean Bernoulli in 1730. The brothers related the pressure to the velocity of a moving fluid.

$$\frac{v^2}{2} + gh + \frac{p}{\rho} = \text{constant} \tag{3.1}$$

where v is the velocity of the fluid, g acceleration due to gravity, h the height of the fluid, p its pressure and ρ its density (Massey and Ward-Smith 1998). This equation represents the conservation of energy along a streamline and shows that when the fluid velocity is increased, the pressure of the fluid decreases, and if the velocity becomes great enough, the pressure of the fluid becomes negative (tension). At a limiting negative fluid pressure the fluid "breaks" and cavities appear within the fluid. This phenomenon is known as cavitation. The tensile strength of the water was thought by Donny (1844) to be due to the cohesion of the molecules to one another. Donny found that the tensile strength of a fluid could be increased if gas was removed from the fluid prior to testing.

The stress required to pull apart two molecules can be calculated using the following formula (Israelachvili 2005)

$$P = \frac{2\gamma}{r} \tag{3.2}$$

where γ is the free surface energy of the molecule and r its effective radius. Taking the case of a water molecule of mean radius 0.32nm, and free surface energy 72mJ/m^2, it can be seen that the stress required to pull two water molecules apart is around 480MPa, which is considered to be the ultimate tensile strength of water. Sjoblom (2000) states that many other estimates of the tensile strength of water using

other molecular models have been made, all of which produce results of the same order of magnitude as that given by Equation (3.2).

3.2.2 Wetting angle

If three fluids come together (or two fluids and a solid surface), the properties of each will determine the angle formed between them, known as the *wetting angle* (Figure 3.1). The wetting angle may be determined by considering the relative magnitudes of adsorption and desorption interaction energies of the particles in adjacent fluids. The wetting angle determines the angle at which a meniscus makes contact with a surface, and may be observed when considering a free bubble on a surface or a meniscus within a tube. In the case of unsaturated soil mechanics, the fluids considered are liquid water and air, joining on a solid surface (for example a sand or clay particle). A change of the wetting angle has been observed when the fluid interface moves, and the wetting angle of a completely dry surface is likely to be different to that of a previously wet surface, where a thin layer of adsorbed fluid may be present on the solid surface.

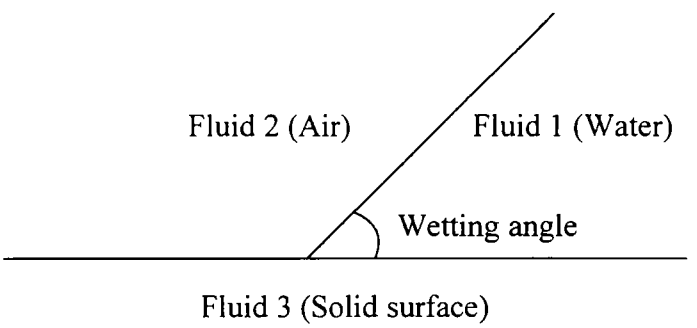

Figure 3.1 Wetting angle

3.2.3 Surface tension

The phenomenon of surface tension exists in all fluids at the vapour-liquid interface and was first been discussed by Pockels (1891). Considering the case of liquid water and air, a molecule which is located within the body of the water is subject to equal attraction in all directions and is in static equilibrium within the body of the liquid. A water molecule within the air is subject to the partial pressure of the water vapour. Where the water vapour pressure is greater than the liquid pressure, there is an unsymmetrical force balance at the interface, and the liquid surface must act in tension to compensate for the difference in the two pressures. This tension is concave

toward the lower pressure. Thus the interface can be seen to act as a membrane in tension. The tensile force of the membrane (or meniscus) is commonly referred to as the *surface tension* (T_s) of the water and has unit of force per unit length. For pure water and air, the tensile force for a given temperature T is given by

$$T_s = 0.1171 - 0.0001516T \text{ N/m} \tag{3.3}$$

The curvature of the interface of two fluids may be determined by considering the membrane stress in a sphere subject to an internal pressure, a solution to which was first proposed by Laplace (1806). Considering a sphere of radius R confining an internal pressure u with a surface under equal biaxial tension σ_T and considering force equilibrium of one hemisphere (Figure 3.2), it can be seen that

$$2\pi R T_s = u\pi R^2 \tag{3.4}$$

therefore

$$u = \frac{2T_s}{R} \tag{3.5}$$

Taking an external air pressure u_a and an internal water pressure u_w, and taking $u_a > u_w$, meaning the net internal pressure is the difference between the air and water pressure, allows equation (3.5) to be written as

$$(u_a - u_w) = \frac{2T_s}{R} \tag{3.6}$$

Taking the curve of the meniscus in two orthogonal directions, and relating the orthogonal radii of curvature to a single radius using the following expression,

$$\frac{1}{R} = \frac{1}{r_1} + \frac{1}{r_2} \tag{3.7}$$

it can be seen that equation (3.6) becomes

$$(u_a - u_w) = 2T_s\left(\frac{1}{r_1} + \frac{1}{r_2}\right) \tag{3.8}$$

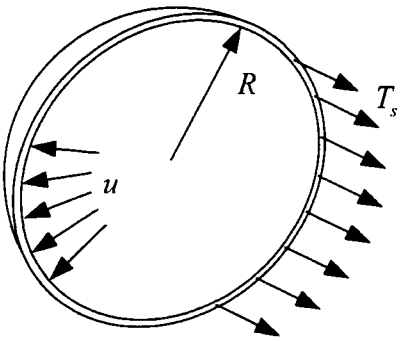

Figure 3.2 Laplace theory of pressure within a sphere

3.2.4 Capillary tubes

Surface tension is often used to explain the phenomenon of capillary rise. Considering the vertical force equilibrium of a water column (Figure 3.3), the level of water will change until the vertical component of the surface tension (acting around the circumference of the container) is equal to the weight of the water column below it

$$2\pi r T_s = \pi r^2 h_c \rho_w g \tag{3.9}$$

giving the height of capillary rise h_c as

$$h_c = \frac{2T_s}{\rho_w g r} \tag{3.10}$$

The water pressures at points A and B are atmospheric, and may be considered a datum for the system (zero elevation). If there is to be no flow between points A and C then their total hydraulic head must be equal. The pressure head at point C is therefore the negative of the elevation head, and the water pressure at point C must be given by

$$u_w = -\rho_w g h_c \tag{3.11}$$

The difference between the air and water pressures $(u_a - u_w)$ is known as the suction. If the air pressure is considered atmospheric, the suction at point C may be expressed as

$$(u_a - u_w) = \rho_w g h_c \tag{3.12}$$

Substituting Equation (3.10) in Equation (3.12) allows suction to be written in terms of surface tension

$$(u_a - u_w) = \frac{2T_s}{r} \tag{3.13}$$

Thus it can be appreciated that the surface tension associated with the meniscus results in a reaction force on the wall of the capillary tube, and the vertical component of the reaction force produces compressive stress in the walls of the tube, therefore the weight of the water column is transferred to the walls of the tube through the meniscus at the interface.

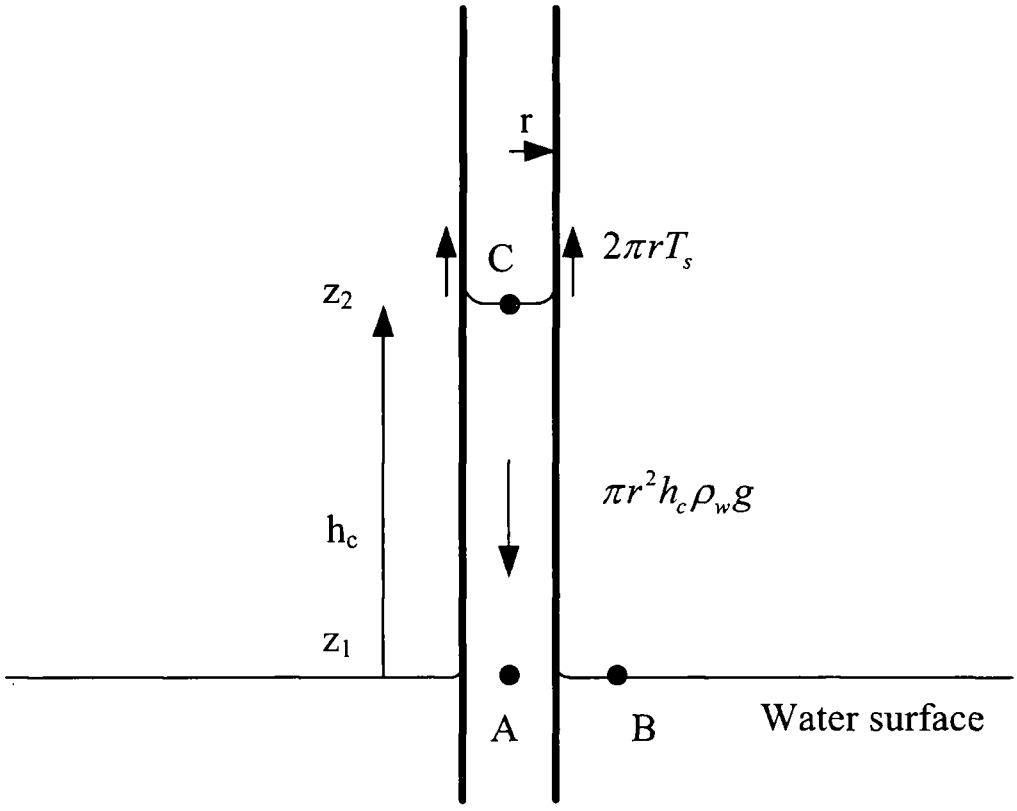

Figure 3.3 Capillary tube

3.2.5 Relative humidity

A body of water contains water molecules in constant random motion by virtue of their kinetic energy. At the surface of the water body, some molecules gain sufficient momentum to escape from the body of water, and join the water molecules in the air surrounding the water. The water molecules in the air are known as water vapour and are also in random thermal motion, sometimes gaining sufficient momentum to enter the body of water. When the number of leaving molecules is equal to the number of arriving molecules, an equilibrium state is reached. When more molecules are leaving than arriving, the body of water can be seen to be evaporating, and when more molecules are arriving than leaving, the body of water will grow through condensation.

The proportion of water molecules in the air to the maximum possible number of water molecules which could be present is known as the relative humidity. Air containing the maximum number of water molecules possible is termed saturated. The relative humidity can be determined by considering the vapour pressures of the fluids in question. If the pressure of the water vapour at the surface of the body of water is p_v and if water vapour is considered to be a perfect gas then

$$p_v = \rho_v R_v T \tag{3.14}$$

where ρ_v is the density of water in kg/m^3, R_v is the gas constant of water vapour (461.5 J/kgK) and T is absolute temperature in Kelvin.

The pressure of the saturated water vapour can be described by equation (3.14) as

$$p_0 = \rho_0 R_v T \tag{3.15}$$

where p_0 is known as the saturated water vapour pressure, which has a density ρ_0.

The ratio of actual vapour pressure to the saturation vapour pressure is known as the relative humidity, RH.

$$RH = \frac{p_v}{p_0} \tag{3.16}$$

3.2.5.1 Relationship between relative humidity and suction

The *hydrostatic* law states that the difference in pressure between two levels in a fluid is caused by the weight of the fluid between these two levels.

$$\mathrm{d}p = \rho g \mathrm{d}z \tag{3.17}$$

using the ideal gas law (Equation (3.14)), to replace the density ρ

$$\mathrm{d}p = \frac{pg}{RT}\mathrm{d}z \tag{3.18}$$

and integrating between pressure p_1 at height z_1 and p_2 at height z_2 we obtain

$$\int_{p_1}^{p_2} \frac{\mathrm{d}p}{p} = \int_{z_1}^{z_2} \frac{g}{RT}\mathrm{d}z \tag{3.19}$$

$$\frac{p_2}{p_1} = e^{\frac{g}{RT}(z_2 - z_1)} \tag{3.20}$$

which is known as the *hypsometric* equation (AMS 2000).

Lord Kelvin (Thomson 1871) realised the height of fluid rise in capillary tubes was due to the difference in water vapour pressures between the base of the tube and the curved meniscus at the top, and that evaporation or condensation will occur such that the water vapour pressure (i.e. relative humidity) will change to suit the height of capillary rise required in the tube (that the surface tension will balance the weight of the water column (Equation (3.9)) . Consider a column of vapour (B to D) adjacent to a closed capillary tube, and that at the datum water surface (flat) the vapour pressure is equal to the saturation vapour pressure p_0 (Figure 3.4). The difference in vapour pressure between a flat surface B, and the meniscus C and top of the vapour column D , noting that the vapour pressure at C is equal to that at D, is given by Equation (3.20). Considering $h_c = (z_2 - z_1)$

$$\ln \frac{p_v}{p_0} = \frac{g h_c}{RT} \tag{3.21}$$

Equation (3.12) gives an expression for h_c as

$$h_c = \frac{(u_a - u_w)}{\rho_w g} \tag{3.22}$$

Therefore

$$\ln \frac{p_v}{p_0} = \frac{(u_a - u_w)}{RT\rho_w} \tag{3.23}$$

Equation (3.16) defines the relative humidity (RH), and taking the specific volume v as the inverse of density ρ

$$(u_a - u_w) = \frac{RT}{v_w} \ln(RH) \tag{3.24}$$

which is the standard form of the *Kelvin* equation used in unsaturated soil mechanics, and may also be derived by considering the Gibbs free energy of the system. Figure 3.5 shows Equation (3.24) plotted at T = 20°C. It can be seen that in the suction range 0 – 1000kPa, the relative humidity of the surrounding air must be close to 100%. As the humidity of the surrounding air drops the suction increases, until a relative humidity of 0.05% where the suction is close to 1GPa, and both the soil and the air are considered dry (Fredlund and Radhardjo 1993).

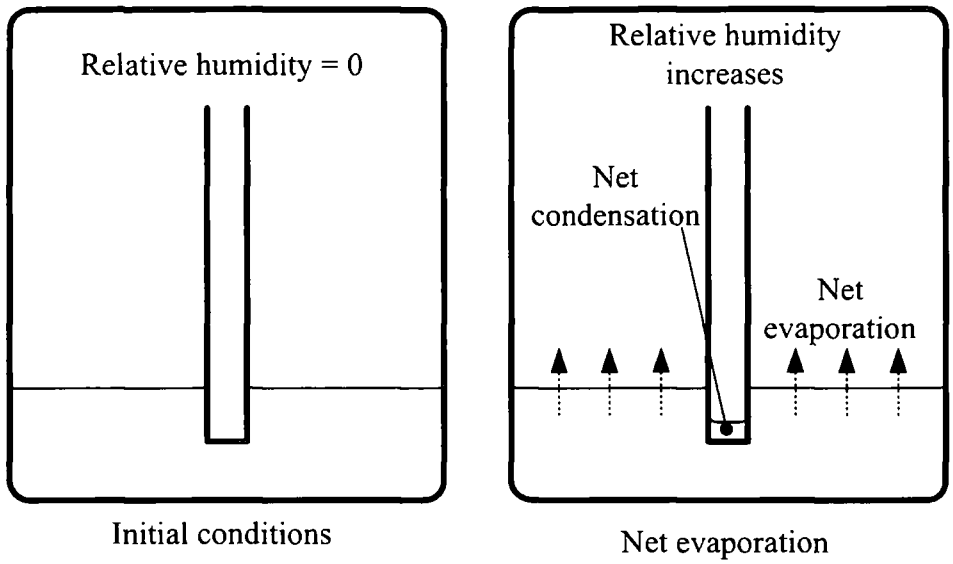

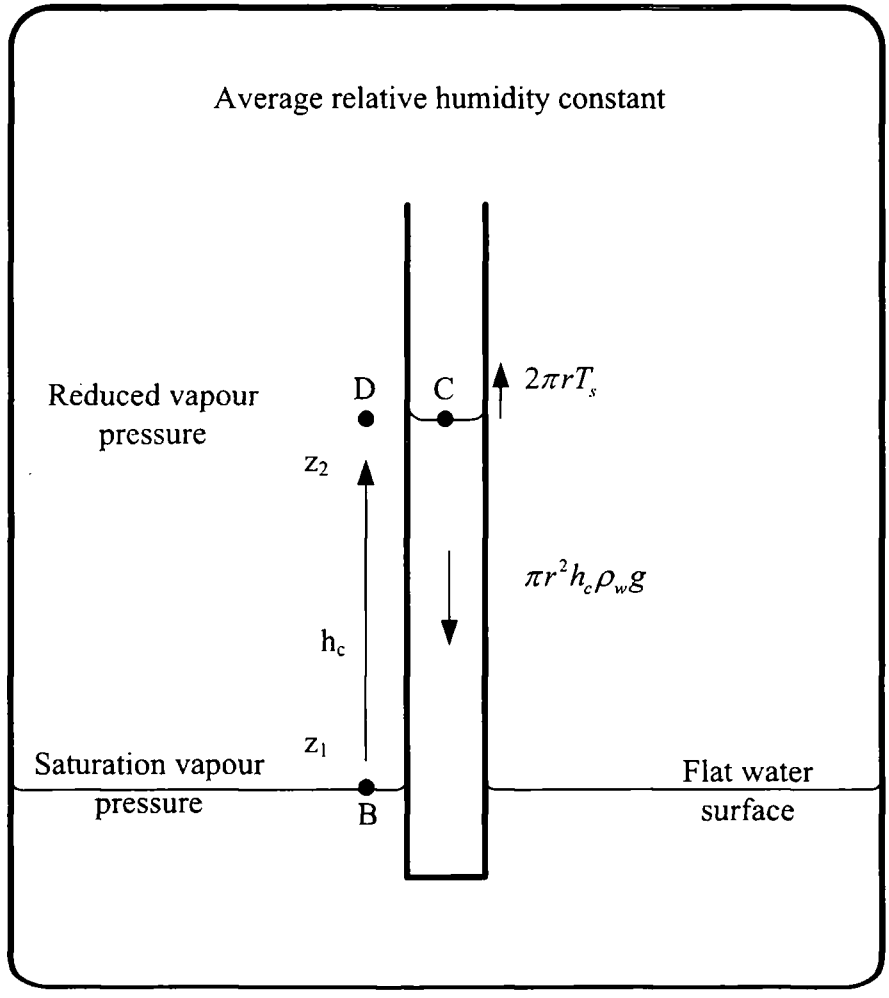

Figure 3.4 Kelvin equation assumptions

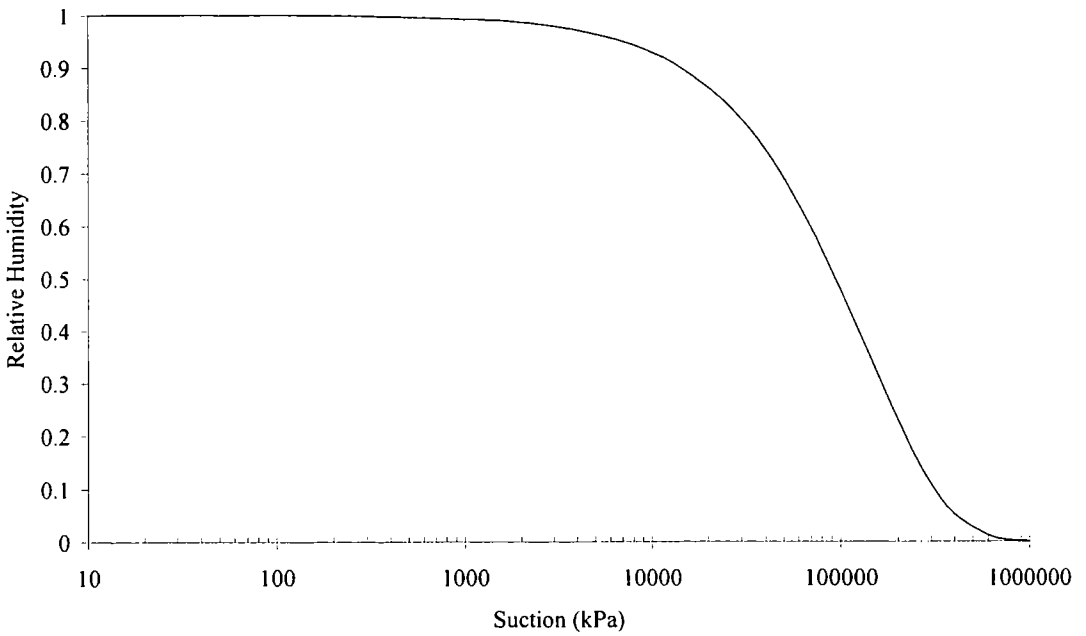

Figure 3.5 Relationship between relative humidity and suction, based on Equation (3.24)

3.3 Suction in soil mechanics

The concept of suction was developed in the field of soil physics in the early 20th century in relation to the soil-water-plant system. The use of soil suction to explain the behaviour of unsaturated soils was first proposed in the 1950s at the Road Research Laboratory in England (Croney, Coleman et al. 1958). Soil suction may be referred to as the potential energy per unit volume of the soil water, and may be defined in terms of relative humidity through *Kelvin's* equation (3.24). This defines *total suction*, of which there are two components, *matrix* and *osmotic* suction. Matrix suction is the height of capillary rise of a sample of soil water, defined by measuring the partial pressure and saturated vapour pressure of the soil water. Osmotic suction is the chemical potential energy difference between the soil water and pure water. Total suction is the total potential energy of the water and is the sum of the matrix and osmotic suction

$$\psi = (u_a - u_w) + \pi \tag{3.25}$$

where ψ is the total suction, $(u_a - u_w)$ is matrix suction and π is osmotic suction.

3.3.1 Pores

The spaces between particles are known as pores, and the size of the pores is related to the fabric of the soil. Gens and Alonso (1992) define two types of pore, based on size. *Microvoids* consist of the spaces between clay platelets (see Section 3.6.1) and small voids between packets of clay. Gens and Alonso (1992) argue these microvoids should always be considered saturated, but Sharma (1998) argues that it is possible that voids between clay packets can become unsaturated and so *microvoids* should be further subdivided. Larger pore spaces, for example between sand particles, are termed *macrovoids* and in an unsaturated soil can contain both air and water (Figure 3.15).

Pores are spaces between particles, but the nature of the pore matrix is difficult to define. Connected and isolated pores must be defined as different entities. An isolated pore has no connection to the rest of the pore matrix, and is simple to imagine in two dimensions. However in three dimensions it is unlikely that a pore will ever be completely isolated. A pore network exists joining a series of interconnected pores,

but a pore network itself may be isolated from the rest of the pore structure. The dimensions of a pore are also difficult to define, but a minimum and maximum radius, together with a length may define a pore for the purposes of meniscus formation and capillarity. These are obviously relatively arbitrary terms, with it highly unlikely that a pore will be cylindrical, and if two particles touch then the minimum radius is reduced to zero (Figure 3.6).

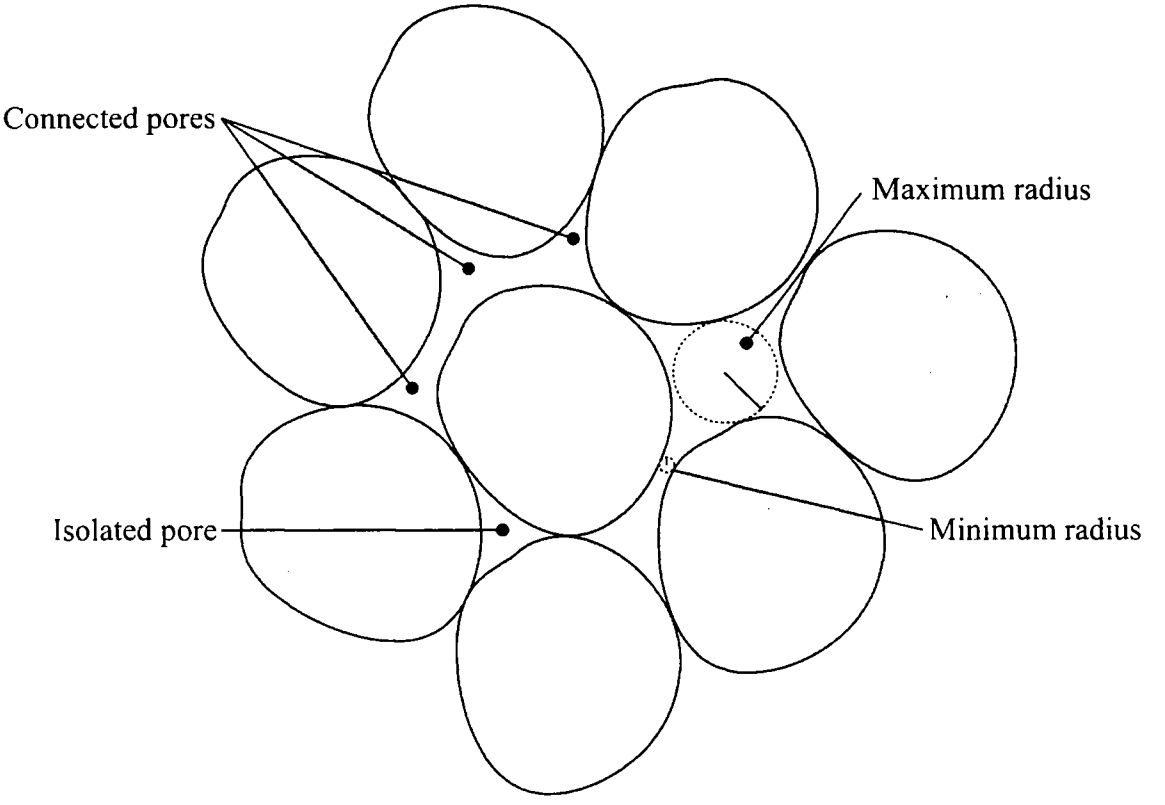

Figure 3.6 Pore radii descriptions

Where two particles are touching, or at a depression in the surface of a particle, and in the presence of a non zero relative humidity, water will condense. Water will continue to condense until the radius of curvature of the meniscus (the air-water interface) is equal to that given by Equation (3.13) for a suction given by the relative humidity (Equation (3.24)). This radius may be defined as the equilibrium radius r_{EQ}. Assuming a contact angle of zero and treating the pore as a parallel sided tube, the radius of the tube would be equal to r_{EQ}, but for finite contact angles, and for non parallel sided pores, the pore radius will be smaller than r_{EQ} (Figure 3.7).

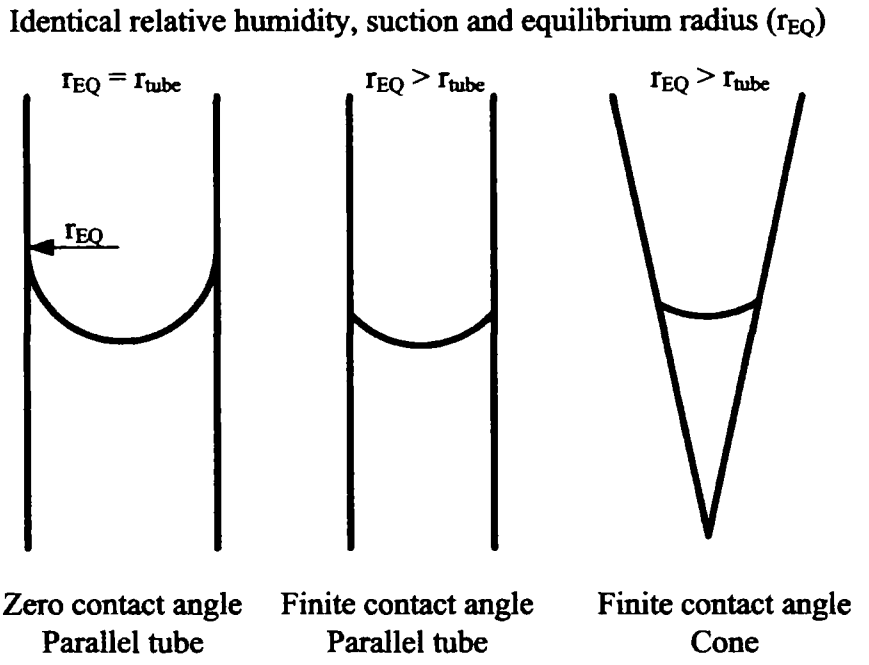

Figure 3.7 Equilibrium radius descriptions

For simplicity a contact angle of zero and a parallel sided pore space will be assumed, meaning Equation (3.26) can be used to define r_{EQ}. It should be appreciated that r_{EQ} given by Equation (3.26) is an overestimate of the true value.

$$\left(u_a - u_w\right)_{EQ} = \frac{2T_s}{r_{EQ}} \tag{3.26}$$

If the maximum pore radius is greater than r_{EQ} then air, and therefore a meniscus, will be present in the pore. If the maximum pore radius is smaller than r_{EQ} then the pore will be completely filled with water, and if the minimum pore radius is larger than r_{EQ} then the pore will be completely filled with air

Figure 3.8 shows the air entry value for changing pore size under given applied suctions. Given Equation (3.24), it can be seen that there will be an applied suction for a given humidity of the pore air. Figure 3.9 thus plots r_{EQ} for a given pore air relative humidity.

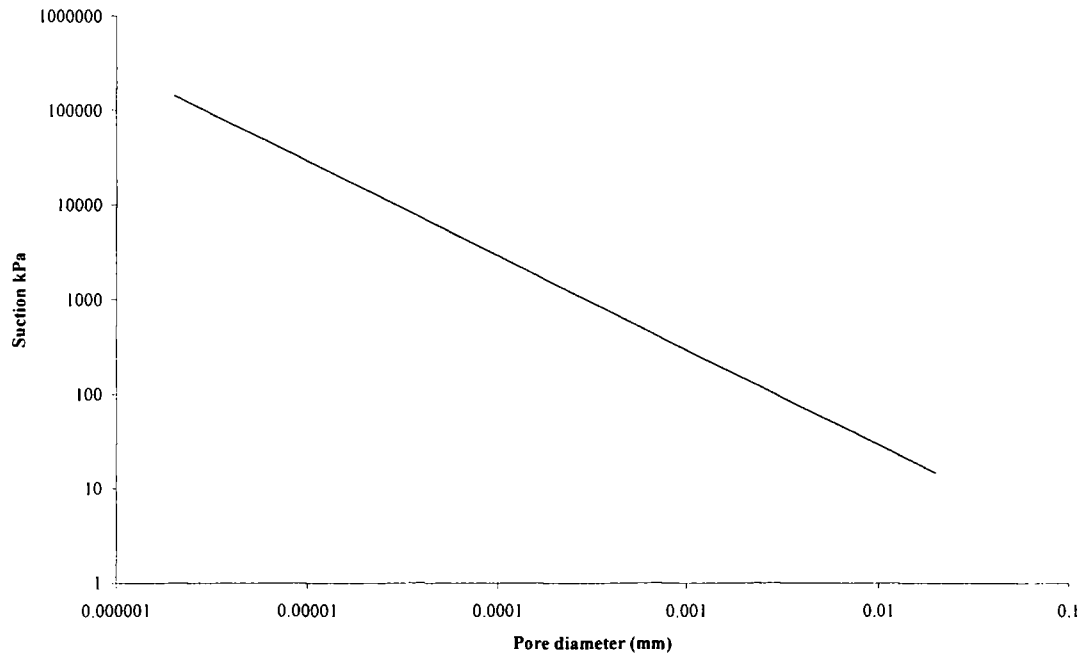

Figure 3.8 $2r_{EQ}$ for changing pore neck diameter, from Equation (3.26)

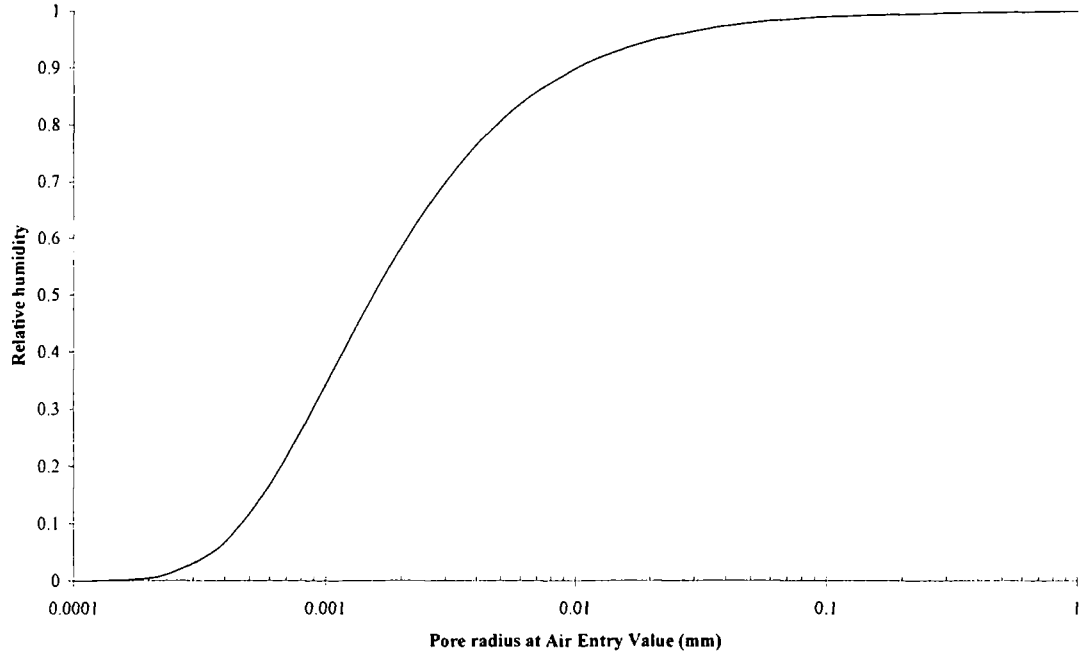

Figure 3.9 r_{EQ} for given relative humidity, given Equation (3.24)

When considering a network of pores, it is likely that there may be different pore radii along the length of the pore. Menisci are stable where $r = r_{EQ}$, and so a situation as shown in Figure 3.10 may occur, where a meniscus may form at a number of points along the pore. This can lead to the phenomenon of entrapped air, and can lead to different water contents being present in the soil for a given suction. For example if a

meniscus is only present at position 1 (Figure 3.10) then the pore space will be filled with water. If a meniscus is present at position 2, then the pore space will be filled with air, but water will be present between 1 and 2. If a meniscus is only present at 3, then the whole pore will be filled with air.

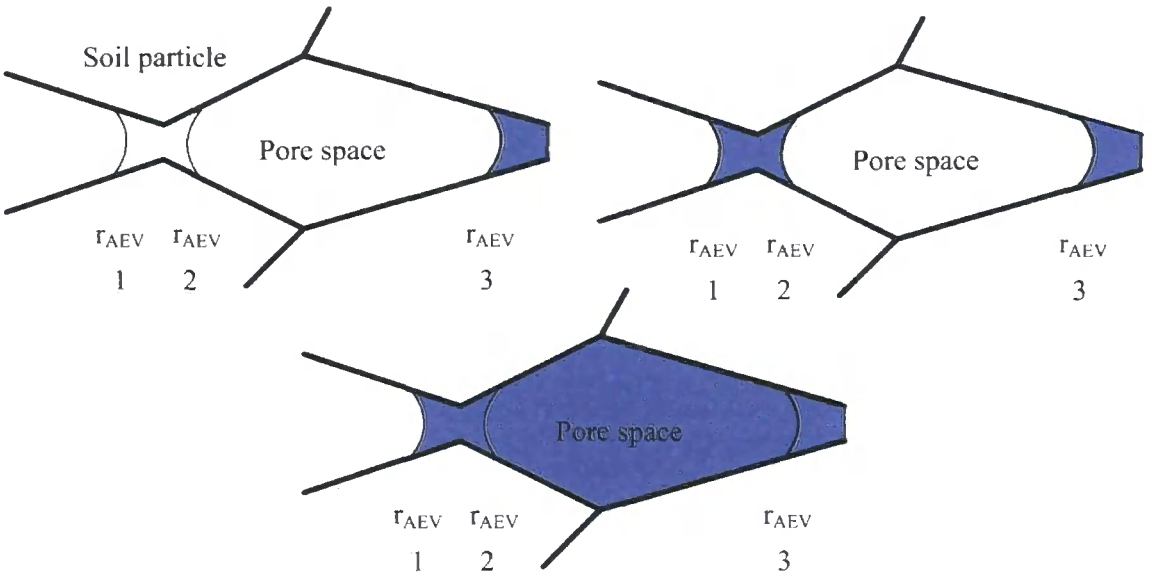

Figure 3.10 Bulb effect

3.3.2 Forms of pore water within unsaturated soil

While a soil as a whole can be considered as unsaturated, it should be understood that each void within the soil is either water filled or air filled, and a collection of continuous water filled voids may exist as a saturated region within an unsaturated soil, this region is termed as *bulk water* or *funicular*. In this range the water is continuous, and at a constant pressure.

Where water is non-continuous, and held only as the contacts of soil particles, it is termed *meniscus water*. *Meniscus* water is the cause of the increase in strength in an unsaturated soil compared to a dry soil. *Adsorbed water* is tightly bound to the soil particles and is not removed unless high levels of suction are applied (Wheeler, Sharma et al. 2003). The thickness of this adsorbed water layer has not been studied in the field of soil mechanics, but Katsube, Scromeda et al. (2000) and Asay and Kim (2005) observe that the thickness of this layer increases with increasing relative humidity from one molecule thick at relative humidity close to zero, to 10 molecules thick at a relative humidity of 100%. A water molecule has an effective diameter of 3.2 Å and so the adsorbed water layer ranges from 0.32 to 3.2 nm thick.

3.3.3 Liquid bridge force

A liquid bridge exists in a pore where both air and water are present in the pore space. The surface tension acting at the interface of the water and solid combined with tension in the water, act to provide an attractive force across the pore, which provides unsaturated soil its increased strength compared to saturated soil. This cohesive force due to capillarity can be idealised as the force between two isodiameteral spheres (Figure 3.11) and was first proposed by Fisher (1926) who used a wetting angle (θ) of zero, Gillespie and Settineri (1967) extended this to a finite wetting angle, and Pietsch (1968) took account of surface roughness of the particles by assuming a separation distance between idealised smooth spheres. Lian, Thornton et al. (1993) provided a mathematical basis for the interactions between a liquid bridge and rough rigid spheres which were applied by Molenkamp and Nazemi (2003). The estimation of the liquid bridge force as described by Fisher (1926) is given below.

The force between these two isodiameteral spheres may be idealised by considering equilibrium of forces as shown in Figure 3.12. The forces considered are

- The surface tension of the air-water interface (the meniscus).
- The resultant force owing to the hydrostatic pressure in the water being lower than the air pressure.

Considering equilibrium at the centre of the neck of the liquid bridge, and defining the radius of the neck as r_2, the surface tension (force per unit length) in the meniscus acting around the neck is equal to

$$F_{meniscus} = 2\pi r_{neck} T_s \tag{3.27}$$

Inside the neck, there exists water at a lower pressure than atmospheric, therefore the net force due to the pressure difference will be

$$F_{pressure} = \pi r_{neck}^2 \left(u_a - u_w\right) \tag{3.28}$$

The attractive force F between the two spheres is thus given by $F_{meniscus} + F_{pressure}$

$$F = \pi r_{neck} \left[2T_s + r_{neck}\left(u_a - u_w\right)\right] \tag{3.29}$$

Many estimations of the liquid bridge force between particles have been made, e.g. Molenkamp and Nazemi (2003), for different values of suction, but these are considered to be of little interest in this thesis as they deal with idealised spheres. This thesis investigates the presence of menisci across pores.

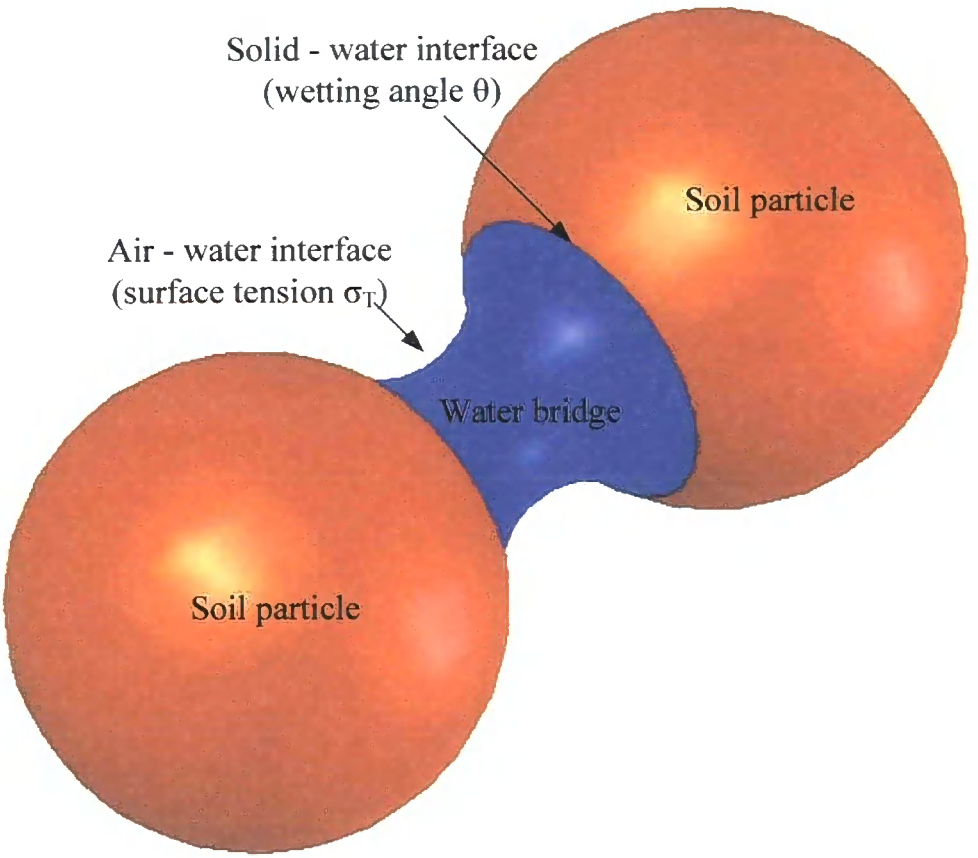

Figure 3.11 Three dimensional representation of isodiameteral spheres

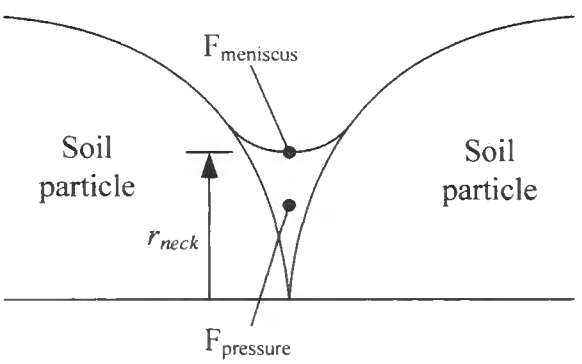

Figure 3.12 Liquid bridge forces, after Fisher (1926)

Applying the reasoning of Fisher (1926) to pores, it can be seen that there are two contributions to the attractive force across pores, the perimeter of the liquid bridge at the contact of the soil particle, and the contribution from the reduced pressure inside the liquid bridge (the tension in the water). Taking a modified example of the bulb shown in Figure 3.10 it may be seen that the two liquid bridges in Figure 3.13a

contribute twice the meniscus force, but that the length of the bridge in Figure 3.13b means that there is a larger contribution to the force from the pressure difference. This implies that in addition to hysteresis of the water volume during wetting and drying cycles (Fredlund and Radhardjo 1993), there may also be a hysteresis of strength.

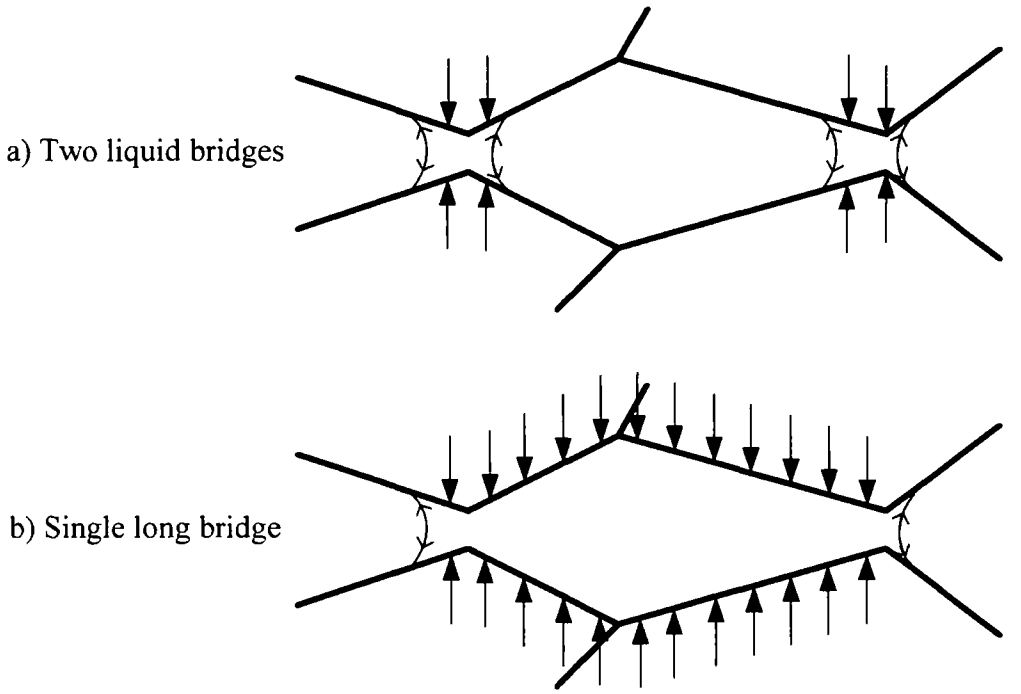

Figure 3.13 Modified bulb showing cross pore forces

3.3.4 Soil water characteristic curve

There is a non-unique relationship between the suction and degree of saturation of a soil. This is known as the soil water characteristic curve (SWCC) and is different for every soil. Fredlund, Wilson et al. (2002) argue that the shape of the SWCC is predominately controlled by the particle size distribution and secondarily influenced by the density of the soil, but this is better expressed as the shape of the SWCC being a direct function of the pore size distribution of the soil. The SWCC may be described as the soil's ability to sustain a water content under a given matrix suction of the pore air, and its shape is determined by the amount of water in the pores of the soil. Hysteresis of the SWCC exists, depending on whether the soil is wetting or drying. The hysteresis has been attributed to a number of different factors, namely different wetting angles depending on if a meniscus is advancing or retreating, and the *bulb effect*, where a meniscus cannot advance into a larger pore for a given relative humidity, but may exist at the smaller entrance to a wide pore filled with water

(Figure 3.10). A typical SWCC is shown in Figure 3.14, and there are a number of common characteristics which can seen on the curve.

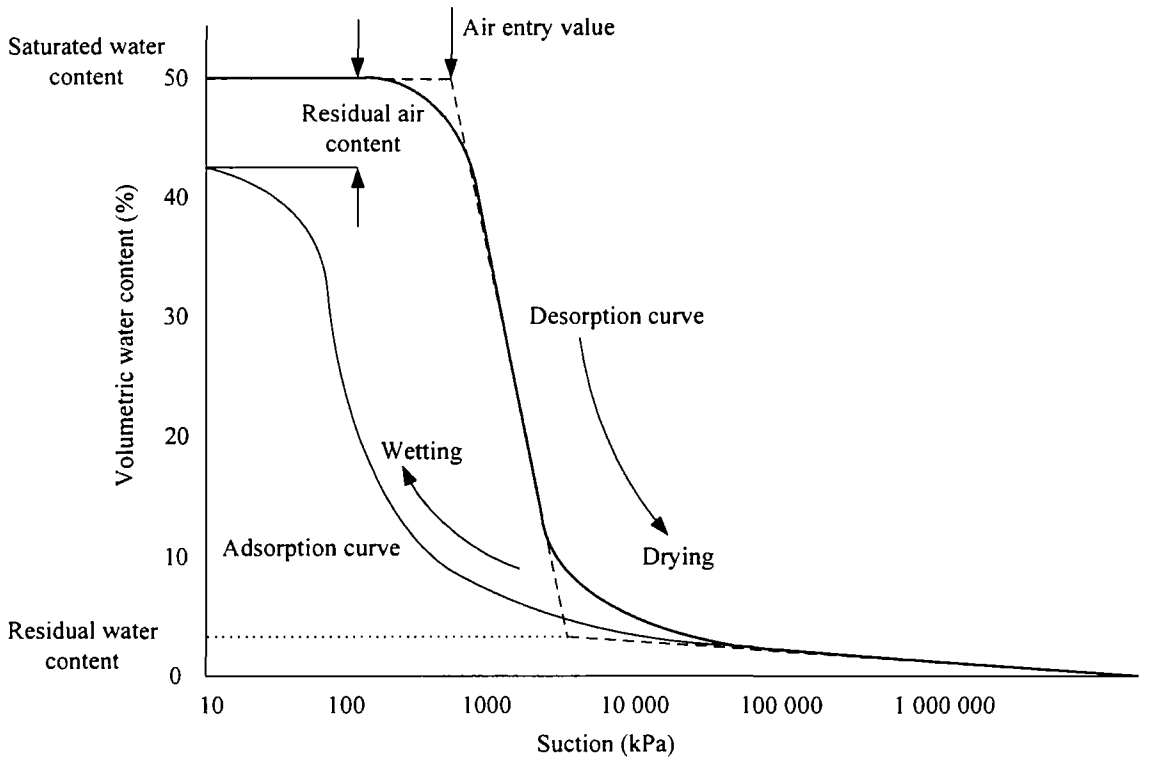

Figure 3.14 Typical Soil Water Characteristic Curve. From Fredlund, Xing et al. (1994)

The *saturated water content* is the maximum water content which can exist in the soil, and is when all of the soil pores are water filled.

The *air entry value* of a soil is the most important variable in the application of unsaturated soil in geotechnical engineering (Fredlund, Wilson et al. 2002). The air-entry value of a soil is the matrix suction value which must be exceeded before air recedes in the soil pores, and is a measure of the maximum pore size in a soil (Section 3.3.1). It is defined (Fredlund and Radhardjo 1993) as the intersection point between the sloping line of the SWCC and the point where the effective degree of saturation is equal to unity.

The *desorption curve* is followed after the air entry value of the largest pores is exceeded, air enters into these pores and liquid bridges then exist in those pores, at a radius given by Equation (3.26). Assuming the water leaves the soil through evaporation, the suction then increases and the volumetric water content reduces. As the suction increases, the air entry value of progressively smaller pores is exceeded,

and the water content of the soil continues to reduce. The shape and position of the desorption curve thus depends solely on the pore size distribution of the soil.

A *residual water content* is defined as the volumetric water content below which it is difficult to go without significant increase in suction. This definition is known to be vague (Fredlund, Xing et al. 1994) and is considered to be a state where air has entered all of the pore spaces and water is held only at grain to grain contacts. From the arguments outlined in Section 3.3.1 it may be stated that both the *saturated* and *residual* water content are never defined points, but functions of the relative humidity and the pore size distribution.

As the water content of a soil increases, the value of suction reduces, following an *adsorption* curve. While the desorption and adsorption curves should follow the same route, hysteresis has been observed in all soils. There are a number of reasons suggested for the difference in volumetric water content for a given suction (Hillel 1982; Likos and Lu 2004)

- The bulb effect (Figure 3.10), for individual pores, where water is able to exist in a large pore though a meniscus across a small entrance, but not able to enter the large pore due to the higher air entry value.
- Entrapment of air within the pores. An increase in the pore air pressure would lead to reduced water content for a given suction, according to Equation (3.6) as the volume of the liquid bridge would be reduced.
- Wetting angle hysteresis. As observed by Lourenço (2008) and documented by Israelachvili (2005), the interface angle between air and water on a surface changes depending on the direction of movement of the interface.
- Different spatial connectivity of pores during wetting and drying. Drying of a soil may lead to collapse or shape change of pores, thus changing the structure of the pore network, meaning adsorption of water cannot take place through the same pores through which it drained.

Gallipoli, Wheeler et al. (2003) note in a rigid soil only hydraulic and wetting angle hysteresis will occur, whereas in a deformable soil there will be changes in the

porosity (void ratio) which mean that a different SWCC will be followed following deformation.

Due to entrapped air within the soil during the adsorption part of the SWCC, a previously dry soil will only absorb a certain volume of water, which is a lower volume than if it were initially fully saturated. The difference between the saturated water content and the adsorption curve water content is known as the *residual air content.*

The curves as shown in Figure 3.14 represent wetting from a fully dry state and drying from a fully saturated state and are known as *primary curves.* If wetting or drying begins from any other point, new curves form within the region bounded by the primary curves. These curves are known as *scanning curves* (Childs 1969). If wetting and drying cycles are performed over a constant suction range it has been observed that the response of the soil approaches a closed hysteresis loop, independent of whether the first cycle starts on the wetting or drying curve.

3.3.5 Empirical fitting of the SWCC to other parameters

Various fitting equations for the SWCC have been suggested, with two main parameters, the air entry value of the soil and the angle of slope of the SWCC. Brooks and Corey (1964) call the slope of the line the *pore size distribution index*, but the model is limited by the linearity of this function. Van Genuchten (1980) improved by introducing an inflexion point into the curve which allowed for better performance close to saturation. Fredlund and Xing (1994) presented a complex theoretical basis for the prediction of the SWCC based on different pore size distribution functions, and Fredlund, Wilson et al. (2002) developed semi-empirical methods for estimation of the SWCC based on particle size distribution data. Most recently estimates of the pore size distribution based on fractal theory (Mandelbrot 1982) have resulted in other estimates of the SWCC for given soils (Ojeda, Perfect et al. 2006).

3.4 Behaviour of unsaturated soils

Unsaturated soils have been observed to behave differently to saturated soils, and the behaviour is considered to be related to the suction $(u_a - u_w)$ in the soil allowing liquid bridges to form between particles. These features can be seen as particularly relevant in the behaviour of rammed earth structures. Two features of unsaturated soil behaviour which cannot be explained in the framework of saturated soil mechanics are increased stiffness and collapse on wetting which were first outlined by Jennings and Burland (1962)

3.4.1 Deviation from saturated soil mechanics

Alonso, Gens et al. (1990) note that increased suction contributes to increased stiffness of the soil against external loading, which is observed both in samples compacted wet and dry of optimum moisture content (Section 2.2.2). This is most easily appreciated in oedometer tests of soil samples carried out at different moisture contents, where drier samples appear stiffer.

Increased strength is given to unsaturated soils by the presence of liquid bridges across the pores. On wetting (a reduction in suction) these bridges are removed and the soil will reduce in strength. A reduction in volume is observed for a high confining stresses where the liquid bridges collapse and interlock is increased. At a low confining stress expansion is observed through the increase in pore water pressure (Alonso, Gens et al. 1990).

3.4.2 Shear strength

The shear strength of unsaturated soil samples is greater than saturated samples. This increased shear strength is derived from the liquid bridges across the pores and is usually interpreted as an increase in cohesion (c) in the Mohr-Coulomb criterion (Chapter 2). This increase in shear strength is highly non-linear with suction and constitutive models including this increased shear strength are discussed in Section 3.5.

3.4.3 Tensile strength

The tensile strength of soil is usually neglected for conservative design purposes, but in some specific aspects of geotechnical engineering, e.g. clay landfill liners, the cores of embankment dams and in the calculation of slope stability of clayey soils (Zeh and Witt 2005) the tensile strength of unsaturated soils is considered important. Methods for the testing of tensile strength of unsaturated soil are very limited (e.g. Tang and Graham 2000, Nahlawi, Chakrabarti et al. 2004) and modelling of the tensile behaviour is seldom undertaken. However the tensile strength of rammed earth structures may be of great importance when determining their behaviour. While this thesis does not investigate the tensile strength of rammed earth, it is important to note that it is non zero, and further investigation is required to quantify this strength.

3.4.4 Particle crushing

If the macroscopic volumetric stress is sufficiently increased, it is possible for crushing and fracturing of the individual soil particles to occur. This is most commonly observed in shear box tests at high compressive loads, and is manifested as a reduced shear angle at high normal stresses. In considering rammed earth as an unsaturated soil, particle crushing will change both the particle and pores size distribution of the soil. A reduced shear angle was observed by Howard (2007) when undertaking large shear box tests on rammed earth samples.

3.4.5 Conceptualisation of microscale mechanical behaviour of unsaturated soils

The mechanical behaviour of an unsaturated soil is governed by the frictional and interlock interactions between the soil particles, and by the behaviour of the liquid bridges and unsaturated regions within the soil.

Wheeler, Sharma et al. (2003) presented a microscale conceptualisation of unsaturated soil similar to that in Figure 3.15. Here three forms of water are present, that of *bulk* water, which is continuous water within a connected pore network, such as water within the water table. *Meniscus water* is that held in liquid bridges at particle to particle contacts, and adsorbed water is that held on the surface of particles which have previously been wetted. Figure 3.15 also shows the *macro-* and *microvoids* of Gens and Alonso (1992) and Sharma (1998) as discussed in Section 3.3.1. Other

forces which may be present within rammed earth and in unsaturated soils are shown in Figure 3.15 and discussed in Section 3.6.

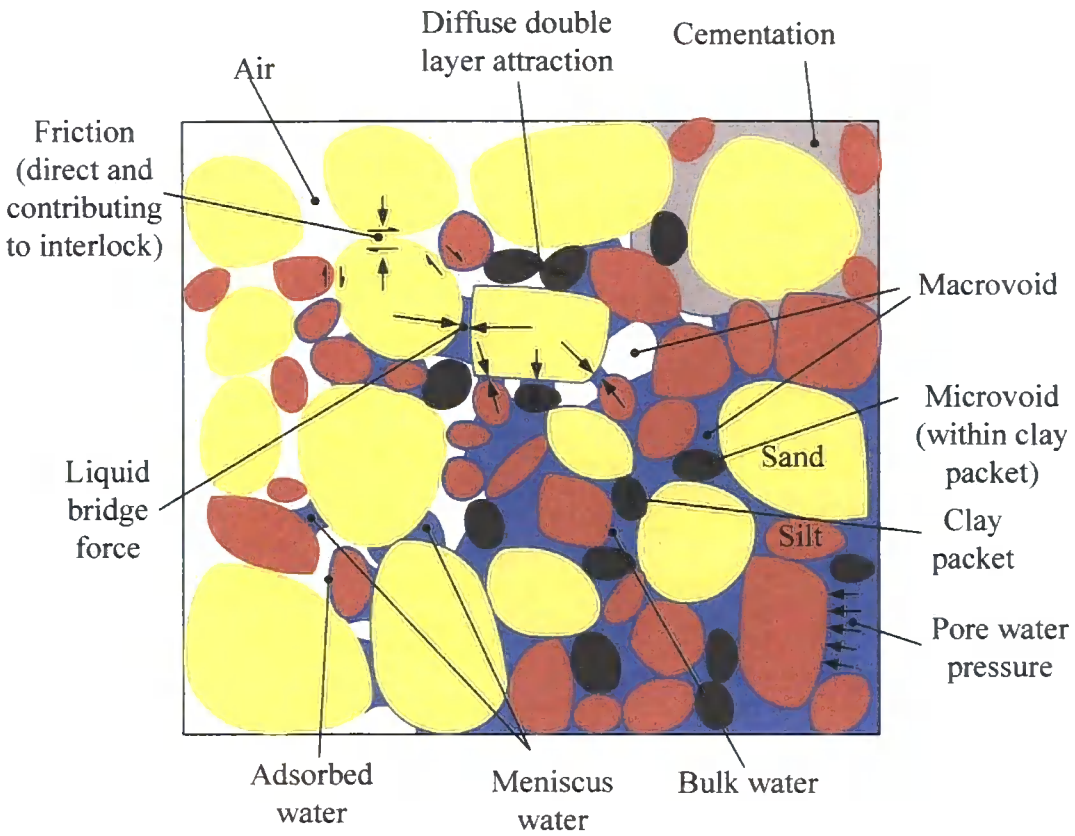

Figure 3.15 Forms of pore water, void spaces and forces within an idealised soil. Based on Gens and Alonso (1992), Sharma (1998) and Wheeler, Sharma et al. (2003)

3.4.6 Double structure

The notion of saturated and unsaturated pores, leading to a double structure approach to unsaturated soils has been advanced by a number of authors. Toll (1990) argues that that an unsaturated soil may behave as coarser than suggested by its particle size distribution due to the formation of macroparticles from the binding together of smaller particles through liquid bridges.

Toll (1990) explains the reduction in suction observed for highly unsaturated samples compared to an increase in suction for low suction samples by considering two levels of fabric - a double structure (Figure 3.16). If saturated clay packets are bound together by liquid bridges across their small pores, then they will act to increase the effective particle size distribution of the sample, resulting in an artificially high

friction angle for the sample. However when these clay packets are subject to volumetric compression they act as a saturated sample, wet of critical, and expel water, therefore increasing the available water content of the sample and reducing the measured suction.

Cunningham, Ridley et al. (2003) also considered the fabric of the soil at two levels, observing that the specific volume of a sample decreases with increasing suction to 1500kPa, then increases slightly and remains constant for further increases in suction. It was postulated that between suctions of 1000 and 1500kPa, silt sized particles are drawn to each other to form a rigid open granular structure, with clay particles occupying pores around the silt contact points. On reduction in suction this open granular structure is retained, but now clay is present between the silt particles and thus the overall volume of the sample remains constant.

A similar phenomenon for unsaturated soils is suggested by Tarantino (2007a), who introduces the notion of *mechanical* and *physical* wetting and drying. Mechanical wetting can be considered as a change in the position of the particles making up the soil skeleton and physical wetting as a change in the suction. The mechanical wetting concept centres around volumetric loading of the sample (mechanical) reducing the size of the pores. If the maximum pore radius is reduced below the air entry value, then the pore will become completely filled with water and act as saturated. Conversely if volumetric unloading takes place then the pore size will be increased, and a pore previously saturated will become unsaturated, and a meniscus form within the pore. *Physical* wetting and drying is achieved through the increase and decrease in suction in a sample. A given pore will be saturated if its maximum radius is smaller than the air entry suction, an increase in suction will result in the air entry radius reducing, so a pore may become unsaturated if its maximum radius is greater than r_{EQ}.

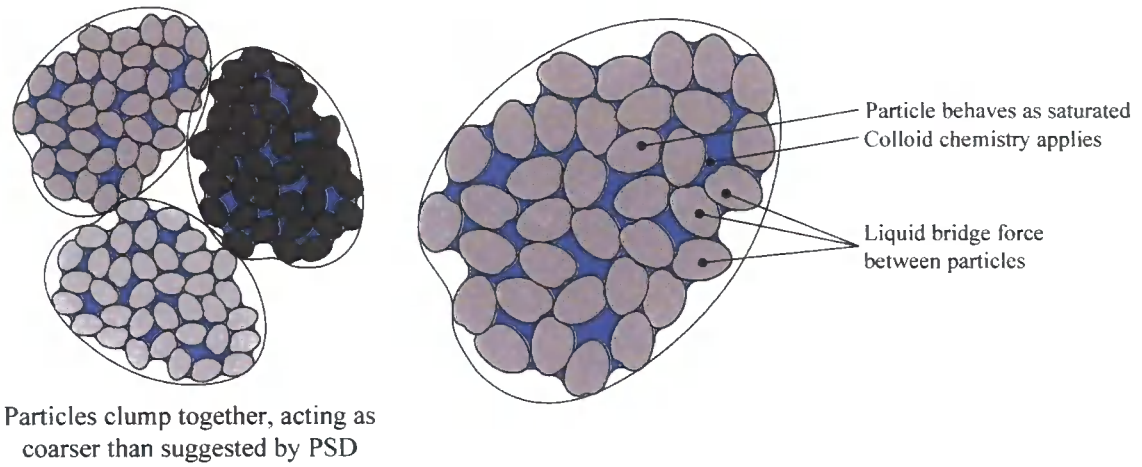

Figure 3.16 Saturated clumped particles, as described by Toll (1990)

3.4.7 Evidence for liquid bridges

Figure 3.17 shows liquid bridges between 5μm Organosilica microspheres (Lourenço 2008) taken using an Environmental Scanning Electron Microscope (ESEM). Figure 3.18 shows an ESEM image of stabilised rammed earth with no menisci, and Figure 3.19shows menisci present (Hall 2006b). Because a cementing (C-S-H) matrix is clearly visible in Figures 3.17 and 3.18, the images indicate that the theory of menisci bonding particles together may be acceptable for unsaturated materials, such as unstabilised rammed earth, but perhaps less acceptable for cemented unsaturated materials such as stabilised rammed earth.

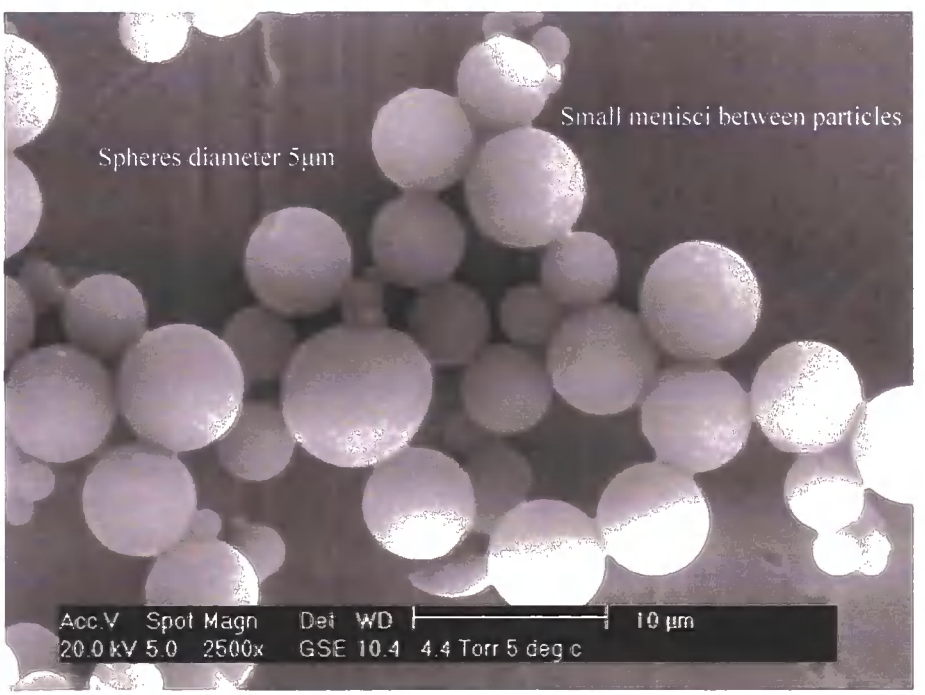

Figure 3.17 ESEM image of spheres at relative humidity of 67%. Photograph: Lourenço (2006)

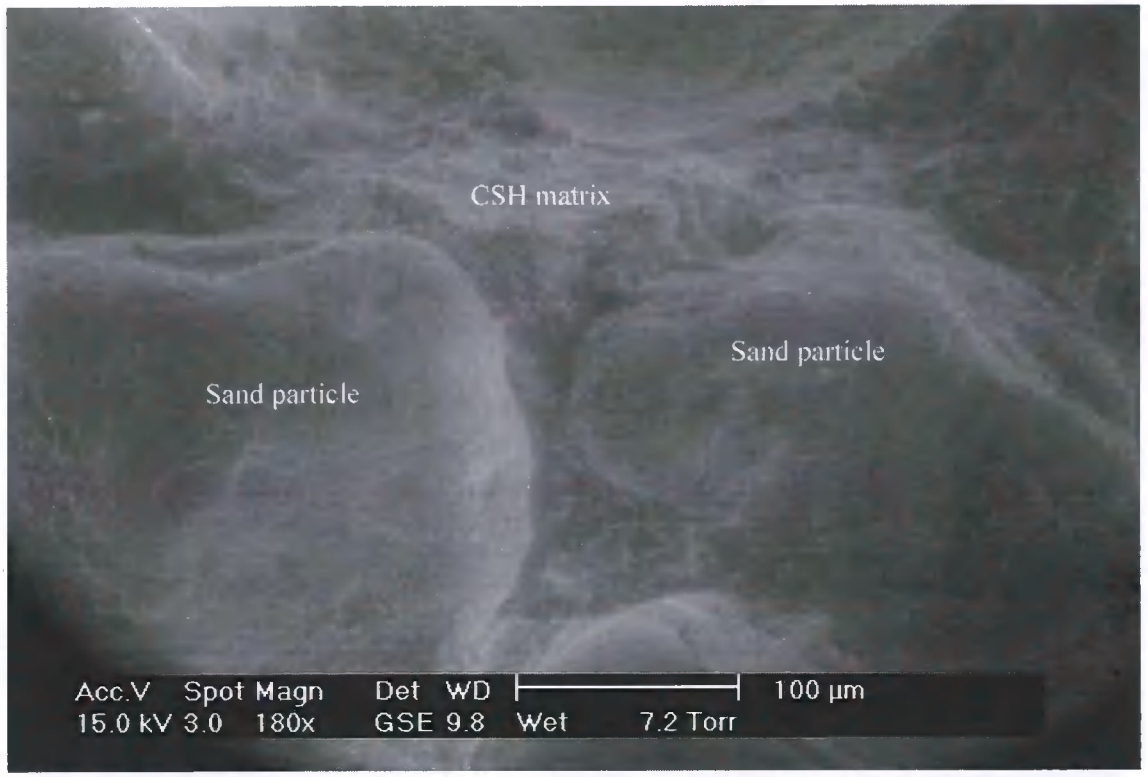

Figure 3.18 ESEM image of stabilised rammed earth with no menisci. Photograph: Hall (2006)

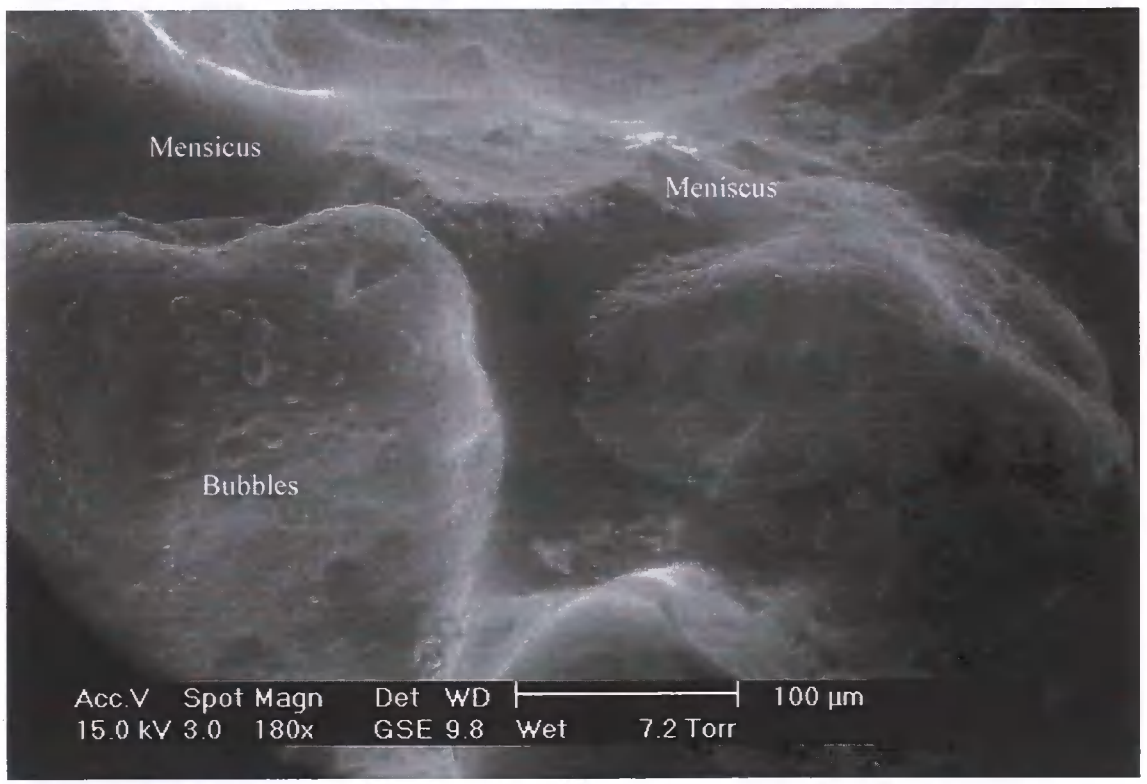

Figure 3.19 ESEM image of stabilised rammed earth where menisci have formed. Photograph: Hall (2006)

3.5 Constitutive models of unsaturated soils

As outlined in Chapters 1 and 2, the placing of rammed earth in a geotechnical engineering framework may help to better explain its behaviour. The unsaturated nature of rammed earth has been discussed above. Therefore, constitutive models for unsaturated soils are now outlined. This section introduces stress state variables for unsaturated soils, and introduces some of the most common constitutive models. These models are only briefly discussed, and are used to qualitatively explain the behaviour of testing described in Section 3.10.

There have been many attempts to model unsaturated soils, taking into account the additional changed behaviour from that of saturated soils as outlined in Section 3.4. An effective stress parameter (χ) was introduced by Bishop (1959) but was shown by Jennings and Burland (1962) to not describe the full range of behaviour of exhibited by unsaturated soils. Fredlund and Morgenstern (1977) showed that two stress state variables were required to fully describe unsaturated soils and introduced a modified Mohr-Coulomb criteria based on the work of Bishop, Alpan et al. (1960). Toll (1990) introduced a critical state approach and the Barcelona Basic Model of Alonso, Gens et al. (1990) now forms the basis of many constitutive models for unsaturated soil.

3.5.1 Stress state variables

The mechanical behaviour of a soil (for example its volume change and shear strength) can be described in terms of the state of stress in the soil. The state of stress in a soil consists of certain combinations of stress variables which are referred to as the stress state variables. These variables should be independent of the physical properties of the soil, and the number of stress state variables required depends on the number of phases in the soil (Fredlund and Radhardjo 1993).

Bishop (1959) was one of the first to present an expression for effective stress (σ') in an unsaturated soil. An effective stress parameter was introduced as a multiplier to the pore water pressure in Terzaghi's equation

$$\sigma' = \sigma - u_w \tag{3.30}$$

where σ is the total stress. The effective stress parameter (χ) varies between zero and unity depending on the degree of saturation, and represents the contribution of the matrix suction to the effective stress.

$$\sigma' = \sigma - u_a + \chi(u_a - u_w) \tag{3.31}$$

While this approach proved capable of producing the phenomenon of increase of shear strength due to suction, Jennings and Burland (1962) recognised that Bishop's approach did not provide a reasonable relationship between volume change and effective stress for most soils at certain degrees of saturation. The degree of saturation for which Equation (3.31) did not apply was found to be 20% for silts and sands, but up to 90% for clays. Morgenstern (1979) found that the values for χ vary between testing of shear strength and volume change of the same soils.

Numerous effective stress equations have been proposed which attempt to incorporate various weighting parameters to produce a single valued effective stress variable. However experimentation has shown that the effective stress equation is not single valued (Fredlund and Radhardjo 1993). It is also difficult to reconcile the use of soil properties through the use of χ in describing the stress state. The effective stress parameter χ in Equation (3.31) attempts to relate unsaturated behaviour of a soil to behaviour of a similar saturated soil. The effective stress variable should be related to equilibrium conditions only and not depend on the constitutive behaviour. Constitutive behavioural relationships relate equilibrium considerations to deformations and should not be introduced into the stress variables. A number of authors, (e.g. Wheeler, Sharma et al. 2003) have noted that changes in suction have a very different effect on the soil structure than changes in applied stress.

Therefore, it is now accepted that two independent stress variables are required to explain the behaviour of unsaturated soils. Given that unsaturated soil is a three phase system, consisting of stresses in the incompressible water (u_w), incompressible solid soil particles (σ), and compressible air (u_a), there are three combinations of stress state variables which could be used to describe the behaviour of unsaturated soils.

- $(\sigma - u_a)$ and $(u_a - u_w)$

- $(\sigma - u_w)$ and $(u_a - u_w)$
- $(\sigma - u_a)$ and $(\sigma - u_w)$

Always assuming that $\sigma > u_w > u_a$.

Fredlund and Morgenstern (1977) proposed the use of independent stress state variables of $(\sigma - u_a)$ and $(u_a - u_w)$ known as net normal stress and matrix suction respectively. This combination takes the pore air pressure (u_a) as the reference pressure (common in both variables), which can be taken as constant atmospheric for most engineering applications. Once the stress state variables are established they can be used to determine the mechanical and failure behaviour of a soil.

3.5.2 Modified Mohr-Coulomb

Bishop, Alpan et al. (1960) were the first to modify the Mohr-Coulomb criteria to include a contribution to shear strength by virtue of the soil being unsaturated.

$$\tau_{ff} = c' + \left[(\sigma - u_a) + \chi(u_a - u_w)\right] \tan\phi' \tag{3.32}$$

This expression treats suction as acting in addition to the net normal stress to produce an increased shear strength for the same effective angle of friction. This is now considered unrealistic and Fredlund and Morgenstern (1977) proposed Equation (3.33), introducing using a variable ϕ^b to describe the nonlinear variation of shear strength with respect to suction. ϕ^b is considered to be a constant property of the soil, independent of suction.

$$\tau_{ff} = c' + (\sigma_f - u_a)_f \tan\phi' + (u_a - u_w)_f \tan\phi^b \tag{3.33}$$

Both of these expressions lead to the construction of an extended Mohr-Coulomb failure surface, with a third orthogonal axis of matrix suction. The Fredlund expression (Equation (3.33)) takes account of the fact that the mechanical behaviour of an unsaturated soil is affected differently by changes in net stress and by matrix suction. A change in shear strength due to an change in net stress is accounted for by the ϕ' parameter, whereas a change in matrix suction is characterised by ϕ^b. However the assumption that ϕ^b is constant is not correct, and it was found by Fredlund, Rahardjo et al. (1987) and Vanapalli and Fredlund (1997) that ϕ^b is equal

to ϕ' at low values of suction, then decreases considerably to a constant low value at high values of suction. Escario and Juca (1989) suggested that at high values of suction ϕ^b becomes negative implying that the increase in apparent cohesion due to suction tends to zero for very dry soils.

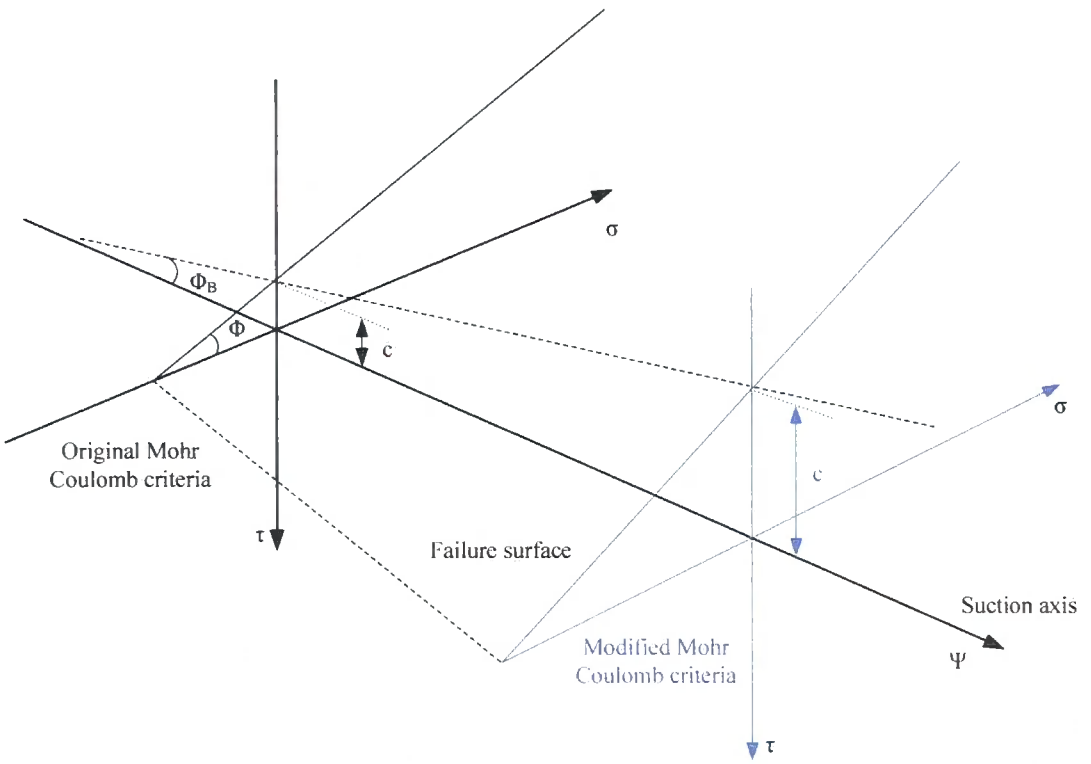

Figure 3.20 Modified Mohr-Coulomb failure criterion. After Fredlund and Radhardjo (1993)

3.5.3 Toll (1990)

Toll (1990) proposed the following expression for critical state shear strength,

$$q = M_a(p - u_a) + M_w(u_a - u_w) \tag{3.34}$$

with M_a and M_w being two parameters named the total stress ratio and the suction ratio, which depend on the degree of saturation and represent the relative proportions of net mean stress and suction to the critical state shear strength. This formulation essentially extends the work of Fredlund and Morgenstern (1977) and others in separating the relative contributions of net mean stress and suction to the shear strength of an unsaturated soil. However determination of M_a and M_w is not straightforward, and cannot be gained from simple soil parameters.

3.5.4 Barcelona Basic Model

An elastoplastic constitutive model for unsaturated soils was developed by Alonso, Gens et al. (1990) and is now known as the Barcelona Basic Model (BBM). As with other models described above, the Barcelona Basic Model aims to capture the increase in strength provided by the suction. This model extends the Modified Cam Clay formulation for saturated soils (Roscoe and Burland 1968) with the introduction of a suction axis (similar to Fredlund and Radhardjo 1993). The model is fully described by Alonso, Gens et al. 1990 and has been subsequently refined (e.g. Wheeler and Sivakumar 1995). The most important aspects for the modelling of rammed earth are the increase in apparent cohesion with increasing suction (introduced by the Suction Increase (SI) yield surface), and the change in effective preconsolidation pressure with suction, defined by the Loading Collapse (LC) yield surface.

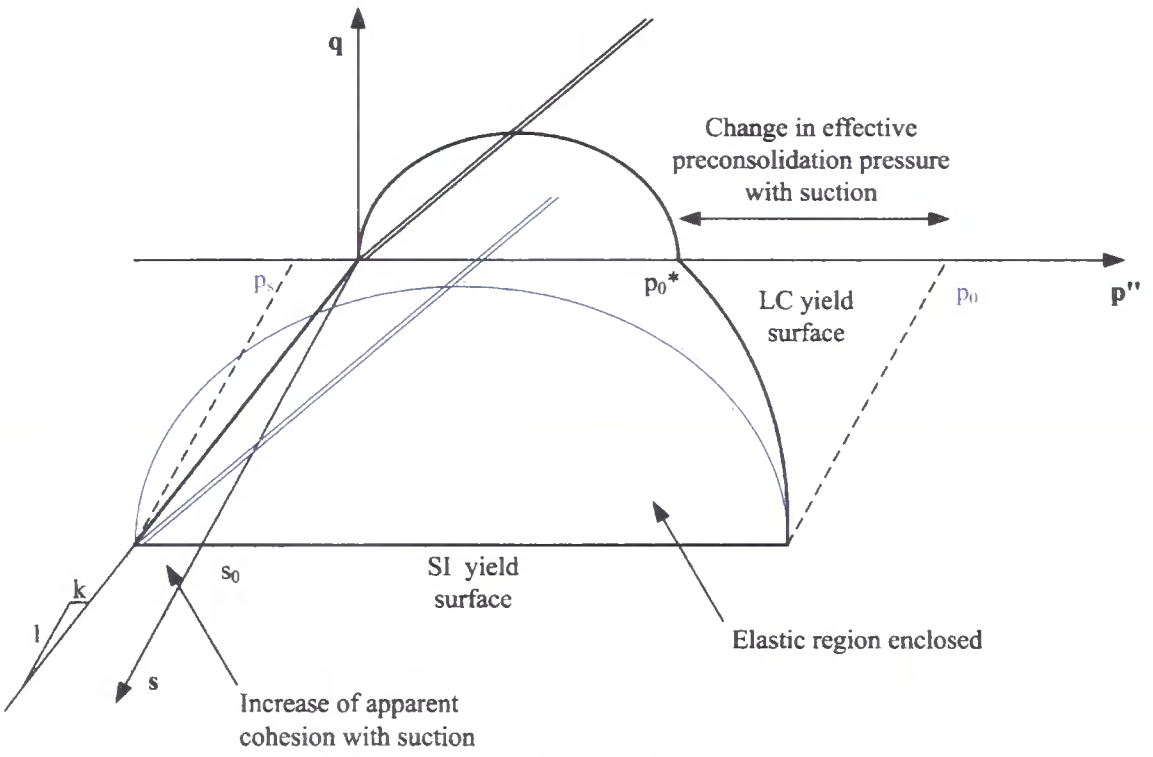

Figure 3.21 Barcelona Basic Model. After Alonso, Gens et al. (1990)

3.6 Origins of strength of earthen materials

It has previously been reported that the strength of earthen materials may be due to a number of interparticle forces, although the relative magnitude of these forces has not been discussed. These mechanisms are usually lumped as 'electrostatic forces' and 'other forces' – described as cementation, capillarity, electromagnetic forces and friction (Houben and Guillaud 1994).

Soil mechanics has only recently begun investigating the relative magnitudes of the interparticle forces. Lu and Likos (2006) identify 'suction stress' which lumps together Van der Waals, diffuse double layer interactions and cementation.

This section introduces clay minerals and discussed the electrostatic forces which are often assumed to be responsible the strength of rammed earth. Van der Waals and double layer forces are described and the DLVO theory explained which allows their net effect to be calculated. Clay bridges are described and it is shown that these may exist at a range of suctions. Cementation in stabilised rammed earth is described, historic rammed earth is often stabilised with lime and modern rammed earth with cement. The formation of a cementing matrix is discussed.

In Section 3.3.1 it was shown that a liquid bridge exists across a certain sided pore for a given relative humidity (Figure 3.9). A minimum pore radius can be defined based on the relative humidity, and at 1% relative humidity, this radius is still much larger than the range over which the forces described below act. Therefore the forces described below can be seen to hold packets of particles together, but not provide strength to the whole sample.

3.6.1 Clay

Clay particles are unique amongst soil particles as they hold an electrostatic charge on their surface. This charged surface means that clay particles are able to adhere to each other and thus provide an apparent cohesion to the soil. This electrostatic clay bonding is often considered to be the source of strength of earthen building materials.

A clay mineral consists of many layers of silica (SiO_4) tetrahedra and alumina (AlO_4) octahedral stacked above each other. Both the sheets of silica and the sheets of alumina have a net negative charge which must be balanced by the addition of other cations. Substitution may occur in the layer, with lower valence ions such as Mg^{2+} or Fe^{2+} substituting for Al^{3+}, in the alumina layer, and Al^{3+} or Fe^{3+} substituting for Si^{4+} in the Silica layer.

If two sheets are brought together, they are able to share oxygen atoms and a 1:1 clay mineral such as Kaolinite is formed. At the silica side of the layer there is a plane of oxygen atoms, whereas at the alumina side there exists a plane of hydroxyls. Bonding between layers therefore occurs via hydrogen bonds from one hydroxyl surface to the adjacent oxygen plane of the neighbouring 1:1 layer. Therefore the overall charge of the layer is always close to zero.

If three layers are brought together then a 2:1 clay mineral such as Smectite is formed. Here it is possible for the layer to have a net charge, which must be balanced by the presence of extra positive charge provided by cations such as Na^+ or K^+.. This allows positively charged ions in the interlayer creating an alternating arrangement of negative and positive charges. The interlayer can also contain water and the separation between 2:1 clay layers depends on the interlayer cations and the ionic strength of the surrounding solution, and therefore these clays are known as *swelling* clays (Giese and Oss 2002).

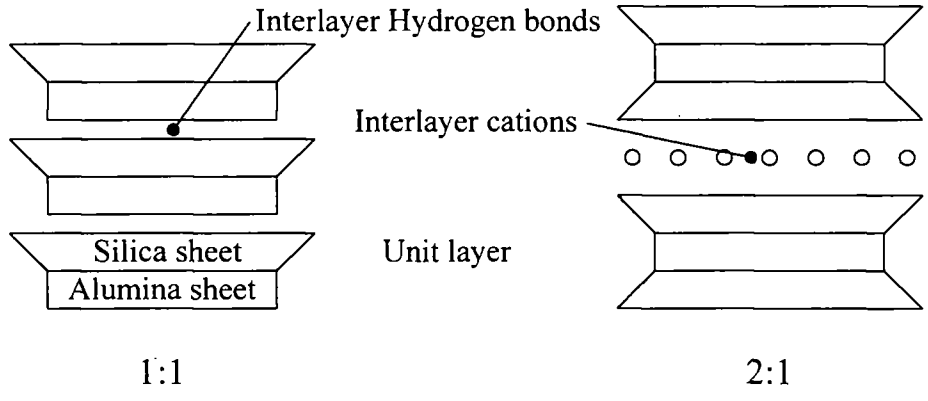

Figure 3.22 1:1 and 2:1 Clay layers

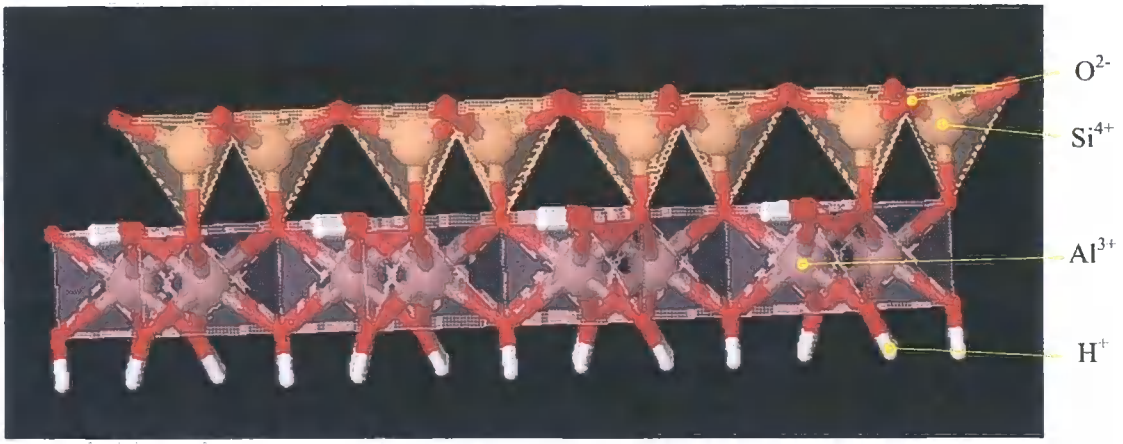

Figure 3.23 1:1 type clay (Kaolinite). Barak and Nater (2003)

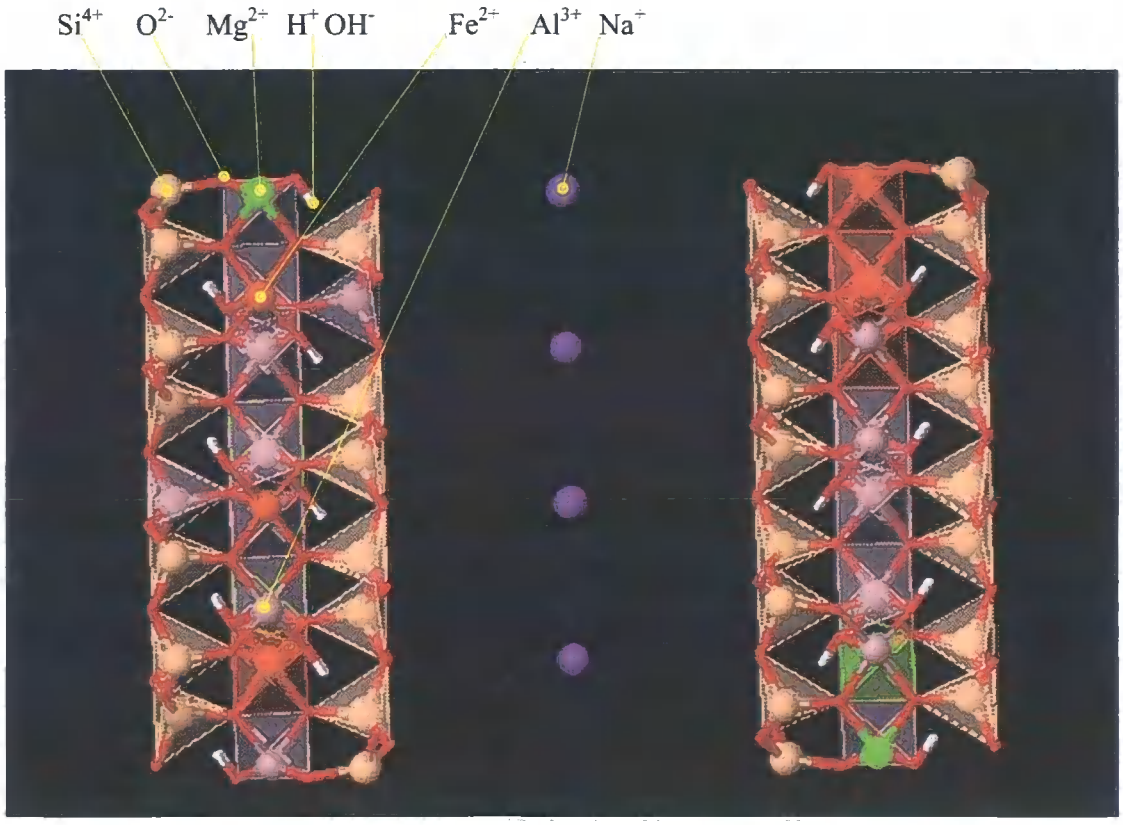

Figure 3.24 2:1 type clay (Smectite). Barak and Nater (2003)

3.6.2 Van der Waals

Johannes Diderik van der Waals was the first to note that there existed interactions between uncharged atoms and molecules which could not be described as covalent (electron sharing) bonding. These interactions became known as van der Waals forces and are much weak than covelent or ionic bonding, they operate because of instantaneous electric dipoles created by fluctuations in the position of charge about

an atom. When two non polar molecules are in close proximity, an instanteous dipole occurs within one molecule, this sets up an electric field which polarises the neighbouring molecule. These forces are almost always attractive and if molecules are treated as hard spheres, the interaction force reduces according to the inverse of the radius raised to the sixth power (Giese and Oss 2002). This implies that the forces are extremely localised (Israelachvili 2005).

3.6.3 Double layer

As explained in Section 3.6.1 clay minerals have charges at their surfaces and as a result of this electrostatic charge, the distribution of ions in the water and water molecules in the vicinity of the particle-water interface is perturbed. This perturbation decreases with increasing distance from the interface. There is a build up of positively charged ions close to the surface of the clay mineral, and the concentration of the charged cations reduces with increasing distance from the mineral surface. The net effect is that the cations form a dispersed layer adjacent to the clay sheet, with the cation concentration reducing with distance from the clay surface, until the concentration is equal to that of the water in the void space. The term *double layer* describes the clay sheet surface and the dispersed layer of cations.

If two clay minerals get too close to each other then the double layers on the surface of each mineral act to repel the minerals from each other. Therefore if the double layer is sufficiently thick then the minerals are dispersed from each other, while if the double layer is thin the minerals are able to approach each other closely, and become flocculated.

3.6.4 DLVO theory

Colloids are broadly defined as a dispersed medium within a continuous medium, in the field of soil mechanics, colloids are most commonly solid clay minerals dispersed in continuous liquid water. The net effect of van der Waals attraction and Double Layer repulsion may be calculated using the DLVO theory of colloids which is named after its four proponents (Derjaguin, Landau, Verwey and Overbeck).

The stability of a colloid system is determined by the sum of attractive van der Waals and repulsive Double layer forces of the particles as they approach each other due to

Brownian motion. The double layer repulsive forces create an energy barrier which prevents two particles from approaching and adhering to each other. However if the particles collide with sufficient energy to overcome this barrier then the attractive van der Waals pull the particles into contact where they adhere strongly.

3.6.5 Clay bridges

Networks of bridges of smaller particles may also form between larger particles as shown in Figure 3.25. These bridges may exist at a range of humidities, and may be formed, for example by clay particles bridging between two larger sand particles. At high humidity, the distance between the sand particles may be equivalent to r_{EQ} and thus a liquid bridge form between the sand particles. Within this bridge the DLVO forces described above will act, but may not contribute to the attractive force between the sand particles. However if the humidity is reduced, then the distance between the clay particles is closer to r_{EQ}. However the clay bridge will remain, held together by the liquid bridges between the clay particles.

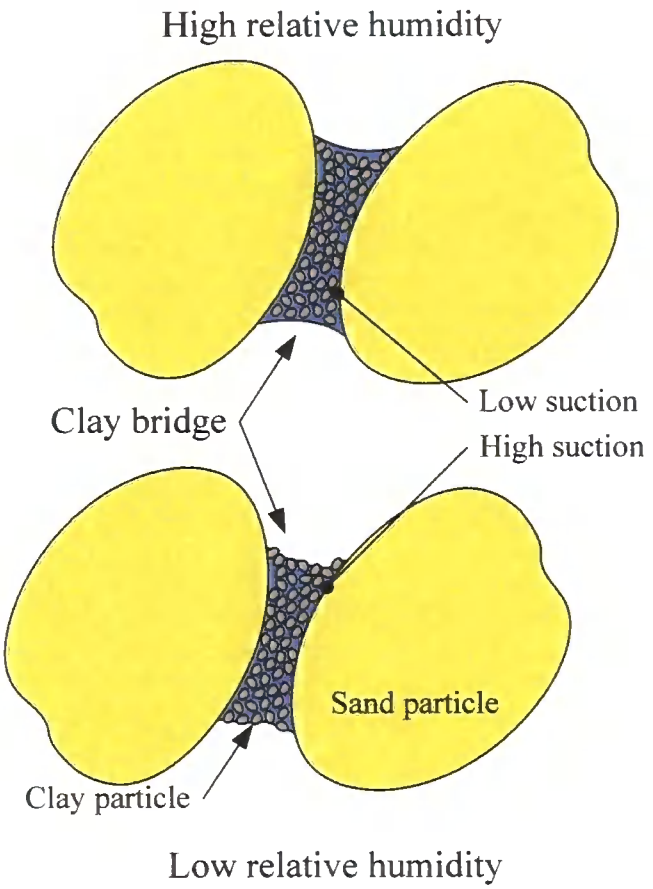

Figure 3.25 Clay bridge at both high and low relative humidity

3.6.6 Cementation

Up to this point this thesis has dealt with rammed earth as a soil, and argued that the strength of rammed earth is derived from particle interlock and the presence of liquid bridges between particles. It will be argued that this holds where no cementing matrix is present, i.e. in *unstabilised* rammed earth. However a number of historic, and many modern rammed earth constructions are *stabilised* with a cementing agent. Although the main focus of this thesis is unstabilised rammed earth, this section briefly explores cementation in rammed earth, and how the cementing matrix may interact with particle interlock and suction as discussed previously.

Historic rammed earth structures are often stabilised with lime (Houben and Guillaud 1994, Arango Gonzalez 1999) while cement is added in modern rammed earth construction (McHenry 1984; Easton 2007). Lime is produced by burning chalk or limestone to form *quicklime* (Calcium Oxide – CaO). If water is then added to this quicklime *slaked lime* is formed (Calcium Hydroxide – $Ca(OH)_2$). If clay is present in

the original clay or limestone then the lime is known as *hydraulic*, and if no clay is present in the limestone then the resulting lime is said to be *non-hydraulic.* Hydraulicity is defined as the ability to set underwater, with non hydraulic limes hardening by reacting with carbon dioxide to form calcium carbonate ($CaCO_3$) in a process known as *carbonation* to form limestone once again. Hydraulic limes react with water to form a solid Hydrated Calcium and Silica matrix (C-S-H). Portland Cement was developed from hydraulic limes in the early 19th century and so named for its similarity to Portland Stone. Portland Cement contains a designed mixture to form a series on reaction products on contact with water which grow to form a series of interlocking needles which provide the strength of the hydrated cementation matrix. The two principal reaction products of cement are Alite which is responsible for the development of early strength, Belite which is responsible for the later strength.

Alite (Tricalcium silicate, C_3S). $2Ca_3SiO_5 + 6H_2O \rightarrow 3CaO.2SiO_2.3H_2O + 3Ca(OH)_2$

Belite (Dicalcium silicate, C_2S). $2Ca_2SiO_4 + 4H_2O \rightarrow 3CaO.2SiO_2.3H_2O + Ca(OH)_2$

Two types of pore structure may be defined within the cement matrix. *Isolated* pores are completely enclosed by hydration products and so material transport into and out of the pore is limited. *Connected* pores offer a continuous pathway between different regions of the microstructure.

The strength of concrete is derived from the combined strength of the inert aggregate held strongly within the cement matrix, but incorrect proportions of cement or aggregate lead to significantly reduced strength concrete. In the context of earthen materials, cement stabilised pressed earth blocks and cement stabilised rammed earth walls have been developed, but the study of this material is currently relatively simplistic and method based (for example Kumar and Reddy 2007; Maini 2007) and the interaction between the cement matrix and the suction and interlock is little understood. Additional study will be required to determine and to quantify the exact mechanisms and interactions between the cement matrix and the unsaturated soil strength gaining mechanisms.

3.6.7 Conclusions of the strength of rammed earth

The previously expressed notions suggested for the origins of strength in rammed earth of van der Waals attraction and Double layer repulsion have been shown only to apply within a saturated region, where colloid theory applies. The Kelvin equation (Equation (3.24)) and observation of the air entry value (Equation (3.26)) allows the placing of limits $\left(r_{EQ}\right)$ on the pores size which will be air or water filled for a given relative humidity. For example a humidity of 99% will allow a fully saturated pore of 0.1mm diameter to be fully saturated with no evaporation. However, at a relative humidity of 50% a pore of 0.0016mm diameter will be saturated with no evaporation. DLVO theory only applicable in a liquid medium, therefore only applicable in a saturated pore or within a liquid bridge. While this controls whether the clay minerals will become flocculated or dispersed, it does not provide the 'cohesion' in unsaturated soil. It may therefore be argued that unstabilised rammed earth consists of clumped particles, held together by menisci at their surface (Section 3.4.6), which are interlocked and also held together by liquid bridges between these clumped particles. Inside these clumped particles, the pores are saturated and colloid chemistry applies.

If the strength of rammed earth were due solely to colloid chemistry, then the strength of a fresh (i.e. saturated) rammed earth would be equal to that when dried. This has been found by many authors not to be the case (for example Houben and Guillaud 1994).

In contrast cement stabilised rammed earth offers a more complex situation, where menisci may be present, but a proportion of the strength may be derived from a solid cementing matrix which is formed over time. This matrix takes the form of limestone if a non hydraulic lime is used, and a C-S-H matrix if hydraulic lime or Portland Cement is used. The formation of this matrix is governed by the availability of water, and there are therefore the conflicting strength forming processes of carbonation and menisci growth. This observation may lead to an explanation of the phenomenon observed by many authors (for example Minke 2007 and Kumar and Reddy 2007) of an optimum cement to clay ratio.

3.7 Measurement of suction

As indicated previously, suction appears to play an important role in the strength of rammed earth. It is therefore important to be able to measure suction accurately. Direct measurement of suction is preferred as pore water pressures changes can be measured in one sample. Methods of direct measurement of matrix suction include the tensiometer and the null-type pressure plate. Indirect measurement of total suction are the filter paper technique which relies on calibration against Kelvin's equation (3.24) and the thermal conductivity sensor (Fredlund and Radhardjo 1993).

Probes for measuring suction, known as tensiometers were first developed at Imperial College (Ridley and Burland 1993) and have subsequently also been constructed and used by others such as Meilani, Radhardjo et al. (2002), Lourenço, Gallipoli et al. (2006) and Rojas, Pagano et al. 2008. The tensiometers used in this investigation are those described by Lourenço, Gallipoli et al. (2006). A tensiometer consists of a high air entry porous ceramic stone disk mounted at the end of a housing, with one face of the disk in contact with the soil. Behind the disk inside the housing is a small reservoir of water and behind this a pressure transducer, which is a flexible diaphragm with strain gauges mounted on it (Figure 3.26 and Figure 3.27).

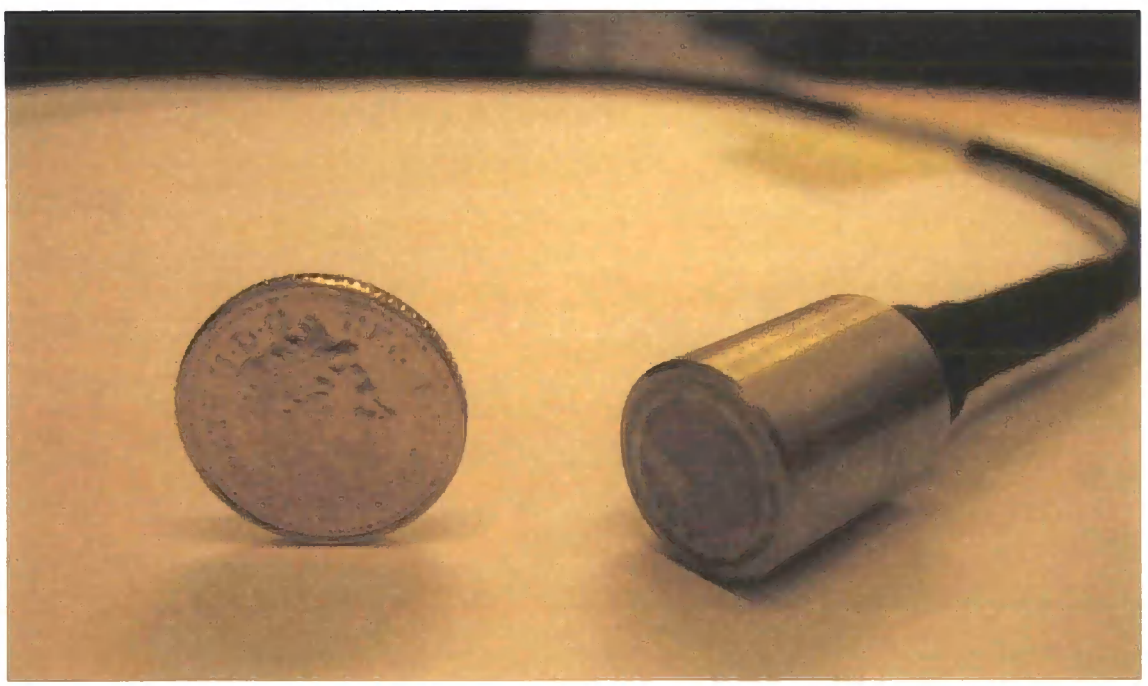

Figure 3.26 Durham University - Wykeham Farrance tensiometer with five pence coin for scale

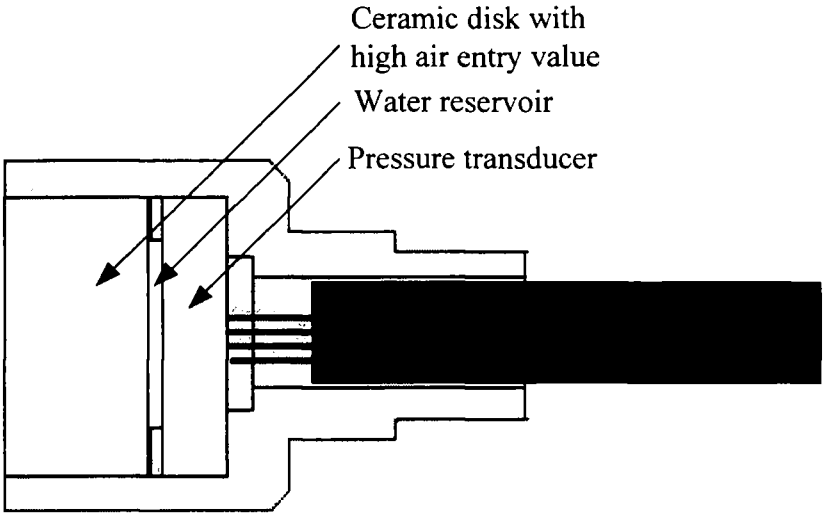

Figure 3.27 The Durham University - Wykeham Farrance tensiometer schematic. After Lourenço, Gallipoli et al. (2006)

The principle of suction measurement using a tensiometer is the equalisation of the pore water pressure in the soil and pore water pressure in the water reservoir behind the ceramic disk (known as a porous stone). Prior to measurement, the tensiometer is placed in a saturation chamber (Lourenço 2008) and de-aired water is applied under pressure to the face of the porous stone. This forces water into the pores in the stone and then into the reservoir behind the stone. This process is known as saturation, and aims to fill the pores of the porous stone and the reservoir completely with water.

To measure the suction in a soil, the tensiometer is placed against the surface of the soil, and steps are taken to ensure a good contact between the stone and the soil. The pore pressures in the soil and in the stone are different, the pore pressures in the porous stone are initially equal to atmospheric and for an unsaturated soil the pore pressures are negative. As a result of this water is drawn from the water reservoir through the porous stone and into the soil. As water is drawn from the reservoir the flexible diaphragm bows to accommodate the reduced volume now present in the water reservoir. This bowing is recorded by the strain gauges on the diaphragm, and can be calibrated against known applied values of pressure (in either the negative or positive range) and thus the pore water pressure in the soil measured. Since suction is the difference between pore air pressure and pore water pressure, the suction can be calculated assuming the pore air pressure is equal to atmospheric. While the results

presented here are given in terms of pore water pressure (negative for unsaturated soils), this is the negative of suction.

As outlined in Section 3.2.1, cavitation occurs when the pressure of the water falls too low and air held in solution in the water comes out of solution in the form of bubbles. When using tensiometers, the water inside the porous stone attempts to equalise in pressure with the water in the sample under test. When a tensiometer is first introduced into the sample, the suction measured is zero, as the water pressure is equal to the air pressure. As water is drawn from the tensiometers into the sample, the water pressure inside the porous stone, and in the reservoir decreases and the suction measured by the tensiometers increases (water pressure becomes more negative). Problems arise when the water pressure becomes too low, and cavitation occurs within the porous stone. This renders the tensiometers unable to measure suction correctly and the tensiometers must be re-saturated before they can be used again.

3.8 Experimentation

The theory presented above has argued that the additional strength in rammed earth is due to the phenomenon of suction. Measurement of suction at Durham University is well advanced and the use of tensiometers routine in the laboratory. A small series of simple tests were proposed to investigate the link between the strength of rammed earth and suction. Unconfined compression tests were performed on samples of rammed earth compacted using the Proctor method (Section 2.2.2) and left to dry to different water contents. Target water contents were achieved by compacting the samples at a known water content, then allowing the samples to dry through evaporation and monitoring the change in mass and hence the water content. Once the required mass was obtained, the samples were wrapped in a water vapour impermeable sheath (shown in Figure 3.28), and secured at the top and bottom to aluminium loading plates. The samples were then left for a further period of time to allow the moisture content to equalise through the sample and to remove the moisture content gradient set up through evaporation (see Section 3.12.3). A tensiometer for the measurement of suction was then placed in contact with the top of the sample such that suction could be measured. Once a steady state suction was recorded by the tensiometer, the sample was tested in unconfined compression to failure, while still recording the suction. Upon failure the whole sample was placed in an oven at 105°C and the moisture content measured.

3.8.1 Issues in testing

Structural materials are most usually tested in uniaxial unconfined compression, uniaxial tension, or in bending tests. Unconfined compression tests $(\sigma_2 = \sigma_3 = 0)$ are usually performed on rock or concrete as simple tests providing a strength value to which other parameters may be fitted. Failure of a sample in an unconfined compression test is through shear and the development of micro cracks (Hudson and Harrison 1997).

The size and shape of samples under test together with the speed of the test have been observed to affect the strength of a sample. The elastic modulus of a sample should not vary significantly with specimen size as the response is an average response for

many aspects of the microstructure, however a larger sample will contain more micro cracks, thus the probability of more extreme cracks is greater, and thus the compressive strength of a larger specimen is reduced. The effect of the shape on the strength of the sample is determined by the contribution of the *end effects* to the stress field within the sample. Due to the mismatch between the elastic properties of the loading platens and the sample, a complex zone of triaxial compression is set up at the ends of the specimen, with the loading platens effectively restraining radial expansion at the ends of the sample. In a squat sample the end effect may dominate the stress field, whereas in a slender sample, the end effect is likely to have a much reduced effect (Hudson and Harrison 1997).

In geotechnical testing the rate of loading is found to affect the strength of the sample, due to the build up of excess pore pressure on loading. Two extremes are defined, quick testing allows a build up of pore pressures and is referred to as quick undrained testing, while slower drained testing allows the pore pressures to dissipate. Because of the increase of pore pressure in saturated samples, failure occurs at a lower stress than in undrained test compared to a drained test. As no water was allowed to leave the sample, and the tests were carried out comparatively quickly (around 20 minutes) they are considered undrained.

3.8.2 Construction and testing procedure

Samples were prepared using a proctor compaction mould, as outlined in Walker, Keable et al. (2005) and as improved by Horncastle (2007). Sample soil was first oven dried at 105°C for 7 days, then placed into re-sealable bags such that two bags could be used for the construction of one cylinder. Distilled water was then added to the bags, such that the water content then matched the predetermined optimum water content. The bags were then turned to distribute the water evenly within the bag, and left to equalise for a further 7 days. Compaction was carried out in 5 layers of soil, each layer being compacted by 15 blows using a 4.5kg hammer.

Following compaction of the 5 layers, a screed of particles passing 425μm sieve was placed on the top surface of the cylinder. This screed served a dual purpose of producing a flat loading surface and producing a fine particle paste on which to place the tensiometer. Immediately following application of this screed, the Proctor split

mould was removed and the mass and height of the sample recorded. The sample was then left to air dry to the required moisture content, calculated by measuring the mass of the sample, and calculating the mass of water lost. Once the sample reached the desired moisture content, it was wrapped in a water impermeable sheath secured with rubber O-rings placed against steel loading plates at the top and bottom of the sample. The samples were then left for at least 7 days to allow water within the sample to distribute evenly through the sample. When it was considered that the samples were ready for testing, the top loading plate was replaced with a loading plate drilled to accommodate a tensiometer.

The tensiometer was placed against the top surface of the sample through a drilled loading plate. As detailed in Lourenço (2008) a small volume of water was added to the hole into which the tensiometer was placed, prior to introduction of the tensiometer. This water acted to make the screed on the surface of the sample more paste like, and thus improve the contact between the tensiometer porous stone and the surface of the sample.

The cylinders were tested uniaxially in a triaxial testing rig. The top loading plate was drilled to accommodate a tensiometer which was free to move on application of load. The sample was placed within a triaxial cell to restrain the loading piston and not allow any horizontal movement, however the cell was not pressurised. An axial displacement transducer was fixed to the base plate of the sample, and the load measured through a load ring at the top of the sample. Loading was carried out at a constant strain rate of 0.1mm/min (as used for a quick, undrained triaixal test, and slower than recommended by Walker, Keable et al. 2005 (1.0mm/min)) and measurements of suction, load and axial displacement taken every 10 seconds using the Triax soil data logging program (Toll 1999). Load, axial displacement and suction were measured and loading continued until failure planes were clearly visible. Following failure the samples were removed from the loading frame and their water content determined. The top and bottom loading plates and the impermeable sheath were removed and the sample weighed. The whole sample was then placed in an oven at 105°C for 48 hours. The samples were then reweighed and the moisture content determined.

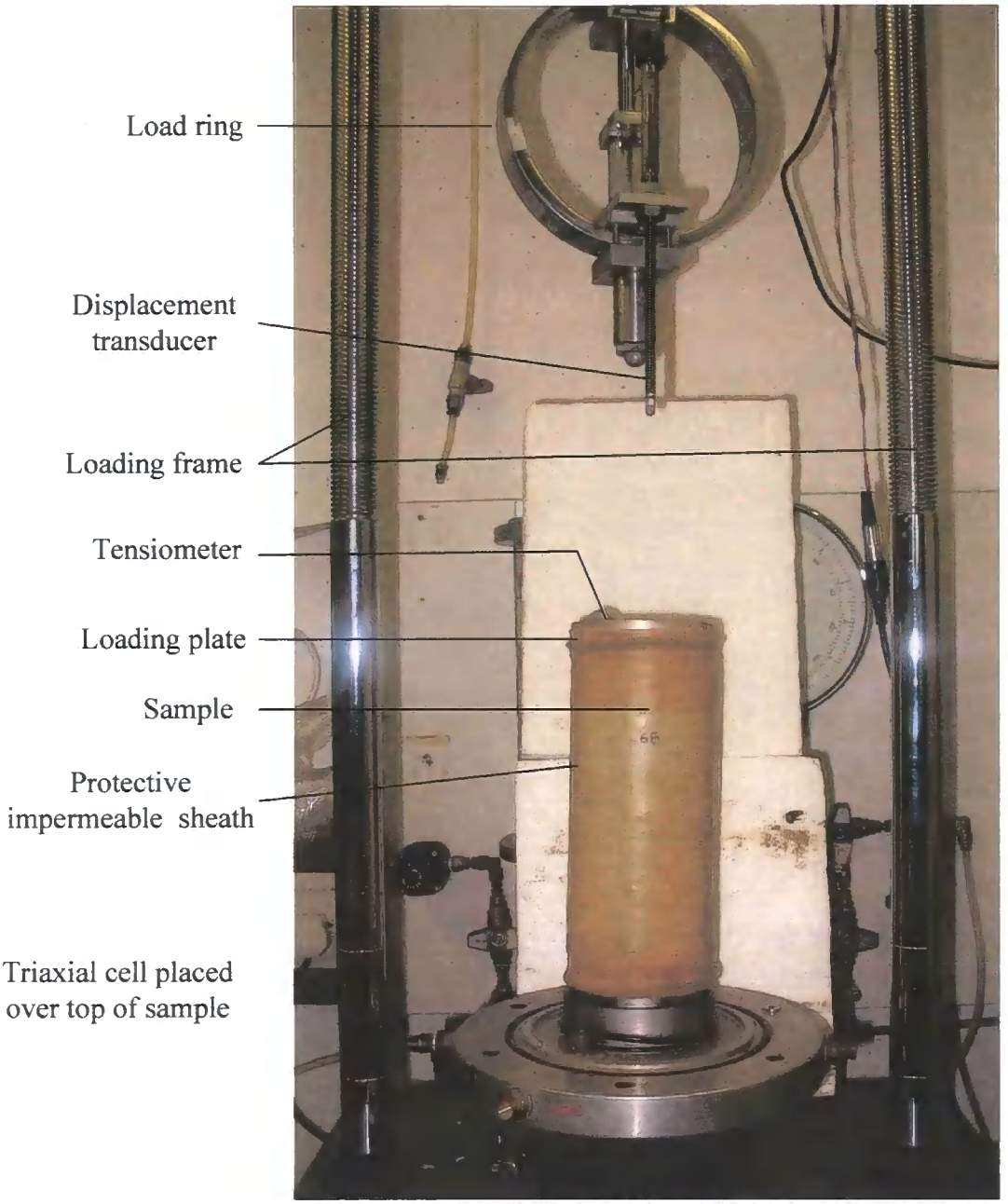

Figure 3.28 Photograph of experimental setup

3.9 Observations

A number of months were spent in the construction and testing of the samples, with particular issues found in the cavitation (Section 3.8.1) and equalisation of the tensiometers, and in the loading and failure mechanisms of the samples.

3.9.1 Tensiometers

Figure 3.29 shows a sample plot of a tensiometer equalising. The plot shows a rapid increase in measured suction to 250kPa in a few hours, followed by a six day period of increasing measured suction, followed by testing. The long period required for each test, coupled with repeated cavitation of the tensiometers (Section 3.7) led to a testing period which extended beyond that originally envisaged. The suction was seen to be constantly reducing during measurement, and a decision had to be made as to when to perform the compression testing. The reason for the continuing reduction was thought to be the slight increase in water content of the sample due to the addition of a small amount of water added on placement of the tensiometer, and the slight permeability of the protective sheath, leading to continuing water loss. Therefore compressive tests were usually performed when the suction changed by less than 1kPa in four hours.

Cavitation was a major issue when measuring suction in the rammed earth samples, as the pore water pressure at low water contents frequently caused cavitation within the tensiometer. Figure 3.30 shows an attempt to measure the suction in one sample, where two tensiometers were used sequentially, both cavitating before reaching a steady state value of suction in the sample.

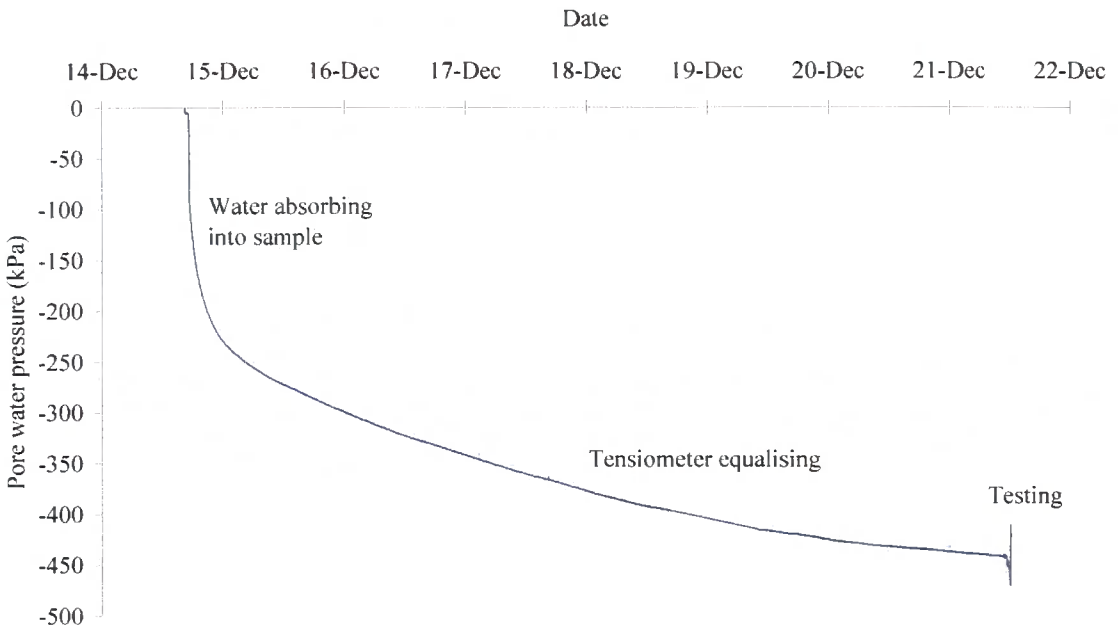

Figure 3.29 Sample tensiometer equalising plot

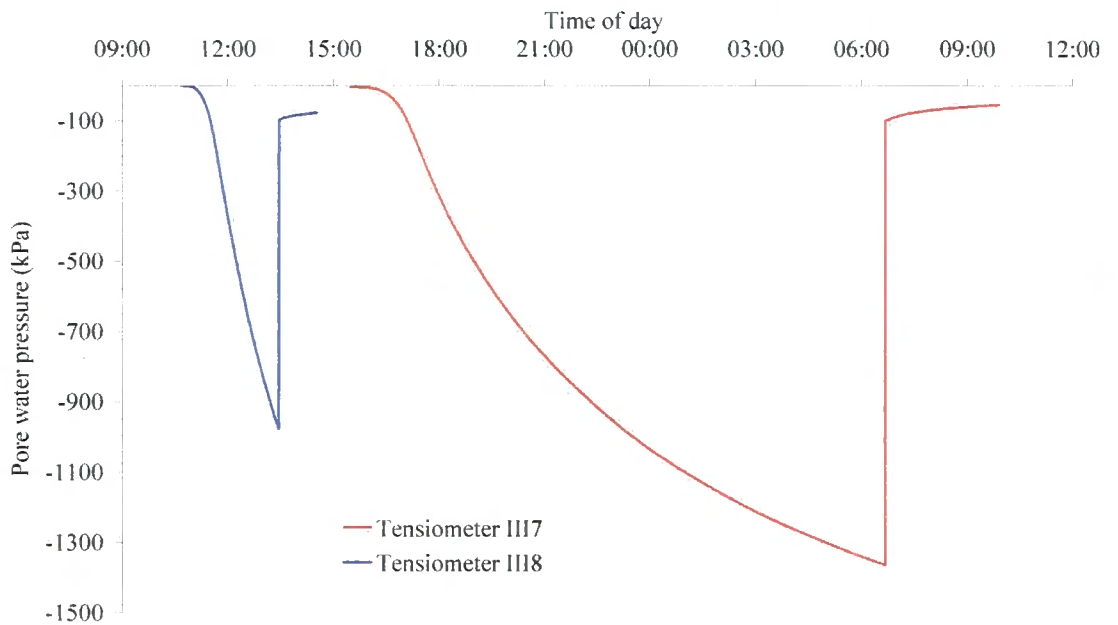

Figure 3.30 Sample cavitation of tensiometers inserted into samples

3.9.2 Failure modes

Previous experimentation (as outlined in Chapter 2) led to the conclusion that failure across the compaction planes is common in rammed earth, if the stresses are applied in a certain orientation. The initial few tests on the rammed earth cylinders were conducted without a triaxial cell surrounding the sample, and this led to imperfect loading to the sample. Non uniformity in the sample (for example a larger particle on one side of the sample) led to slight buckling of the cylinder. This buckling was exacerbated by the ability of the loading ram to rotate with the bucking attempting to always load the top of the sample normally (perpendicular). This buckling induced shear stresses across the weaker compaction plane, leading to failure across that plane. This problem was solved by placing a triaxial cell over the sample which acted to keep the loading ram vertical, thereby reducing any buckling tendencies of the sample. Subsequent samples tested failed through diagonal shear as expected.

Figure 3.31 Cylinder failure through horizontal delamination (left) and shear (right)

3.10 Results

A total of 15 successful cylinder tests were carried out, at water contents ranging from 2.2% to 10.2%. The tensiometers are able to measure a suction of up to 1500kPa, but the maximum suction measured was 773kPa, at a water content of 5.5%. At water contents lower than this the suction exceeded 1500kPa. Attempts to measure the suction were made for each of the samples, but those where suction is recorded as N/A, the suction as measured by the tensiometers exceeded 1500kPa. Table 3.1 shows the cylinder ID, together with measurements taken during testing, Sx denotes cylinders where suction was measured and Nx where it was not measured during testing.Bboth the initial and the final suction values are given. The maximum stress achieved, and the axial strain at that stress are given. The failure mode is recorded (D – delamination, S – shear, B – barrelling). The final water content, determined by oven drying of the whole sample at the end of the test is also given.

ID	Test date	Water content (%)	Initial suction (kPa)	Suction at max. stress (kPa)	Max. stress (kPa)	Axial strain at max. stress	Failure mode	Stiffness (MPa)
S1	25/09/06	10.2	-9	-3	160	0.0364	D	4.4
S2	03/10/06	9.4	-43	-27	164	0.0328	S	5.0
S3	22/08/06	8.6	-119	-104	211	0.0266	B	7.9
S4	25/09/06	8.4	-179	-128	338	0.0174	S	19
S5	21/08/06	8.3	-168	-120	128	0.0110	D	11
S6	22/12/06	7.2	-412	-274	470	0.0183	B	26
S7	21/12/06	7.1	-469	-220	437	0.0170	B	26
S8	14/08/06	5.8	-687	-565	444	0.0008	D	-
S9	15/08/06	5.5	-773	-538	596	0.0144	S	41
N1	01/02/07	4.6	N/A	N/A	843	0.0112	S	75
N2	01/05/07	2.8	N/A	N/A	773	0.0154	S	50
N3	02/05/07	2.7	N/A	N/A	1030	0.0065	S	160
N4	03/05/07	2.3	N/A	N/A	979	0.0364	S	26
N5	08/05/07	2.2	N/A	N/A	813	0.0112	S	72
N6	05/02/07	2.2	N/A	N/A	1078	0.0095	D	113

Table 3.1 Cylinder test results

3.10.1 Strength - water content relationship

Figure 3.32 shows that there appears to be a linear relationship between failure stress and water content. This relationship is intuitive, and tests on a wide range of earthen building materials have recognised this (for example Greer 1996; Houben and Avrami 2000; Walker, Keable et al. 2005). It is proposed that at a simple level, the strength of an earthen material is proportional to the suction, and that the suction is proportional to the water content, thus the strength of an earthen material is proportional to its water content. The water content of a sample depends on the unique soil water characteristic curve and the relative humidity of the surrounding air. Thus for a given relative humidity of 50%, this particular soil sample will achieve a moisture content of around 2%, and thus a maximum strength of around 1.0MPa. However the saturated water content of the soil is close to 10%, where the failure stress is only 0.2MPa. Walker, Keable et al. (2005) note that if rammed earth is liable to become damp, then its design strength should be 50% of that for a 'dry' sample. It can be thus seen that this is not the case, and the reduction in strength is much greater than that discussed by Walker, Keable et al. (2005).

The spread of the failures of the samples is due to the quality of sample preparation and of loading. As outlined in Section 3.9.2 some of the first samples failed through horizontal layer delamination, and thus the recorded failure stress is lower than would otherwise be expected.

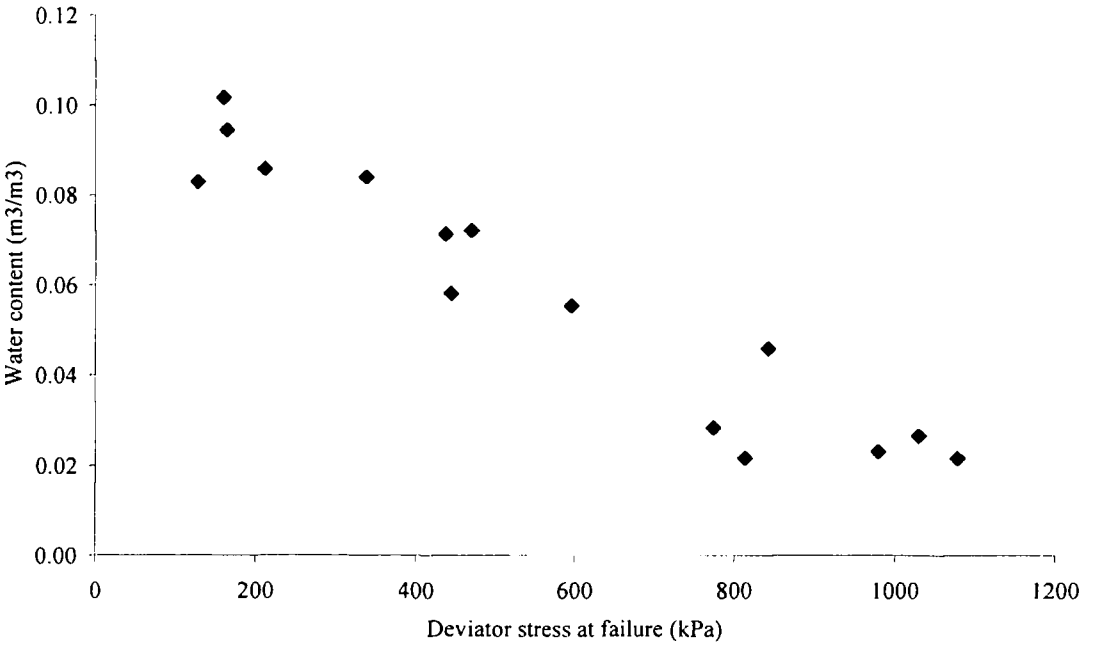

Figure 3.32 Strength - water content relationship

3.10.2 Initial suction - strength relationship

Figure 3.33 shows that there appears to be a linear relationship between initial suction and failure stress, showing that there is a minimum failure strength of 160kPa, which occurred at an initial suction of 9kPa. It is assumed that this graph is only linear in the range which is shown, and as shown in Figure 3.32 the failure stress does not increase dramatically for a corresponding reduction in water content. Filter paper tests (Jaquin, Augarde et al. 2007) show that at a water content of 2%, the suction is close to 30000kPa (corresponding to a pore air relative humidity of 80%), and it is assumed that when the pore air humidity reaches that of the surrounding air (50%), the suction will be close to 100 000 kPa. There is obviously no corresponding increase in strength, and the reasons for this are discussed in Section 3.11.

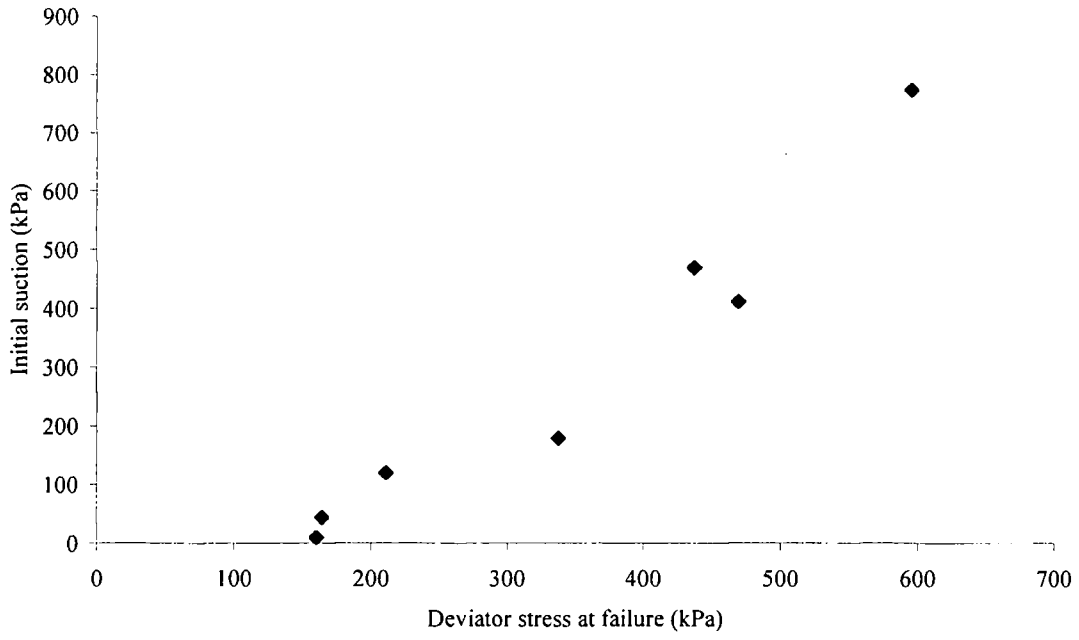

Figure 3.33 Relationship between initial suction as measured in the samples and deviator stress at failure

3.10.3 Change in suction on loading

Figure 3.34 shows the deviatoric stress versus suction relationship, for loading of the samples. As all loading was unconfined, the deviatoric stress is equal to the axial load ($q = \sigma_1$). A number of observations can be taken from Figure 3.34. With all samples, suction decreases on initial application of load. At high water contents (low suction) the suction then increases until failure, whereas a lower water contents, the suction continues to reduce until failure. A water content of 5.5% shows little change in suction on loading. A failure envelope can be drawn encompassing the low water content samples, but it can be seen that this does not extend to the higher water content samples. Problems with recording the load of the sample at 7.2% water content means that only a small number of points are recorded. Similar unconfined tests, with suction measured using tensiometers have been carried out by Cunningham, Ridley et al. (2003) and similar behaviour was observed. It should be noted that only seven of the fifteen samples tests are presented in Figure 3.34 as suction was only measured for these samples. The tensiometers are only able to measure a suction of 1500kPa, and remaining samples exceeded this suction. There are two issues with this; firstly that that the change in suction on loading cannot be measured; and secondly that in order for a suction, and a change in suction to be

measured, there must be a continuous network of pores filled with water, through which to transmit information from the shearing regions to the tensiometer. It is possible that at high levels of suction, such a continuous pore network might not exist.

The samples were sheared very quickly (0.1mm/min) which would not allow sufficient time for excess pore water pressures to dissipate. Meilani, Radhardjo et al. (2002) also noted a change in suction on loading, but observed that there was no change when the samples were sheared extremely slowly (0.0008mm/min).

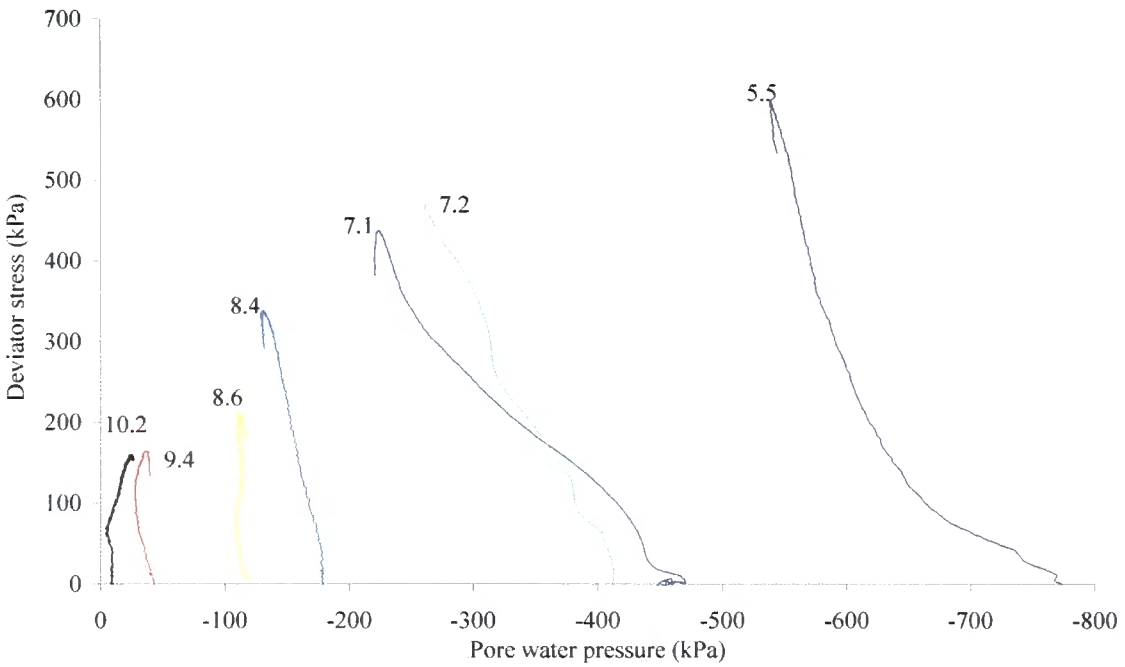

Figure 3.34 Measured change of pore water water pressure on loading

3.10.4 Strain - suction relationship

Figure 3.35 shows the relationship between axial strain and suction on loading. As only axial strain was measured, it is not possible to directly infer the volumetric behaviour of the sample. There appears to be a relationship between the strain at failure and the suction, and Figure 3.35 also clearly presents the change in suction on loading. It can be observed that there is a large reduction in suction on loading for samples with initially low water content, and a small increase in suction for samples with an initially high water content.

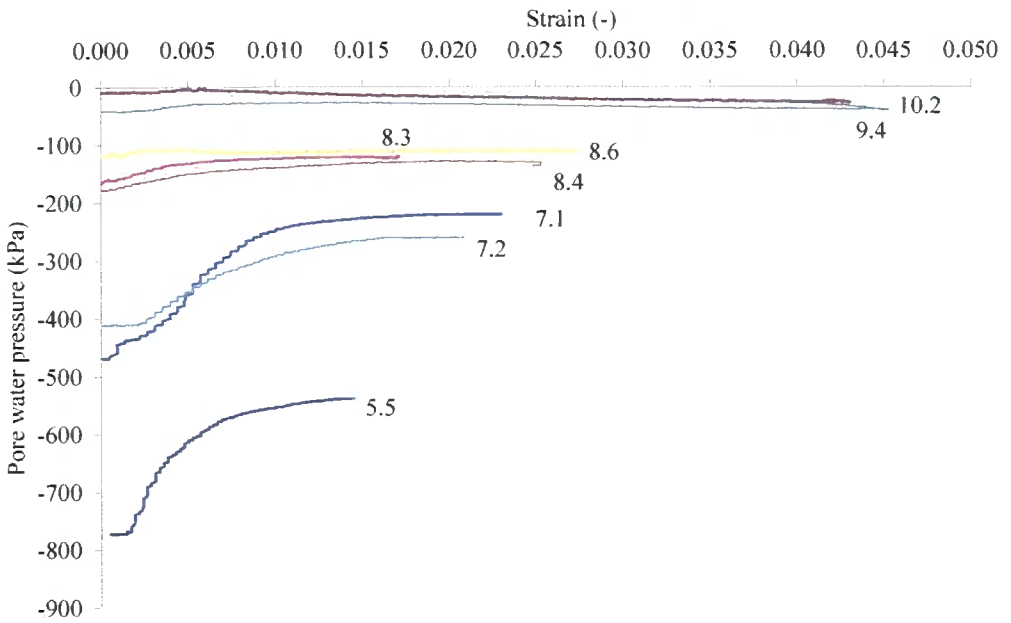

Figure 3.35 Strain - suction relationship

3.10.5 Modulus - water content

Figure 3.36 shows the axial stress – strain relationship for the samples where suction was measured and Figure 3.37 shows the axial stress – strain relationship for all samples. The lower water content samples fail at a higher axial stress than those at higher water contents. It can be seen that ductile behaviour is observed in the high water content samples, and brittle behaviour in the low water content samples. The modulus of the samples increases with decreasing water content, and both figures show increasing failure strain with increasing water content. Figure 3.36 shows that where suction increases, the modulus is low, and where suction increases the modulus is higher, and constant regardless of failure strain. Figure 3.37 shows that the modulus continues to increase with reducing water content. Three distinct regions are seen in Figure 3.37; a region of distinct brittle behaviour, where there is a significant reduction in post peak strength; a slightly ductile region where there is a defined peak strength, but only a slight reduction in post peak strength; and a very ductile region, where there is only large straining at a relatively constant stress level. Table 3.1 shows that the stiffness values range between 4.4MPa at the highest water content to a maximum of 160MP at the air dry state, which was the reference stiffness used in the Hardening Soil model of the walls constructed in the laboratory (Table 2.5), but significantly lower than the stiffness (56GPa) recorded by Gonzalez (1999).

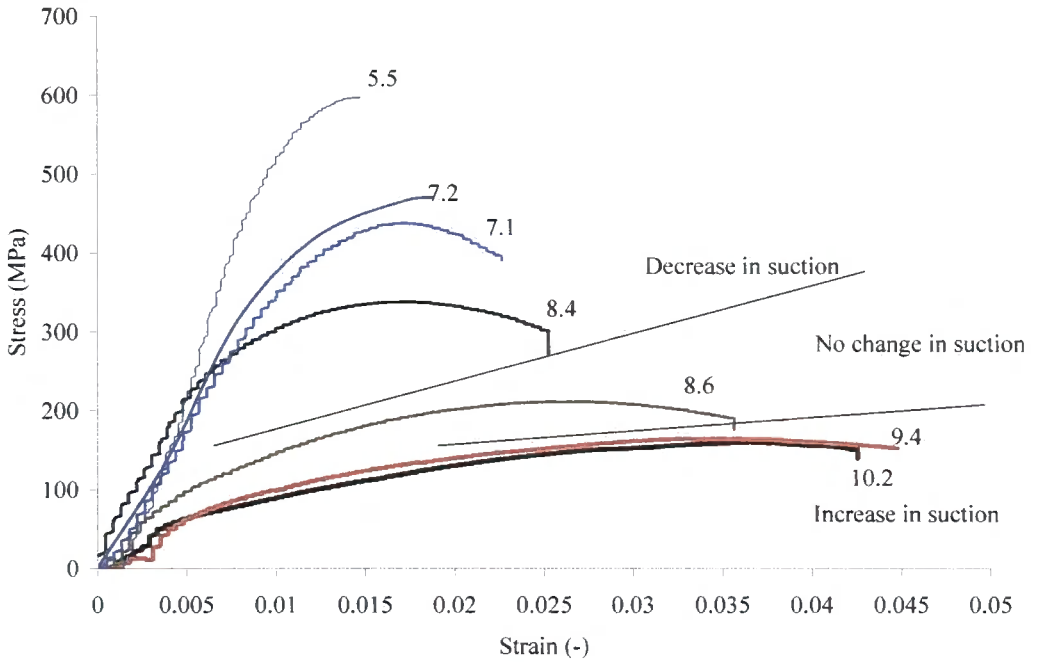

Figure 3.36 Stress - strain relationship for samples with measured suction

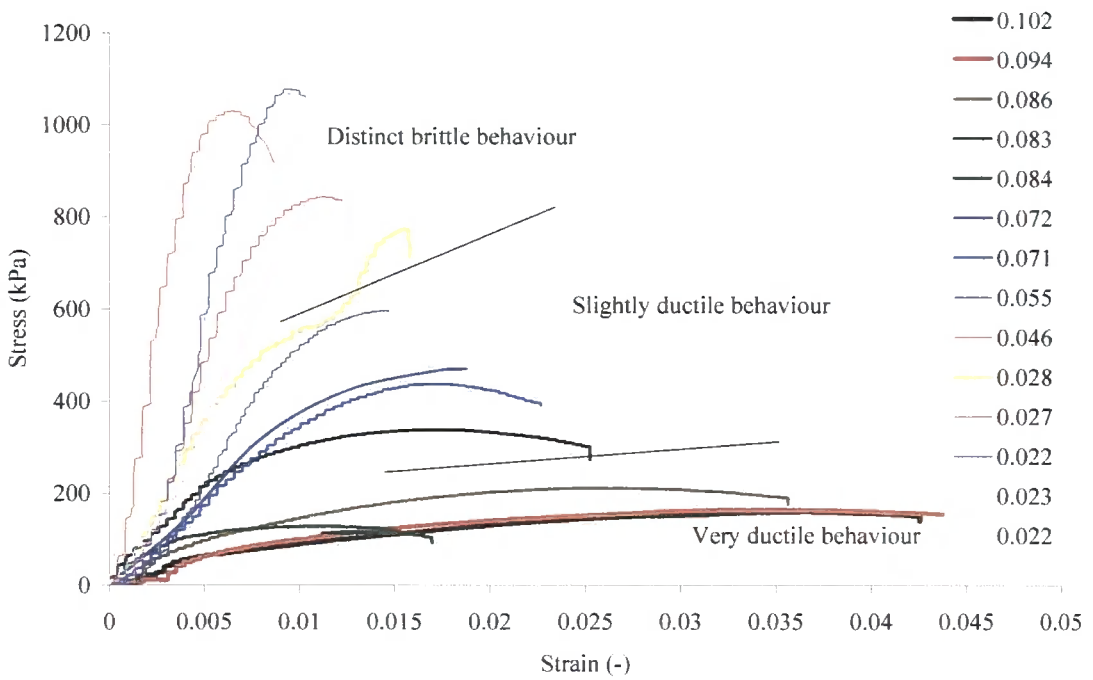

Figure 3.37 Stress - strain relationship for all samples. Key indicates water content

3.10.6 Pseudo soil water characteristic curve

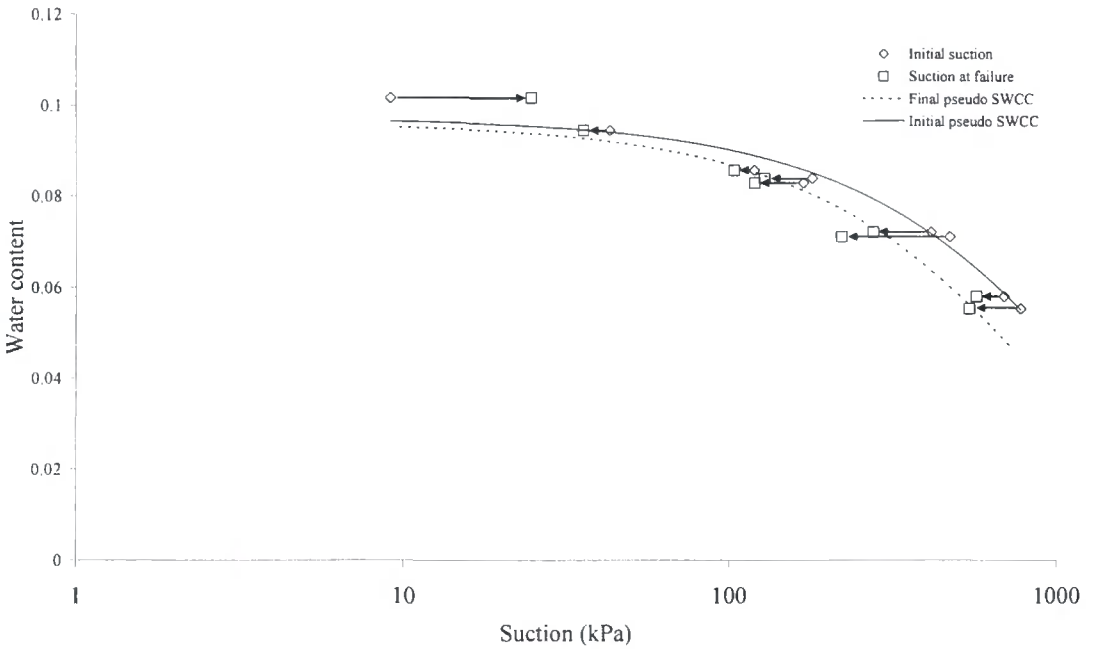

Figure 3.38 Water content - suction points

The suction in the samples was measured prior to and during each test, and the water content of each sample determined following each test. Figure 3.38 shows the water content and suction for each of the samples. Given that each of the samples was prepared at the same compactive effort and water content, Figure 3.38 can be seen as an approximation to the drying section of the Soil Water Characteristic Curve for the samples (a *pseudo SWCC*). On loading, the suction in each of the samples changed and thus another approximation to a SWCC can be drawn. Figure 3.38 shows that all the samples reduced in suction, with the exception of the highest water content sample which increased in suction.

3.11 Discussion

Although a small range of simple experiments was carried out, significant conclusions may be drawn from these when interpreted in the light of other similar work and the theories outlined in Section 3.3. This section attempts to interpret the results, drawing conclusions for rammed earth as a building material and viewing the tests as further evidence for the double structure nature of unsaturated soils alluded to by Cunningham, Ridley et al. (2003).

3.11.1 Expected saturated results

An increase in pore water pressure (reduction in suction) was observed at high moisture contents, and a decrease in pore water pressure (increase in suction) was seen at low water contents. If a saturated constant water content sample is considered, a dilation (increase in volume) of the sample would lead to a reduction in the pore water pressure. A contraction of the sample at constant water content would increase the pore water pressure, and a reduction in suction. Unfortunately, it is impossible to determine the magnitude of the sample dilation because while axial strain was measured, the circumferential strain was not. Given that the samples were unconfined, it seems reasonable to assume that there was some radial expansion, but the magnitude of this was not determined.

3.11.2 Double structure framework

The concept of a double structure, as outlined in Section 3.4.6, is considered to be useful in explaining the results of the sample testing. Two facts should be considered when interpreting the results of the tests in the light of the double structure theory – that air is more compressible than water, therefore the air filled pores will reduce in volume in preference to the water filled pores. As these were quick, undrained tests, the water content of the samples remained constant. As an unsaturated sample is loaded, the air filled pores will reduce in volume first, and the suction will reduce as outlined in Section 3.4.6. Air is able to escape from those pores connected to the surface of the sample (the membrane is air permeable). This reduction in suction should then continue until all of the air filled pores become water filled, through reduction of their maximum radius below the required air entry value (explained in Section 3.3.1). Continued shearing (and volume reduction, i.e. 'wet' of critical) will

lead to a sample where all of the pores are water filled, and therefore the sample may be considered saturated. However the water is still under tension due to the presence of menisci at the surface of the sample, a state which may be considered the Air Entry Value suction for the sample. As outlined in Section 3.11.3, an unsaturated soil sample where the suction is above the air entry value of the soil may be considered to behave as saturated.

This idea may also be extended to consider all of the soil particles in the sample, and the formation of clumped particles as outlined by Toll (1990). Each clumped particle must consist of a number of smaller particles held together by water menisci at the clumped particle surface. The clumped particles interact with each other through the liquid bridges between them and through 'dry' interlock. Inside the clumped particles the particles interact through 'wet' interlock. Although the relative magnitudes of each of these processes is difficult to determine, it would seem possible that the change in sample strength from saturated to unsaturated may be explained by considering the sample strength as a summation of the interlock plus liquid bridge force between saturated clumped particles, and that on shearing, the clumped particles are gradually destroyed by becoming larger and larger as the air gaps between them are removed, until eventually a saturated sample remains, where the bulk water is under tension. Figure 3.39 shows an idealisation of the volumetric compression of clumped particles, where a more compressible air void is reduced in volume prior to the water filled pores. It may be appreciated that with further volumetric compression, the air filled pore would disappear and a larger macro particle would be formed. This may happen at many levels throughout the sample, eventually leading to the whole sample becoming saturated, when the pressure of the bulk water is equal to the air entry suction of the sample. It should be noted that as the sample is volumetrically loaded, the mean pore size is reduced, and thus the air entry value of the sample is also reduced, therefore it is unlikely that the initial air entry value suction at failure will be equal to that initially because the pore volume distribution will change on loading.

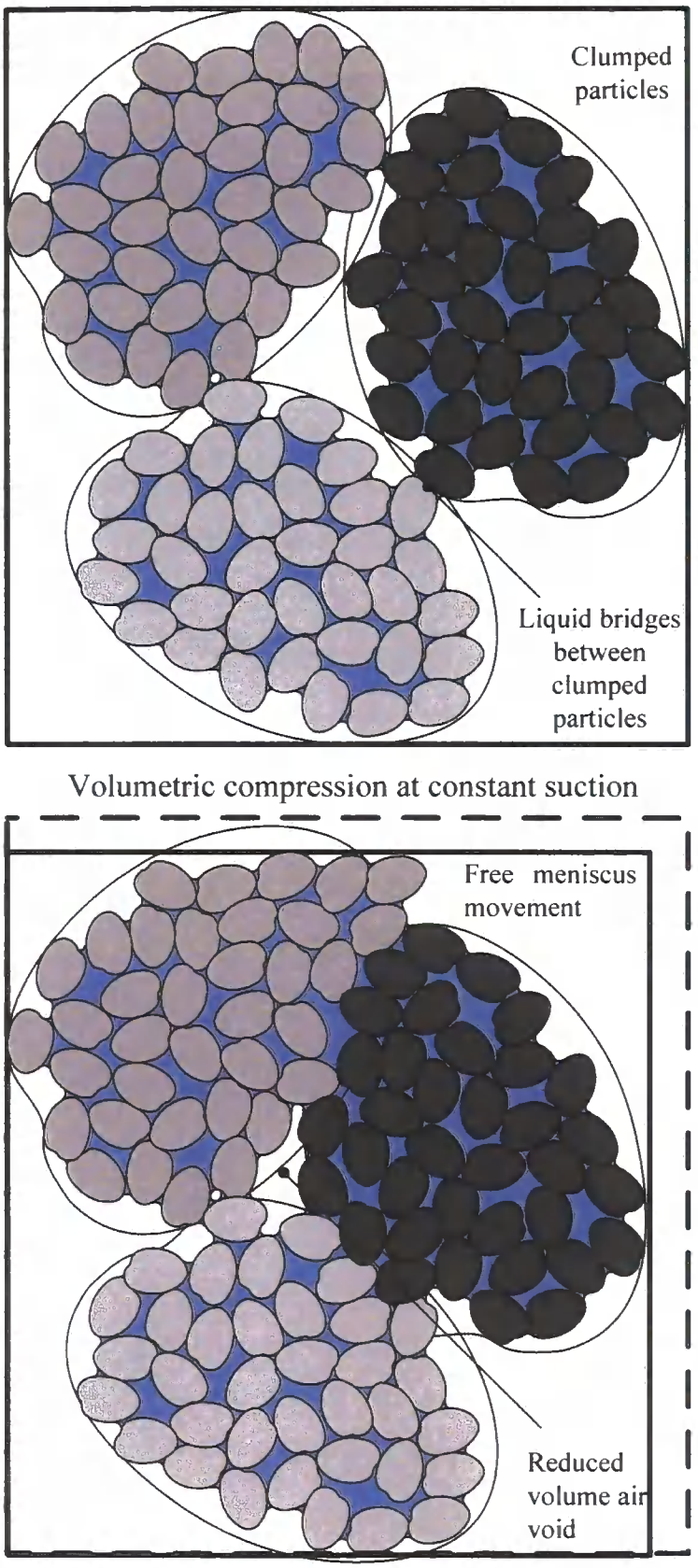

Figure 3.39 Volumetric compression of clumped particles

The notion of void ratio (e), as the total volume of the pores compared to the total volume of the sample, is less useful in unsaturated soil mechanics, and the idea of pore size distribution should be developed. This way those pores which are saturated and those which have a meniscus across them may be identified, and therefore the relative contributions of the strength identified. Sharma (1998) argues that the cross pore force is of less importance than the number of pores across which the liquid bridges act. Therefore it may be seen that the strength of an unsaturated soil below its air entry value is the sum of strength derived from interlock (which may be determined using critical state soil mechanics) and an additional strength due to liquid bridges across pores, that strength being a summation of the strength and the number of the liquid bridges.

Pore size distribution is a function of both particle size (and shape) distribution and density. The reduction or increase in volume in critical state theories may be viewed in terms of changing the effective pore size distribution, but as noted previously, changing the pore size, leads to mechanical wetting or drying of the sample (Tarantino 2007), therefore changing both the effective particle size distribution and the number of liquid bridges contributing to the strength of the sample. Figure 3.40 shows a simple indication of this theory. The graphs on the left are a line drawing of Figure 3.9, and those on the right an estimation of a cumulative pore volume distribution curve for a sample. A saturated sample (top) will have all the pores filled, and thus the only contribution to strength would be due to interlock. In contrast an unsaturated sample, at a relative humidity of 50% (bottom) would have only some of the pores saturated (those whose maximum radius is below the given air entry radius for that suction), the rest would contain menisci at the air entry radius, therefore the strength of the sample would be greater due to the presence of the menisci. Shearing of the sample would reduce both the number and the volume of the air filled pores, changing the pore volume distribution to that shown by the dotted line in Figure 3.40. Sample failure then occurs through shear failure in the saturated (but under tension) regions of the sample.

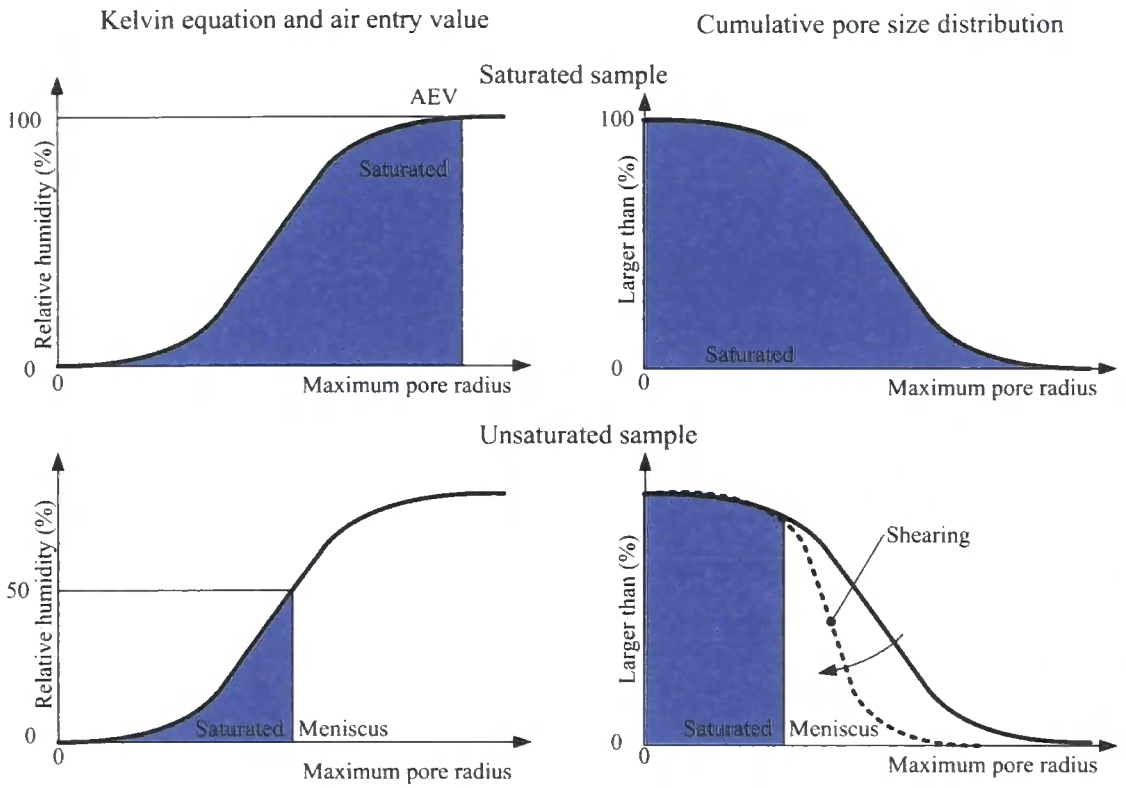

Figure 3.40 Cumulative pore distribution and relative humidity

The presence of clay bridges, as shown in Figure 3.25 may indicate why there will be less of a strength change in the higher suction regions. If the proportion of small particles (clay) in a sample is high enough, then bridges are likely to form between larger (sand) particles. Figure 3.25 shows that if a clay bridge is present at high suctions (top), where the clays are held in a saturated medium through colloid interaction, then an increase in suction will merely introduce menisci between the smaller particles, and the stability of the bridge will be maintained. If the smaller particles are physically touching, then the suction may increase indefinitely, and menisci will always exist between the small particles, until all the water is removed from the sample.

3.11.3 The pseudo - SWCC

The SWCC of a soil should be considered as a summation of the air entry values of the pores which make up the soil, with the total volume of water being the sum of the volume of those pores which are saturated $\left(r_{\max} < r_{EQ}\right)$ and the volume of the liquid bridge in those pores across which a meniscus is present $\left(r_{\max} < r_{EQ}\right)$. The volume of

air in a sample is the sum of those pores which are air saturated $\left(r_{\min} > r_{EQ}\right)$ and the volume of the air in those pores in which a meniscus is present $\left(r_{\max} > r_{EQ}\right)$.

The pseudo SWCC obtained for the rammed earth samples (Figure 3.38) may be considered as the drying curve of a single rammed earth sample, and while not exact, does allow some conclusions about the rammed earth to be drawn. The initial air entry suction value for the rammed earth may be seen to be around 80kPa if the falling part of the curve is considered, but may be as low as 10kPa when all the points are considered. Many authors (e.g. Fredlund and Radhardjo 1993) accept that the air entry value of a soil is not an exact value, and as outlined above must be considered to be an artefact of the pore size distribution of the soil. Figure 3.8 shows the air entry pore radius for a given suction, and it may be observed that the pore radius for a suction of 10kPa is greater than 0.01mm, and the pore radius for a suction of 80kPa is closer to 0.001mm. However, given the highly compacted nature of rammed earth, a pore radius of 0.001mm is within the range of dimensions of a silt particle, and therefore a pore of this radius would likely be filled by a silt particle if sufficient were available.

Figure 3.38 shows both the initial and final suction points measured using the tensiometers during loading of the samples. As outlined in Section 3.10.6, in the high water content samples the suction increased slightly, and in the lower suction samples the suction reduced. If the high water content samples are considered as saturated, then axial loading coupled with dilation, as outlined in Section 3.11.1 suggests an increase in suction, which is as observed. However the lower water content samples showed an increase in pore water pressure on loading, which is shown as a reduction in suction. This may be explained by considering that the tensiometer measures the pressure of the continuous bulk water in the sample. As liquid bridges are destroyed through the reduction in size of the pores (mechanical wetting) below r_{EQ}, water is able to join the body of continuous bulk water, and so both the volume of bulk water is increased and the volume of the pore network is reduced, leading to an increase in bulk water pressure. An increase in bulk water pressure is a reduction in suction.

This leads to the conclusion that there are two regions to consider when the pore water pressure is negative; a region when the suction is above the air entry value of the soil,

which may be considered to behave as a saturated soil; and a region where the suction is below the air entry value of the soil, and therefore must be considered more as a weakly bonded soil, with the liquid bridges acting as bonds between larger particles.

As explained in Section 3.3.4 the SWCC must be considered as the function of the air entry values of the pores of the soil. Therefore the initial SWCC may be considered as a function of the initial pore size distribution of the rammed earth, and the final SWCC as a function of the final pore size distribution of the rammed earth.

3.11.4 Brittle - ductile behaviour

Figure 3.37 shows increasing brittleness with increased suction. The brittle behaviour of unsaturated samples was explained by Cunningham, Ridley et al. (2003) through the formation of an open structure of silt particles stabilised by menisci, with clay particles within the menisci. It was argued that during shearing the silt particles become more closely pack and the stabilising effect of the menisci is reduced. At failure the menisci do not play a part and sample strength is a function only of the friction between particles on two independent rigid blocks.

This explanation may be further developed by considering the development of saturated pores within the sample, as the sample tends to the air entry value of the soil. Ductile behaviour may be expected from an interlocked saturated sample at its critical state, and brittle behaviour from a sample whose strength is derived from rigid bonds between each of the particles in the sample. On shearing of a highly unsaturated sample, the air filled pores reduce in volume and become saturated, which is why the stabilising effect of the menisci is reduced. At failure of the samples, the pores are all water filled (with water under tension), and thus sample strength may again be determined by critical state methods. However, the critical state parameters of the soil are likely to have changed because the effective pore size distribution of the soil is changed, as outlined by Toll (1990).

Due to the significantly greater compressibility of air compared to water (neglecting any resistance to movement of the meniscus), the meniscus filled pores compress easier than the water filled ones. On mechanical wetting the mean maximum radius of the meniscus filled pores reduces. This reduction in radius leads to the smallest of the

meniscus filled pores becoming saturated, and thus reducing to zero the stabilising effect of the liquid bridges, which are not now present.

3.11.5 Unsaturated sample strength

In this chapter is has been argued that there is a link between sample strength and measured suction, through the increasing strength and increasing number of inter particle bonds provided by the menisci, which arise as a result of the negative pore water pressure (suction). Figure 3.32 and Figure 3.37 shown that there is a relationship between both water content and strength, and suction and strength.

Considering Figure 3.33 (initial suction – deviator stress at failure), it can be seen that the sample deviator stress at failure increases linearly with suction, but comparison with the Figure 3.32 (Strength – water content) and Figure 3.38 (pseudo-SWCC) leads to the conclusion that sample strength cannot increase linearly with suction, and thus that Figure 3.33 may be viewed as a linear section of an exponential graph. While interparticle force increases linearly with suction, it can be seen that sample strength does not. The fact that sample strength does not increase linearly with suction was noted by Fredlund, Rahardjo et al. (1987), who noted the variation of the ϕ^b parameter.

The strength of an unsaturated soil sample below the air entry value, may be described by saturated soil mechanics, due to all the pores being water filled. However, the additional sample strength once the air entry suction is exceeded is due to the unsaturated nature of the soil. Figure 3.42 shows an idealised version of Figure 3.34, showing that the pore water pressure reduces (suction increases) below the sample air entry value, and increases (suction reduces) above the AEV. As outlined in Section 3.11.2, this is due to the higher compressibility of the air filled pores when compared to the water filled pores.

An increase in strength with suction is due to the unsaturated nature of the sample. This increase in strength is likely to be due to a combination of the following:

- Changed effective particle size distribution

Toll (1990) argues that the effective particle size distribution of an unsaturated soil alters as suction changes, this is shown in Figure 3.16. Therefore the determination of material parameters for the soil is difficult, as they are likely to also change with suction. The changing effective particle size distribu, tion cannot completely explain the strength of the samples tested due to their vertical sides which would be impossible to form through only interlock, and so some cohesion between the particles must exist.

- Increased colloid forces

Section 3.6 argues that the strength of earthen building materials is due to their unsaturated nature and that the colloid forces which have previously been attributed as strength providing mechanisms are only able to act in saturated media. However, the double structure theories presented above argue that as shearing occurs, the number of saturated pores increases. Therefore it is possible that the cross pore colloid forces also increase, increasing the strength of the sample. This postulate would be difficult to measure and requires knowledge of the relative magnitudes of colloid and frictional interlock forces at particle contacts.

- Increased cross pore strength

The relationship between suction and interparticle force, first developed by Fisher (1926) (Equation (3.29)) may be responsible for increased sample strength. The relationship between microscale interparticle strength and macroscale sample strength is complex, and the subject of much research, for example Cundall and Strack (1979). If a rigid soil body were considered then it may be suggested that a higher suction, therefore higher interparticle strength sample would be stronger than a lower suction one. Figure 3.41 shows the relationship between cross pore force and pore radius at the air entry value of the pore, given Equations (3.26) and (3.29). This shows that the relationship between interparticle force and pore radius is approximately linear between 100% and 90% RH, but then reduces when the relative humidity is below 90%. This relationship may help to explain the linear increase in strength observed

with reducing water content, and the non-linear relationship between strength and suction as described in Section 3.11.5. However, as described below, the whole sample strength is likely to be a function of the pore size distribution as well as the cross pore strength, and therefore further research in this area is required in order to determine the relative contributions of these aspects.

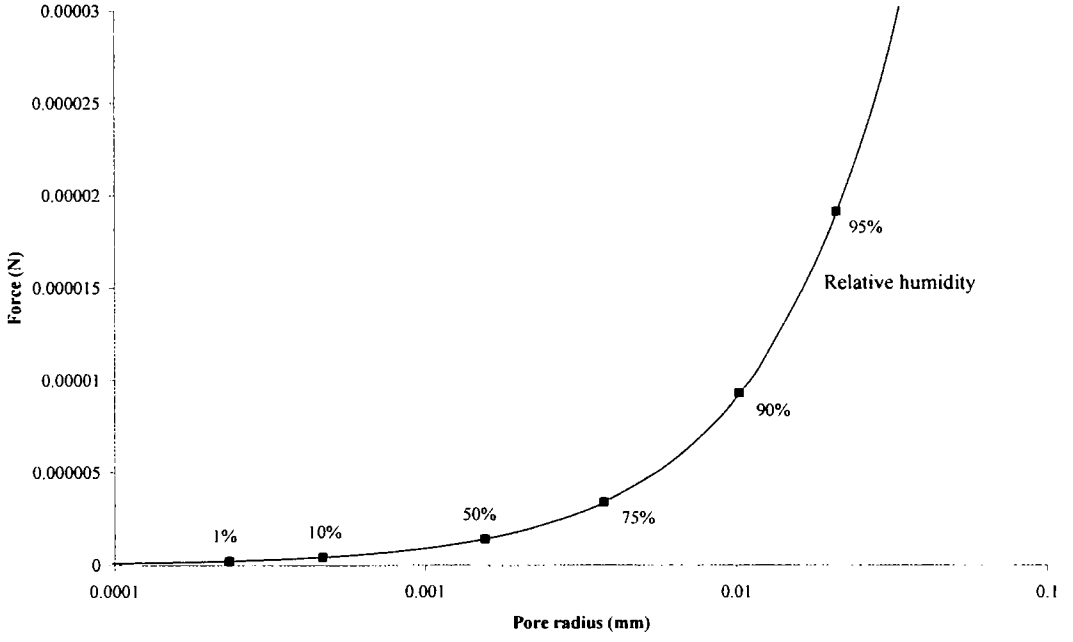

Figure 3.41 Force - pore radius

- Increased number of meniscus pores

Sharma (1998) argues that the number of pores across which menisci act will act to increase sample strength, and a brief extension of this theory is outlined below. Those pores across which a meniscus is present may be defined as those having a radius greater than the air entry radius as shown in Figure 3.9 and replicated in Figure 3.40. Therefore for a given relative humidity, it is possible to determine the maximum pore radius, below which pores will be saturated, and above which a meniscus will exist across the pore. This maximum pore radius may then be transferred to the cumulative pore size distribution curve, and the percentage of pore containing a meniscus, thus contributing to strength determined, as shown in Figure 3.40. However pore size distribution is extremely difficult to quantify, both in terms of physical definition of the pore and measurement of the pore shape and volume. Instruments and methods

exist which are able to scan an object to determine the pore volume distribution of a sample, and utilisation of these may allow further development of this area.

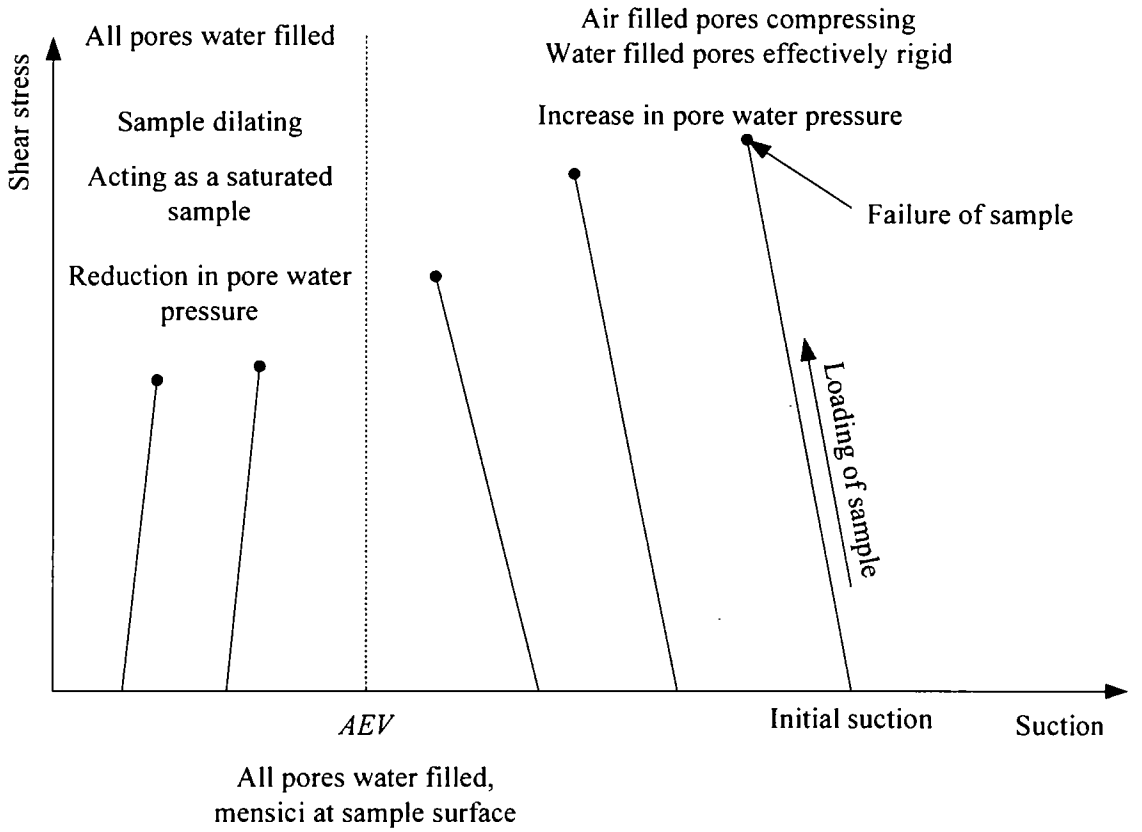

Figure 3.42 Idealised shear strength - suction relationship. Compare to Figure 3.34

3.11.6 Further investigation required

The arguments presented above propose that the additional strength of an unsaturated sample is likely to be a function of the number of pores across which a meniscus is present, and the strength of these menisci. However at the microscale the relative magnitudes of the interparticle contact forces is not known, and it is not known for example if the liquid bridge is stronger or weaker than the frictional forces at the interparticle contacts. The movement of the liquid bridge, its growth and shrinkage have not been addressed and in all considerations so far, the soil particles have been treated as within a rigid framework and not drawn together by the liquid bridge force. The behaviour of particles under negative pore water pressure, without consideration of an air water interface should be investigated.

3.12 Water movement in rammed earth

Having established that the additional strength in rammed earth is due to the presence of small amounts of water acting as liquid bridges between the particles, it is now possible to investigate the movement of this water within a body of rammed earth. It is well known that a rammed earth wall will not perform satisfactorily if it becomes too wet, and myths persist about not allowing earth buildings to dry out (Trotman 2007). Flow of moisture through a rammed earth wall is very important as it affects both the initial drying process, ingress of water during a rainfall event, and release of water following a rainfall event. Rammed earth buildings have often been noted for their constant internal relative humidity and temperature, and it will be shown that this is related to the flow of water through a wall.

The drivers of flow through any medium are fluid concentration difference, temperature and gravity. Evaporation from a surface causes a fluid concentration difference, leading to flow through the medium. A rammed earth wall presents a large surface to volume ratio compared to a region of unsaturated soil in the ground.

Flow of water through a porous medium can be split into two parts, that of liquid water flow and of water vapour flow. In an unsaturated soil liquid water flow can occur in two ways, liquid water and vapour movement. Flow of liquid water occurs through fully saturated pores, or by the advance of a wetting front into previously air filled pores. At high degrees of saturation the mass flow of liquid water dominates compared to water vapour flow, as the majority of the pores are water filled. At low degrees of saturation water vapour flow dominates, with the pores being air filled and water only present at the edges of pores as liquid bridges, or as bulk water between very small pore spaces. This section will explore the flow of both liquid water and water vapour in rammed earth. First the macroscale flow of water in saturated and unsaturated media is discussed, and it may be seen that predictions of water flow are impossible without physical measurement of permeability. Next. flow in capillary tubes is outlined, and here simple conclusions are drawn based on elementary capillarity theory.

3.12.1 Macroscale flow

Flow of fluid through a saturated medium was first described by Darcy, who postulated that the one dimensional rate of flow(q) through a porous medium was proportional to the hydraulic head gradient.

$$q = k\frac{\partial h}{\partial z} \tag{3.35}$$

Where k is the constant of proportionality known as the coefficient of permeability (or hydraulic conductivity), and $\frac{\partial h}{\partial z}$ the hydraulic gradient.

Taking the derivative of Equation (3.35) to find the rate of flow with respect to position gives

$$\frac{\partial q}{\partial z} = -\frac{\partial}{\partial z}\left[k\frac{\partial h}{\partial z}\right] \tag{3.36}$$

Defining volume of stored water as θ and considering conservation of mass, it can be seen that the rate of change of stored water with respect to time is equal to the change in rate of flow with respect to distance.

$$-\frac{\partial \theta}{\partial t} = \frac{\partial q}{\partial z}. \tag{3.37}$$

Combining equations (3.36) and (3.37) yields

$$\frac{\partial \theta}{\partial t} = \frac{\partial}{\partial z}\left[k\frac{\partial h}{\partial z}\right] \tag{3.38}$$

which is known as *Richards* equation (Richards 1931) for horizontal flow.

Solution of Richards equation, both exact and numerical, form the basis for prediction of flow of water in many aspects of soil physics. However all solutions rely on knowledge of permeability coefficients.

The coefficient of permeability k for a saturated soil is constant, but for an unsaturated soil k is predominantly a function of the water content. This is because the water can only flow through pore spaces which are filled with water (bulk water), and the air filled pores can be seen to be reducing the permeability of the soil (Fredlund and Radhardjo 1993, Fredlund, Xing et al. 1994)

Terzaghi (1943) formulated a simple theory for predicting the rate of capillary rise in a one dimensional column of soil. This theory made two assumptions, that Darcy's law (Equation (3.35)) for saturated flow holds for unsaturated flow, and that the hydraulic gradient (i) responsible for capillary rise can be approximated as follows:

$$i = \frac{h_c - z}{z} \tag{3.39}$$

Where h_c is the ultimate height of capillary rise, and z is a distance measured vertically upwards from the water table. h_c represents the drop in pressure head across the air-water interface at the wetting front in the soil pores.

Solving equations (3.35) and (3.39) and setting initial conditions of zero capillary rise at zero time, the following formula describes the location of the wetting front as a function of time.

$$t = \frac{nh_c}{k_s}\left(\ln\frac{h_c}{h_c - z} - \frac{z}{h_c}\right) \tag{3.40}$$

where n is the soil porosity and k_s is the saturated permeability. Unfortunately this equation is difficult to implement for rammed earth structures, as it is intended to describe the capillary rise above a constantly replenished water table. When considering a rammed earth wall drying, and suction increasing, the capillary rise (h_c) is determined by the relative humidity (Equation (3.21)) and z as a vertical distance from the water table, whereas drying and wetting from a rammed earth wall is likely to take place horizontally through capillary flow rather than capillary rise.

3.12.2 Flow in capillary tubes

Poiseuille's law concerns the volume of laminar flow of an incompressible viscous fluid through a cylindrical tube of constant circular cross section under an external pressure, and is formulated by considering the internal friction between cylinders of laminar flow in a tube.

$$\frac{dV}{dt} = v\pi R^2 = \frac{\pi R^4}{8\eta}\left(\frac{-\Delta P}{\Delta x}\right) = \frac{\pi R^4}{8\eta}\frac{|\Delta P|}{L} \tag{3.41}$$

where V is the volume of liquid, v the fluid velocity, R the tube radius, η the dynamic fluid viscosity, ΔP the pressure difference and L the length of the tube.

Washburn (1921) calculated the depth and rate of penetration into a small capillary by applying Poiseulle's law for fluid motion in a circular tube. Assuming that the wetting front (meniscus) is able to slip up to the tube freely, and taking

$$dV = \pi r^2 dl \tag{3.42}$$

Equation (3.41) becomes

$$\frac{dl}{dt} = \frac{\Sigma P r^4}{8 r^2 \eta l} \tag{3.43}$$

where ΣP is the sum over the participating pressures. The first order differential equation is thus formed. Assuming horizontal infiltration into the wall (no influence of gravity), and the external pressure to be equal to atmospheric, and a wetting angle of zero, the only pressure driving capillary rise is capillary pressure, therefore

$$\frac{dl}{dt} = \frac{\left[\frac{2\sigma_l}{r}\right] r^2}{8\eta l} \tag{3.44}$$

$$l = \int_0^t \frac{2r\sigma_l}{8\eta l} dt \tag{3.45}$$

$$L^2 = \frac{D\sigma_l t}{4\eta} \tag{3.46}$$

Equation (3.46) may provide a reasonable estimation of capillary flow through rammed earth walls.

Currently earth walls are tested using the spray test where a sample of wall is wetted by a known rate of water spray known as the *accelerated spray test* (Walker 2002). The mass of water absorbed and the depth of erosion is measured, but there are currently no guidelines on methods of changing the mass of water absorbed or reducing the depth of erosion. Recent investigations into moisture ingress into rammed earth walls (Hall and Djerbib 2004a; Hall and Djerbib 2006a; Hall and Djerbib 2006b) have shown that particle size distribution affects the rate of moisture ingress and mass of absorbed water, and Hall (2007) has further recognised the advantages in reducing the effective hydraulic pore radius of the material.

The liquid water ingress into an earthen building may be determined by considering capillary flow into the pore spaces in the material. It is likely that an earthen structure will only survive for a significant length of time if the pore spaces are of the correct

size for the surrounding relative humidity. These sizes ensure that liquid bridges are able to form across the pores and provide the structure with additional strength above that derived from frictional interlock.

Rammed earth is an interlocked granular material with menisci present at the particle-particle contacts. There exist pores whose minimum radius is smaller than that required for a given relative humidity and whose largest dimension is greater than that required for the given relative humidity. A meniscus exists at the pore radius $\left(r_{EQ}\right)$ for the given relative humidity. In the presence of a replenished water source on the surface of the wall (for example a heavy rain storm causing water to run over the surface, Figure 5.29 water will ingress into the wall through capillarity. In the local region of the water source, the relative humidity will increase, allowing menisci to form across larger pores, and increasing the size of menisci across previously joined pores. A wetting front will advance through capillary rise, in an attempt to equalise the vapour pressures as described by Kelvin (Equation (3.24)). The speed of advance of this wetting front may be given by Equation (3.46), but is likely to be slower due to energy required to overcome slip of the meniscus. In addition pores are unlikely to be perfectly cylindrical and thus advance of a wetting front through a pore network is highly complex.

A simple conclusion may be drawn from Equation (3.46). Assuming the ambient relative humidity to the 50%, and the corresponding air entry value (maximum pore radius at which a meniscus will be present) to be 0.0016mm, taking the dynamic viscosity of water to be 0.00089 Pa·s (Massey and Ward-Smith 1998), Equation (3.46) shows that water would take one hour to penetrate 13mm into a wall and two weeks to penetrate 23cm. This may explain the "overcoat" effect reported by Hall and Djerbib (2006b), and allow a quantification of the depth of this overcoat (Figure 3.43).

Capillary absorption is limited by the viscosity of water (Equation (3.46)) and by the slip of the meniscus (not included in this simple analysis) and thus there is a finite rate at which water can be absorbed (Equation (3.41)). Excess incident water flows as a surface runoff. Erosion occurs when the surface becomes saturated, and the liquid

bridges are not able to form across saturated pores. When this occurs a particle or group of particles are dependent only on internal friction, remembering that they are unconstrained in the out of plane direction, and will thus fall to their angle of repose if the whole structure becomes saturated. A single particle may detach from the body of the wall if it becomes part of a saturated region, and gravity overcomes any other frictional or electrostatic forces holding it to the wall. The depth of erosion, as measured by the *spray test*, may be indicative of the depth of full capillary penetration, but as Equation (3.46) shows, it takes longer for a wetting front to advance up a larger diameter pore than a smaller pore, and thus the small pores may become saturated while the larger pores remain unsaturated, leading to increasing large regions of low suction, which eventually reduce to regions of zero suction and can be considered saturated. Once this saturation occurs, erosion is likely to happen.

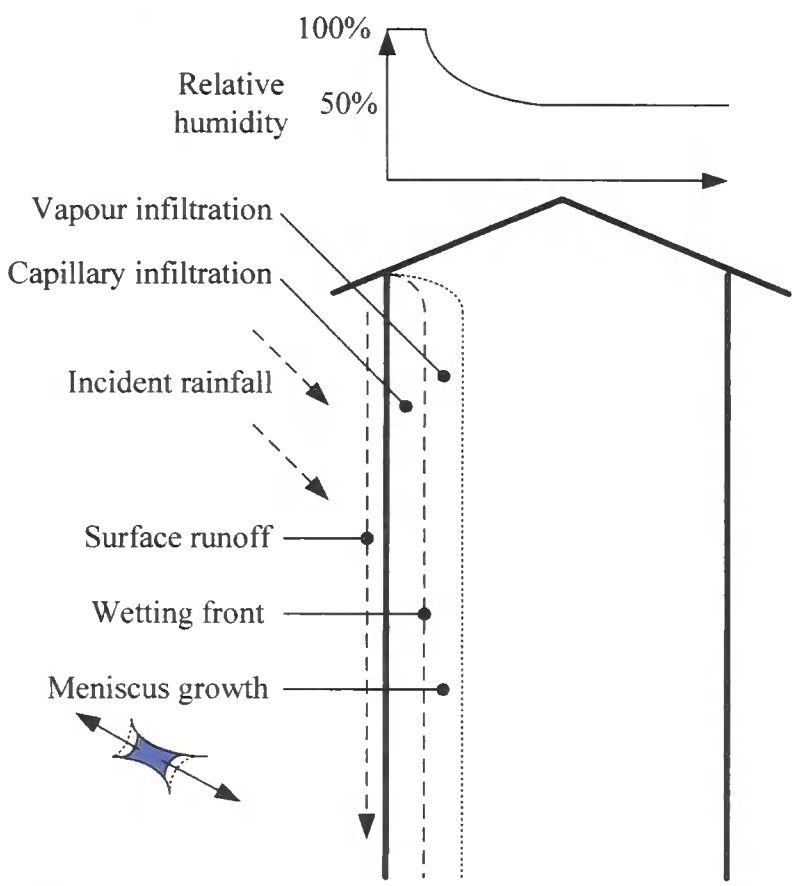

Figure 3.43 Overcoat effect (Hall and Djerbib 2006a) explained

3.12.3 Evaporation

At the low water contents found in 'dry' rammed earth structures, the transport of water is likely to occur in the form of water vapour evaporating and condensing, and

the transfer of water vapour through the pore matrix. The magnitude of vapour transport is related to the gradient of vapour pressure (i.e. relative humidity), and on a macroscale on the tortuosity of the pore matrix. The movement of water vapour has not been studied in this thesis, but the process of evaporation is now examined.

The water held within the soil must be in equilibrium with the air in the soil pores, otherwise there is a transfer of water from the liquid phase to the vapour phase more commonly called evaporation. The conditions for this are outlined below.

At a free flat body of water, the vapour pressure above the body of water will be the saturation vapour pressure p_0. However above a meniscus, Kelvin's equation shows that the vapour pressure will be reduced. It is the difference in these vapour pressures which causes capillary rise. At the free surface the vapour pressure equals the saturation vapour pressure $(p_v = p_0)$, there will be no evaporation, since saturation vapour pressure implies an equal number of water molecules leaving as entering the liquid phase. Similarly at a meniscus there will be no evaporation if the vapour pressure is equal to that required for the given size of the meniscus, determined by considering Kelvin's Equation (3.24) and the air entry value of the pore (Equation (3.26)), because the number of molecules entering will equal the number of molecules leaving the liquid.

However, if the vapour pressure is not equal to that required for a given meniscus curvature, then evaporation or condensation will occur. In the case of a rammed earth wall, the external vapour pressure (which may now be referred to as the relative humidity, through the relationship described in Equation (3.16)), is not usually equal to that within the wall, therefore evaporation and condensation occur between the wall and the external environment.

Evaporation is defined as the quantity of water per unit time which is removed from a body to the atmosphere (Wilson, Barbour et al. 1995). The evaporation from a free body of water was first described by Dalton (1802, 1805) considering the theory of partial pressures.

$$E = f(u)(p_0 - p_v) \tag{3.47}$$

Where $f(u)$ is known as the turbulent exchange function, and takes account of the temperature and turbulence of the air. p_0 is the saturation vapour pressure of water at the temperature of the surface and p_v is vapour pressure of the air in the atmosphere above the water surface. Given that the relative humidity(RH) is the ratio of the saturation vapour pressure to the actual vapour pressure (Equation (3.16)), the rate of evaporation from a surface may be expressed as

$$E = f(u)\, p_0 [1 - RH] \tag{3.48}$$

The evaporation of water from an unsaturated soil occurs through evaporation from progressively smaller pores, beginning with evaporation from the largest pores and continuing to smaller pores until only pores small enough to be filled under a given relative humidity are left filled with water. Evaporation from unsaturated soil may be considered as analogous to evaporation from capillary tubes. The evaporation which takes place from a meniscus depends on the difference between the ambient and the meniscus partial pressures (relative humidities).

Evaporation from unsaturated soils has previously been studied in the "vadose" zone (soil above the water table), where a constant recharge is available, and has not looked at the drying (and therefore increasing suction) of soils.

Wilson, Barbour et al. (1995) defined Actual Evaporation (AE) and Potential Evaporation (PE) fluxes, where PE is the evaporation flux which would be expected for an ambient relative humidity, and AE is the evaporation flux which would be expected for a given relative humidity (i.e. suction). The ratio of these evaporations for a given suction was then determined and a close correlation was observed (Figure 3.44) but not explained.

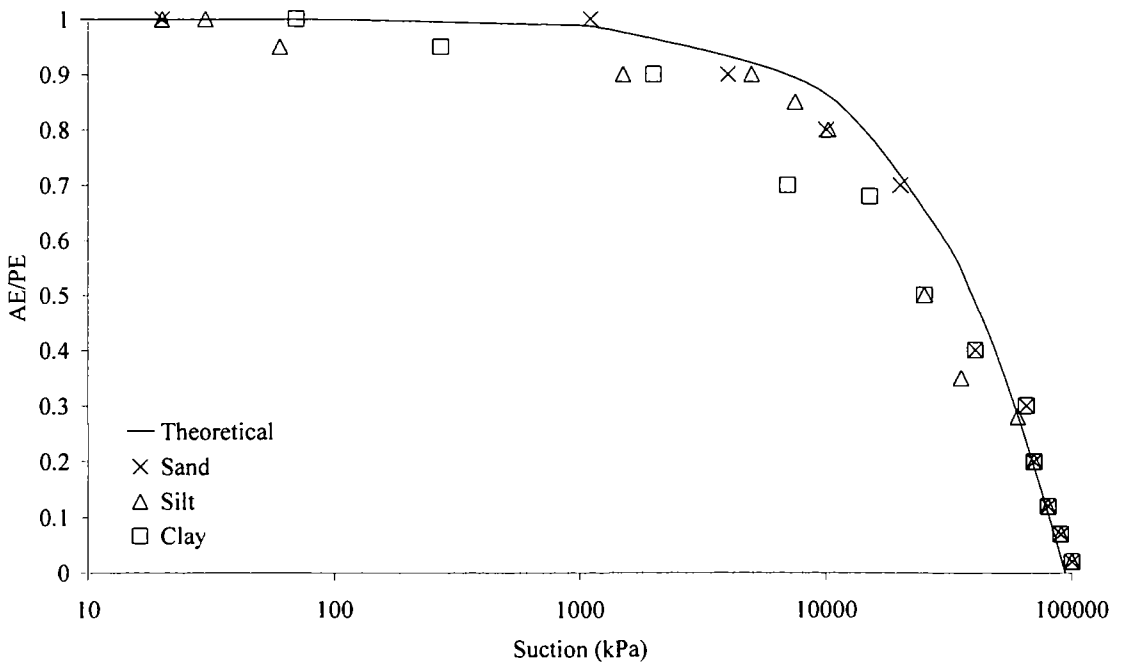

Figure 3.44 Ratio of AE/PE for a given suction, from Equation (3.50) at $RH_{Ambient}$ = 50%, and results from Wilson, Barbour et al. (1995)

The relationship between suction and evaporation may be explained by expressing Equation (3.48) in terms of suction by relating relative humidity to suction through Equation (3.24).

$$E = f(u)\,p_0\left[1 - e^{(u_a - u_w)\frac{RT}{V}}\right] \tag{3.49}$$

The ratio may therefore be expressed as

$$\frac{AE}{PE} = \frac{\left[1 - RH_{Ambient}\right]}{\left[1 - e^{(u_a - u_w)\frac{RT}{V}}\right]} \tag{3.50}$$

which is plotted in Figure 3.44. The variation between the curves may be explained by considering a relative humidity and water content gradient within the samples, set up by the evaporation. The suction values were obtained by comparison with the SWCC of the soils, which were derived using samples at constant suction. It may be observed that the sand values fall closest to the theoretical curve, and the clay values furthest away, suggesting that evaporation is easier from a sand than from a clay, so the suction values are closer to those expected.

This simple insight into evaporation from unsaturated soils helps to explain why earth walls dry to a small but finite water content. Evaporation from pores ceases when the humidity of the pore air is equal to the humidity of the surrounding air. This corresponds to a suction which may be derived from Equation (3.24), and thus a pore size which may be derived from Equation (3.13). If, for a given relative humidity, the maximum pore size exceeds that required, then a meniscus will exist in the pore and thus an attractive force across it. If the maximum pore size is less than required then the pore will be filled with water and may be considered saturated. Conversely if the minimum pore size is greater than required then a meniscus could not be sustained within the pore.

This insight leads to the attractive prospect of being able to determine the drying characteristics of different rammed earth mixes, by establishing the pore size distribution and the vapour diffusivity coefficients. Without knowing these, it may be appreciated that a samples with a smaller mean pore size will take longer to dry out than a sample with a larger mean pore size, as is observed when considering the difference between dense clay bricks and dense sand drying.

3.12.4 Water in rammed earth

The above discussions highlight the rate of liquid and vapour flow in rammed earth walls. This section draws together these discussions to describe the flow of water in a rammed earth wall. Earthen structures act as a relative humidity flywheel, using a variety of processes to attempt to equalise the relative humidity of the external environment with that of the pores within the walls. The stabilised relative humidity inside a rammed earth building has been observed by the author and Heathcote (2007), and is often highlighted as an advantage of rammed earth when compared to other construction materials, but has yet to be explained.

Following the compaction of a rammed earth wall, the initial drying phase is dominated by evaporation from the free surfaces of a wall, which may also act to provide a driving capillary pressure to draw water from the centre of the wall (Equation (3.41)) to the face through capillarity. At the same time the difference in relative humidities causes direct evaporation both at the surface and within the pores

of the wall. Evaporation and capillary movement will continue until the humidity of the pore air is equal to that of the surrounding air (Phases 1, 2 and 3, Figure 3.45).

When rainfall occurs against a surface (Phase 5, Figure 3.45) liquid water initially flows through the wall by capillary action, but this raises the relative humidity in the pores close to the wetting front, so water vapour diffusion takes place ahead of the wetting front leading to an increase in relative humidity and thus condensation and growth of the liquid bridges in the central section of the wall.

When rainfall ceases (Phase 5, Figure 3.45) the water content of the wall is increased and the relative humidity of the pores is also slightly increased. If the relative humidity of the external air returns to the ambient (say 50%) then the relative humidity of some of the pores is greater than ambient, and thus evaporation takes place from these pores.

If the roof is deficient or missing then water is able to enter the body of a wall (Phase 6, Figure 3.45) then the water content of the wall will increase. If the ambient relative humidity is less than 100% then evaporation will occur from the body of the wall to the atmosphere, and if the rate of removal of water is less than the rate of infiltration, then the water content of the wall will increase, eventually leading to collapse.

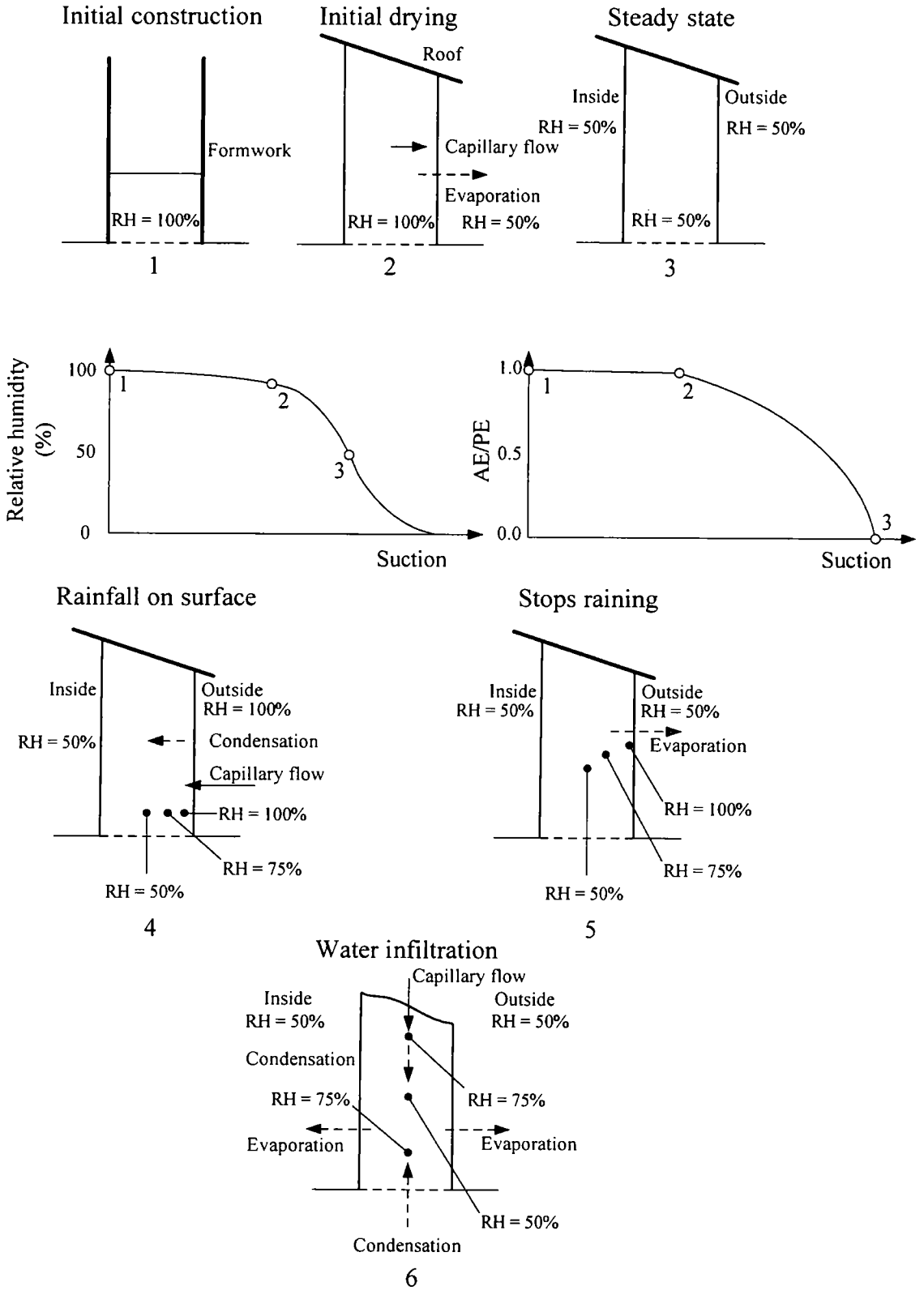

Figure 3.45 Infiltration and evaporation in a rammed earth wall

3.13 Further work

A series of very simple tests have been carried out, and during the course of testing a huge number of ideas for further work arose. It has not been possible to fully characterise the material, as insufficient tests were carried out. Therefore, further work would include triaxial tests at various confining pressures, in order to measure Mohr-Coulomb and Critical State parameters and later parameters for the BBM. In addition, the rammed earth mix should also be characterised as a saturated soil, such that a comparison between saturated and unsaturated behaviour can be observed. More displacement instrumentation should be added, such that it can be properly ascertained as to whether the material is dilating or contracting, the addition of strain belts around the sample, would provide a simple method of measuring volumetric behaviour. The small number and discrete nature of each of the tests carried out meant that issues of variability were not addressed, and further work should look to measuring the inherent variability within rammed earth. Other types of test should be performed, perhaps treating rammed earth as a weak rock. Brazilian tests have already been carried out (Jaquin, Augarde *et al.* 2007b), but direct shear tests, and shear testing of wallets would be of great value. The rate of loading should be carefully investigated as it is known that loading rate plays a large role in saturated soil mechanics, and it is considered that the same is true for highly unsaturated soils such as found in building.

One of the main arguments of this chapter is that strength is related to pore size, and while indirect evidence has been provided, a measurements of the pore size distribution, would further validate that argument. While it has been argued that an increase in the number of pores across which a meniscus exists produces an increase in total sample strength, no proof of this has been provided. Analyses using the Discrete Element Method (Cundall and Strack 1979) might provide evidence for such arguments.

An argument has been presented which attempts to explain the distribution of relative humidity within a rammed earth wall, but there has yet to be any physical testing of

the pore air relative humidity of a rammed earth wall. Such testing would be relatively simple, and would provide evidence to back up the theories proposed.

Finally, all of the work in this chapter is related to unstabilised rammed earth. Much of the rammed earth currently under construction, and much historic rammed earth is bonded in some way. The inclusion of cementing in an unsaturated soil mechanics framework would mean that the behaviour of stabilised earthen architecture could be better understood.

3.14 Implications for rammed earth buildings

Chapter 3 has shown that many aspects of the behaviour of rammed earth building material can be explained by considering rammed earth as an unsaturated soil. It has been shown that the saturated strength of the samples tested is around 20% (Figure 3.33) of the unsaturated strength, and as explained previously that the maximum sample strength corresponds to a minimum water content, which is controlled by the relative humidity of the surrounding air. Furthermore it has been suggested that the strength of a rammed earth sample is a function of the pore size distribution, and that rammed earth 'works' as a structural material due to its low mean pore size, allowing the formation of menisci at the relative humidity where rammed earth is used as a building material. It has been shown that the strength of the material reduces as water flows from bulk water to menisci, either through reduction in pore size or through an increase in water content, and has suggested that the rate of loading is important in the strength of a structure. If evaporation and pore water dissipation is allowed to take place, then the strength of an earthen structure is increased compared to if pore water dissipation is not allowed to take place (analogous to saturated soil mechanics). It can thus be seen that rapid loading, such as occurs during seismic events, may cause a reduction in strength, and thus collapse, as was observed in rammed earth structures during the Bam earthquake (Langenbach 2004).

Figure 3.36 and Figure 3.37 show the change in modulus and in strain at peak deviatoric stress of the samples tested with changing water content. This helps to explain the observed ability of earthen building to 'flow' when wet without appearing to lose any strength (Houben and Avrami 2000). If a 'dry' load bearing structure is wetted, it can be seen that its modulus may reduce slightly, and it is likely that there will be a small reduction in the failure strength of the material. A reduction in the modulus will lead to increased strains for the applied load, but provided the strength of the material is not exceeded, the building may 'flow', but will not actually collapse.

Previous work, detailed in Chapters 1 and 2, looked at producing the optimum particle size distribution for rammed earth construction. It was assumed that maximum density would be achieved by approximating the particle size distribution to the Fuller

distribution, but there was no explanation as to why an increased density produced a stronger material. It has been shown that strength is derived from the pore size distribution of a mix, and that pore size distribution is a function of the particle size distribution, compactive effort, and water content at compaction. A strong rammed earth mix is then a mix in which the mean pore size in minimised, but that pores still exist in which menisci are able to form and thus provide strength to the material.

The 'drop test' (Houben and Guillaud 1994; Lilley and Robinson 1995; Keable 1996) appears to provide a moisture content wet of optimum when compared to the Proctor compaction test (BS1377-2 1990). Compacting wet of optimum moisture content leads to a dispersed structure, with small interaggregate pores, while compacting dry of optimum leads to a flocculated structure of many soil packets with more large interaggregate pores. If the suction is sufficiently high to prevent breakdown of these packets, the soil then acts in a more granular way than justified by its grading. If the suction is reduced, then the soil becomes unstable and collapse occurs through breakdown of the packet structure (Toll 1990). It is therefore preferable to compact the soil wet, rather than dry, of optimum.

The optimum pore size distribution for rammed earth is then one in which the pores are small enough to allow the formation of menisci across pores, but large enough such that they are not fully saturated at all ranges of relative humidities. Figure 3.9 shows the pore radii which will be saturated for a given relative humidity. It can be seen that for a relative humidity of 50%, pores of maximum radius smaller than 0.0016mm will be saturated. Therefore a rammed earth sample should have a particle size distribution which allows pores of radius greater than 0.0016mm.

The Fuller formula, recommended by Houben and Guillaud (1994), is intended to provide a maximum density, but it can be seen that a particle size distribution close to the Fuller formula will also reduce the pore size distribution, and for spherical particles the pore size distribution may be considered to be the difference between the particle size distribution and the Fuller formula.

Current state-of-the-art modelling of rammed earth (Walker, Keable et al. 2005) is simplistic and does not consider the unsaturated nature of rammed earth. It has been

shown that 'dry' rammed earth has a strength of close to 1MPa, and can be considered to have both tensile and shear strength. However when considering new rammed earth, the strength on removal of the formwork is usually most critical, and it has been shown that this should be the saturated strength, which has been shown to be of the order of 20% of the dry strength.

3.15 Concluding remarks

This chapter has shown that rammed earth can be successfully treated as an unsaturated soil, and doing so allows prediction of the strength, stiffness and water retention behaviour. While the idea that suction may be responsible for the additional strength of earthen materials has previously been proposed (for example Gelard, Fontaine et al. 2007), this chapter has aimed to further develop these ideas by introducing the concept of pore size distribution and relative humidity. It has been argued that there should be a change of emphasis from liquid bridge forces acting between particles to acting across pores. By considering these aspects, it is possible to theorise on both the strength and moisture retention characteristics of rammed earth. The previously held notions of colloid chemistry being responsible for the strength of rammed earth have been challenged, and it has been argued that these colloid interactions occur only within saturated pores, and that dry rammed earth must, through equalisation of the relative humidities of the pore and external air, be treated as an unsaturated medium. The non-zero water content of dry rammed earth has been shown to be due to this evaporation driven by differences in the relative humidities, and that the final water content is the sum of the volume of water held in the saturated pores and in the pores where menisci are present. It is also possible to use the same theories to argue that all non-stabilised earthen architecture (cob, adobe) also gain strength through these same mechanisms.